

**UNIVERSITY OF ALBERTA**

*Fluid Chemistry of Base-Metal Mineralizing and Non-Mineralizing Fluids of the N81  
Deposit at Pine Point, Northwest Territories, Canada*

by

*Paulina Gromek* ©

A thesis submitted to the Faculty of Graduate Studies and Research  
in partial fulfillment of the requirements for the degree of

Master of Science

Department of Earth and Atmospheric Sciences

Edmonton, Alberta

Fall 2006



Library and  
Archives Canada

Bibliothèque et  
Archives Canada

Published Heritage  
Branch

Direction du  
Patrimoine de l'édition

395 Wellington Street  
Ottawa ON K1A 0N4  
Canada

395, rue Wellington  
Ottawa ON K1A 0N4  
Canada

*Your file* *Votre référence*  
*ISBN: 978-0-494-22272-0*  
*Our file* *Notre référence*  
*ISBN: 978-0-494-22272-0*

**NOTICE:**

The author has granted a non-exclusive license allowing Library and Archives Canada to reproduce, publish, archive, preserve, conserve, communicate to the public by telecommunication or on the Internet, loan, distribute and sell theses worldwide, for commercial or non-commercial purposes, in microform, paper, electronic and/or any other formats.

The author retains copyright ownership and moral rights in this thesis. Neither the thesis nor substantial extracts from it may be printed or otherwise reproduced without the author's permission.

**AVIS:**

L'auteur a accordé une licence non exclusive permettant à la Bibliothèque et Archives Canada de reproduire, publier, archiver, sauvegarder, conserver, transmettre au public par télécommunication ou par l'Internet, prêter, distribuer et vendre des thèses partout dans le monde, à des fins commerciales ou autres, sur support microforme, papier, électronique et/ou autres formats.

L'auteur conserve la propriété du droit d'auteur et des droits moraux qui protègent cette thèse. Ni la thèse ni des extraits substantiels de celle-ci ne doivent être imprimés ou autrement reproduits sans son autorisation.

---

In compliance with the Canadian Privacy Act some supporting forms may have been removed from this thesis.

Conformément à la loi canadienne sur la protection de la vie privée, quelques formulaires secondaires ont été enlevés de cette thèse.

While these forms may be included in the document page count, their removal does not represent any loss of content from the thesis.

Bien que ces formulaires aient inclus dans la pagination, il n'y aura aucun contenu manquant.

  
**Canada**

## ABSTRACT

Mineralizing and non-mineralizing fluids involved in the N81 deposit at Pine Point were characterized using microthermometric, bulk geochemical and strontium isotopic analyses. The mineralizing fluids are highly calcic brines (23 wt% CaCl<sub>2</sub>-NaCl), which formed at a minimum temperature of 82°C. Geochemical data suggests that at least two fluids were responsible for the mineralization, which varied in salinity and strontium composition, (<sup>87</sup>Sr/<sup>86</sup>Sr=0.7073 to 0.7152; average=0.7116) but were relatively isothermal and likely derived from a mixture of highly evaporated seawater and an <sup>87</sup>Sr-rich fluid. The post-ore fluids were highly radiogenic (<sup>87</sup>Sr/<sup>86</sup>Sr<sub>avg</sub>=0.7149) NaCl-CaCl<sub>2</sub> brines (0 to 15 wt% equivalent NaCl-CaCl<sub>2</sub>; average=9 wt% equivalent) and geochemical data suggest the fluids may have been a mixture of a saline brine and meteoric water. In general, Sr isotope ratios suggest that the fluids became more radiogenic with the progression of the paragenetic sequence and that the <sup>87</sup>Sr is likely sourced from clastics and/or basement rocks.

## ACKNOWLEDGMENTS

A sincere thanks is given to Dr. Sarah Gleeson for allowing me to do this study. Her continued support, guidance, discussion and input significantly improved the quality of this thesis.

Dr. Jeremy Richards is thanked for the generous use of fluid inclusion analysis equipment in his fluid inclusion laboratory. Dr. Antonio Simonetti is thanked for his technical expertise of strontium isotopic analysis. Don Resultay and Mark Labbe are thanked for the preparation of thin and thick sections.

A warm thanks to my family and friends, especially to my mother and Shannon Zurevinski, for their continued support, patience and encouragement throughout the completion of this thesis.

## TABLE OF CONTENTS

### CHAPTER 1: GENERAL INTRODUCTION

1.1	Scope and Intent .....	1
1.2	Study Area .....	2
1.3	Geological Background .....	4
1.4	Previous Studies .....	5
1.4.1	Petrographic Analysis – Paragenetic Sequence Development .....	6
1.4.2	Microthermometric Analysis .....	6
1.4.3	Bulk Geochemical Analysis .....	7
1.4.4	Strontium Isotopic Analysis .....	7
1.5	Objectives .....	8

### CHAPTER 2: METHODOLOGY

2.1	Introduction .....	10
2.2	Methodology of Petrographic Study .....	10
2.3	Methodology of Fluid Chemistry Analyses .....	10
2.3.1	Microthermometric Analysis .....	10
2.3.2	Bulk Geochemistry Analysis .....	11
2.3.3	Strontium Isotopic Analysis .....	13

### CHAPTER 3: PETROGRAPHY

3.1	Introduction .....	14
3.2	Fluid Inclusions .....	14
3.2.1	Background Information .....	14
3.2.2	Trapping and Characterization .....	15
3.3	Petrographic and Fluid Inclusion Sample Descriptions .....	15

3.3.1	N81-65 0249 .....	15
3.3.2	N81-68A 2969 375' .....	17
3.3.3	N81-69 2754 195' .....	17
3.3.4	N81-69 2758 217' .....	18
3.3.5	N81-69 2764 235' .....	19
3.3.6	N81-69 2766 240' .....	20
3.3.7	N81-75 3358 260' .....	20
3.3.8	N81-75 3386 322' .....	21
3.3.9	N81-84 1078 .....	21
3.3.10	N81-98 3181 287' .....	22
3.3.11	N81-98 3205 355' .....	23
3.3.12	N81-98 3205 360' .....	24
3.3.13	N81-98 3208 367' .....	24
3.3.14	N81-98 3214 .....	25
3.3.15	N81-98 3225 450' .....	25
3.4	Mineral Phase Summaries .....	26
3.4.1	Host Dolomite .....	26
3.4.2	Coarse White Dolomite .....	26
3.4.3	Sphalerite .....	27
3.4.4	Galena .....	27
3.4.5	Calcite .....	27
3.4.6	Native Sulphur .....	28
3.4.7	Bitumen .....	28
3.4.8	Summary of the Paragenetic Sequence .....	28
3.5	Discussion – Comparison to Previous Petrographic Analyses .....	30
3.5.1	Introduction .....	30

3.5.2	Phase Description Summary – Krebs and MacQueen (1984) .....	30
3.5.3	Phase Description Summary – Qing (1991) .....	31
3.5.4	Paragenetic Comparisons .....	33
3.6	Remarks .....	35

## **CHAPTER 4:           MICROTHERMOMETRIC ANALYSIS**

4.1	Introduction .....	62
4.2	Background Information .....	62
4.3	Microthermometric Results .....	63
4.3.1	Coarse White Dolomite .....	63
4.3.2	Sphalerite .....	64
4.3.3	Calcite .....	65
4.4	Interpretation .....	67
4.4.1	Calculation Information .....	67
4.4.2	Coarse White Dolomite .....	67
4.4.3	Sphalerite .....	68
4.4.4	Calcite .....	68
4.5	Discussion – Comparison of Phases .....	70
4.6	Discussion – Comparison to Previous Microthermometric Analyses .....	72
4.6.1	Microthermometric Summary – Roedder (1968) .....	72
4.6.2	Microthermometric Summary – Kyle (1977) .....	72
4.6.3	Microthermometric Summary – Qing (1991) & Qing & Mountjoy (1992) .....	73
4.6.4	Microthermometric Summary – Turner (2003) .....	75

4.6.5	Comparison of Previous Microthermometric Data to this Study ....	75
4.7	Remarks .....	76
<b>CHAPTER 5:                  BULK FLUID INCLUSION ANALYSIS</b>		
5.1	Introduction .....	89
5.2	Sample Selection .....	89
5.3	Suitability of Samples .....	91
5.4	Results .....	91
5.4.1	Contamination .....	91
5.4.2	Charge Balance .....	92
5.4.3	Ratios versus Absolute Data .....	93
5.4.4	Anion Data.....	94
5.4.5	Cation Data .....	97
5.5	Discussion .....	102
5.5.1	Na-Cl-Br Systematics .....	102
5.5.2	Geochemical Implications for Fluid Sources .....	103
5.5.3	Comparison of Telser (1999) to this Study .....	107
5.5.4	Comparison of Gleeson and Gromek (in press) to this Study .....	108
5.6	Remarks .....	113
<b>CHAPTER 6:                  STRONTIUM ISOTOPE GEOCHEMISTRY</b>		
6.1	Introduction .....	114
6.2	Strontium Isotopic Results .....	114
6.2.1	Host Dolomite .....	114
6.2.2.	Coarse White Dolomite Dolomite .....	116

6.2.3	Saddle Dolomite .....	118
6.2.4	Calcite .....	120
6.3	Comparison to Previous Work .....	120
6.3.1	Host dolomite .....	120
6.3.2	Coarse White Dolomite and Saddle Dolomite .....	122
6.3.3	Calcite .....	123
6.4	Geochemical Implications for Fluid Sources .....	123
<b>CHAPTER 7:</b>	<b>DISCUSSION</b>	
7.1	Introduction .....	142
7.2	Summary of Fluids Involved in the N81 Deposit .....	142
7.2.1	Pre-Ore Fluid .....	142
7.2.2	Ore-Stage Fluid .....	142
7.2.3	Post-Ore Fluid .....	143
7.3	Fluid Origins and Water-Rock Interactions .....	144
7.3.1	Nature of Clastics and Basement Rocks .....	144
7.3.2	Pre-Ore Fluid .....	145
7.3.3	Ore Fluid .....	147
7.3.4	Post-Ore Fluid .....	149
7.4	The Role of Fluid Mixing in Mineralization of the N81 Deposit .....	150
7.5	Source of the Metals .....	151
7.6	Timing of Mineralization and Formation of the Deposits .....	152
<b>CHAPTER 8</b>	<b>CONCLUSIONS</b> .....	156
<b>CHAPTER 9</b>	<b>REFERENCES</b> .....	158

<b>APPENDIX I:</b>	Fluid inclusion microthermometric results .....	164
<b>APPENDIX II:</b>	Fluid inclusion calculated salinities .....	170
<b>APPENDIX III:</b>	Pine Point microthermometric data from previous authors ...	173
<b>APPENDIX IV:</b>	Geochemical data from ion chromatography .....	175
<b>APPENDIX V:</b>	Geochemical data from AAS analysis .....	178
<b>APPENDIX VI:</b>	Geochemical data from ICP-MS analysis .....	180
<b>APPENDIX VII:</b>	Normalized cation concentrations (ICP-MS) .....	183
<b>APPENDIX VIII:</b>	Anion and cation molar ratio results (IC and AAS) .....	186
<b>APPENDIX IX:</b>	Cation molar ratio results (ICP-MS) .....	188
<b>APPENDIX X:</b>	In-situ Sr isotope results (MC-ICP-MS) .....	190
<b>APPENDIX XI:</b>	Average Sr isotope results .....	194
<b>APPENDIX XII:</b>	Sr isotopic data from previous authors (Pine Point and related areas) .....	197

## LIST OF TABLES

Table 4.1	Average microthermometric results .....	75
Table 5.1	Charge balance calculation data .....	93
Table 5.2	Absolute anion concentrations (IC) .....	97
Table 5.3	Absolute cation concentrations (AAS) .....	99
Table 5.4	Absolute cation concentrations (ICP-MS) .....	100
Table 5.5	Seawater evaporation trajectory data .....	101
Table 7.1	Average molar ratios and absolute values .....	143
Table 7.2	Zn/Pb molar ratio data from coarse white dolomite .....	152

## LIST OF FIGURES

Figure 1.1	Middle Devonian geology of Alberta and surrounding areas .....	2
Figure 1.2	Location map of Pine Point .....	3
Figure 1.3	The Pine Point ore region boundary .....	4
Figure 3.1	Mineral phase summaries (including previous authors) .....	29
Figure 3.2	Paragenetic summary from Krebs and MacQueen (1984) .....	31
Figure 3.3	Paragenetic summary from Qing (1991) .....	32
Figure 3.4	Paragenetic summary from this thesis .....	33
Figure 4.1	Hydrohalite melting temperature histogram .....	64
Figure 4.2	Ice melting temperature histogram .....	65
Figure 4.3	Homogenization melting temperature histogram .....	66
Figure 4.4	Formula used for salinity calculations .....	67
Figure 4.5	Homogenization temperatures compared to Na:Ca ratios .....	68
Figure 4.6	Plot of ice melting temperatures versus homogenization temperatures ...	69
Figure 4.7	Plot of salinity versus homogenization temperatures .....	70
Figure 4.8	Plot of hydrohalite melting temperatures versus homogenization temperatures .....	71
Figure 4.9	Plot of hydrohalite melting temperatures versus ice melting temperatures .....	71
Figure 4.10	Plot of salinity and homogenization temperature data from previous authors compared to data from this thesis .....	73
Figure 4.11	Hydrohalite melting and homogenization temperature comparison plot	74
Figure 5.1	Numeric summary of samples analyzed by IC, AAS and ICP-MS analyses .....	90
Figure 5.2	Charge balance equation .....	92
Figure 5.3	Absolute concentration formula .....	93
Figure 5.4	Histogram of molar Cl/Br ratios .....	95

Figure 5.5	Log-log plot of absolute Cl and Br concentrations .....	104
Figure 5.6	Na/Br-Cl/Br plot .....	105
Figure 5.7	Cl/Br-K/Br plot .....	106
Figure 5.8	K/Na-Li/Na plot .....	106
Figure 5.9	Na/Br-Cl/Br plot of data from Telser (1999) .....	107
Figure 5.10	Na/Br-Cl/Br comparison plot of host dolomite and correlative units from Gleeson and Gromek (in press) and Telser (1999) .....	109
Figure 5.11	Na/Br-Cl/Br comparison plot of coarse white dolomite and correlative units from Gleeson and Gromek (in press) and Telser (1999) .....	110
Figure 5.12	Na/Br-Cl/Br comparison plot of sulphides from this study, Gleeson and Gromek (in press) and Telser (1999) .....	111
Figure 5.12	Na/Br-Cl/Br comparison plot of calcites from this study, Gleeson and Gromek (in press) and Telser (1999) .....	112
Figure 6.1	Strontium isotope results from host dolomite .....	115
Figure 6.2	Strontium isotope results from coarse white and saddle dolomite .....	116
Figure 6.3	Strontium isotope results from saddle dolomite growth zones from sample N81-65 0249 .....	117
Figure 6.4	Strontium isotope results from saddle dolomite growth zones from sample N81-98 3205 360' .....	119
Figure 6.5	Strontium isotope results from calcite .....	121
Figure 6.6	Box and whisker plot of $^{87}\text{Sr}/^{86}\text{Sr}$ values from host dolomite, coarse white dolomite and calcite .....	122
Figure 6.7	Plot of strontium ratios from Pine Point ore region from previous authors compared those of this study .....	124
Figure 7.1	$^{87}\text{Sr}$ and metal source diagram for the N81 deposit .....	154

## LIST OF PLATES

Plate 3.0	Host dolomite petrographic photographs .....	36
Plate 3.1	Host dolomite petrographic photographs .....	38
Plate 3.2	Coarse white dolomite petrographic photographs .....	40
Plate 3.3	Coarse white dolomite petrographic photographs .....	42
Plate 3.4	Coarse white dolomite petrographic photographs .....	44
Plate 3.5	Coarse white dolomite petrographic photographs .....	46
Plate 3.6	Sulphide petrographic photographs .....	48
Plate 3.7	Sulphide petrographic photographs .....	50
Plate 3.8	Sulphide petrographic photographs .....	52
Plate 3.9	Sulphide petrographic photographs .....	54
Plate 3.10	Calcite petrographic photographs .....	56
Plate 3.11	Calcite petrographic photographs .....	58
Plate 3.12	Calcite petrographic photographs .....	60
Plate 4.0	Coarse white dolomite-hosted fluid inclusion photographs .....	77
Plate 4.1	Coarse white dolomite-hosted fluid inclusion photographs .....	79
Plate 4.2	Coarse white dolomite-hosted fluid inclusion photographs .....	81
Plate 4.3	Sphalerite-hosted fluid inclusion photographs .....	83
Plate 4.4	Calcite-hosted fluid inclusion photographs .....	85
Plate 4.5	Calcite-hosted fluid inclusion photographs .....	87
Plate 6.0	Photographs of strontium isotope laser tracks in host dolomite .....	126
Plate 6.1	Photographs of strontium isotope laser tracks in coarse white dolomite ...	128
Plate 6.2	Photographs of strontium isotope laser tracks in coarse white dolomite ...	130
Plate 6.3	Photographs of strontium isotope laser tracks in coarse white dolomite ...	132
Plate 6.4	Photographs of strontium isotope laser tracks in coarse white dolomite ...	134

Plate 6.5	Photographs of strontium isotope laser tracks in calcite .....	136
Plate 6.6	Photographs of strontium isotope laser tracks in calcite .....	138
Plate 6.7	Photographs of strontium isotope laser tracks in calcite .....	140

# CHAPTER 1

## GENERAL INTRODUCTION

### 1.1 Scope and Intent

Carbonate-hosted base metal deposits are important worldwide producers of lead and zinc. Many of the exploration models for these deposits are based on early work carried out at the Pine Point ore district in the Northwest Territories. In spite of a multitude of previous studies, the origin and accumulation of the world-class zinc-lead ore at Pine Point is still enigmatic. The source and pathways of the base metal mineralizing fluids and the associated non-mineralizing fluids and the potential role of fluid mixing have yet to be fully resolved in this classic ore region.

Roedder (1968) suggested that the base metals could have been leached from crystalline basement and/or sedimentary rocks, noting that circulation would have had to be deep enough to account for the elevated temperatures deduced from the fluid inclusions of ore-related phases. He indicated that mineralization at Pine Point may have been caused by hot, metal bearing and upward flowing brines mixing with fresh and cold surface waters. Similarly, Krebs and MacQueen (1984) suggested that ore mineralization, and related saddle dolomite formation, may have been caused by ascending hydrothermal solutions. These solutions are proposed to have ascended through pathways in hinge zones of the McDonald Fault (see Figure 1.1) hosted by Precambrian rocks. Alternatively, it has also been suggested that tectonically driven large-scale formation water flow has resulted in several generations of diagenetic cements in the Western Canada Sedimentary Basin and is also responsible for the formation of zinc-lead deposits of the Pine Point ore district (Garven, 1985; Nesbitt and Muehlenbachs, 1994). Qing and Mountjoy (1992) suggest that mineralization was caused by the combination of regional fluid flow of hotter more radiogenic basinal fluids migrating updip (east direction) along the barrier complex mixing with cooler ambient formation waters.

This study was undertaken to provide additional and necessary information on the fluid chemistry of Pine Point, focusing on a concentrated geochemical characterization of the fluids involved in the N81 deposit system. Petrographic analyses of selected drill cores introduce the minerals studied in this thesis and produce a solid background for fluid analyses of various phases in the deposit. Fluid inclusion microthermometric findings yield temperature, salinity and fluid compositional data, which are correlated with bulk geochemical data from ion chromatographic, inductively coupled plasma-mass spectrometry (ICP-MS) and atomic absorption spectrometry (AAS) analysis. Strontium isotopic analysis was carried out on

carbonate phases from the N81 drill cores. This analysis was selected to determine whether radiogenic strontium was introduced into ore forming and non-ore associated fluids from a source other than the Devonian seawater from which the host rocks were formed. The findings of this study aim to give a better understanding and more precise interpretation of the complex fluid activity at Pine Point.

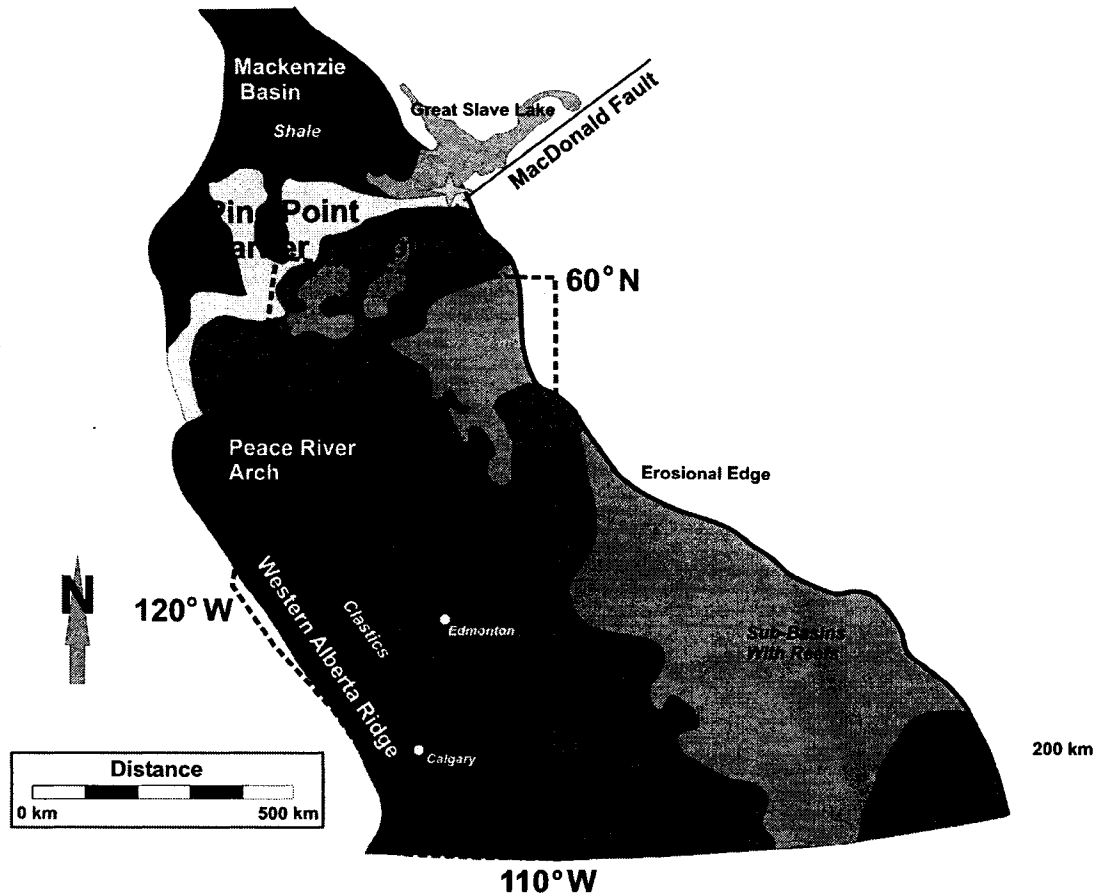


**Figure 1.1** Middle Devonian geology of Alberta and surrounding areas (modified from Qing and Mountjoy, 1994 and Rhodes et al., 1984).

## 1.2 Study Area

The Pine Point zinc-lead ore region is located just south of Great Slave Lake in the Northwest Territories of Canada (Figure 1.2). The region is approximately 180 km south of Yellowknife and 90 km east of Hay River and is contained in Middle Devonian carbonate rocks of the Presqu'île barrier reef complex, also known as the Pine Point barrier complex (Figure 1.1). The barrier extends approximately 400 km to the southwest from Pine Point and

is buried to an approximate 2 km depth in northeastern British Columbia (Qing, 1998). The Pine Point deposit system is located in the eastern portion of the barrier and is approximately 100 km long and 20 km wide. The N81 deposit is located in the southwestern portion of the ore district (Figure 1.3).

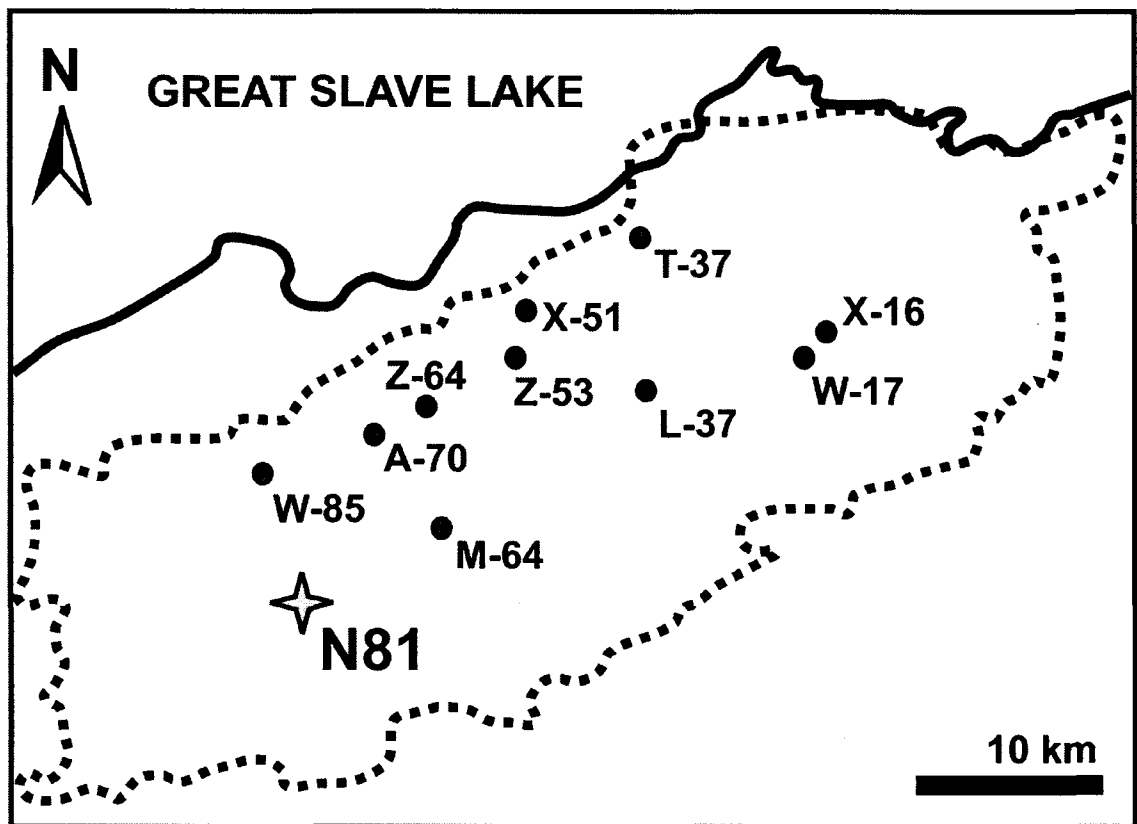
The Pine Point ore region is composed of over 80 Middle Devonian carbonate-hosted deposits (Qing, 1998). These strata-bound base metal deposits contained average grades of 6.7 % zinc and 3.0 % lead and produced over 60 million tons of zinc-lead ore (Rhodes et al., 1984) in over 30 years. Mining commenced in the mid 1960's and ceased in the summer of 1988 by Pine Point Mines Ltd.



Figure 1.2 Location map of Pine Point (modified from Cumming et al., 1990).

### 1.3 Geological Background

The basement rocks in the Pine Point area include granites, granite gneisses and quartzites (Norris, 1965). Over 100m of Early Paleozoic clastic and evaporitic rocks unconformably overlie the basement rocks. The Early Paleozoic rocks are in turn unconformably overlain by the Middle Devonian Chinchaga Formation. The Chinchaga Formation is comprised of evaporites, limestones and dolomites, which lie beneath the open-marine platform carbonates of the Early Givetian Keg River Formation. The Presqu'île barrier reef complex, which hosts the ore of the Pine Point district, was developed in the Middle Givetian following the deposition of the Keg River Formation (Krebs and Macqueen, 1984).



**Figure 1.3** The Pine Point ore region boundary (dashed line) including some ore body locations (modified from Qing, 1998).

The development of the southwest-northeast trending Presqu'île barrier reef complex (Figure 1.1) was partly constrained by the reactivation of the MacDonald Fault system causing differential subsidence along the associated faults. This differential subsidence allowed for the deposition of various lithologies of variable thicknesses to develop in between the North, Main

and South Hinges of the barrier complex (Krebs and MacQueen, 1984). Hinge zones of the MacDonald Fault have been suggested as possible pathways for ascending hydrothermal fluids from Precambrian rocks (Krebs and MacQueen, 1984), which are proposed to be a potential base metal conduit system or at least a source of the metals.

A regional regression occurred at some point between Middle and Upper Givetian times. Subsequent uplift (up to 30m above sea-level) sub-aerially exposed a portion of the Pine Point barrier complex resulting in the development of a karst surface known as the Watt Mountain Disconformity (Krebs and MacQueen, 1984). The Watt Mountain Formation disconformably overlies the karsted surface. Brecciated zones beneath the Watt Mountain Formation have been interpreted to be due to sinkhole collapse during the sub-aerial exposure (Kyle, 1981). A tilting event occurred after the Mississippian causing a gentle southwest dip in the Paleozoic strata. The underlying strata are covered by Pleistocene sediments of till, clay, sand and gravel (Krebs and MacQueen, 1984).

The Pine Point deposits are epigenetic, however, the timing of the mineralization is contentious. Proposed times include, but are not limited to, Carboniferous (Late Pennsylvanian) (Cumming et al., 1990), Post-Cretaceous (Garven, 1985) and Late Cretaceous, Early Tertiary (Qing, 1991) and Devonian-Mississippian (Nelson et al., 2002).

#### **1.4 Previous Studies**

The majority of previous studies on the Pine Point district have included stratigraphic, mineralogic and isotopic work (e.g., Roedder, 1968; Kyle, 1977; Skall, 1975; Kyle, 1981; Medford et al., 1983; Krebs and MacQueen, 1984; Rhodes et al., 1984; Garven, 1985; Mountjoy et al., 1992; Qing, 1991; Qing and Mountjoy, 1992; Nesbitt and Muehlenbachs, 1994; among others). Emphasis has been placed on either the ore or the host-rock itself depending on the authors and their area of expertise. The bulk of published studies focus on field and petrogenetic relationships, light stable isotopes ( $\delta^{18}\text{O}$ ,  $\delta^{13}\text{C}$ ,  $\delta\text{D}$ ,  $\delta^{34}\text{S}$ ) and strontium isotopes (Medford et al., 1983; Qing, 1991; Qing and Mountjoy, 1992; Mountjoy et al., 1992; Nesbitt and Muehlenbachs, 1994; among others). Only a small number of fluid inclusion studies have been carried out on gangue and ore minerals in the deposits and/or on carbonate minerals on a regional scale (Roedder, 1968; Kyle, 1977; Qing, 1991; Nesbitt and Muehlenbachs, 1994; Telser, 1999; Turner, 2003).

#### *1.4.1 Petrographic Analysis – Paragenetic Sequence Development*

Several studies have been carried out on the paragenesis of the Pine Point district (Kyle, 1981; Krebs and MacQueen, 1984; Qing, 1991; among others) however, a single paragenetic sequence has yet to be wholly accepted by the geologic community. This is primarily due to the difficulty in resolving the various stages of diagenesis, multiple and often over-lapping phases of dolomitization and ore mineralization that have occurred throughout the formation of the deposits. In general, there are pre-, syn- and post-ore dolomitization events, including the development of ore-related coarse white dolomite, which often occurs in the saddle-like textural variety (often termed saddle dolomite). These phases are often post-dated by calcite, fluorite, anhydrite, elemental sulphur and bitumen (Kyle, 1981; Krebs and MacQueen, 1984; Qing, 1991).

#### *1.4.2 Microthermometric Analysis*

A small number of fluid inclusion studies have been carried out on this world-class deposit. Most of the studies were carried out on samples that were not well constrained paragenetically and/or a full set of microthermometric data was not collected (e.g. concentration on homogenization ( $T_h$ ) and ice-melting temperatures ( $T_{m,ice}$ )). Although Roedder (1968) mentioned and tentatively identified hydrohalite on the fluid inclusion freezing cycle, only Turner (2003) recorded hydrohalite melting temperatures, thereby allowing for the Ca:Na ratios of the mineralizing fluids to be calculated. The findings of Turner (2003) indicate that the fluids had exceptionally high  $Ca^{2+}$  contents, which differ remarkably from some of the extant formation waters in the basin today.

The first microthermometric work on Pine Point minerals, from unspecified locations, produced a small set of homogenization and ice melting temperatures (Roedder, 1968). Although, the presence of hydrohalite was mentioned, no hydrohalite melting temperatures were recorded, likely due to the difficulty of finding suitable fluid inclusions large enough to measure the phase change. However, homogenization and/or ice melting temperature data were collected from fluid inclusions in sphalerite, dolomite and calcite. Kyle (1977) published homogenization and salinity data from sphalerite and celestite. Limited microthermometric work on assumed primary inclusions in coarse crystalline and saddle dolomite from the Pine Point area is presented in Qing (1991). The data indicate that dolomitization occurred at temperatures that exceeded those allowed by maximum burial. Microthermometry was performed on saddle dolomite and calcite. Although Qing (1991) infers a multicomponent salt

system ( $\text{NaCl} \pm \text{CaCl}_2 \pm \text{KCl} \pm \text{MgCl}_2$ ) from a small number of eutectic temperature measurements, no hydrohalite melting temperatures were recorded. The previously mentioned study did not document the relationships between the paragenesis and the fluid inclusions, thereby making the data difficult to interpret. On a more regional scale, Qing and Mountjoy (1992) published microthermometric data from saddle dolomite-hosted fluid inclusions spanning the length of the Presqu'ile Barrier (Pine Point Barrier Complex). Their study produced homogenization and salinity data that indicated saddle dolomite was precipitated from hot saline brines. This is in agreement with the findings of a recent study by Al-Aasm et al. (2000) on saddle dolomites in stratigraphically related formations in northwestern Alberta. Their study not only proposed that the saddle dolomite was precipitated by hot saline brines but inferred that it was a result of structurally controlled hydrothermal fluid flow. Turner (2003) produced microthermometric data from sphalerite, dolomite, saddle dolomite and calcite, which included hydrohalite melting, homogenization and ice melting temperatures.

#### *1.4.3 Bulk Geochemical Analysis*

Only a few studies on Pine Point have incorporated bulk fluid geochemical analyses. Telser (1999) and Gleeson & Gromek (in press) suggested that most of the mineralizing fluids at Pine Point originated as highly evaporated seawater. Some samples from these studies do however stray from the seawater evaporation curve. Most of the samples analyzed in these studies did not have correlated microthermometric data and it is not known if multiple generations of inclusions were analyzed.

#### *1.4.4 Strontium Isotopic Analysis*

Previous strontium isotopic work on Pine Point carbonates has been compared and/or related to that of Middle Devonian seawater. Carbonate minerals that precipitate from seawater will have the same  $^{87}\text{Sr}/^{86}\text{Sr}$  as the fluid from which they formed (Veizer and Compston, 1974; Burke et al., 1982) unless they have been infiltrated by other sources of strontium (e.g. radiogenic variety). Carbonates formed from Middle Devonian seawater should have an approximate  $^{87}\text{Sr}/^{86}\text{Sr}$  value of 0.7080 (Burke et al., 1982).

Strontium isotopic analyses have been documented on host dolomites, dolomites associated with ore mineralization and post-ore calcites at Pine Point (Maxwell, 1976; Medford et al., 1983; Mountjoy et al., 1992 and Qing, 1998; among others). Most studies suggest that the host and ore-related dolomites were formed from Middle Devonian seawater and late-stage

calcites have had a radiogenic strontium input (see Chapter 6). Host dolomite equivalent phases were analyzed by Medford et al. (1983), Mountjoy et al. (1992), Qing (1998), among others. The composition of coarse white dolomite equivalent phases were reported in Maxwell (1976), Medford et al. (1983), Mountjoy et al. (1992) and Qing (1998). Calcite  $^{87}\text{Sr}/^{86}\text{Sr}$  values were obtained by Maxwell (1976), Medford et al. (1983) and Mountjoy et al. (1992). This thesis expands the  $^{87}\text{Sr}/^{86}\text{Sr}$  database at Pine Point by 112 data points including  $^{87}\text{Sr}/^{86}\text{Sr}$  values from host, coarse white dolomite (including saddle-textured variety) and calcite phases.

### 1.5 Objectives

The primary objective of this thesis is to characterize the mineralizing and non-mineralizing fluids involved at Pine Point with particular focus on the N81 deposit. The specific scientific objectives are:

- (1) to construct a paragenetic sequence of major pre-, syn- and post-ore phases, via petrographic analyses, from fifteen well-constrained drill core samples of the N81 Pine Point deposit;
- (2) to integrate the petrography with a detailed fluid inclusion microthermometric study of the syn- and post-ore phases in the deposit;
- (3) to conduct a petrographically-based bulk fluid chemistry study on suitable samples to ascertain the origin and evolution of the mineralizing fluids;
- (4) to determine strontium isotopic compositions of the mineralizing and non-mineralizing associated carbonates;
- (5) to constrain whether mixing of fluids took place in the deposit and whether it played a role in the ore mineralization (using the above mentioned analytical techniques), and
- (6) to compare the data with previous geochemical analyses.

Chapter 2 includes the methodology of all the analyses undertaken in this thesis. Chapter 3 provides a detailed petrographic analysis of all drill core samples that were geochemically analysed, defines the major mineral phases present and produces a paragenetic sequence of the N81 deposit at Pine Point. Chapter 4 delineates the fluid chemistry of ore, ore-related and non-ore related phases in the N81 deposit using temperature, salinity and fluid composition data from microthermometric analyses. Chapter 5 includes the bulk geochemical characterization of mineralizing and non-mineralizing fluids. Anion and cation concentrations are presented and interpreted for the fluids. Chapter 6 defines the strontium isotopic composition of pre-, syn-

and post-ore carbonate phases in the ore deposit. Chapter 7 includes a discussion of all the observations and interpretations from the analyses of this thesis and generates a geochemical characterization of the mineralizing and non-mineralizing fluids involved in the Pine Point N81 deposit.

The determination of the fluid compositions of mineralizing and non-mineralizing fluids in the N81 deposit at Pine Point (e.g. temperatures, salinities, fluid compositions) using fluid inclusion microthermometry, bulk geochemical analysis and strontium isotopic analysis may be potentially useful for future work regarding fluids involved in Mississippi Valley-type (MVT) lead-zinc ore deposits.

## CHAPTER 2

### METHODOLOGY

#### 2.1 Introduction

Drill core was sampled from Pine Point deposit N81, housed at the University of Alberta. Initially a detailed petrographic study of all the samples was carried out to provide a framework for the subsequent geochemical analyses. Fluid inclusion studies (microthermometry and bulk crush-leach analyses) were combined with strontium isotopic analyses to characterize the fluids involved in the mineralization processes. These three geochemical approaches were used to understand the origin of, and processes acting upon, the mineralizing and non-mineralizing fluids involved at Pine Point deposit N81.

#### 2.2 Methodology of Petrographic Study

A petrographic study was carried out using a Zeiss Axioskop 40 microscope equipped with a Zeiss AxioCam MRc digital photo-microscopic system. Petrography was performed on thick mounted fluid inclusion wafers and standard thin sections. Samples were selected to build a paragenetic model of the multiple carbonate and sulphide phases, to determine the nature of the fluid inclusions in their host minerals and to select subsequent samples for strontium isotope work.

#### 2.3 Methodology of Fluid Chemistry Analyses

##### 2.3.1 Microthermometric Analysis

Fluid inclusion microthermometric analyses were conducted on a Linkam THMSG600 heating-freezing stage mounted on an Olympus BX50 microscope equipped with a color video camera and video copy processor. Calibration of the stage was carried out using SynFline synthetic fluid inclusion standards. The standards used included the CO<sub>2</sub> melting point (-56.6°C), H<sub>2</sub>O-NaCl eutectic (-21.2°C), pure water melting (0.0°C) and the alpha/beta quartz transition (573°C). The shape and degree of fill of all inclusions was recorded before any heating/freezing measurements as well as any subsequent changes in appearance of the inclusions. Sub-zero and low temperature measurements (e.g., first melting (T<sub>f</sub>), hydrohalite melting (T<sub>m<sub>HH</sub></sub>) and ice melting (T<sub>m<sub>ice</sub></sub>)) have an accuracy of ±1°C, ±1°C and ±0.3°C, respectively, and high temperature measurements (e.g., homogenization temperature (T<sub>h</sub>)) an accuracy of ±1°C. Most inclusions were approximately 5µm or smaller in size, therefore, sub-zero measurements were difficult and at times impossible to ascertain.

Heating measurements for calcite and dolomite hosted fluid inclusions were made prior to freezing measurements. The heating-freezing cycle has a tendency to allow fluid inclusions in soft minerals, such as calcite and dolomite, to stretch or leak (caused during cooling), which can alter homogenization temperature values. Unless differential leakage occurs this should not effect the composition of the inclusions. Homogenization temperature was measured first to minimize such effects. Degree of fill was carefully observed at room temperature before and after temperature of homogenization was obtained. Inclusions with a variable degree of fill or necked appearance were avoided.

### 2.3.2 Bulk Geochemistry Analysis

Carbonate and sulphide mineral phases from 15 drill cores of the N81 deposit and one hand sample were selected based on paragenetic relevance and availability and cut using a rock saw. The samples were crushed using a cast iron mortar and pestle and sieved to produce a 1 to 1.7mm size fraction. These separates were hand picked using a binocular microscope to produce approximately 3 grams of pure mineral separate. A pure mineral separate could not be picked for a small number of these samples, the carbonates and sulphides contained minute amounts of sulphides (e.g. sphalerite and galena). In this case information on the contaminating phases was recorded (see Section 5.4.1). Subsequent to crushing and sieving the mineral separate was washed five times in 20.0MΩcm water on a hot plate heated to 75 °C and, lastly, dried in an oven. The mineral separate was powdered using an agate mortar and pestle under a laminar flow hood in a controlled environment. Approximately 1.5 grams of powdered sample was placed in an unreactive sterlin pot and shaken with 3mL of 20.0 MΩcm water for 1 minute. The mixture was allowed to settle and the supernatant liquid was filtered through a 0.2µm pore size 13mm diameter Whatman nylon media syringe filter. Chloride, Br<sup>-</sup>, F<sup>-</sup> and SO<sub>4</sub><sup>2-</sup> were analyzed using a Dionex DX600 ion chromatograph (IC) at the University of Alberta. Detection limits for the IC analysis of Cl<sup>-</sup>, Br<sup>-</sup> and F<sup>-</sup> are 0.02 ppm and 0.05 ppm for SO<sub>4</sub><sup>2-</sup>. Bromide and F<sup>-</sup> were often below the detection limits of the ion chromatograph (see Appendix IV). Due to the small amount of leachate produced it was not possible to routinely run duplicates, however, two mineral separates from the same sphalerite phase from drill core N81-98 3205 355' were analyzed by ion chromatography. The ion chromatographic results are shown in Appendix IV (see sample N81-98 3205 355'SPH (DUP)) and are very similar (Cl (ppm) = 6.27 & 6.49 and Br (ppm) = 0.05 and 0.06), which confirms that two separate crush leachates from the same sample phase would likely yield similar concentrations. Replicate

analyses of known standards showed that the precision and accuracy of the ion chromatograph was within 5% for all anions (S. Gleeson pers. comm.)

The leachate used for the IC analysis was also used for major cation analysis. The leachates were analyzed for Na, K and Li cations using an Atomic Absorption Spectrometer Varian 880 (AAS) at the University of Alberta. The calibration range was estimated from Cl<sup>-</sup> values of the ion chromatographic analysis. When necessary, samples were diluted to reach the Na, K and Li values required for AAS analyses (i.e., Na < 5ppm, K < 1ppm and Li < 1ppm). The diluted cation values were then back calculated to their undiluted values as shown in Appendix V. Detection limits for the AAS analysis of Na, K and Li are 0.0002 ppm, 0.003 ppm and 0.002 ppm, respectively.

The remainder of the crushed pure mineral separate (approximately 1.5 grams) was combined with 10mL of acidified lanthanum-doped solution (200 ppm) and shaken vigorously for one minute. The solution was centrifuged at 4000 rpm for ten minutes. The supernatant leachate was pipetted out from the residual solids and filtered through a 0.2 µm pore size 13mm diameter Whatman nylon media syringe filter into sterile unreactive bottles. Norwest labs in Edmonton analyzed the La-doped leachate by Inductively Coupled Plasma-Mass Spectrometry (ICP-MS) for major (Na, K, Mg, Mn, Fe and Ca) and minor/trace (S, Ba, B, Cd, Co, Pb, Li, Ni, Sr and Zn) elements.

The AAS method had lower detection limits for Na, K and Li (0.0002, 0.003 and 0.002 ppm, respectively) in comparison to the ICP-MS analyses (0.4, 0.4 and 0.01 ppm, respectively). All Mg and Mn values in the leachates were above the detection limits of the ICP-MS analyses (0.1 and 0.005 ppm, respectively). Magnesium levels, however, are more likely to be derived from the carbonate host phases than to be truly from the leachate. Iron was often below the detection limit of 0.01 ppm. Commonly, Ca was above the detection limit (0.2 ppm) but not reported when the host mineral was a calcite or dolomite. Similarly, sphalerite and galena leachates yielded high values of S, Zn and Pb and are assumed to be contaminated by the host minerals. Sulphur was detected in most samples and had a detection limit of 0.3 ppm. Barium, Sr and Zn all had the same detection limit of 0.001 ppm. Cobalt and Pb share the same detection limit of 0.0001 ppm. Boron, Ni and Cd have detection limits of 0.002, 0.0005 and 0.00001 ppm, respectively.

### 2.3.3 Strontium Isotopic Analysis

In-situ Sr isotope analyses were determined using a Nu Plasma (MC-ICP-MS) instrument coupled to a 213 nm Nd:YAG laser system (New Wave Research) housed at the University of Alberta with an analytical protocol similar to that described by Schmidberger et al. (2003). Thin and thick sections containing carbonate (calcite and dolomite) phases were ablated in spot and mostly raster (line) mode using a spot size of 160 $\mu$ m, a repetition rate of 10 Hz and an approximate 3 mJ laser output. The laser ablation runs varied in time, largely dependant on the amount of time taken to ablate through the calcite and dolomite phases analyzed. Reproducibility and accuracy was verified using a modern day coral (Indian Ocean) internal standard, which yielded an average  $^{87}\text{Sr}/^{86}\text{Sr}$  value of  $0.70910 \pm 0.00005$  ( $2\sigma$ ,  $n>50$ ; Schmidberger et al. 2003).

Previous strontium isotopic studies used bulk crushed samples. This method may have resulted in inaccurate results due to the analyses of multiple phases at once (e.g. thin calcite overgrowths on coarse white dolomite crystals). The in-situ Sr isotopic analytical technique of this thesis produced a total of 112  $^{87}\text{Sr}/^{86}\text{Sr}$  values from targeted areas in carbonate phases from nine drill core samples. Strontium values were obtained directly from thin and thick sections (up to  $\sim 100\mu$ m). Calcite and various phases of dolomite were analyzed with special attention given to specific zones in saddle-textured coarse white dolomites including rims and cores that had microthermometry performed on them.

## CHAPTER 3

### PETROGRAPHY

#### 3.1 Introduction

The objectives of the petrographic study were to: 1) identify the major mineral phases in drill core samples from N81 deposit at Pine Point; 2) establish a paragenetic relationship between the major phases; and 3) establish the fluid inclusion population types and assess the number of inclusions of the appropriate phases. These objectives were achieved by petrographic analysis carried out on fifteen drill core samples. Standard thin sections and also thick sections (used for strontium laser isotopic analyses) were described and photographed. The results from this chapter provide the framework necessary for the interpretation of the microthermometric, bulk geochemical and strontium isotope studies (Chapters 4, 5 and 6, respectively). Individual drill core samples are summarized in the following text and fluid inclusion petrographic descriptions are given for each sample.

#### 3.2 Fluid Inclusions

##### 3.2.1 Background Information

Fluid inclusions have provided insight into the nature of fluids involved in a multitude of geological settings. Analysis of fluid inclusions is the only way to directly sample ancient fluids (Roedder, 1984). Inclusions that have been trapped during the growth of a mineral are a direct representation of the precipitating fluid. As a mineral is precipitating from a fluid, irregularities or imperfections in the growing minerals (e.g. on the surface) often allow small amounts of the precipitating fluid to be trapped, and in effect, sealed by the growth (Bodnar, 2003), resulting in the formation of fluid inclusion assemblages (Goldstein and Reynolds, 1994). Assemblages are composed of groups of inclusions that occur together in clusters, which have a similar appearance and/or growing in the same fashion e.g. along growth bands or in healed fractures (Goldstein and Reynolds, 1994). Analyses of these inclusions by microthermometry confirm these groups are assemblages that yield similar microthermometric data. The specific information gained from fluid inclusion microthermometry is further discussed in Chapter 4. Since fluid inclusions are samples of crustal fluids trapped in rocks, they can be composed of melt, aqueous, carbonic or hydrocarbon liquids, volatile phases, supercritical fluids and/or solid daughter phases. The fluid inclusions in this study are dominantly aqueous liquid and liquid-vapour types. Characterizing the types, quantities, and

appearance of fluid inclusions within a host mineral gives an abundant amount of information and provides a necessary background for geochemical analyses such as microthermometry and the bulk geochemical work done in this thesis (see Chapters 4 and 5, respectively). This study used fluid inclusions to characterize both mineralizing and non-mineralizing fluids in the N81 deposit at Pine Point.

### *3.2.2 Trapping and Characterization*

A temporal classification of fluid inclusions is an integral part of fluid inclusion studies. One of the basic objectives of the petrographic study was to determine the timing of fluid inclusion entrapment relative to the age of the host mineral. Inclusions are characterized as primary, secondary or pseudosecondary types (Roedder, 1984). Primary fluid inclusions, as described by Roedder (1984), are single inclusions (or small 3-dimensional groups) in an otherwise inclusion-poor crystal, that may contain daughter crystals, may occur parallel to a crystal face and close to its centre (e.g. along growth zones) and may have an equant or negative crystal shape. Secondary inclusions are inclusions formed after a mineral has precipitated from a fluid. These can occur when fractures are infiltrated with a later fluid and sealed, thereby, trapping fluid inclusions that do not represent the original fluid. These often occur in trails that can cut across grain boundaries. Pseudosecondary inclusions are visually similar to secondary inclusions but are formed during the crystallization of the mineral. They can be distinguished from secondary inclusions because the inclusion trails end at growth zones or crystal boundaries. Sometimes it is not possible to confidently classify inclusions as primary, secondary or pseudosecondary. In such cases the inclusions are classified as indeterminate (Goldstein, 2003). The nature of the mineral phases encountered in this study, and the relationship of these phases to the fluid inclusion populations, is the focus of the remainder of this chapter.

## **3.3 Petrographic and Fluid Inclusion Sample Descriptions**

### *3.3.1 N81-65 0249*

#### Petrographic Discussion

This sample contained four main phases: host dolomite, coarse white dolomite, calcite and native sulphur. The host dolomite varied from light greyish brown to medium brown in colour and was composed primarily of blocky interlocking crystals but rare voids between crystal boundaries existed (Plate 3.0-A & B). No original limestone textures were preserved in

this sample. The next phase to form in the sample was white to very pale grey coarse white dolomite (CWD), which occasionally displayed excellent saddle-like textures (Plate 6.1-C to H). Commonly, the boundary between the host dolomite and coarse white dolomite appeared transitional but in some areas the host dolomite contained minor fractures that were filled by the coarse white dolomite. Some host dolomite crystals appeared to have a feature that looked like a replacement by coarse white dolomite. The medium brown original colour of the host dolomite was muted to a light greyish brown colour but the original crystal habit of the host dolomite was preserved (Plate 6.0-A & B). The coarse white dolomite had a larger average crystal size (average ~700  $\mu\text{m}$ ) and saddle-like textures were frequently developed when the coarse white dolomite had grown into void space. The final phases to precipitate in this sample were late-stage calcite and native sulphur, which filled or lined vugs in the drill core. The calcite was clear and colourless and occurred with clear to bright yellow native sulphur (Plate 3.10-A).

#### Fluid Inclusion Petrography

The fluid inclusions in host dolomite were abundant, generally sub-rounded in shape and much smaller than 5  $\mu\text{m}$  in length. The larger inclusions were dominantly two-phase (L-V) and had an average degree of fill (DOF) of 0.90. The high fluid inclusion population density often obscured thin and especially thick section clarity making microthermometric analyses impossible (Plate 3.0-A & B). Most of the inclusions in this phase appeared to be primary and were restricted to defined growth zones. The coarse white dolomite was host to abundant, small (generally <5  $\mu\text{m}$ ), aqueous inclusions that were dominantly primary (Plate 3.2-A & B). The inclusions were sub-rounded to elongate in shape and tended to have their long axis parallel to growth zone lineations. Larger, discernable inclusions contained two phases (L-V) with an average degree of fill of approximately 0.85. Some larger inclusions had small tails that were indicative of leaking and these were avoided during microthermometry. A very small number of secondary inclusion assemblages did exist and were found associated with fractures. Coarse white dolomite that displayed saddle-like textures had fluid inclusions that clearly followed the growth zones of their host.

Microthermometric analysis of saddle dolomite rims was easier than that of their cores or non-saddle textured coarse white dolomite crystals since there was a much smaller number of fluid inclusions and the optical transmissivity of the sample was high (Plate 3.2-B). Calcite-hosted inclusions were much less abundant than those of coarse white dolomite (Plate 3.10-B & C). The rare inclusions could be classified as mostly primary but secondary inclusions did

exist, albeit infrequently. In calcite, the two-phase (L-V) primary inclusions were often larger ( $>5\ \mu\text{m}$ ), sub-rounded to elongate (pseudo-rectangular), isolated and randomly spaced in the crystals and had an average DOF of 0.95. Calcite-hosted secondary fluid inclusions frequently occurred along healed fractures in trail assemblages. One small area of calcite contained an uncharacteristically high percentage of liquid-rich (L-V; DOF=0.95) primary inclusions (Plate 3.10-D).

### 3.3.2 N81-68A 2969 375'

#### Petrographic Discussion

Three mineral phases existed in this sample: sphalerite, galena and calcite. Sphalerite colour ranged from honey yellow to reddish brown and often displayed colloform textures (Plate 3.6-B). Galena was dark grey and metallic. The galena appeared largely cogenetic with sphalerite but occasionally showed both pre- and post-sphalerite mineralization relationships (e.g. pieces of galena both within and in between colloform bands). Both galena and sphalerite had late fractures, which were infilled by calcite (Plate 3.6-A & B). The last phase to form in the sample was clear and colourless to cloudy white (due to the abundance of inclusions) calcite. Calcite generally existed as interlocking blocky crystals (average 1mm size) with good twinning visible and occasionally contained broken pieces of sulphides (e.g. sphalerite crystals).

#### Fluid Inclusion Petrography

Sphalerite in sample N81-68A 2969 375' had numerous tiny, primary,  $<<5\ \mu\text{m}$  inclusions (Plate 3.6-C) and many inclusions of a similar size located along healed fractures as secondary trails. Their small size made them impossible to describe further.

Primary (L-V) calcite-hosted fluid inclusion assemblages and isolated fluid inclusions are shown in Plate 3.10-F. Primary inclusions in calcite were generally irregularly shaped and occasionally showed some evidence of leaking (e.g. small tails are present). Many large ( $>20\ \mu\text{m}$ ) inclusions were opened by the thin section making process. Calcite contained abundant, smaller ( $<5\ \mu\text{m}$ ), subhedral to elongate shaped, secondary inclusions in trails along healed fractures often crosscutting crystals (Plate 3.10-E).

### 3.3.3 N81-69 2754 195'

#### Petrographic Discussion

Host dolomite, coarse white dolomite, sphalerite and galena were present in this sample. The host dolomite was fine grained (with an average grain size of  $75\ \mu\text{m}$ ) and medium

to dark greyish brown (Plate 3.0-C to E). No original limestone textures were present in this sample. Sphalerite blebs within the host dolomite were common and appeared post-host dolomite and were replacive in nature. There was abundant coarse white dolomite in the sample that replaced the host dolomite, suggesting it was a younger phase. Coarse white dolomite was white in colour and occurred as open space fillings often with saddle-textures present in between growths of galena and sphalerite crystals (Plate 3.2-C to E). Sphalerite occurred as both crystalline and colloform textures and ranged in colour from honey to reddish brown. Galena was dark grey and metallic and occurred as large anhedral to subhedral crystals often connecting to each other by neck-like structures (Plate 3.2-C). The sphalerite and galena had clearly precipitated post-host dolomite and were cogenetic with coarse white dolomite.

#### Fluid Inclusion Petrography

Abundant, primary, small ( $\ll 5\mu\text{m}$ ), fluid inclusions were present in the host dolomite but were too small to be described in more detail. The poor optical clarity of this phase was the result of the mineral colour and the density of fluid inclusions and made microthermometry impossible (Plate 3.0-D). Coarse white dolomite contained abundant, small ( $<5\mu\text{m}$ ), subrounded to elongate shaped, almost entirely primary, generally two-phase (L-V) inclusions (Plate 3.2-D & E). Secondary fluid inclusion trails existed very infrequently in this phase. There were fluid inclusions present in the sphalerite in this sample but they were very small ( $\ll 5\mu\text{m}$ ). Most of the sphalerite-hosted inclusions were primary and were located along growth zones of optically clear light coloured sphalerite. Primary inclusions that were larger ( $> 5\mu\text{m}$ ) were two-phase (L-V) and had an average degree of fill of approximately 0.8. Secondary inclusions occurred in trails and healed fractures cross cutting growth zones and interlocking crystals.

#### 3.3.4 *N81-69 2758 217'*

##### Petrographic Discussion

Host dolomite, sphalerite, galena and calcite were present in this sample. The host dolomite was fine grained (average size is  $50\mu\text{m}$ ) and light to dark grey coloured (Plate 3.0-F to H; Plate 3.1-A). It occurred as irregular interlocking blocks that occasionally appeared to have been brecciated, fractured and cemented by sphalerite. Pseudo-layers of light and dark host dolomite crystals existed in a small portion of the thin section (Plate 3.0-G). Clasts of host dolomite acted as nuclei for crystalline sphalerite and occasional galena growth. Sphalerite was dominantly very pale honey brown in colour but did appear to be reddish brown in places. The

two colours appeared in alternating bands but a true colloform texture was not observed. Commonly, sphalerite occurred as irregular or subrounded blebs growing on the host dolomite or as irregular interlocking grains in fractures or vugs. Galena was dark grey and metallic and grew anhedrally to subhedrally and also in fracture fills along with sphalerite and later-stage calcite. In this sample, calcite was clear and colourless and occurred as infillings between galena, sphalerite and clasts of the brecciated host dolomite, clearly demonstrating that it was the last phase to precipitate.

#### Fluid Inclusion Petrography

There were abundant inclusions present in the host dolomite and sphalerite but they were of very small size ( $\ll 5 \mu\text{m}$ ) as shown in Plate 3.0-H and could not be discriminated any further. The late calcite contained a smaller amount of inclusions compared to the inclusion density of host dolomite and sphalerite. The calcite-hosted inclusions were generally larger, subrounded to irregularly shaped, mainly primary and occasionally displayed evidence of leaking such as tails and increased degree of fill ratios. Secondary fluid inclusions ( $< 5 \mu\text{m}$ ) occurred in trails along healed fractures.

### 3.3.5 *N81-69 2764 235'*

#### Petrographic Discussion

This sample contained four phases: host dolomite, sphalerite, galena, and calcite. Traces to small amounts of light to medium brown host dolomite were found in this sample and no original limestone textures were present in this phase. The sample was dominated by well-developed colloform sphalerite (Plate 3.7-A & B) and coarse galena. Galena acted as a nucleus for some of the colloform sphalerite and also was present as an infill between colloform growth ends, suggesting that galena was precipitated both before and after sphalerite. The calcite precipitated in voids in between sphalerite and galena growths and as such was considered late-stage.

#### Fluid Inclusion Petrography

Abundant, small, primary and secondary fluid inclusions were visible in the sphalerite phase. The number of tiny inclusions ( $\ll 5 \mu\text{m}$ ) often destroyed optical clarity in the sample and made microthermometric analyses very difficult. Some sphalerite colloform textures had inclusion-poor rims and inclusion-rich cores with a distinct boundary between the two (Plate 3.7-C). Small ( $< 5 \mu\text{m}$ ), primary, calcite-hosted fluid inclusions were common along growth zones.

### 3.3.6 N81-69 2766 240'

#### Petrographic Discussion

This sample was dominated by fine-grained light brown host dolomite (Plate 3.1-B & C), which showed no evidence of any original limestone textures. A lesser amount of coarse white dolomite was present as pore infillings. Pale brown to reddish brown coloured sphalerite was also found in the sample and occurred as irregular to sub-rounded blebs in both the host and coarse white dolomite. Minor amounts of crystalline sphalerite were found in the sample. A small amount of clear and colourless calcite was present with native sulphur. Both of these phases precipitated last in this sample, as both filled the remaining void space.

#### Fluid Inclusion Petrography

Primary fluid inclusions in host dolomite were very small ( $\ll 5\mu\text{m}$ ) and could not be measured in the microthermometric study (Chapter 4). The coarse white dolomite was dominated by small (generally  $< 5\mu\text{m}$  in size) primary, irregular to subrounded shaped, inclusions (Plate 3.2-F). Larger, discernable, inclusions were generally two-phase (L-V). Sphalerite hosted inclusions (largely mono-phase) were rare but when present were found in the crystalline variety of sphalerite. Primary, mono- and two-phase (L-V) inclusions were present in the clear calcite (Plate 3.11-A). Secondary calcite-hosted inclusions ( $< 5\mu\text{m}$ ) occurred in trails interpreted to be healed fractures (Plate 3.10-H).

### 3.3.7 N81-75 3358 260'

#### Petrographic Discussion

In this sample, host dolomite was rare, had a pale brown colour and had no evidence of any precursor limestone textures. This sample was dominated by coarse white dolomite, which generally occurred as irregularly shaped masses to blocky well-defined equant crystals but occasionally developed saddle-like morphologies exhibiting sweeping and undulatory extinction in crossed polarized light (Plate 3.3-A to D). Sub-rounded voids (with an average size of 1.5mm) in coarse white dolomite were common and were often lined with bitumen and filled by clear and colourless calcite (Plate 3.3-E & F). The bitumen often stained the surrounding coarse white dolomite. This was in agreement with the "pyrobitumen" found on the walls of many vugs and consequent staining of host minerals as noted by Roedder (1968). Calcite in this sample often displayed excellent twinning and also occurred in non-bitumen stained voids within the coarse white dolomite.

### Fluid Inclusion Petrography

The host dolomite contained abundant very small ( $\ll 5\mu\text{m}$ ) unworkable primary inclusions. Coarse white dolomite was dominated by small ( $<5\mu\text{m}$ ), irregular to subrounded, generally two-phase (L-V), primary inclusions that often followed growth zones (Plate 3.3-A to C). Calcite contained numerous, isolated, very small ( $\ll 5\mu\text{m}$ ), subrounded, primary fluid inclusions but their frequency was much less than those hosted by coarse white dolomite. Secondary, small inclusions in calcite occurred along fractures and as cross cutting trails (Plate 3.11-C). Larger, calcite-hosted, inclusions occasionally showed evidence of leaking including the formation of tails on some of the inclusions and variable degree of fill in single inclusion assemblages.

#### 3.3.8 N81-75 3386 322'

### Petrographic Discussion

This sample contained three phases, namely coarse white dolomite, bitumen and calcite. Coarse white dolomite was white to pale grey in colour and dominated this sample. It grew in interlocking blocky and saddle-like textures (Plate 3.3-G & H). Very fine ( $\sim 1\text{ mm}$ ) fractures (almost appearing stylolitic) cut across the interconnected coarse white dolomite crystals. These features consisted of speckles of medium to dark brown blebs, which were likely to be bitumen. The coarse white dolomite had an irregular morphology to lath-like textures away from the void space and was more transparent and saddle-like in vugs. Calcite cemented the void space and fractures in the coarse white dolomite. It was clear and colourless with subhedral to euhedral crystals and twinning was often visible (Plate 3.3-G & H).

### Fluid Inclusion Petrography

Coarse white dolomite had abundant, small ( $<5\mu\text{m}$ ), two-phase (L-V), blocky to subrounded, primary fluid inclusions often located along growth zones (Plate 3.3-G; Plate 3.4-A). Calcite had mostly small ( $<5\mu\text{m}$ ) but occasionally moderately sized ( $>20\mu\text{m}$ ), often irregularly shaped, two-phase (L-V), primary inclusions (Plate 3.11-D). Secondary trails of very small ( $\ll 5\mu\text{m}$ ) fluid inclusions existed along healed fractures.

#### 3.3.9 N81-84 1078

### Petrographic Discussion

The host dolomite in this sample was light brown to medium brown and occurred as interlocking, irregularly shaped crystals. No original limestone textures were preserved in this

sample. This host dolomite predated coarse white dolomite. The coarse white dolomite was white to very pale grey and often displayed saddle-like textures that had a sweeping extinction pattern when viewed in crossed polarized light. When the coarse white dolomite was in proximity to host dolomite, it had the same crystal size and texture of the host dolomite (evidence that the host dolomite was older and the coarse white dolomite was replacing it). The further away from the host dolomite, the more the coarse white dolomite developed a distinctive texture. The crystal shape was less uniform and larger in size than that of the host dolomite. The coarse white dolomite had an average grain size of 750  $\mu\text{m}$  and often grew into vugs often terminating with saddle-like textural development. The best examples of saddle textures were growing into void spaces (Plate 3.4-B to D). As seen in other samples, the saddle features often had clear rims growing on the cloudier core of the crystals. The late phase in the paragenesis was clear and colourless calcite. Calcite grew as coarser interlocking crystals and filled vugs in the samples.

#### Fluid Inclusion Petrography

Coarse white dolomite had abundant, small ( $<5 \mu\text{m}$ ), irregular to subrounded, primary fluid inclusions (Plate 3.4-E) along growth zones. The cores of the saddle-textured dolomite were cloudy due to the abundance of fluid inclusions and the rims were often devoid of them (Plate 3.4-B to D). Calcite had both moderately sized ( $>20 \mu\text{m}$ ), isolated, irregularly shaped, primary inclusions and smaller ( $<<5 \mu\text{m}$ ), irregular to subrounded, secondary assemblages located in trails along healed fractures. Some areas of calcite were inundated by the presence of inclusions although many of these inclusions appeared to be secondary assemblages trapped along these healed fractures.

#### *3.3.10 N81-98 3181 287'*

#### Petrographic Discussion

This sample contained four mineral phases: host dolomite, sphalerite, galena, and calcite. The host dolomite was medium to dark brown in colour and very fine grained (Plate 3.1-D & E). It occurred solely as clasts cemented by the later sulphide and calcite growth and no original limestone textures were present in this sample. The sample was dominated by pale honey to dark reddish brown coloured sphalerite and dark grey metallic galena. The sphalerite occurred as coarse crystals with a vitreous lustre and as fine-grained, banded colloform sphalerite. The transition between the two was gradual; commonly, the colloform masses became single, large (1 to 5 mm), highly fractured, crystals displaying dark banding at irregular

intervals. The galena, with large (over 5mm) irregular crystals, grew between colloform sections as well as acting as nucleation points for some of the colloform sphalerite development (Plate 3.7-H). On the basis of these observations galena and sphalerite were considered to be cogenetic. Plate 3.7 (photographs E & F) shows an interesting relationship between galena and calcite. These two minerals appeared to be growing cogenetically in a void space and clearly post-dated sphalerite mineralization. Calcite was clear and colourless, often fractured, and found dominantly as a later-stage vein filling and pore space filling (Plate 6.5-B & C).

#### Fluid Inclusion Petrography

The host dolomite in this sample was very dark in colour and it was not possible to optically resolve individual fluid inclusions. Sphalerite contained many small ( $\ll 5 \mu\text{m}$ ), dominantly primary inclusions along growth zones and abundant secondary inclusion trails (Plate 3.7-D, G & H). Primary calcite-hosted inclusions were found in clusters (some moderately sized,  $>20 \mu\text{m}$ ) (see Plate 4.4-G & H) and also frequently as smaller size ( $\ll 5 \mu\text{m}$ ) inclusions along secondary trails (Plate 3.11-E & F). Many of the larger inclusions had been split open during the thin section making process.

#### *3.3.11 N81-98 3205 355'*

#### Petrographic Discussion

This sample contained sphalerite, galena and calcite. Sphalerite was the most abundant mineral and grew mostly with colloform textures ranging from honey brown to dark reddish brown in colour (Plate 3.8-B to D). Galena in the sample was dark metallic grey and did not have a well-developed crystal habit. It could occur earlier in the paragenesis than sphalerite, as galena often acted as a nucleation site for colloform sphalerite growth (Plate 3.8-D). In other areas it was observed to be cogenetic growing within colloform bands of sphalerite. Calcite was clear and colourless and was composed mostly of large interlocking blocky crystals that had an average size of 2 mm. It was the last mineral phase to grow in the sample and filled void space in between the colloform sphalerite and occasionally contained pieces of broken sulphides within it (Plate 3.12-B&C).

#### Fluid Inclusion Petrography

Sphalerite-hosted fluid inclusions were small, dominantly primary, irregularly shaped and found along growth zones (Plate 3.8-A). Abundant very small ( $\ll 5 \mu\text{m}$ ), secondary inclusion trails existed along healed fractures. Calcite was dominated by small, mostly secondary, irregular to subrounded, inclusions but larger ( $\sim 20 \mu\text{m}$ ) primary inclusions with

average degrees of fill of 0.80 were present along growth zones (Plate 3.11-G, Plate 3.11-H; Plate 3.12-A). Some larger inclusions had small tails and increased degrees of fill and were therefore, considered to be leaked.

### 3.3.12 N81-98 3205 360'

#### Petrographic Discussion

This sample contained coarse white dolomite, sphalerite and galena. Coarse white dolomite was white to pale grey and was generally highly fractured. It appeared to occur largely pre-mineralization but in some areas could be seen as later infills between sulphides and it sometimes occurred as a substrate for colloform sphalerite development and galena crystallization. Most of the sphalerite was dark reddish brown in colour but in a few areas it was honey brown (Plate 3.8-F & G). Galena was finer grained (average 1.5mm) than that of sample N81-98 3205 355' but had the same colour and texture. It appeared to have precipitated at the same time as the sphalerite.

#### Fluid Inclusion Petrography

The coarse white dolomite had abundant, small ( $\ll 5 \mu\text{m}$ ), dominantly primary inclusions. Some of the discernable two-phase inclusions were large enough for microthermometric analysis. The sphalerite contained dominantly primary inclusions ( $< 5 \mu\text{m}$ ) but was largely too opaque to see the inclusions. Frequently, secondary trails of very small ( $\ll 5 \mu\text{m}$ ) inclusions existed along healed fractures.

### 3.3.13 N81-98 3208 367'

#### Petrographic Discussion

This sample consisted of coarse white dolomite, sphalerite and calcite. Coarse white dolomite was white to pale grey in colour and appeared to pre-date medium to very dark reddish brown colloform sphalerite (Plate 3.8-H) but was coeval with crystalline, pale honey yellow coloured sphalerite. The final phase to precipitate, calcite, was clear and colourless and occurred as blocky irregular crystals. The calcite cemented fractures that crosscut much of the colloform sphalerite.

#### Fluid Inclusion Petrography

Inclusions in coarse white dolomite were small ( $< 5 \mu\text{m}$ ), irregular to subrounded in shape, and dominantly primary. Although, secondary inclusion trails existed in sphalerite (sometimes cutting across crystal boundaries), the mineral was dominated by very small

(<<5 $\mu\text{m}$ ), generally subrounded, primary inclusions often found along growth zones (Plate 3.9-A to C). The calcite contained mostly primary, small (<5  $\mu\text{m}$ ) and irregular to subrounded inclusions, which were randomly distributed and irregularly shaped, but small (<5  $\mu\text{m}$ ) inclusions in secondary trails were also present (Plate 3.12-D).

#### 3.3.14 N81-98 3214

##### Petrographic Discussion

This sample contained three phases: sphalerite, galena, and calcite. The sphalerite phase colour ranged from transparent to opaque pale honey to dark reddish brown and appeared to be cogenetic with coarse galena. Sphalerite occurred in both crystalline and colloform textures (Plate 3.9-D to F). Both sulphide phases were highly brecciated and cemented by clear and colourless to opaque white calcite, which also grew into vugs near colloform terminations. The calcite grew in void spaces near colloform terminations but generally appeared to brecciate much of the sphalerite.

##### Fluid Inclusion Petrography

Sphalerite-hosted very small (<<5  $\mu\text{m}$ ), irregular to subrounded, primary inclusions occurred frequently along growth zones (Plate 3.9-G) and occasionally as secondary and pseudosecondary trails (Plate 3.9-H). Calcite contained irregularly to subrounded shaped, usually less than 5  $\mu\text{m}$  in size, primary inclusions in clusters and along growth zones. Some larger (>10  $\mu\text{m}$ ; average degree of fill = 0.80) fluid inclusions were interpreted to have leaked due to the presence of tails and variable degrees of fill. Secondary inclusion trails occurred along healed fractures and contained abundant, small (<5  $\mu\text{m}$ ), fluid inclusions (Plate 3.12-E).

#### 3.3.15 N81-98 3225 450'

##### Petrographic Discussion

This sample contained three phases: host dolomite, coarse white dolomite and calcite. A very small amount of host dolomite occurred in this sample and this dolomite had destroyed the original limestone mineralogy and textures. It appeared as though most of the host dolomite had been replaced by coarse white dolomite. The host dolomite was fine grained and medium brown and had abundant dark brown speckles throughout it, which were interpreted to be bitumen blebs (Plate 3.1-F). Coarse white dolomite dominated this sample and occurred as blocky interlocking crystals and was also frequently observed with saddle textures (Plate 3.4-H; Plate 3.5-A to C). Calcite was clear and colourless and post-dated the coarse white dolomite. It

precipitated in any porosity left in the sample after coarse white dolomite precipitation (Plate 3.5-B & C; Plate 3.12-F & G).

#### Fluid Inclusion Petrography

Coarse white dolomite had numerous, small (<5  $\mu\text{m}$ ), primary, dominantly two-phase (L-V) inclusions, especially along growth zones. Saddle textures in coarse white dolomite had inclusion-poor rims and inclusion-rich cores (Plate 3.4-H; Plate 3.5-A). Calcite was dominated by small (<5  $\mu\text{m}$ ), irregularly shaped, secondary inclusions along healed fractures (Plate 3.12-F & G).

### **3.4 Mineral Phase Summaries**

#### *3.4.1 Host Dolomite*

Host dolomite ranged from light to dark brown in colour and had a relatively uniform fine-grained crystal size (generally 20-150  $\mu\text{m}$ ) in all of the drill core samples studied. Only one sample contained what might be a remnant texture (N81-69 2758 217') from the original limestone, represented by light and dark layers of dolomite crystals. The host dolomite was frequently replaced to some degree by coarse white dolomite (e.g. N81-65 0249, N81-69 2754 195', N81-84 1078 and N81-98 3225 450'), though this replacement could be rare to pervasive. When partially replaced, the host dolomite appeared light greyish brown and could be mistaken for another dolomite phase (such as a discoloured coarse white dolomite phase). However, crystal size and shape suggested whether the phase was a variant of the host dolomite. The host dolomite phase was dominated by very small, generally much less than 5 $\mu\text{m}$ , primary inclusions that were not suitable for a microthermometric study.

#### *3.4.2 Coarse White Dolomite*

Coarse white dolomite, as the name implies, was generally white in colour but did vary to a pale grey colour in some samples. This phase of dolomite was post-host dolomite in every sample studied and had a coarser grain size than the host dolomite, with an average crystal size of approximately 500  $\mu\text{m}$ . It often displayed saddle textures where open space was available for its development. Where saddle textures were developed the rims of the crystals formed from clear transparent dolomite, and were, on average, approximately 200  $\mu\text{m}$  in width. These rims were largely inclusion poor, unlike the cores of the crystals, which, like the non-zoned coarse white dolomites contained abundant, small (5  $\mu\text{m}$ ), dominantly primary inclusions. These primary inclusions were frequently found in growth zones. Often the shear numbers of

these inclusions severely reduced the optical clarity of this phase. Secondary inclusions were identified in the petrographic study but were relatively rare and, therefore, these phases were particularly suitable for bulk geochemical techniques such as those outlined in Chapter 2.

#### 3.4.3 *Sphalerite*

Sphalerite was the more abundant of the two sulphide phases present in the N81 deposit. It occurred in two main forms: crystalline sphalerite and colloform sphalerite. Crystalline sphalerite was often pale in colour (pale honey to light brown) and occurred largely in blebs (e.g. N81-98 2754 195') or interlocking crystals (e.g. N81-98 3181 287'). Colloform sphalerite varied in colour from pale honey to very dark reddish brown (e.g. N81-98 3208 367'). Colloform textures were usually developed on the millimetre scale up to centimetre scale and individual colloform bands were on average approximately 1 mm wide. Clear and pale coloured sphalerite contained abundant primary inclusions along growth zones and had few to moderate numbers of very small (<5 µm) inclusions formed along healed fractures as secondary trails. The darker coloured sphalerites were opaque to the petrological microscope and were unsuitable for fluid inclusion microthermometric analyses.

#### 3.4.4 *Galena*

Galena was generally consistent in appearance and texture throughout all the samples studied. It had a dark grey colour and metallic lustre. It often occurred as irregular blocks and sometimes angular blebs growing with sphalerite. In one sample it occurred with calcite (N81-98 3181 287'). Galena could precipitate before, be coeval with or post-date sphalerite. In general, however, the galena could be considered to be broadly cogenetic with sphalerite. Since galena was an opaque mineral, it was not possible to carry out a microthermometric analyses on this phase.

#### 3.4.5 *Calcite*

Calcite was generally clear and colourless but occurred in one sample with an opaque white colour (N81-98 3214). Calcite crystals tended to be coarser than the two previously mentioned carbonate phases and averaged approximately 1mm in size with a range from approximately 500µm to over 2500 µm and often displayed twinning in thin section. Through petrographic analyses of all the N81 deposit core samples, it evident that calcite was a late-stage, post-mineralization phase. It was often found filling remaining voids or porosity and/or

fractures in the previously mentioned phases. However, one occurrence of calcite growing contemporaneously with galena but post-dating sphalerite existed (sample N81-98 3181 287' – see Plate 3.7-E & H). Calcite contained both primary and secondary inclusions. Primary (L-V) inclusions tended to be larger (e.g. >5 µm) and more irregularly shaped than secondary ones. Secondary inclusion trails were common along healed fractures in most of the drill core samples. This has implications for bulk geochemical analysis interpretations with respect to the geochemical data characterizing a combination of both primary and secondary fluids associated with calcite precipitation.

#### 3.4.6 *Native Sulphur*

Native sulphur occurred in two samples, N81-65 0249 and N81-69 2766 240', as coarse crystalline grains and disseminations, respectively. The sulphur was associated with calcite and was considered to be late-stage with respect to the other dominant phases of the N81 drill cores studied.

#### 3.4.7 *Bitumen*

Bitumen occurred in at least one, potentially two samples of the drill cores studied. Sample N81-75 3358 260' contained vugs in coarse white dolomite that were lined with bitumen and frequently filled with calcite. Sample N81-75 3368 322' contained medium to dark brown disseminations that might be bitumen. Where observed, bitumen was associated with calcite and as such was considered to be a late-stage phase.

#### 3.4.8 *Summary of the Paragenetic Sequence*

Host dolomite contained vugs, fractures and other porosity features subsequently filled by largely contemporaneous later coarse-white dolomite and sulphides. Coarse white dolomite (including saddle-textured coarse white dolomite) was interpreted to be intimately associated with ore mineralization in most samples from the N81 deposit. Sphalerite blebs could be seen within coarse white dolomite (Plate 3.2-G and H) and sphalerite, galena and coarse white dolomite intergrowths were also observed (Plate 3.2-C). In a small number of samples, coarse white dolomite precipitated before sulphides. Bitumen appeared pre-calcite but post-coarse white dolomite (Plate 3.3-E & F). Calcite was classified as a late-stage, post-mineralization precipitate. It was paragenetically later than host dolomite, coarse white dolomite (including saddle-texture variety), sulphides and bitumen. Calcite was typically found filling fractures

Author	Phase Type	Size Dimension	Features
Krebs & MacQueen (1984)	<b>fine-grained dolomite</b>	<30 $\mu$ m	Original sedimentary textures preserved, uniformly sized mosaic
	<b>Presqu'ile Dolomite</b>	20 to >100 $\mu$ m	Medium to coarsely crystalline, ~ no sedimentary textures, abundant vugs
	<b>coarse-grained dolomite</b>	—	Coarsely crystalline, rhombohedral & also saddle-textures, pre-, syn- & post-ore
	<b>late calcite</b>	mm to cm	Late-stage filling remaining porosity, post-ore, post-coarse grained dolomite
Qing (1991)	<b>fine-crystalline dolomite</b>	5 to 25 $\mu$ m	Well preserved original sedimentary textures, interlocking crystals
	<b>medium-crystalline dolomite</b>	150 to 250 $\mu$ m	Recognizable sedimentary features, vugs and fractures filled with saddle dolomite
	<b>coarse-crystalline dolomite</b>	500 to 2mm	Original texture destroyed, vugs and fractures, hosts ore mineralization
	<b>saddle dolomite</b>	—	Curved faces, saddle shapes, associated with ore mineralization
	<b>late-stage coarse-crystalline calcite</b>	mm to cm	Encrusts onto saddle dolomite and sulphides
	<b>white calcite</b>	—	Associated with ore bodies
Gromek (this study)	<b>host dolomite</b>	20 to 150 $\mu$ m	Original sedimentary textures destroyed (one possible relic occurrence), frequently overprinted by coarse white dolomite
	<b>coarse white dolomite</b>	AVG 500 $\mu$ m	No original textures, saddle-like textures sometimes developed, associated with ore mineralization
	<b>late-stage calcite</b>	500 $\mu$ m to mm	Fills voids, vugs, fractures, post-coarse white dolomite and ore mineralization

**Figure 3.1** Mineral phase summaries from Krebs and MacQueen (1984), Qing (1991) and this study.

and remnant voids (Plate 3.6-A, B and H) and occasionally cemented sulphide breccias. One occurrence of calcite (N81-98 3181 287'; Plate 3.7-E & F) was coeval with galena, suggesting that there may have been some sulphide precipitation or remobilization associated with the calcite forming fluids. Native sulphur was post-coarse white dolomite and appeared to be cogenetic with calcite (see Plate 3.10-A).

### **3.5 Discussion – Comparison to Previous Petrographic Analyses**

#### *3.5.1 Introduction*

Petrographic analyses of various phases at Pine Point are documented by Kyle (1981), Krebs and MacQueen (1984), Qing and Mountjoy (1990), Qing (1991), Qing and Mountjoy (1994), Qing (1998), Telser (1999), among others. The main petrographic studies cited are by Qing and co-workers and by Krebs and MacQueen. The papers by Qing are based on a more regional study of the carbonate host rocks and their alteration whereas the Krebs and MacQueen paragenesis was produced for the Pine Point deposits. Paragenetic summaries from Krebs and MacQueen and that of Qing, and the paragenesis from this study are outlined below and in Figures 3.2, 3.3 and 3.4 respectively. A comparison between the three studies can be found in Section 3.5.4.

#### *3.5.2 Phase Description Summary– Krebs and MacQueen (1984)*

A phase summary and a paragenetic sequence for data from Krebs & MacQueen are given in Figures 3.1 and 3.2, respectively. Fine-grained dolomite ranges from grey, yellow grey to brown grey and has original sedimentary structures preserved. This phase occurs as uniformly sized mosaics of dolomite crystals that are less than 30µm (Krebs and MacQueen, 1984). Presqu'ile dolomite is medium to coarsely crystalline dolomite with a colour range of buff-brown, buff-grey to grey. Generally, no original sedimentary features are preserved in this phase but relic textures are sometimes seen. The dolomite crystal size ranges from 20 to greater than 100µm. Abundant vugs are present and are filled or lined with coarse-grained dolomite, sulphides, calcite, altered bitumen and native sulphur (Krebs and MacQueen, 1984). Coarse-grained dolomite (saddle dolomite) is white to yellowish-white coloured dolomite that lines fractures, veins and vugs. This dolomite phase has a rhombohedral morphology and also occurs as saddle-like textures. The crystal faces of the saddle dolomite are curved and display sweeping extinction when viewed in crossed polarized light. This phase has a complex paragenetic relationship to the ore mineralization at Pine Point and can occur as a pre-, syn-,

and post-ore phases (Krebs and MacQueen, 1984). Largely euhedral “whitish” coloured calcite crystals range from millimetre to centimetre scale size. This calcite is late-stage phase filling in remaining vugs, fractures and other voids between or in, sulphides and coarse-grained dolomite (Krebs and MacQueen, 1984). Bitumen phases post-date ore mineralization (Krebs and MacQueen, 1984).

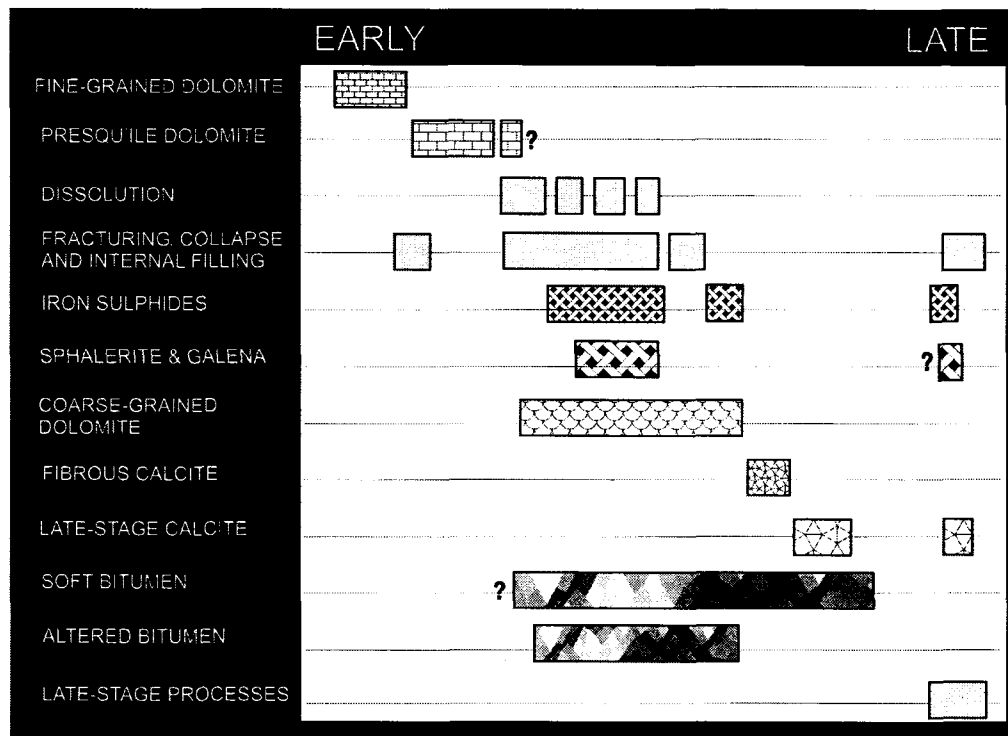


**Figure 3.2** Paragenetic summary from Krebs & MacQueen (1984).

### 3.5.3 Phase Description Summary – Qing (1991)

The first phase described by Qing (1991) is a fine-crystalline dolomite, which is brown to grey in colour and has well preserved original limestone features (e.g. fossils and sedimentary structures) (Qing, 1991). The dolomite crystals are subhedral to euhedral, ranging from 5 to 25 $\mu\text{m}$  with an average size of 8 $\mu\text{m}$ . The dolomite has an interlocking texture and does not display undulatory extinction. The crystal size increases (up to 100 $\mu\text{m}$ ) near the ore bodies (Qing, 1991). Medium-crystalline dolomite is medium to dark brown in colour and has original sedimentary features that are “generally recognizable”. Porosity in the form of dissolution vugs and fractures are occasionally filled with “saddle dolomite” and anhydrite. Fine-crystalline dolomite is anhedral to subhedral with well-defined crystal boundaries and ranges in size from 150 to 250  $\mu\text{m}$  (the average is 200  $\mu\text{m}$ ). Similar to fine-crystalline

dolomite, it does not display undulatory extinction (Qing, 1991). Coarse crystalline dolomite is light brown to buff coloured and most of the original sedimentary textures are destroyed (Qing, 1991). Vugs and fractures occur at the millimetre to metre scale and host ore mineralization in the deposit. This dolomite crystal size ranges from 500  $\mu\text{m}$  to 2 mm and displays undulatory extinction (Qing, 1991). Saddle dolomite is described as coarse (millimetre scale crystals), generally white in colour and rhombohedrally shaped with curved faces sometimes having symmetrical saddle-like textures. This dolomite typically occurs in vugs and fractures and is

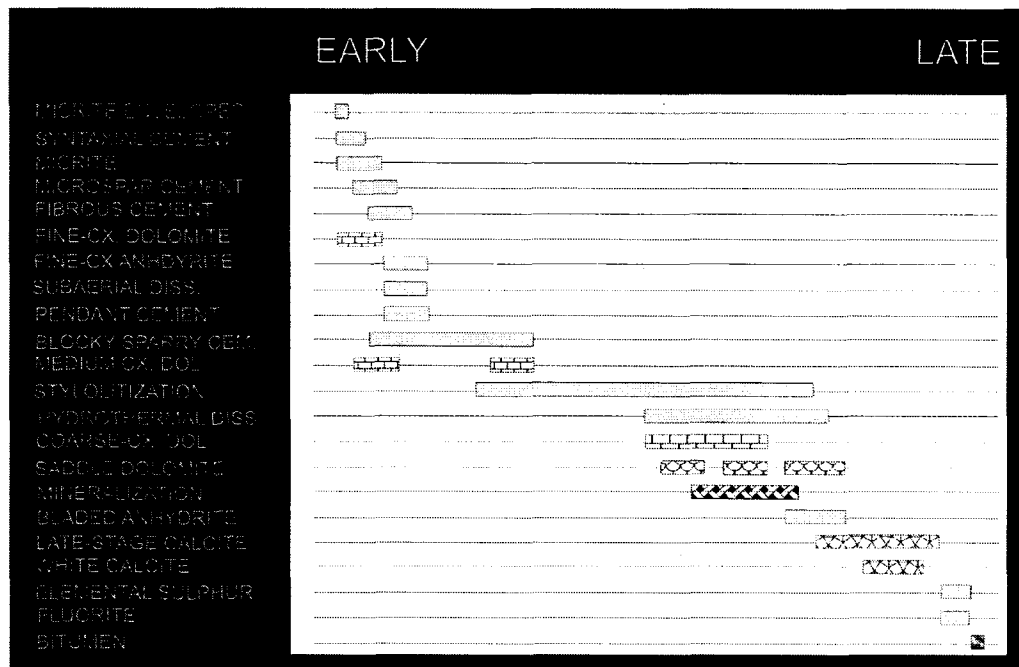


**Figure 3.3** Paragenetic Summary from Qing (1991).

associated with ore mineralization (pre-, syn-, post-mineralization textures are observed). Saddle dolomite displays sweeping extinction in crossed polarized light (Qing, 1991). Late-stage coarse-crystalline calcite (millimetre to centimetre scale) is semi-translucent to white coloured and often found in vugs and encrusting saddle dolomite and sulphide phases. This phase is considered to post-date saddle dolomite and ore mineralization (Qing, 1991). White calcite, forms anhedral crystals and is found in between layers of saddle dolomite. This phase is closely associated with the ore bodies (Qing, 1991). Elemental sulphur is anhedral to euhedral in form and occurs in vugs and fractures. This phase is paragenetically later than both saddle dolomite and late-stage coarse-crystalline calcite (Qing, 1991). Bitumen is massive and black coloured postdating late-stage coarse-crystalline calcite and is found in fractures and

vugs. Two types of bitumen are described, unaltered (“representing indigenous organic matter”) and altered bitumen. The latter, is interpreted to likely be produced via thermochemical sulphate reduction during dolomitization of the coarse-crystalline dolomite, saddle dolomite and ore phases (Qing, 1991).

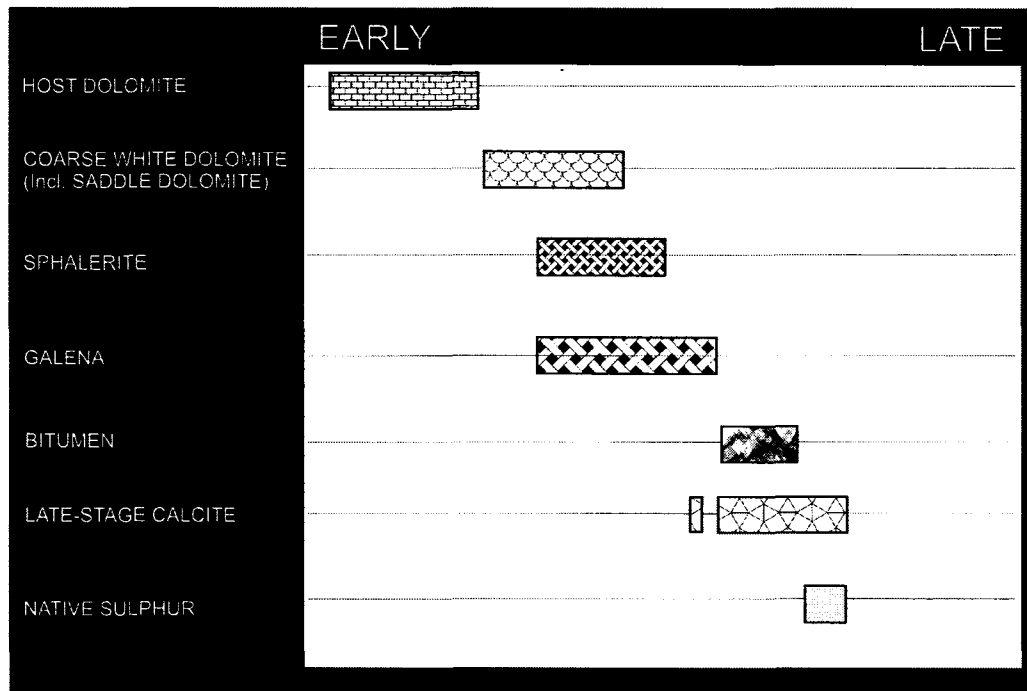


**Figure 3.4** Paragenetic summary from this thesis.

#### 3.5.4 *Paragenetic Comparisons*

The paragenetic sequence descriptions from both Krebs & MacQueen (1984) and Qing (1991) are generally correlative to those of this study. It is important to note that only the N81 deposit was studied in this thesis and both the Krebs & MacQueen (1984) and Qing (1991) studies encompass a much larger range of deposits at Pine Point and on a more regional scale. As such, some differences are inevitable between the published studies and this one. The following is a list of basic similarities between the other studies and this study, focussing specifically on the carbonate phases:

- 1) A dolomite exists that contains porosity or accommodation space for precipitation of minerals (e.g., dolomite and sulphide phases):

The host dolomite encountered in this study contains no major signs of original sedimentary textures and it pre-dates coarse white dolomite precipitation and ore mineralization. This phase is inferred to be correlative to “Presqu’ile dolomite” of Krebs & MacQueen (1984), which hosts the mineralization and has a very similar size range (see Figure 3.1). It is similar in its lack of evidence of the original limestone to the “coarse-crystalline dolomite” of Qing (1991) but has a crystal size ratio that is more similar to the “fine and medium-crystalline dolomites”. It is likely that the host dolomite in this study may be encompassing more than one phase of finer grained dolomite. The main aim of this thesis is to understand the nature of the fluids responsible for the mineralization and therefore, it is not within the scope of this study to separate the various phases of pre-ore dolomites. Some of these dolomites are included in the geochemical study but are intended to give more of a “background” analyses to compare with the mineralization.

2) A coarse, dominantly white, dolomite exists that is associated with mineralization:

Coarse white dolomite post-dates the host dolomite and is associated with ore mineralization. Largely syn-ore textures were observed and saddle-like features developed in vugs and porous zones. This phase is inferred to correlate to “saddle dolomite” of Qing (1991) and “coarse-grained dolomite” of Krebs & MacQueen (1984). Both of these studies related these phases to mineralization and are equivalent to coarse white dolomite of this study.

3) A late-stage (post-ore) calcite phase fills remaining porosity:

Calcite is generally a late-stage precipitate in these samples. One occurrence of calcite and galena precipitating cogenetically was found but all other calcites studied are inferred to be the last stage of carbonate precipitation. This phase correlates well with the “late-stage coarse-crystalline calcite” of Qing (1991) and “late-stage calcite” of Krebs & MacQueen (1984). Qing (1991) contains a “white calcite” phase that is associated with ore bodies. This could be a correlative phase to the calcite seen in sample N81-98 3181 287’ that appears cogenetic with galena. Krebs and MacQueen

(1984) discuss calcite intergrowths with sulphides from Fritz (1969), which supports this hypothesis.

### **3.6 Remarks**

This petrography chapter forms the basis for all fluid chemistry analyses of this thesis. Microthermometric fluid inclusion studies on coarse white dolomite, sphalerite and calcite-hosted fluid inclusions are reported in Chapter 4. Crush-leach analysis on host and coarse white dolomite, sulphide and calcite mineral phases are outlined in Chapter 5. Chapter 6, further characterizing the fluids involved in the N81 deposit, reports strontium isotopic data from carbonate phases of coarse white dolomite and calcite. Geochemical data from the subsequent three chapters will characterize the fluids and suggest fluid-evolution processes in the deposit.

Plate 3.0

A. Photograph of host dolomite from sample N81-65 0249. Note the abundance of very small inclusions and the poor clarity of sample (plane polarized light).

B. Photograph of host dolomite from sample N81-65 0249 showing very small primary inclusions viewed in plane polarized light.

C. Photograph of host dolomite (HDOL), galena (GN) and coarse white dolomite (CWD) from sample N81-69 2754 195' (viewed in plane polarized light). This photograph shows the crystal size difference between host and coarse white dolomite.

D. Host dolomite from previous photograph (C) at a higher magnification photographed in plane polarized light. Note the very small fluid inclusion size.

E. Photograph of host dolomite (HDOL), galena (GN) and sphalerite (SPH) from sample N81-69 2754 195' (viewed in reflected light).

F. Host dolomite (HDOL) and sphalerite (SPH) from sample N81-69 2758 217' photographed in plane polarized light.

G. Photograph of host dolomite banding from sample N81-69 2758 217' taken in plane polarized light.

H. Photograph of host dolomite in sample N81-69 2758 217' viewed in plane polarized light. The photograph shows the very small size of the inclusions.

Plate 3.0

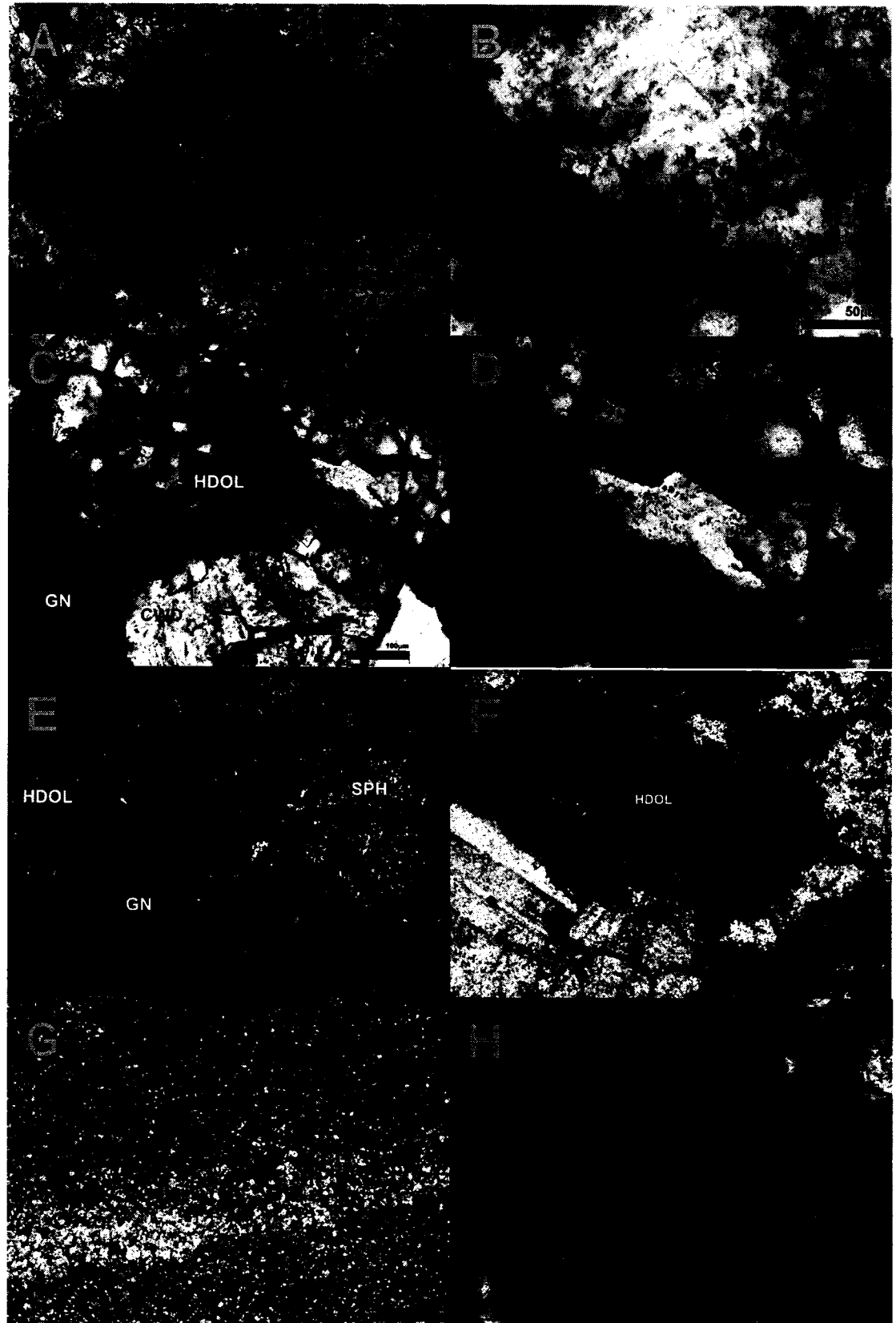


Plate 3.1

A. Photograph of host dolomite (HDOL), sphalerite (SPH) and galena (GN) viewed in plane polarized light from sample N81-69 2758 217'.

B. Photograph of host dolomite, viewed in plane polarized light, from sample N81-69 2766 240'.

C. Photograph of host dolomite, under a higher magnification than previous photograph, from sample N81-69 2766 240' (viewed in plane polarized light). The photograph shows the small fluid inclusion size.

D. Host dolomite photographed in plane polarized light from sample N81-98 3181 287'. Photograph shows the dolomite with a greyish-brown colour and relatively uniform sized crystals.

E. Photograph of host dolomite viewed in crossed polarized light from sample N81-98 3181 287'.

F. Photograph of host dolomite viewed in plane polarized light from sample N81-98 3225 450' (note abundant bitumen speckles throughout mineral phase).

Plate 3.1

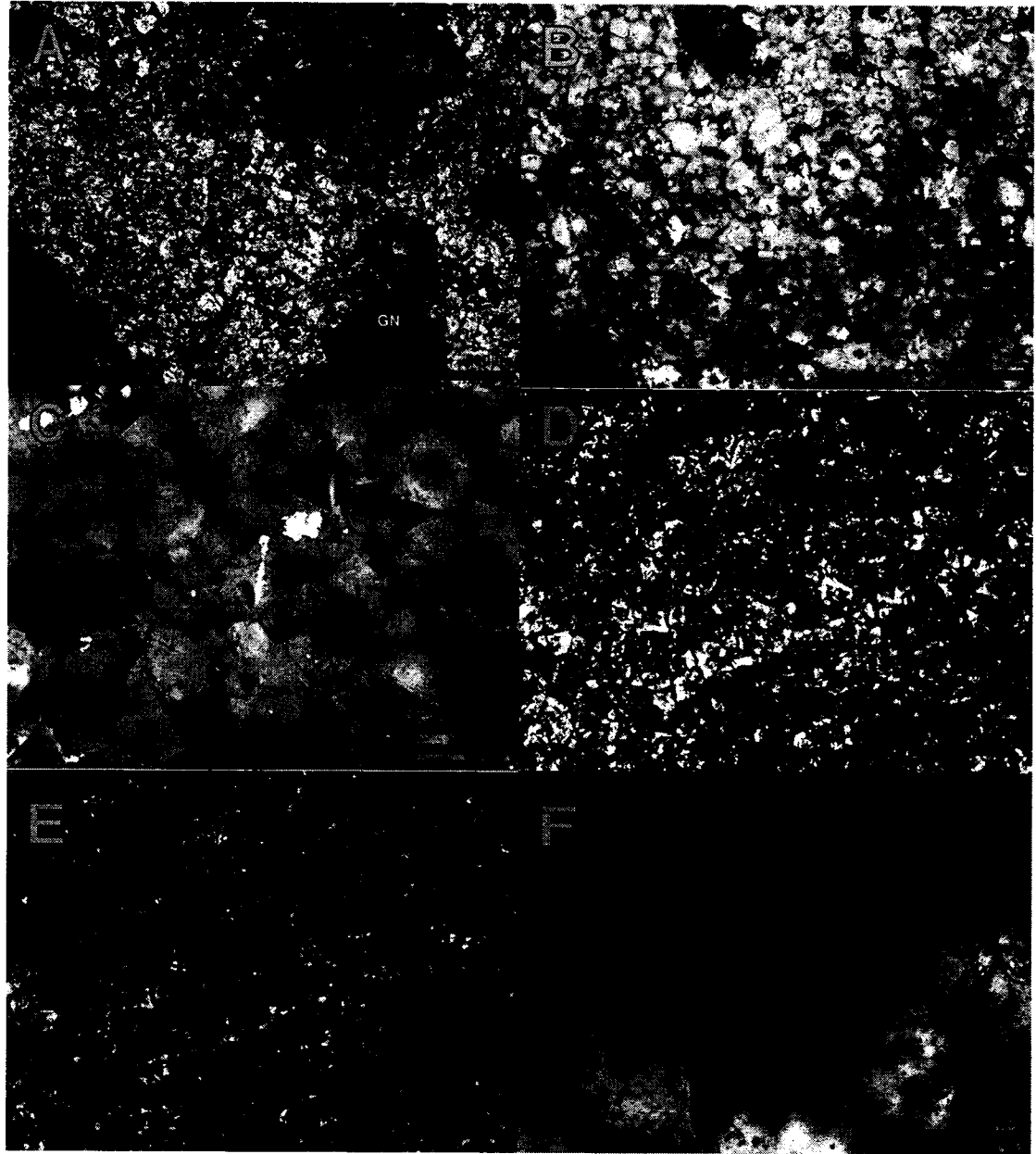


Plate 3.2

A. Photograph of primary fluid inclusions in coarse white dolomite viewed in plane polarized light from sample N81-65 0249.

B. A saddle rim and core zone of coarse white dolomite from sample N81-65 0249 photographed in plane polarized light. Note the difference in fluid inclusion population densities between the rim and core areas. The red tinted mineral in top right corner of photograph is calcite.

C. Photograph of galena (GN), sphalerite (SPH) and coarse white dolomite (CWD) from sample N81-69 2754 195' viewed in reflected light.

D. Photograph of primary fluid inclusions following growth zones in coarse white dolomite from sample N81-69 2754 195' (viewed in plane polarized light).

E. Photograph of primary fluid inclusions in coarse white dolomite, viewed in plane polarized light, from sample N81-69 2754 195'.

F. Primary fluid inclusions in coarse white dolomite from sample N81-69 2766 240' photographed in plane polarized light.

G. Photograph of dark reddish brown sphalerite (SPH) surrounded by coarse white dolomite (CWD) from sample N81-69 2766 240' (viewed in plane polarized light).

H. Same field of view as photograph (G) but viewed in crossed polarized light. The sphalerite is surrounded by coarse white dolomite.

Plate 3.2

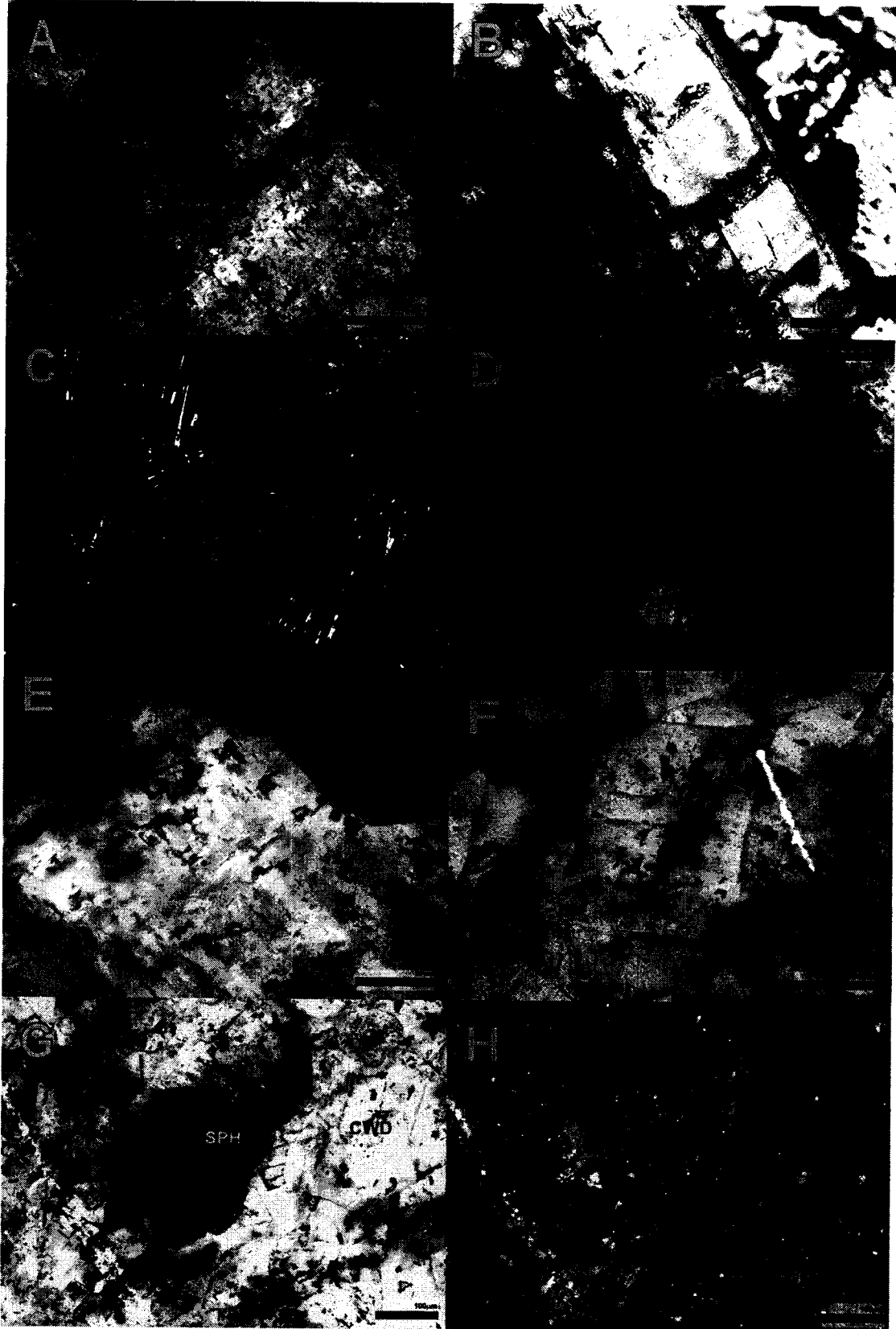


Plate 3.3

A. Photograph of a coarse white dolomite crystal with a saddle-like texture (SDOL) from sample N81-75 3358 260' viewed in plane polarized light.

B. Primary fluid inclusions along growth zones in coarse white dolomite from sample N81-75 3358 260' photographed under plane polarized light.

C. Primary fluid inclusions along growth zones, under high magnification, in coarse white dolomite from sample N81-75 3358 260' photographed in plane polarized light.

D. Photograph of coarse white dolomite (CWD) and calcite (CC) (from sample N81-75 3358 260') showing characteristic high and low fluid inclusion population densities, respectively. The photograph was taken in plane polarized light.

E. Photograph of a vug in coarse white dolomite lined with bitumen and filled by calcite from sample N81-75 3358 260' (viewed in plane polarized light). Good twinning is visible in the calcite.

F. Same field of view as photograph (E) except viewed in crossed polarized light.

G. Photograph of coarse white dolomite displaying saddle texture and late-stage calcite (top right) from sample N81-75 3386 322' viewed in plane polarized light.

H. Same field of view as photograph (G) except viewed in crossed polarized light. Good twinning is visible in the calcite.

Plate 3.3

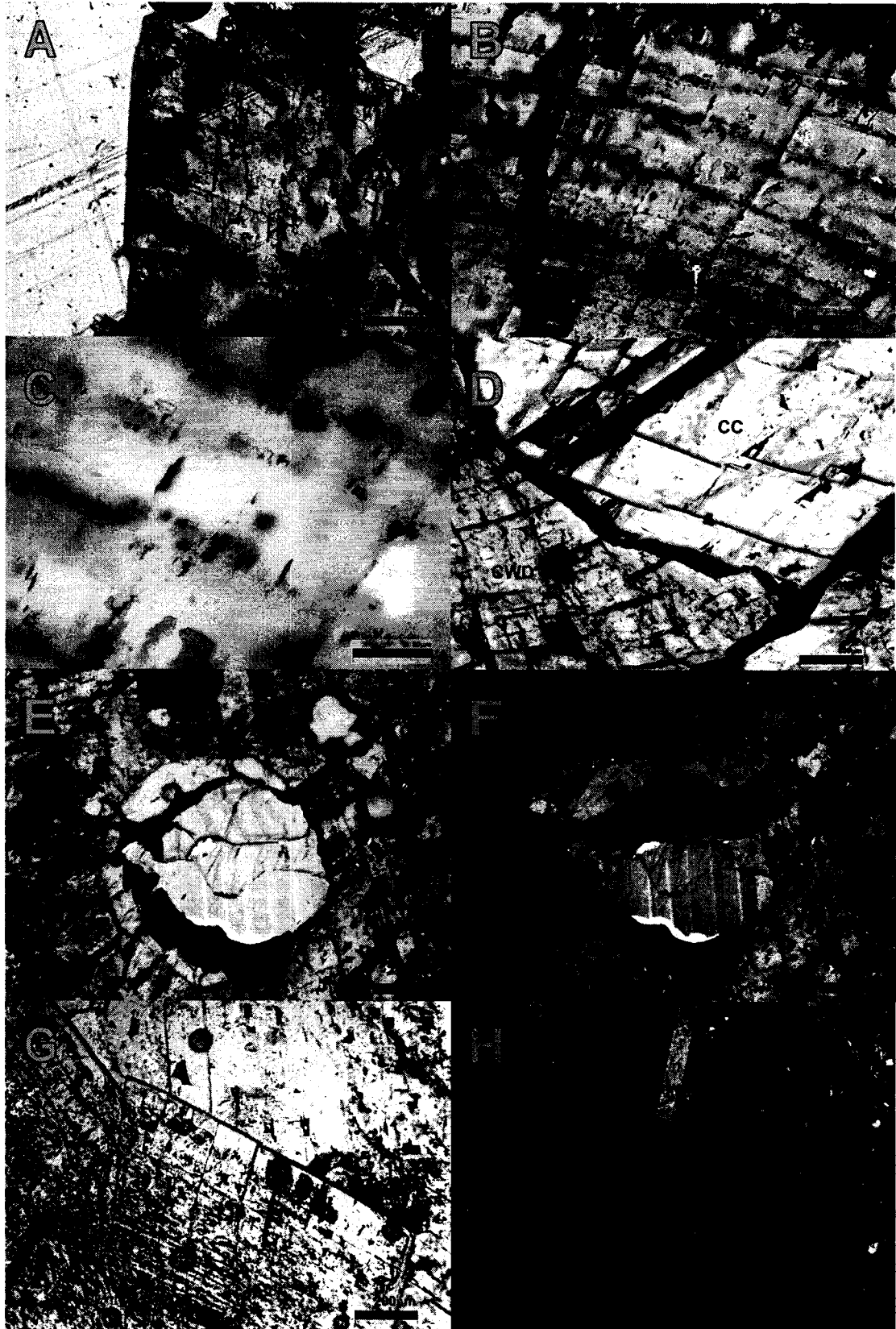


Plate 3.4

- A. Photograph of primary fluid inclusions in coarse white dolomite from sample N81-75 3386 322' viewed in plane polarized light.
- B. Coarse white dolomite with saddle-like texture (SDOL) and later stage calcite (CC) from sample N81-84 1078 photographed in plane polarized light.
- C. Same crystal as above photograph (B) except photographed under higher magnification. The photograph shows how the rim of the saddle shape is more clear (e.g. lower fluid inclusion density) than the core of the crystal.
- D. Same crystal as above photograph (C) except viewed under higher magnification. Primary fluid inclusions dominate this phase and are visibly increasing in numbers towards core of crystal.
- E. Photograph of primary fluid inclusions following growth zones in coarse white dolomite from sample N81-84 1078 (viewed in plane polarized light).
- F. Primary fluid inclusions in coarse white dolomite from sample N81-98 3205 360' photographed in plane polarized light.
- G. Photograph of primary fluid inclusions in coarse white dolomite from sample N81-98 3208 367' viewed in plane polarized light.
- H. Photograph of a saddle dolomite crystal displaying rim and core zone fluid inclusion assemblages from sample N81-98 3225 450' (viewed in plane polarized light).

Plate 3.4

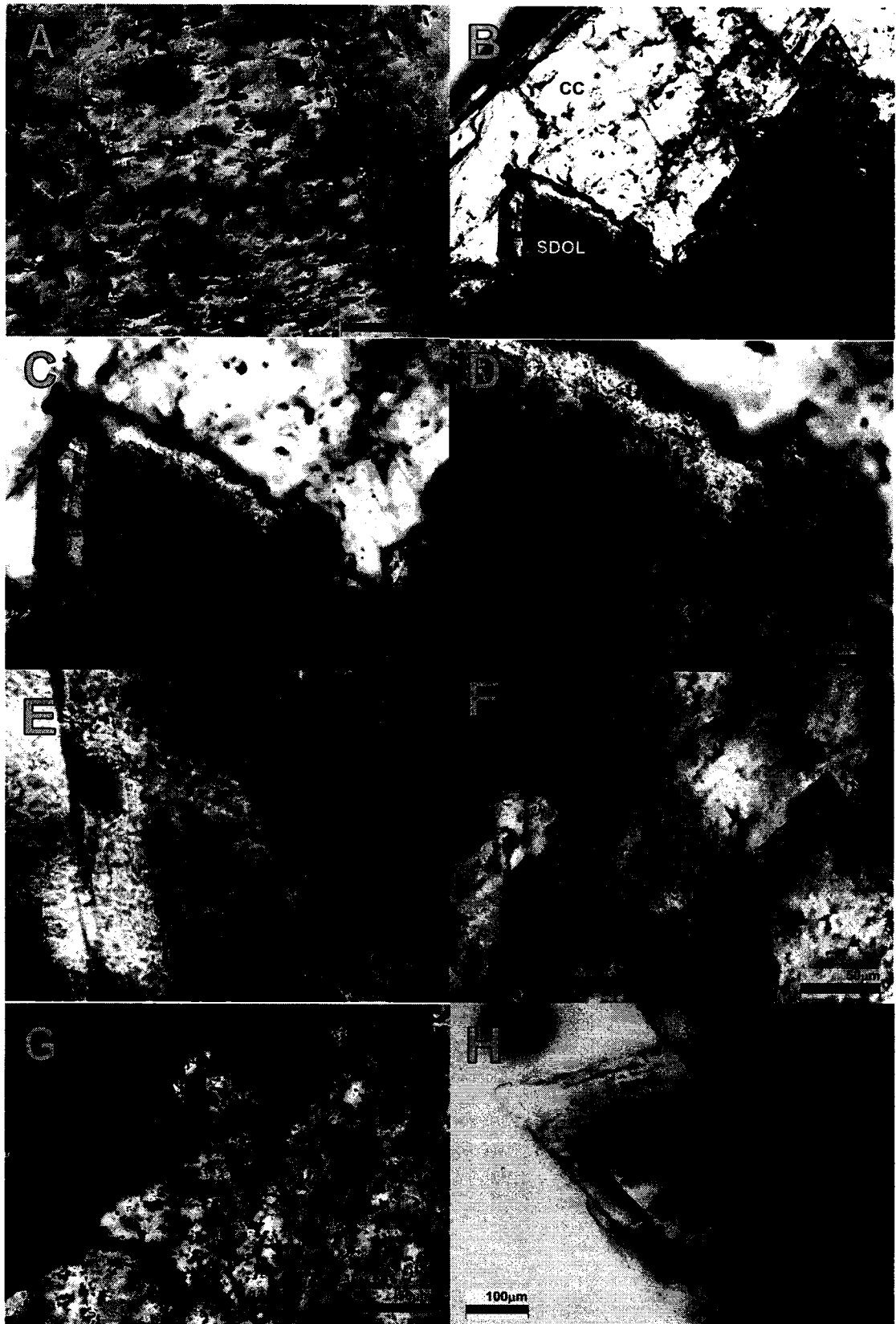


Plate 3.5

A. Same coarse white dolomite crystal as photograph H in Plate 3.4 except viewed under higher magnification. Photograph of primary fluid inclusions in coarse white dolomite from sample N81-98 3225 450' viewed in plane polarized light.

B. Photograph of coarse white dolomite with saddle texture terminations and calcite from N81-98 3225 450' viewed in plane polarized light. This photograph shows the abundance of fluid inclusions towards the core of the dolomite crystals, which severely reduce the optical clarity of the thin section and appear very dark in the photograph.

C. Same field of view as above photograph (B) except viewed in crossed polarized light.

Plate 3.5



Plate 3.6

- A. Photograph of a calcite filled fracture within sphalerite and galena mineralization from sample N81-68A 2969 375' (viewed in plane polarized light).
- B. Colloform sphalerite and galena mineralization from sample N81-68A 2969 375' photographed in plane polarized light.
- C. Typical sphalerite-hosted primary fluid inclusions from sample N81-68A 2969 375' viewed in plane polarized light.
- D. Photograph of sphalerite-hosted primary fluid inclusions occurring along growth zones viewed in plane polarized light (sample N81-69 2754 195').
- E. Photograph of secondary fluid inclusions in sphalerite from sample N81-69 2754 195' viewed in plane polarized light.
- F. Coarse sphalerite (SPH), galena (GN) and late stage calcite (CC) from sample N81-69 2758 217' photographed in plane polarized light.
- G. Photograph taken in plane polarized light showing the variation in sphalerite (SPH) colour from sample N81-69 2758 217' (note the calcite (CC) in the bottom portion of photograph).
- H. Photograph of sphalerite (SPH) with void filling late-stage calcite (CC) from sample N81-69 2764 235' viewed in plane polarized light.

Plate 3.6

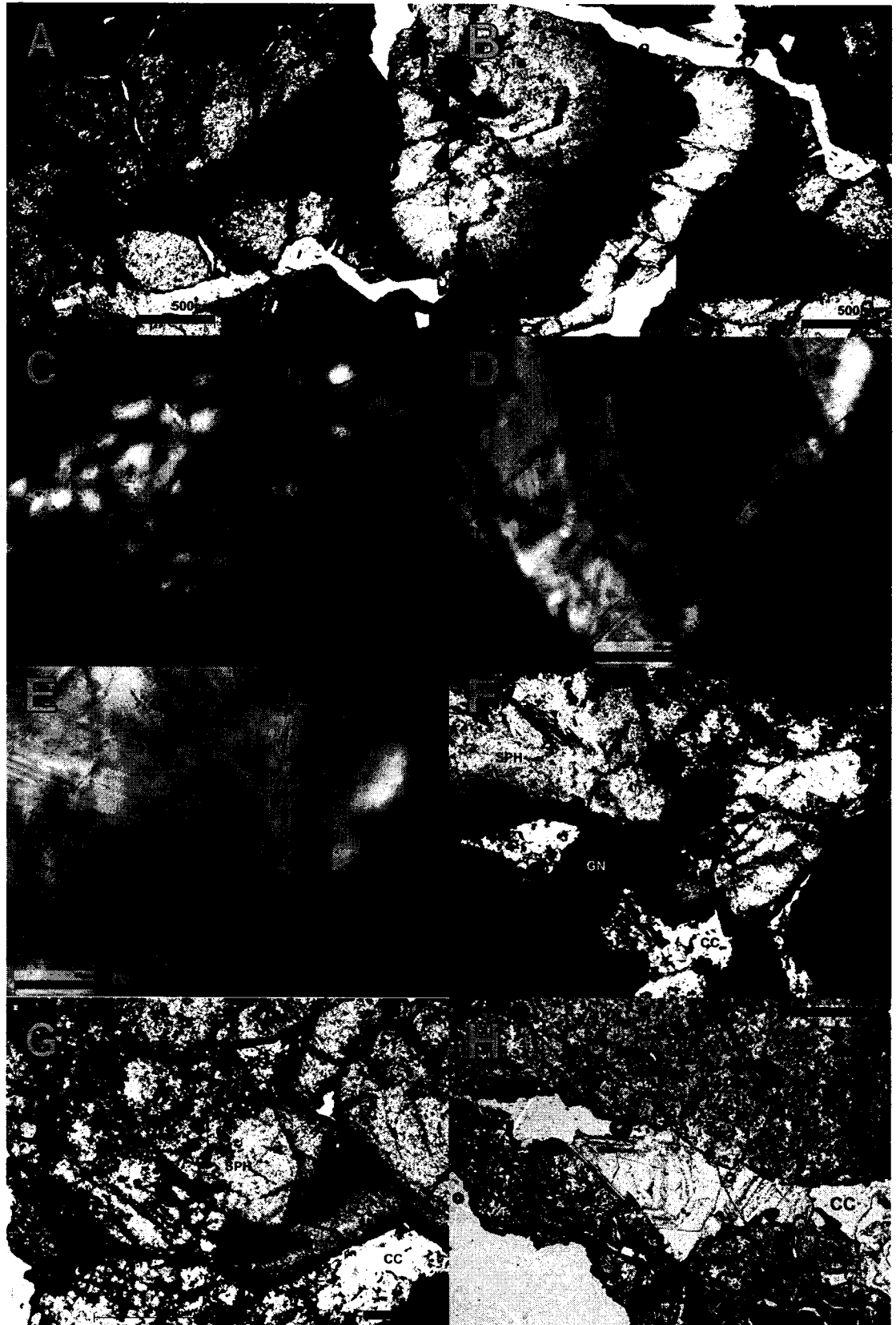


Plate 3.7

- A. Photograph of sphalerite with colloform development from sample N81-69 2764 235' (viewed in plane polarized light).
- B. Same field of view as photograph (A) except viewed in reflected light.
- C. Sphalerite with clear and fluid inclusion poor rim from sample N81-69 2764 235' photographed in plane polarized light. The dashed line highlights the abrupt change in the fluid inclusion population density.
- D. Photograph of primary sphalerite-hosted fluid inclusions located along growth zones from sample N81-98 3181 287' (viewed in polarized light).
- E. Colloform sphalerite (SPH), galena (GN) and calcite (CC) from sample N81-98 3181 287' photographed in plane polarized light.
- F. Same field of view as photograph (E) except viewed in crossed polarized light.
- G. Photograph of secondary sphalerite-hosted fluid inclusions located in healed fractures from sample N81-98 3181 287' (viewed in plane polarized light).
- H. Primary fluid inclusions along growth zones in sphalerite photographed in plane polarized light (sample N81-98 3181 287').

Plate 3.7

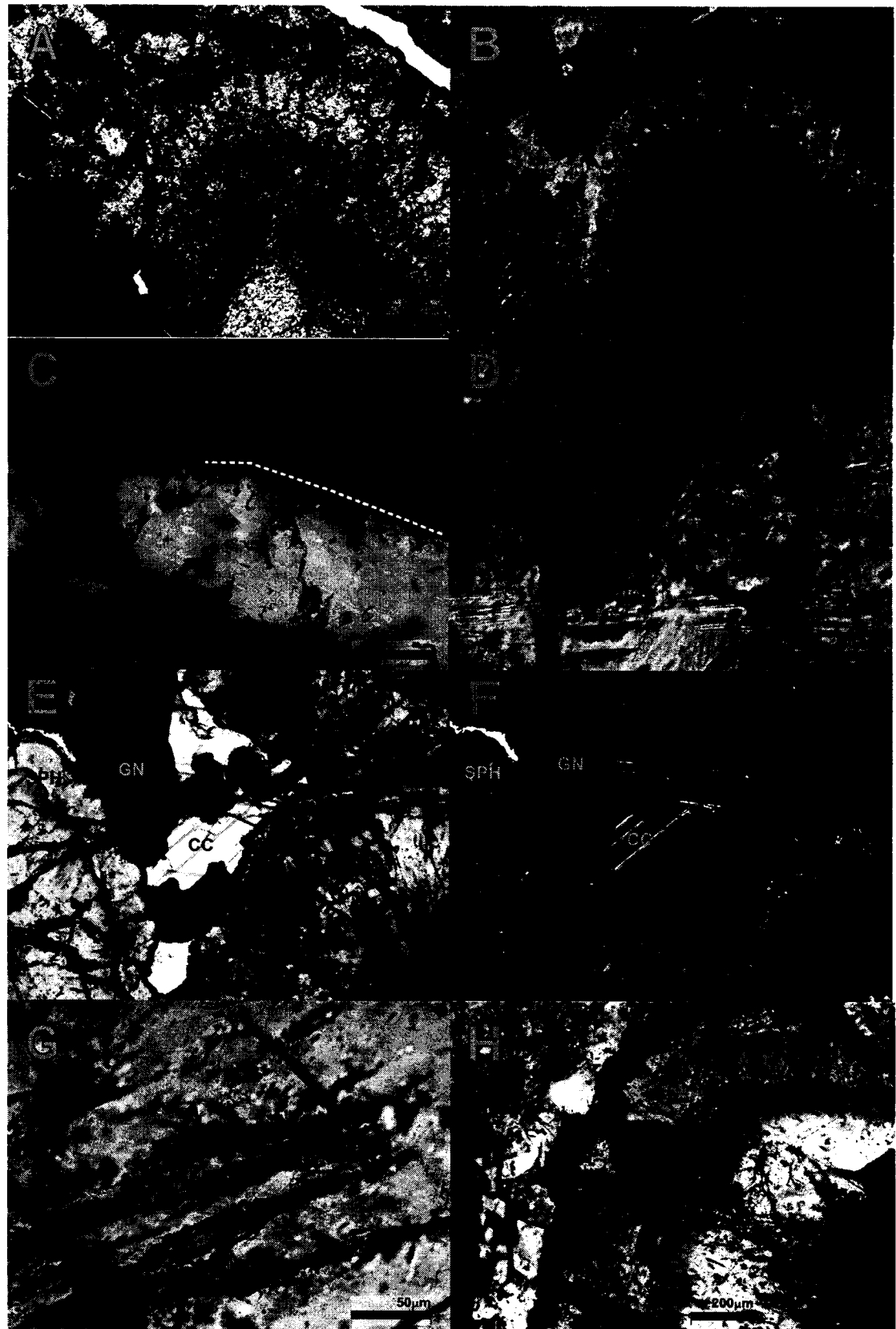


Plate 3.8

A Primary fluid inclusions along growth zones in sphalerite from sample N81-98 3205 355' photographed in plane polarized light.

B. Photograph of colloform sphalerite from drill core sample N81-98 3205 355' viewed in plane polarized light.

C. Colloform sphalerite and late-stage calcite (clear coloured) from sample N81-98 3205 355' photographed in plane polarized light.

D. Photograph of galena (black) and radiating colloform sphalerite from sample N81-98 3205 355' viewed in plane polarized light.

E. Photograph of a secondary fluid inclusion trail in sphalerite from sample N81-98 3205 355' viewed in plane polarized light.

F. Sphalerite and galena from drill core sample N81-98 3205 360' photographed in reflected light.

G. Photograph of reddish brown sphalerite from sample N81-98 3205 360' taken in reflected light.

H. Highly fractured sphalerite from sample N81-98 3208 367' photographed in plane polarized light.

Plate 3.8



Plate 3.9

- A. Photograph of sphalerite hosted fluid inclusions from sample N81-98 3208 367' viewed in plane polarized light.
- B. Primary fluid inclusions following growth zones in sphalerite photographed in plane polarized light (sample N81-98 3208 367').
- C. Secondary sphalerite-hosted fluid inclusions from sample N81-98 3208 367' photographed in plane polarized light.
- D. Photograph of colloform and crystalline sphalerite from sample N81-98 3214 taken in reflected light.
- E. Photograph of galena and crystalline sphalerite from sample N81-98 3214 viewed in reflected light.
- F. Pale beige to dark reddish brown sphalerite and galena from sample N81-98 3214 photographed in plane polarized light.
- G. Photograph of primary inclusions along growth zones in sphalerite viewed in plane polarized light (sample N81-98 3214).
- H. A sphalerite-hosted secondary fluid inclusion trail from sample N81-98 3214 photographed in plane polarized light.

Plate 3.9

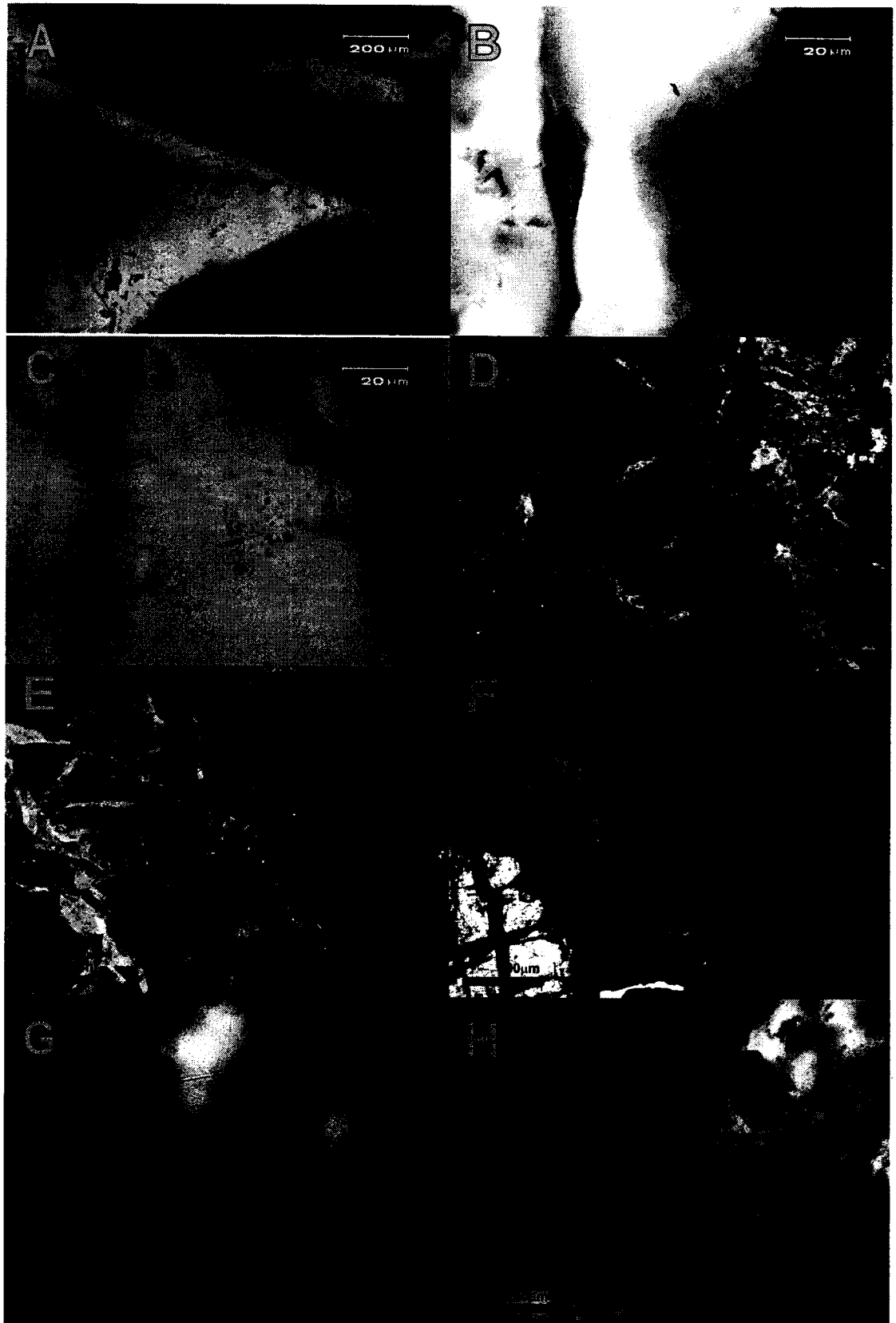


Plate 3.10

- A. Photograph of native sulphur (yellow) and late-stage calcite (red tinted) from sample N81-65 0249 viewed in plane polarized light.
- B. Primary fluid inclusions in calcite from sample N81-65 0249 photographed in plane polarized light.
- C. A primary calcite-hosted fluid inclusion assemblage from sample N81-65 0249 photographed in plane polarized light.
- D. Photograph of an area containing abundant uniformly sized primary inclusions in calcite from sample N81-65 0249 (viewed in plane polarized light).
- E. Secondary calcite-hosted fluid inclusion trails from sample N81-68A 2969 375' photographed in plane polarized light.
- F. Photograph of calcite-hosted primary fluid inclusions following growth zones from sample N81-69 2764 235' taken in plane polarized light.
- G. Calcite-hosted primary fluid inclusions following growth zones from sample N81-69 2764 235' photographed in plane polarized light.
- H. A secondary fluid inclusion trail in calcite from sample N81-69 2766 240' (see dashed lines) photographed in plane polarized light.

Plate 3.10

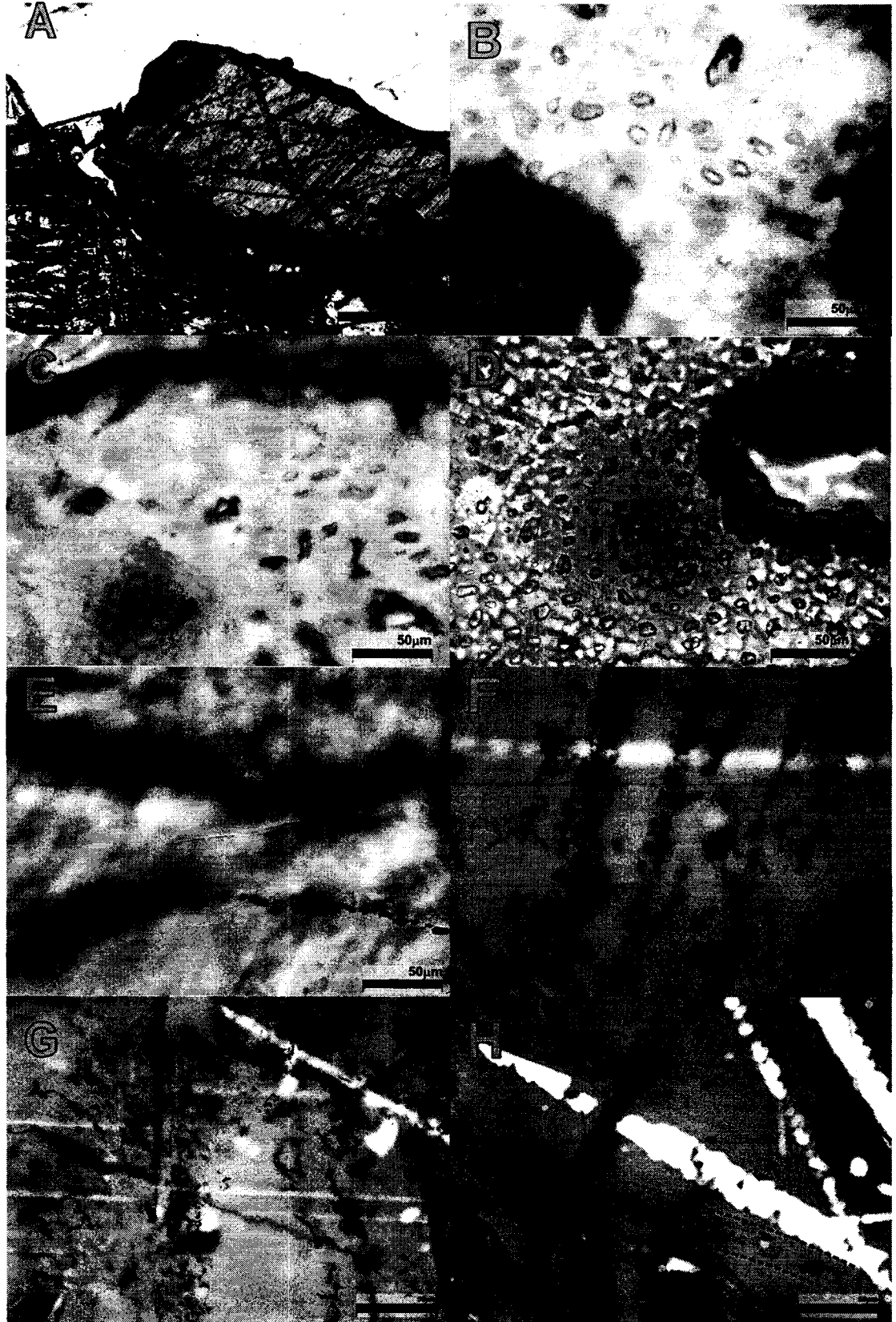


Plate 3.11

- A. A primary fluid inclusion (L-V) in calcite from sample N81-69 2766 240' (see dashed border) photographed in plane polarized light.
- B. Photograph of a primary calcite-hosted fluid inclusion (L-V) from sample N81-75 3358 260' taken in plane polarized light.
- C. Secondary calcite-hosted fluid inclusion trails from sample N81-75 3358 260' photographed in plane polarized light.
- D. Photograph of primary fluid inclusions in calcite from sample N81-75 3386 322' taken in plane polarized light.
- E. Secondary fluid inclusion trails in calcite photographed in plane polarized light (sample N81-98 3181 287').
- F. Photograph of a primary fluid inclusion cluster in calcite viewed in plane polarized light (sample N81-98 3181 287').
- G. Calcite-hosted fluid inclusions from sample N81-98 3205 355' photographed in plane polarized light.
- H. Photograph of dominantly primary fluid inclusions along growth zones in calcite from sample N81-98 3205 355' (viewed in plane polarized light).

Plate 3.11

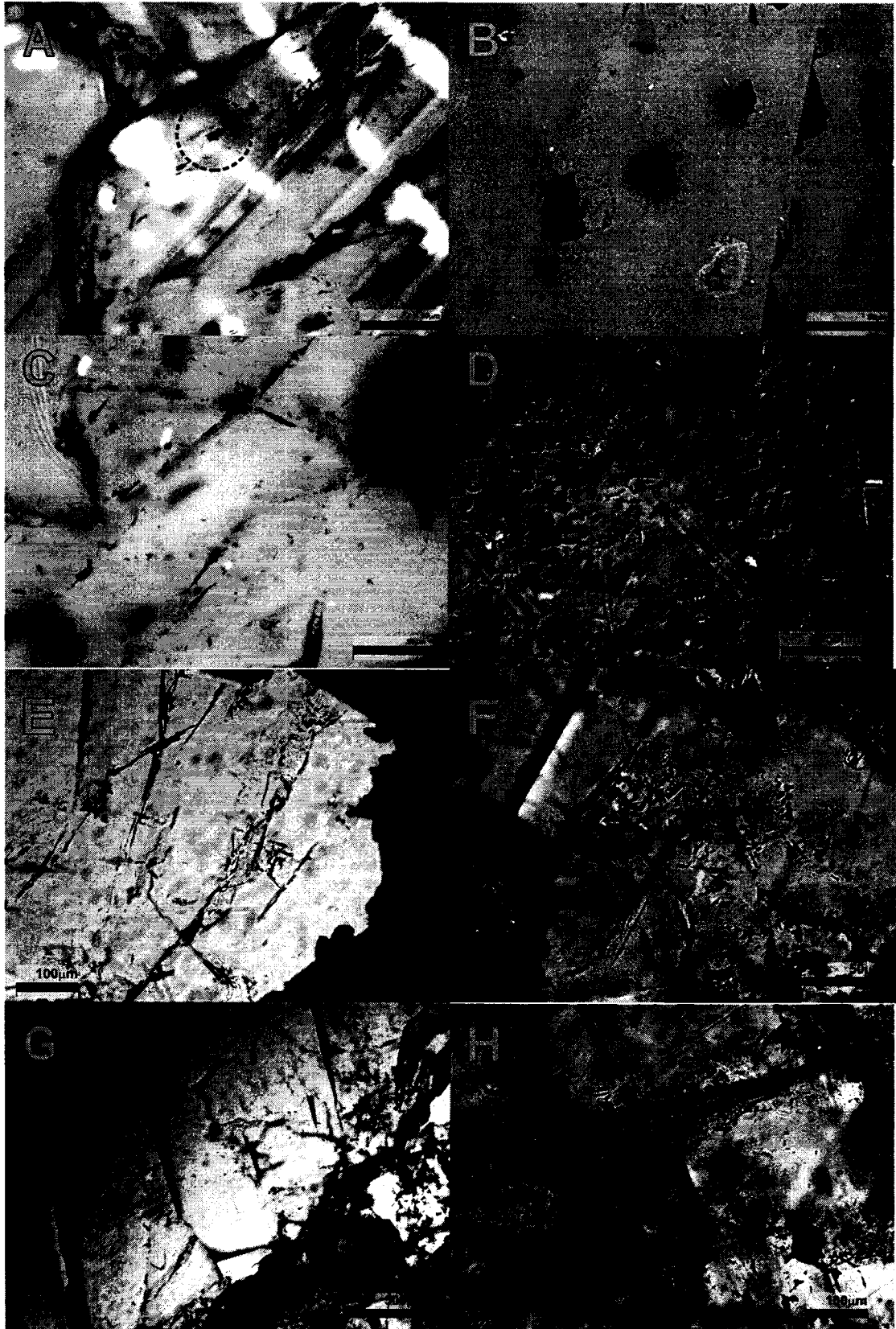
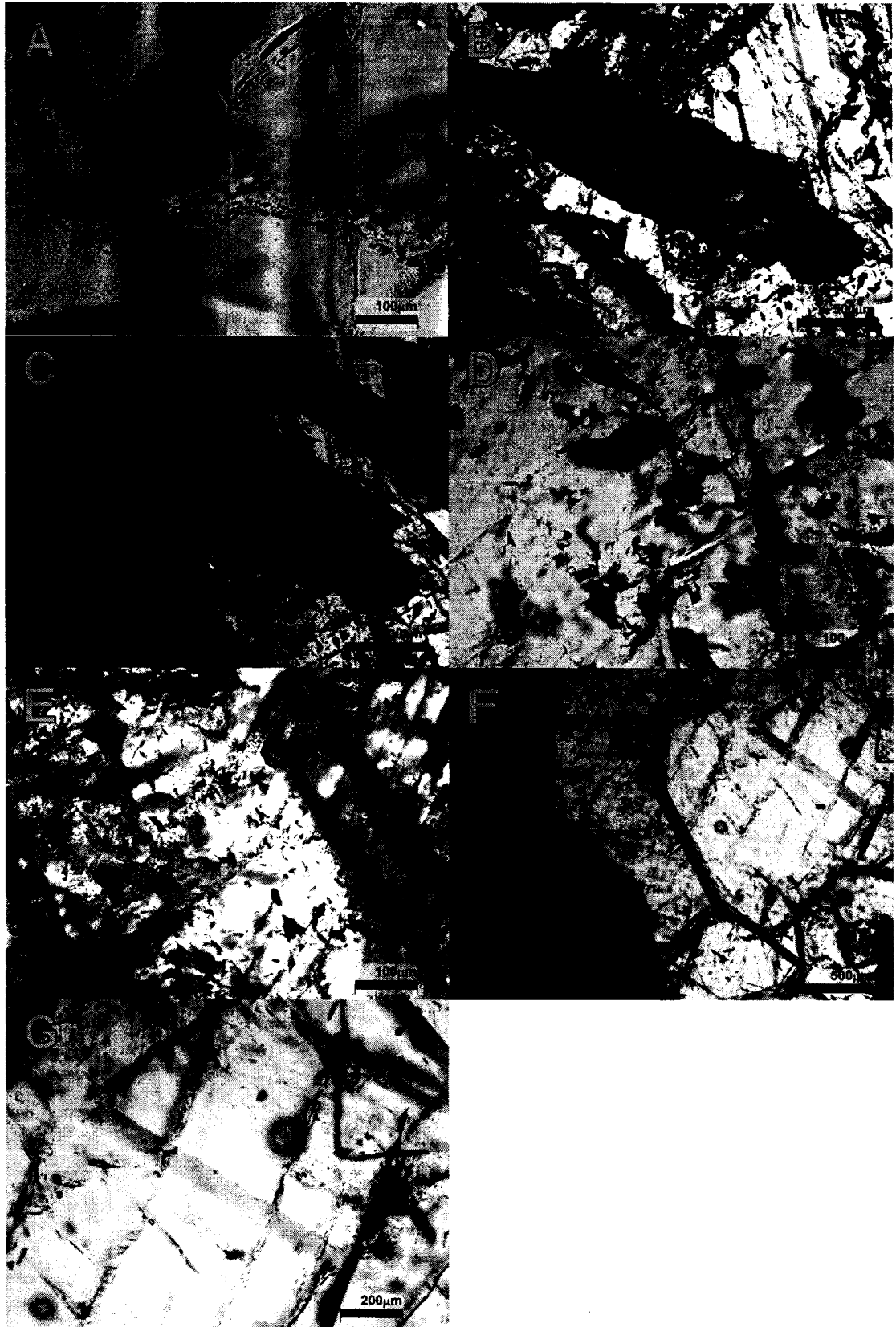


Plate 3.12

- A. Secondary fluid inclusion trails in calcite from sample N81-98 3205 355' photographed in plane polarized light.
- B. Photograph of late-stage calcite surrounding a broken clast of sphalerite from sample N81-98 3205 355' (viewed in plane polarized light).
- C. Same field of view as photograph (B) except viewed in crossed polarized light.
- D. Photograph of primary irregularly shaped calcite-hosted fluid inclusions from sample N81-98 3208 367' taken in plane polarized light.
- E. Fluid inclusion assemblages in calcite photographed in plane polarized light (sample N81-98 3214).
- F. Photograph of coarse white dolomite (dark) and calcite from sample N81-98 3225 450' viewed in plane polarized light.
- G. Secondary calcite-hosted fluid inclusion trails from sample N81-98 3225 450' photographed in plane polarized light.

Plate 3.12



## CHAPTER 4

### MICROTHERMOMETRIC ANALYSIS

#### 4.1 Introduction

The objectives of this microthermometric study were to: 1) establish minimum trapping temperatures for syn- and post-ore phases; 2) identify syn- and post-ore fluid salinities; and, 3) characterize syn- and post-ore fluid compositions. These objectives were achieved by carrying out microthermometric analysis on 11 phases from 9 drill core samples. Samples were selected to reflect syn-ore and post-ore fluids and include ore-related coarse white dolomite, sphalerite and late-stage calcite. The majority of phases were extremely difficult to work with. Host dolomite was often dark in thick section and had a very high number of fluid inclusions. This severely reduced the optical clarity of the mineral phase and consequently, no microthermometric analysis was possible on this phase. Coarse white dolomite had abundant small inclusions. The sheer quantities and very small size ( $<5\mu\text{m}$ ) of these inclusions made focussing on an assemblage or even a single inclusion very difficult. The small average size of the inclusions and reduced optical clarity made freezing measurements such as first melting, hydrohalite and ice melting temperatures very difficult to determine precisely. This is reflected in the uncertainties of the analysis ranging from  $\pm 0.3$  to  $\pm 1^\circ\text{C}$ . Sphalerite was often very dark in thick section and had a very small average inclusion size ( $<5\mu\text{m}$ ), which made finding microthermometrically-suitable inclusions difficult. Calcite was generally clear and colourless and frequently had larger inclusions, which made microthermometric analysis less difficult. Microthermometry was carried out on a transmitted-light microthermometric stage/microscope and as such opaque galena was not studied.

The integration of the petrographic results from Chapter 3 with this chapter's detailed fluid inclusion microthermometric analysis characterizes the composition of syn- and post-ore fluids in the N81 deposit. Microthermometric analytical procedures are outlined in Section 2.3.1. Microthermometric results are summarized in the following text and fluid inclusion petrographic descriptions are given in Sections 3.2 and 3.3, respectively.

#### 4.2 Background Information

Microthermometry is a non-destructive analytical technique that involves heating and freezing fluid inclusions to acquire fluid compositional data. Data obtained from microthermometry, such as minimum trapping temperatures, dominant salts present and fluid salinities, relies on the assumption that fluid inclusions are closed systems. During cooling,

after mineral crystallization, differential shrinkage occurs between a trapped mono-phase inclusion and the host mineral. This causes the formation of a contraction bubble, which gives the fluid inclusion a two-phase appearance at surface conditions. During microthermometry, heating this two-phase bubble to a temperature at which the vapour bubble disappears is the minimum trapping temperature for the inclusion. This temperature reflects the minimum crystallization temperature for the mineral host that contains the observed fluid inclusion and is more commonly referred to as homogenization temperature ( $T_h$ ). The homogenization temperatures are considered to be real trapping temperatures since the pressure correction is assumed to be negligible. Three sub-zero microthermometric measurements were attempted. First melting temperature ( $T_f$ ), also referred to as initial melting temperature in the literature, is the temperature at which melting was first observed in a fluid inclusion that was being heated from sub-zero conditions, after all the phases were in a solid frozen state. This is equivalent to the eutectic temperature for the system. Two additional melting temperatures were observed, hydrohalite ( $T_{m_{HH}}$ ) and ice ( $T_{m_{ice}}$ ) melting. These were used in determining salt composition and salinity, respectively (see Section 4.4). Hydrohalite is a salt hydrate ( $NaCl \cdot 2H_2O$ ) that is difficult to distinguish between ice but it often had (in this study) a brighter white colour and slightly higher relief than ice.

Microthermometric data from a total of 188 fluid inclusions from 11 phases of 9 drill core samples were obtained (see Appendix I). First melting was observed in 42 inclusions (37 from primary inclusions), hydrohalite melting was identified in 41 inclusions (34 from primary inclusions) and ice melting was observed in 63 primary inclusions (80 inclusions in total). Homogenization temperatures were derived from 186 fluid inclusions, 149 of these temperatures being observed in primary fluid inclusions, hosted by coarse white dolomite, sphalerite or calcite. The following section includes the microthermometric results for all the phases studied.

### **4.3 Microthermometric Results**

#### **4.3.1 Coarse White Dolomite**

First melting was often observed in primary coarse white dolomite-hosted inclusions. First melting temperatures were observed in 28 primary fluid inclusions and ranged from approximately  $-75^\circ C$  to  $-57^\circ C$ . During the subsequent heating of 25 primary inclusions in coarse white dolomite, hydrohalite was observed to melt from  $-56.5^\circ C$  to  $-31.0^\circ C$  (average  $T_{m_{HH}} = -43.4^\circ C$ ;  $n=25$ ; Figure 4.1). Upon further heating, ice melting was observed. Ice

melting from 40 primary coarse white dolomite-hosted inclusions occurred between  $-28.8^{\circ}\text{C}$  and  $-12.6^{\circ}\text{C}$  ( $T_{m_{ice}}$  average =  $-21.0^{\circ}\text{C}$ ;  $n=40$ ; Figure 4.2). Coarse white dolomite fluid inclusions homogenized into the liquid phase. Homogenization temperatures from 98 coarse white dolomite-hosted primary fluid inclusions ranged from  $56^{\circ}\text{C}$  to  $129^{\circ}\text{C}$  (average =  $82^{\circ}\text{C}$ ; see Appendix I and Figure 4.3). Data from four paragenetically undetermined coarse white dolomite-hosted inclusions are also included in Appendix I. No suitable secondary inclusions were found for microthermometric analysis therefore, no secondary inclusion data are reported for coarse white dolomite hosted fluid inclusions.

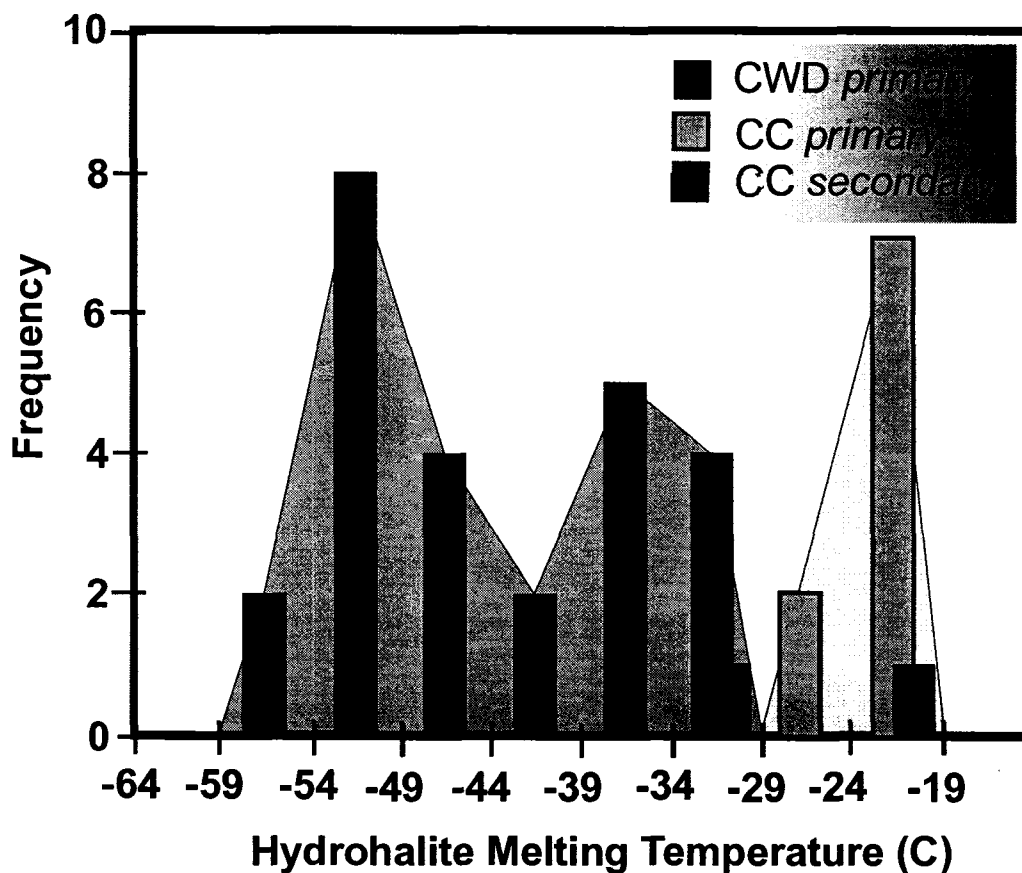


**Figure 4.1** A histogram of hydrohalite melting temperatures (CWD=coarse white dolomite; CC=calcite).

#### 4.3.2 Sphalerite

First melting and hydrohalite melting were not observed in sphalerite-hosted inclusions due to the poor optical clarity of this mineral phase and small size of the inclusions. Upon further heating, ice melting was observed in sphalerite. Sphalerite-hosted primary inclusions

yielded an average ice melting temperature of  $-17.4^{\circ}\text{C}$  (range =  $-17.7^{\circ}\text{C}$  to  $-16.9^{\circ}\text{C}$ ;  $n=3$ ; Figure 4.2). No values are reported for ice melting temperatures of secondary inclusions in sphalerite due to their very small size and the poor optical clarity of the sphalerite. Sphalerite-hosted primary and secondary fluid inclusions homogenized into the liquid phase. Primary sphalerite-hosted fluid inclusions had an average homogenization temperature of  $74^{\circ}\text{C}$  ( $n=4$ ; range =  $67^{\circ}\text{C}$  to  $80^{\circ}\text{C}$ ) (Figure 4.3). Secondary inclusions in sphalerite homogenized between  $60^{\circ}\text{C}$  and  $79^{\circ}\text{C}$  (average =  $70^{\circ}\text{C}$ ;  $n=2$ ) (see Appendix I). Data from three sphalerite-hosted inclusions that could not be paragenetically classified are included in Appendix I.

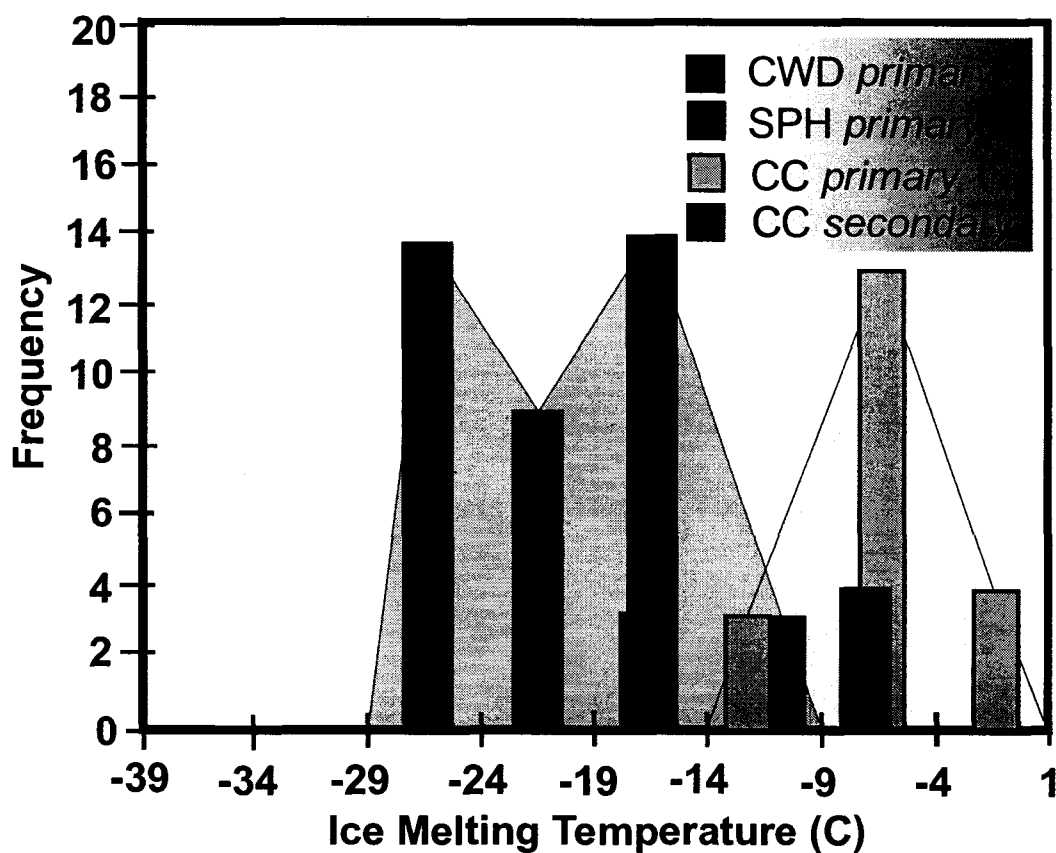


**Figure 4.2** A histogram of ice melting temperatures (CWD=coarse white dolomite; SPH=sphalerite; CC=calcite).

#### 4.3.3 Calcite

First melting was observed in 9 calcite-hosted primary inclusions between approximately  $-76^{\circ}\text{C}$  to  $-37^{\circ}\text{C}$ . Upon further heating, two other phase changes were observed, melting of hydrohalite and ice. Hydrohalite melting occurred between  $-27.5^{\circ}\text{C}$  and  $-20.0^{\circ}\text{C}$  in 9 primary

inclusions (average =  $-22.1^{\circ}\text{C}$ ; Figure 4.1). With further heating, melting of ice occurred. Ice melting was observed in 20 primary inclusions at temperatures between  $-11.3^{\circ}\text{C}$  and  $0.0^{\circ}\text{C}$  (average =  $-6.2^{\circ}\text{C}$ ;  $n=20$ ; Figure 4.2). Secondary inclusions yielded data. First melting was observed in two inclusions at approximately  $-64$  and  $-50^{\circ}\text{C}$ . Hydrohalite melting occurred between  $-30.0^{\circ}\text{C}$  and  $-20.0^{\circ}\text{C}$  (average =  $-25.0^{\circ}\text{C}$ ;  $n=2$ ). Upon further heating, ice melted between  $-8.8^{\circ}\text{C}$  and  $-6.9^{\circ}\text{C}$  (average =  $-7.8^{\circ}\text{C}$ ;  $n=4$ ). Calcite hosted primary and secondary fluid inclusions homogenized into the liquid phase. Primary inclusions homogenized between  $56$  and  $195^{\circ}\text{C}$  (average= $92^{\circ}\text{C}$ ;  $n=47$ ). Secondary inclusions homogenized between  $58^{\circ}\text{C}$  and  $109^{\circ}\text{C}$  (average= $77^{\circ}\text{C}$ ;  $n=11$ ; Figure 4.3). Calcite-hosted pseudosecondary inclusions yielded a homogenization range between  $63^{\circ}\text{C}$  and  $66^{\circ}\text{C}$  (average =  $64^{\circ}\text{C}$ ;  $n=3$ ). One hydrocarbon-rich inclusion (length =  $13.6\mu\text{m}$ ) was observed in calcite from sample N81-98 3208 367'. Calcite-hosted fluid inclusion microthermometric data is presented in Appendix I including data from 12 paragenetically unclassified calcite-hosted inclusions.

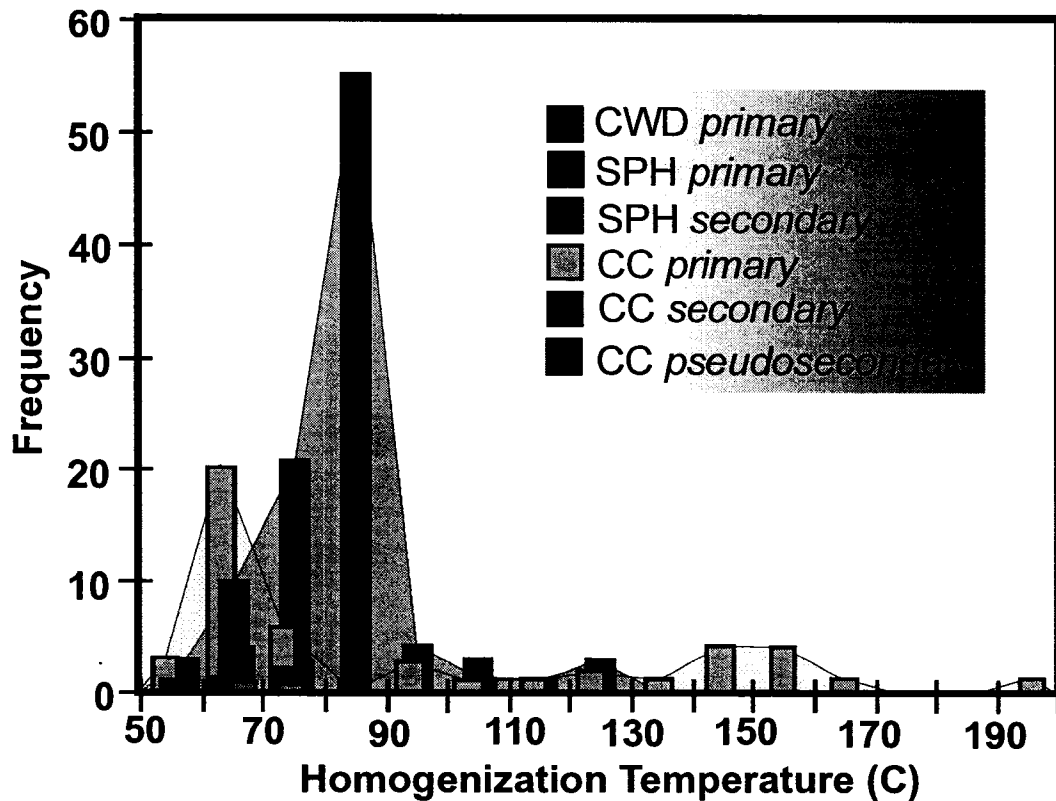


**Figure 4.3** A histogram of homogenization temperatures (CWD=coarse white dolomite; SPH=sphalerite; CC=calcite).

## 4.4 Interpretation

### 4.4.1 Calculation Information

Precise first melting temperatures were very difficult to determine due to small inclusion size and diminished optical clarity under high magnification. This difficulty can be seen in the values reported for first melting in Appendix I. The first melting is represented not by a specific temperature but by a temperature limitation (e.g. <-63°C). First melting temperatures were frequently very low (generally below -60°C) in the samples studied. This indicates that there were salts other than NaCl present. Eutectics for the H<sub>2</sub>O-NaCl-KCl and H<sub>2</sub>O-NaCl-CaCl<sub>2</sub> systems are -22.9 and approximately -52°C (Bodnar, 2003). First melting temperatures from coarse white dolomite and calcite-hosted fluid inclusions were closest to the eutectic of (and likely composed of) the H<sub>2</sub>O-NaCl-CaCl<sub>2</sub> system but were frequently much lower than its eutectic temperature (-52°C). This indicates that other divalent cations may be present, or more likely, that there is a metastable assemblage forming at low temperatures (Bodnar, 2003). Hydrohalite melting temperatures can be used to determine the sodium-calcium ratios of brines in fluid inclusions. This thesis uses the procedure outlined by Oakes et al. (1990) to determine Na-Ca ratios of the fluid inclusion brines. Fluid salinities can be calculated from ice melting temperatures of fluid inclusions. Figure 4.4 shows the salinity formula given by Bodnar, 1993 that is used to calculate salinity (wt% NaCl equivalent) from ice melting temperatures.

$$\begin{array}{l} \text{Salinity wt\%} \\ \text{NaCl Equiv.} \end{array} = 0 + [1.78 \times (T_{m_{ice}})] - [0.0442 \times (T_{m_{ice}})^2] - [0.000557 \times (T_{m_{ice}})^3]$$

**Figure 4.4** Formula used to derive salinity (from Bodnar, 1993).

### 4.4.2 Coarse White Dolomite

The depressed first melting temperatures (likely due to metastability of fluid components) are indicative of the breakdown of salt hydrates in the NaCl-CaCl<sub>2</sub>-H<sub>2</sub>O system. Hydrohalite melting temperatures from primary inclusions in coarse white dolomite indicate the fluids are calcic. These fluids have a weight fraction NaCl/(NaCl+CaCl<sub>2</sub>) range from 0.01 to 0.23 with an average of 0.05. This value can also be represented as Na:Ca of 0.05, indicating that the salts within the inclusions are highly calcic (some being composed of nearly pure

CaCl<sub>2</sub>). Eighty percent of the coarse white dolomite samples gave an average NaCl/(NaCl+CaCl<sub>2</sub>) of ≤0.06 (see Figure 4.5). Salinities derived from the ice melting temperatures of primary coarse white dolomite-hosted fluid inclusions (using the formula in Figure 4.4) ranged from 16.5 to 27.9 wt% CaCl<sub>2</sub>-NaCl equivalent (average = 23 wt% CaCl<sub>2</sub>-NaCl equivalent; n=39).

#### 4.4.3 Sphalerite

Sphalerite-hosted primary inclusions yielded an average ice melting temperature of -17.4°C and have a corresponding average salinity of 21wt% CaCl<sub>2</sub>-NaCl equivalent (n=3). This value is very similar to that of the fluids responsible for the precipitation of coarse white dolomite. This confirms petrographic evidence that the coarse white dolomite and sulphides are related and suggests that the phases likely precipitated from the same fluid.

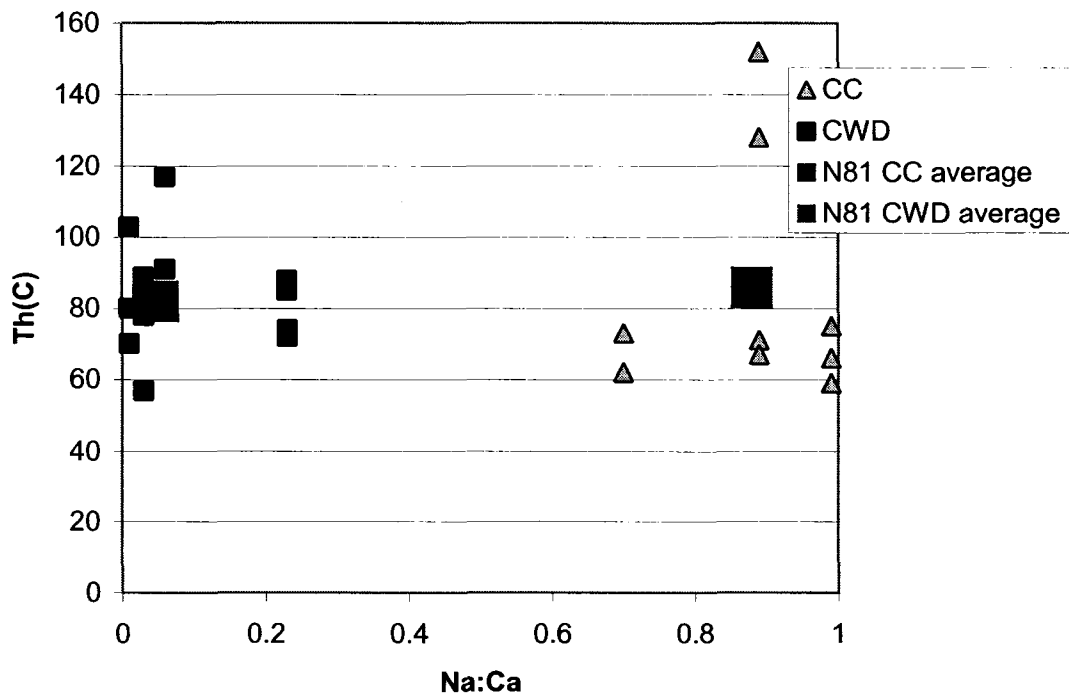


**Figure 4.5** Plot of homogenization temperatures and Na:Ca ratios from coarse white dolomite- and calcite-hosted fluid inclusions (CC=calcite and CWD=coarse white dolomite).

#### 4.4.4 Calcite

First melting was observed in 9 calcite-hosted primary inclusions between -76°C to -37°C. Similar to coarse white dolomite-hosted inclusions, the temperature of this group of phase changes indicates a breakdown of salt hydrates in the NaCl-CaCl<sub>2</sub>-H<sub>2</sub>O fluid ternary system.

The average hydrohalite melting temperature translates to a weight fraction NaCl/(NaCl+CaCl<sub>2</sub>) of 0.88. This high Na:Ca value (~0.9) indicates salts within the inclusions are composed primarily of NaCl. Salinities, as calculated from ice melting temperatures (Bodnar, 1993), had a range of 0 to 15.3 wt% NaCl-CaCl<sub>2</sub> equivalent (average = 9 wt% NaCl-CaCl<sub>2</sub> equivalent; n = 19). First melting (-64 and -50°C) and hydrohalite melting (-30.0°C and -20.0°C) temperatures observed in two secondary inclusions yielded values that fall within the range of the primary inclusion melting temperatures. Ice melting temperatures from secondary fluid inclusions indicate a salinity range of 10.4 and 12.6 wt% NaCl-CaCl<sub>2</sub> equivalent with an average of 11.4 wt % NaCl-CaCl<sub>2</sub> equivalent. The composition of the fluids and salinities of primary and secondary calcite-hosted inclusions confirms that the secondary inclusions will not substantially affect the salinity budget when bulk geochemical analyses are carried out on calcite phases.

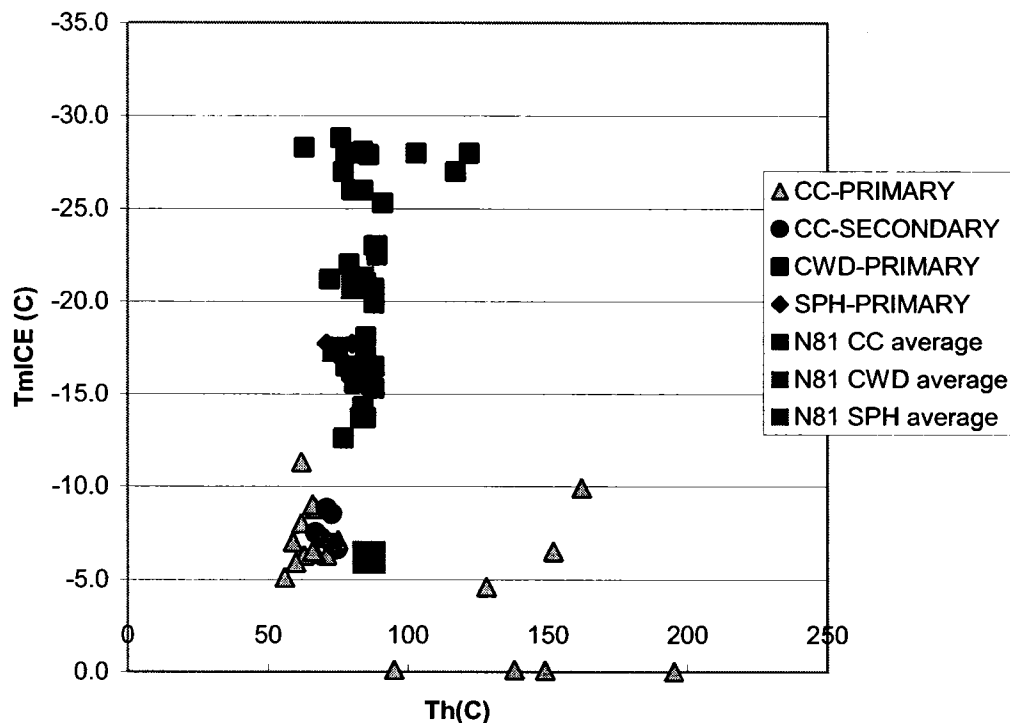


**Figure 4.6** Plot of ice melting and homogenization temperatures from calcite-, coarse white dolomite- and sphalerite-hosted primary inclusions (CC=calcite; CWD=coarse white dolomite; SPH=sphalerite).

#### 4.5 Discussion – Comparison of Phases

Primary coarse white dolomite hosted-inclusions are composed of high salinity calcic fluids with moderately variable trapping temperatures (Figures 4.3 and 4.5). The fluid responsible for the precipitation of this type of dolomite is similar to the fluid responsible for the precipitation of sphalerite and varies considerably from the fluid that precipitated the late-stage calcite. Sphalerite-hosted fluid inclusions, yielding consistent salinity values and generally consistent trapping temperatures, are similar to, and fall within, the fluid composition/temperature ranges of coarse white dolomite (see Figure 4.6). Both coarse white dolomite and sphalerite precipitating fluids appear to be similar in salinity and homogenization temperature and consequently, the two mineral phases have likely precipitated from the same fluid. This agrees with the petrographic association made between coarse white dolomite and sulphides in Chapter 3.

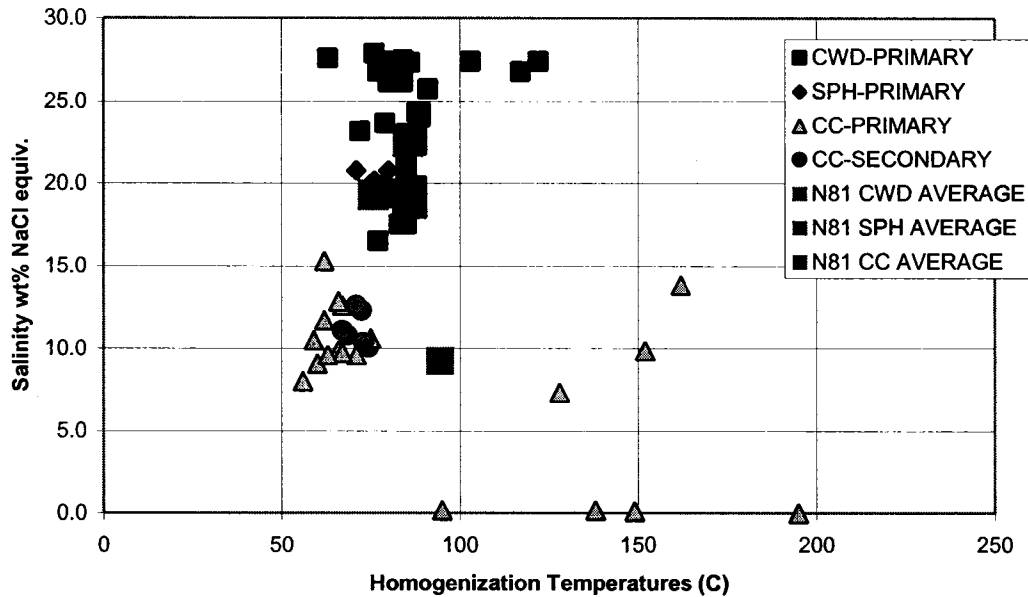


**Figure 4.7** Salinity and homogenization temperatures from calcite-, coarse white dolomite- and sphalerite-hosted primary inclusions.

Primary calcite-hosted inclusions yield lower salinity brines (Figure 4.2) with a much less calcic (higher Na:Ca) salt component (see Figures 4.2 and 4.5) compared to the fluid that precipitated the coarse white dolomite and sphalerite. Figure 4.9 demonstrates the difference

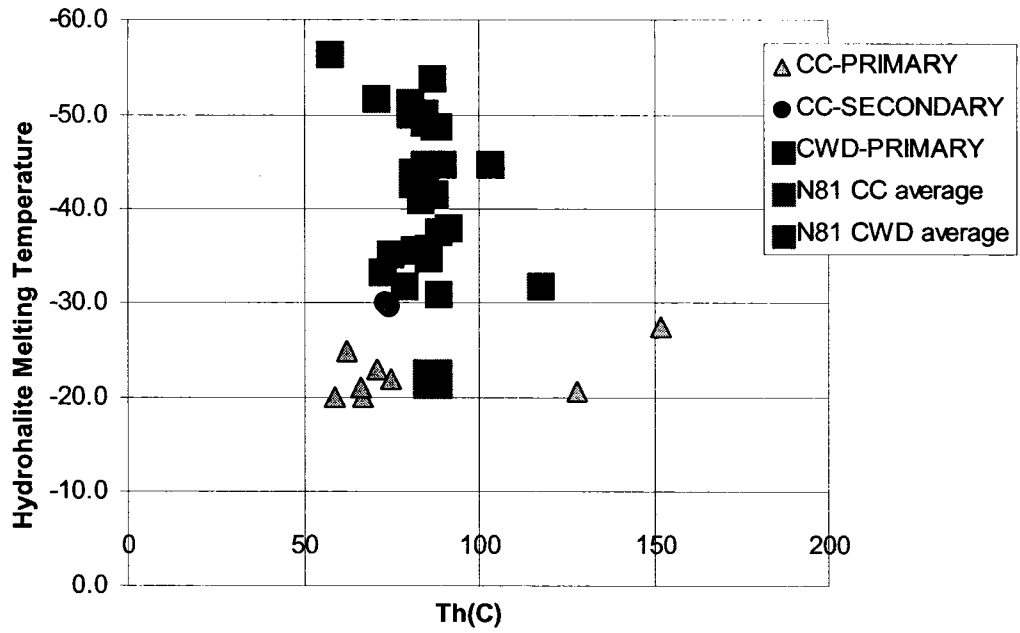


**Figure 4.8** Plot of hydrohalite melting and homogenization temperatures from coarse white dolomite- and calcite-hosted fluid inclusions (CC=calcite; CWD=coarse white dolomite).

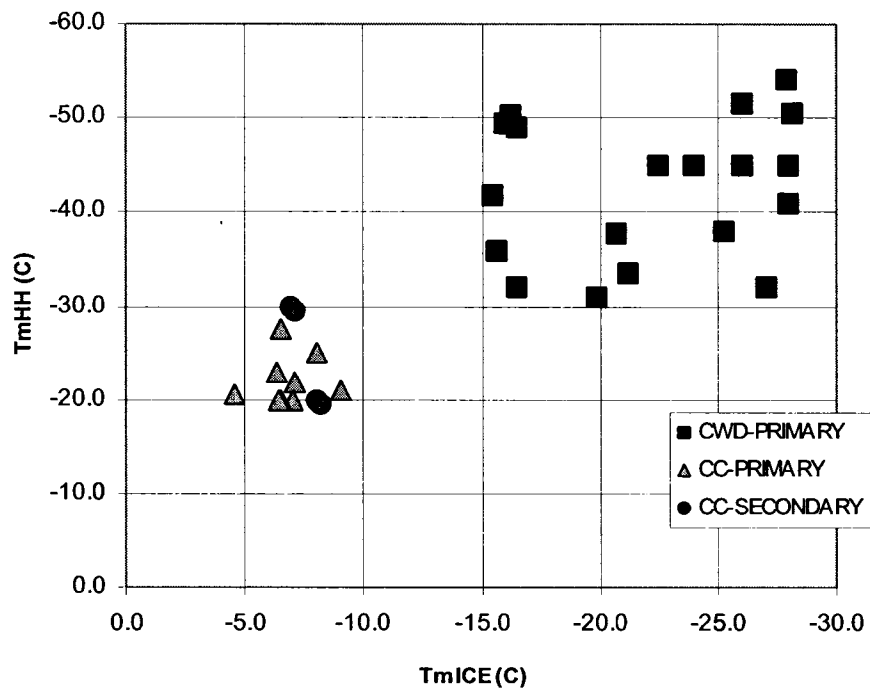


**Figure 4.9** Plot of hydrohalite and ice melting temperatures from coarse white dolomite- and calcite-hosted fluid inclusions.

between the brine composition of the two distinct fluids responsible for the precipitation of coarse white dolomite and calcite. Two separate fluids are visible in the plot as well as the similarity of primary and secondary fluid inclusion brine compositions in calcite-hosted inclusions. As noted previously, this similarity indicates that the saline budget for primary calcite-hosted inclusions will likely not be affected by secondary inclusions in the bulk geochemical analyses of Chapter 5.

Minimum trapping temperatures for the late-stage calcite phase are much more variable than those for both the sphalerite and coarse white dolomite (see Figure 4.6). The fluid responsible for precipitating calcite varies from approximately 50 to 200°C, whereas, the fluid precipitating coarse white dolomite and sphalerite average is more consistent and has an approximate minimum trapping temperature of 80°C (see Figure 4.3).

#### **4.6 Discussion – Comparison to Previous Microthermometric Analyses**

##### *4.6.1 Microthermometric Summary– Roedder (1968)*

Roedder (1968) carried out the first microthermometric study on Pine Point minerals. That study produced a small set of homogenization and ice melting temperatures but only mentioned the presence of hydrohalite. Sphalerite-hosted fluid inclusions gave homogenization temperatures ranging from 51 to 97°C ( $n_{Th}=112$ ) and an average calculated salinity of approximately 25 wt% NaCl equivalent ( $n_{T_{mice}}=133$ ). The high salinities were interpreted by Roedder (1968) to suggest that the mineralizing fluid resulted from the dissolution of evaporites. Dolomite-hosted fluid inclusions were also analyzed and gave homogenization temperatures of 90 to 100°C ( $n_{Th}=23$ ) and an average salinity of approximately 21 wt% NaCl equivalent (Roedder, 1968). No homogenization temperatures were reported from calcite-hosted fluid inclusions but fourteen ice melting temperatures gave an average salinity of approximately 5 wt% NaCl equivalent.

##### *4.6.2 Microthermometric Summary– Kyle (1977)*

In 1977, Kyle reported homogenization temperatures and salinities from microthermometry of sphalerite-hosted fluid inclusions. Fifty-six homogenization temperatures ranged from 51 to 99°C and 31 ice melting temperatures produced an average salinity of 20 wt% NaCl equivalent. Four celestite-hosted fluid inclusions were also analyzed and found to have a Th range of 86 to 98°C and salinity of 10 to 15wt % NaCl equivalent (Kyle, 1977).

4.6.3 *Microthermometric Summary—Qing (1991) & Qing & Mountjoy (1992)*

Limited microthermometric work on assumed primary inclusions in coarse crystalline and saddle dolomite from Pine Point and the adjacent area indicates that dolomitization occurred at temperatures that exceeded those allowed by maximum burial (Qing, 1991). Saddle dolomite microthermometry by Qing (1991) yielded homogenization temperatures of 85

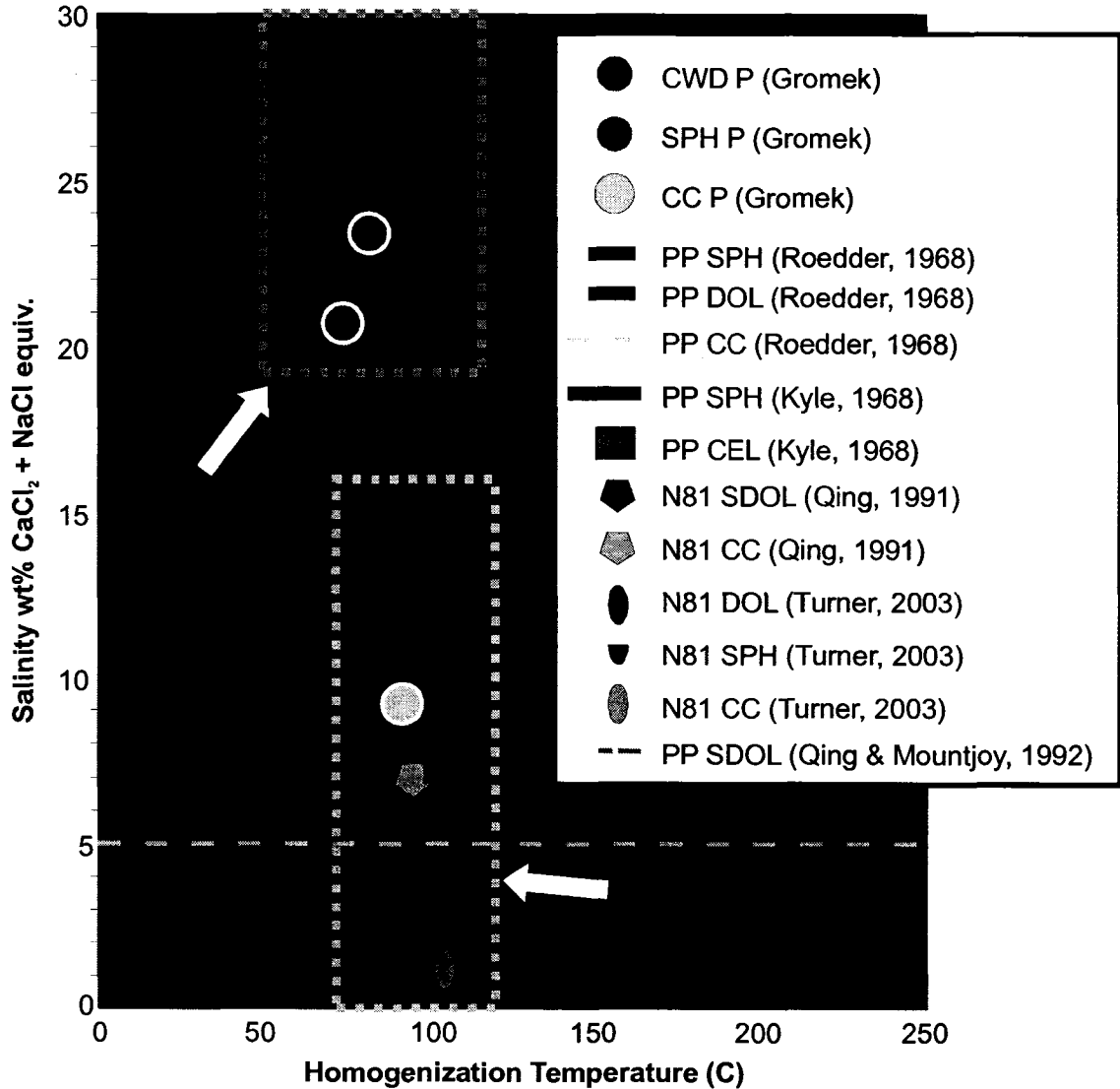


**Figure 4.10** A comparison plot of this study's findings and previous salinity and homogenization temperature data from the Pine Point ore region (CWD=coarse white dolomite; SPH=sphalerite; CC=calcite; CEL=celestite; SDOL=saddle dolomite; PP=Pine Point Mine).

to 210°C and salinities of 10 to 31 wt% NaCl equiv. Calcite-hosted fluid inclusions yielded homogenization temperatures of 70 to 176°C and ice melting temperatures of -3.6 to -15.1°C, equating to a salinity of 6 to 19 wt% NaCl equivalent. Saddle dolomite and calcite from the N81 deposit are also reported. Thirteen homogenization temperatures yielded an average of 106°C (95 to 118°C) and 2 ice melting temperatures averaged -22.8°C (24.5 wt% salinity). Calcite-hosted inclusions from Pit N81 yielded homogenization temperatures ranging from 71.8 to 124.5°C (average = 95°C; n = 8) and 8 ice melting temperatures averaging -4.5°C (range of -5.8 to -3.6°C; average salinity of 7.1 wt% NaCl). Although Qing (1991) infers a multi-component salt system (NaCl±CaCl<sub>2</sub>±KCl±MgCl<sub>2</sub>), no hydrohalite melting temperatures were recorded. Qing and Mountjoy (1992) published microthermometric data (homogenization and ice melting temperatures) from saddle dolomite-hosted fluid inclusions from the Presqu'île Barrier (Pine Point Barrier Complex). Homogenization temperature ranged from 92 to 178°C across the barrier, and locally at Pine Point from 92 to 106°C. These microthermometric data infer that hot saline brines were responsible for the precipitation of the saddle dolomite.

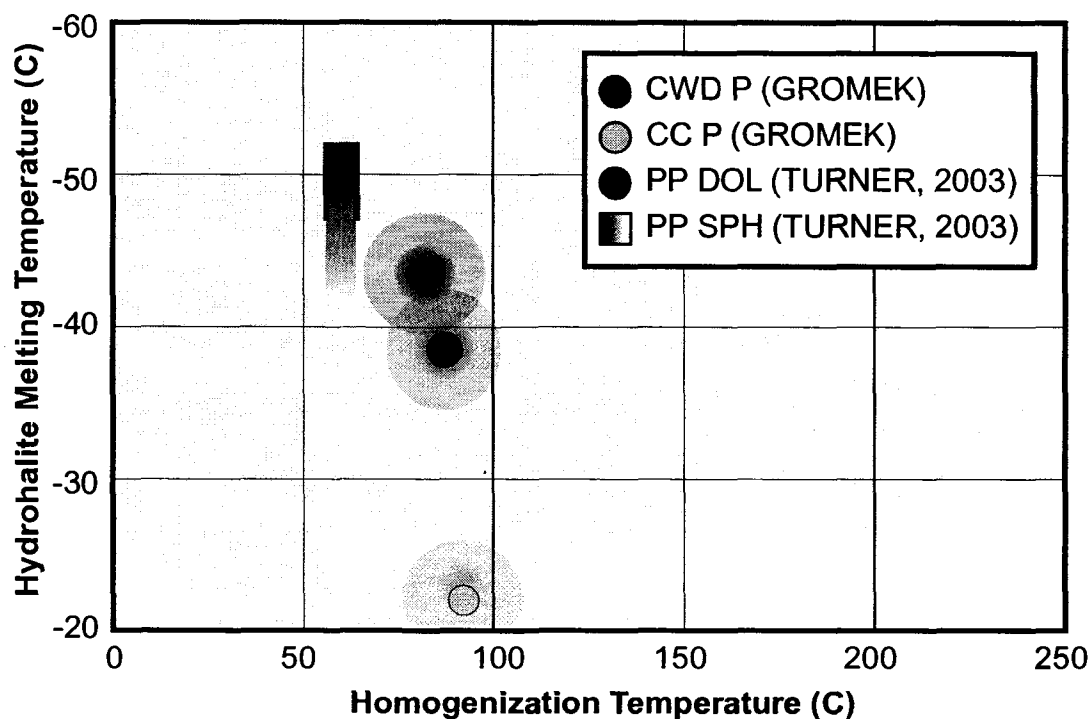


**Figure 4.11** A comparison plot of hydrohalite melting and homogenization temperatures between this study and the only other study to report hydrohalite melting temperature data (Turner, 2003).

#### 4.6.4 Microthermometric Summary– Turner (2003)

Turner (2003) produced microthermometric data from sphalerite, dolomite, saddle dolomite and calcite-hosted fluid inclusions. The data included hydrohalite and ice melting and homogenization temperatures. Two types of fluids were found from these data. “Type 1” fluid, comprised of dolomite and sphalerite-hosted inclusions, was characterized as a moderately low temperature (averages 86 to 100°C, respectively), high salinity, calcic brine (25 to 27 wt% CaCl<sub>2</sub>-NaCl) with a weight fraction NaCl (NaCl/NaCl+CaCl<sub>2</sub>) of less than 0.1 (dominantly CaCl<sub>2</sub> salt hydrates) and inferred to be directly involved in the mineralization process. “Type 2” fluid (calcite and celestite?) had a slightly lower temperature (~85°C) and salinity (average ~9wt% CaCl<sub>2</sub>-NaCl equivalent), hydrohalite melting temperatures indicative of a weight fraction NaCl (NaCl/NaCl+CaCl<sub>2</sub>) variance between 1 and 0.40 and is not inferred to be involved in the mineralization.

	T <sub>m<sub>HH</sub></sub> (°C)	n (T <sub>m<sub>HH</sub></sub> )	T <sub>m<sub>ice</sub></sub> (°C)	n (T <sub>m<sub>ice</sub></sub> )	Th (°C)	n (Th)
<b>CWD P</b>	-43.4	25	-21.0	40	82	98
<b>SPH P</b>	n/a	n/a	-17.4	3	74	4
<b>ORE FLUID*</b>	-43.4	25	-20.7	43	82	102
<b>CC P</b>	-22.1	9	-5.8	20	92	47
<b>CWD S</b>	n/a	n/a	n/a	n/a	n/a	n/a
<b>SPH S</b>	n/a	n/a	n/a	n/a	70	2
<b>CC S</b>	-25	2	-7.8	4	77	11
<b>CWD PS</b>	n/a	n/a	n/a	n/a	n/a	n/a
<b>SPH PS</b>	n/a	n/a	n/a	n/a	n/a	n/a
<b>CC PS</b>	n/a	n/a	n/a	n/a	64	3

**Table 4.1** Average microthermometric results from this study (CWD=coarse white dolomite; SPH=sphalerite; CC=calcite; P=primary; S=secondary; PS=pseudosecondary; ORE FLUID\*=primary fluid inclusion data from coarse white dolomite and sphalerite).

#### 4.6.5 Comparison of Previous Microthermometric Data to this Study

A summary of the previously discussed microthermometric data from the Pine Point mine site and data from Pine Point surrounding and/or related regions are reported in Appendix III. A graphical representation of all Pine Point mine site microthermometric data is shown in Figure 4.10. The diagram confirms, as previously established in Section 4.5, two distinct fluid regimes involved in the Pine Point ore field. A high salinity (~20 to 30 wt% CaCl<sub>2</sub>-NaCl equivalent), calcic and moderately warm brine related to ore mineralization and a less saline (~0 to 15 wt% NaCl-CaCl<sub>2</sub> equivalent), slightly warmer brine responsible for the precipitation of

late-stage calcite. Although coarse white dolomite fluid inclusions show a range of salinities, they have fairly consistent homogenization temperatures (see Figure 4.7). This may be indicative of mixing and will be further examined in the bulk geochemical and strontium isotopic analyses. Figure 4.7 also suggests that the late-stage fluids may be formed from the mixing of two fluids (a lower temperature moderately saline brine and a higher temperature fluid with a very low salinity) or from meteoric water that is dissolving halite in various amounts.

#### **4.7 Remarks**

This microthermometric chapter characterizes the salinity, salt composition and trapping temperatures of the precipitating fluids involved in the N81 deposit. It is evident that at least two fluids are responsible in precipitated mineral phases in the N81 deposit. Coarse white dolomite and sphalerite-precipitating fluids are very similar and potentially have the same source. Bulk geochemical analyses on host and coarse white dolomite, sulphide and calcite mineral phases are outlined in the following chapter and will further characterize the fluids involved in the deposit and the relationships between them. Chapter 6 will provide additional geochemical data to characterize the precipitating fluids via reporting strontium isotopic data from coarse white dolomite and calcite.

Plate 4.0

- A. A primary coarse white dolomite hosted fluid inclusions at 25°C from sample N81-65 0249 photographed in plane polarized light.
- B. Same area as photograph (A) except photographed under high magnification. Photograph of primary coarse white dolomite hosted fluid inclusions at 24°C from sample N81-65 0249 (viewed in plane polarized light).
- C. A primary fluid inclusion in coarse white dolomite from sample N81-65 0249 photographed in plane polarized light at 23°C.
- D. A primary fluid inclusion in coarse white dolomite (saddle-texture variety) from sample N81-65 0249 photographed at 45°C in plane polarized light.
- E. A primary fluid inclusion in coarse white dolomite from sample N81-75 3386 322' viewed in plane polarized light at -55°C.
- F. A coarse white dolomite-hosted primary fluid inclusion from drill core sample N81-75 3386 322' photographed at -22°C in plane polarized light.
- G. Photograph of a primary coarse white dolomite-hosted fluid inclusion from sample N81-75 3386 322' showing both hydrohalite and ice at -44°C (viewed in plane polarized light).
- H. Same field of view as previous photograph (G) except at -23°C (no hydrohalite is visible).

Plate 4.0



Plate 4.1

- A. A primary fluid inclusion in coarse white dolomite from sample N81-84 1078 viewed in plane polarized light at 45°C.
- B. A large primary fluid inclusion in coarse white dolomite from drill core sample N81-84 1078 at 26°C and photographed in plane polarized light.
- C. Photograph of a primary fluid inclusion (see dashed circle) in coarse white dolomite from sample N81-84 1078. Photograph taken in plane polarized light at 27°C.
- D. A primary fluid inclusion in coarse white dolomite from sample N81-84 1078 at 23°C (viewed in plane polarized light).
- E. Photograph taken in plane polarized light of a primary fluid inclusion in coarse white dolomite at 35°C (from sample N81-98 3205 360').
- F. A primary fluid inclusion in coarse white dolomite from sample N81-98 3205 360' in plane polarized light at 67°C.
- G. A large primary fluid inclusion in coarse white dolomite from sample N81-98 3205 360' photographed in plane polarized light at 23°C.
- H. Same field of view as above photograph (G) except at -70°C.

Plate 4.1

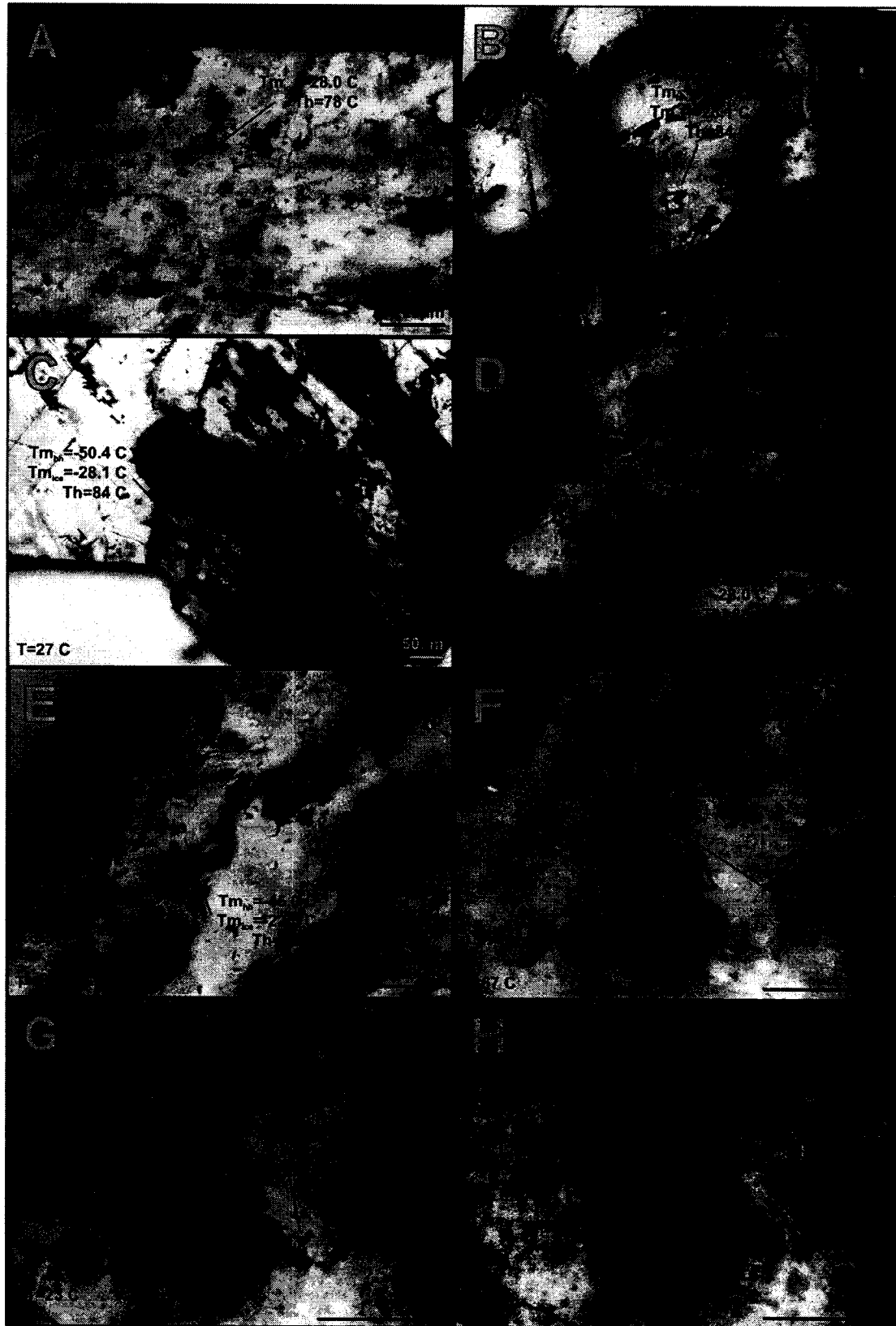


Plate 4.2

A. Photograph of a primary coarse white dolomite-hosted fluid inclusion at 67°C from sample N81-98 3205 360' (viewed in plane polarized light).

B. Primary inclusions hosted by coarse white dolomite from sample N81-98 3225 450' (photographed in plane polarized light).

C. Primary inclusions in coarse white dolomite from sample N81-98 3225 450' (photographed in plane polarized light).

D. Photograph of a primary inclusion hosted by coarse white dolomite from sample N81-98 3225 450' (viewed in plane polarized light).

Plate 4.2

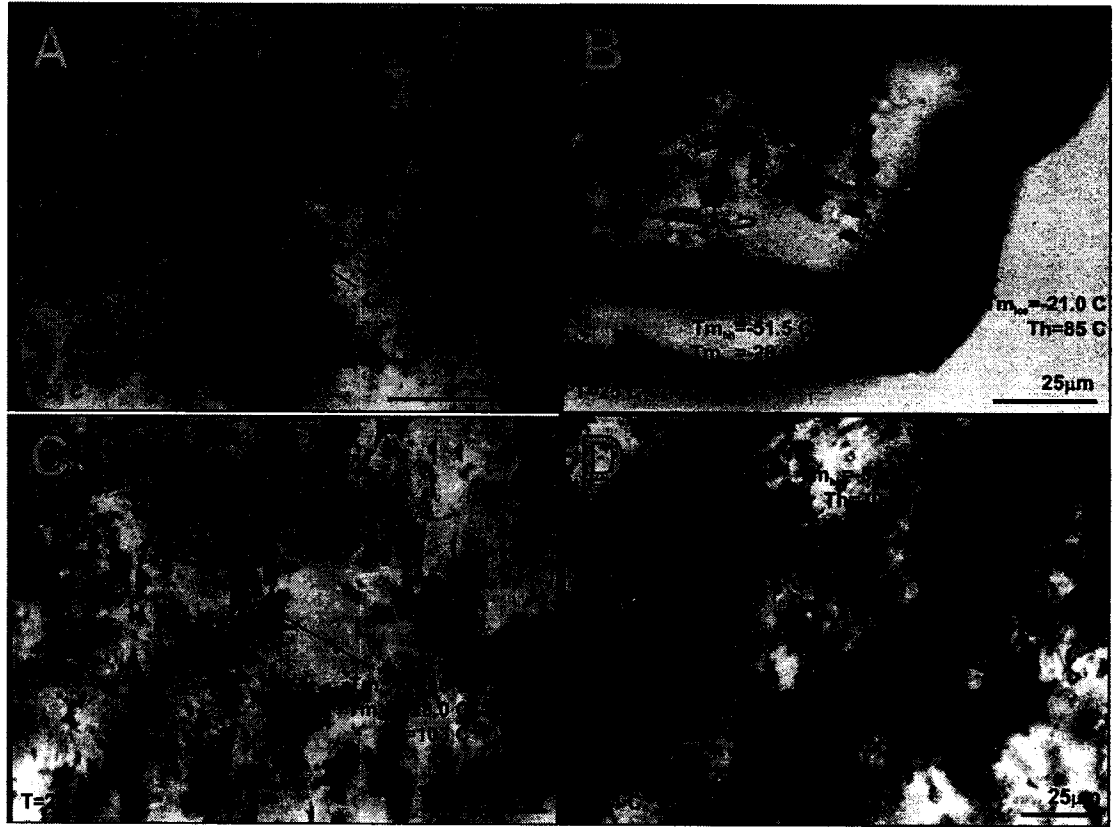


Plate 4.3

A. Photograph of a secondary fluid inclusion trail in sphalerite from sample N81-98 3205 360' at 45°C (photographed in plane polarized light).

B. A large primary sphalerite-hosted fluid inclusion from sample N81-98 3205 360' photographed in plane polarized light at 23°C.

C. Photograph of a healed fracture in sphalerite with secondary inclusions from sample N81-98 3205 360'. Photographed at 61°C in plane polarized light.

Plate 4.3

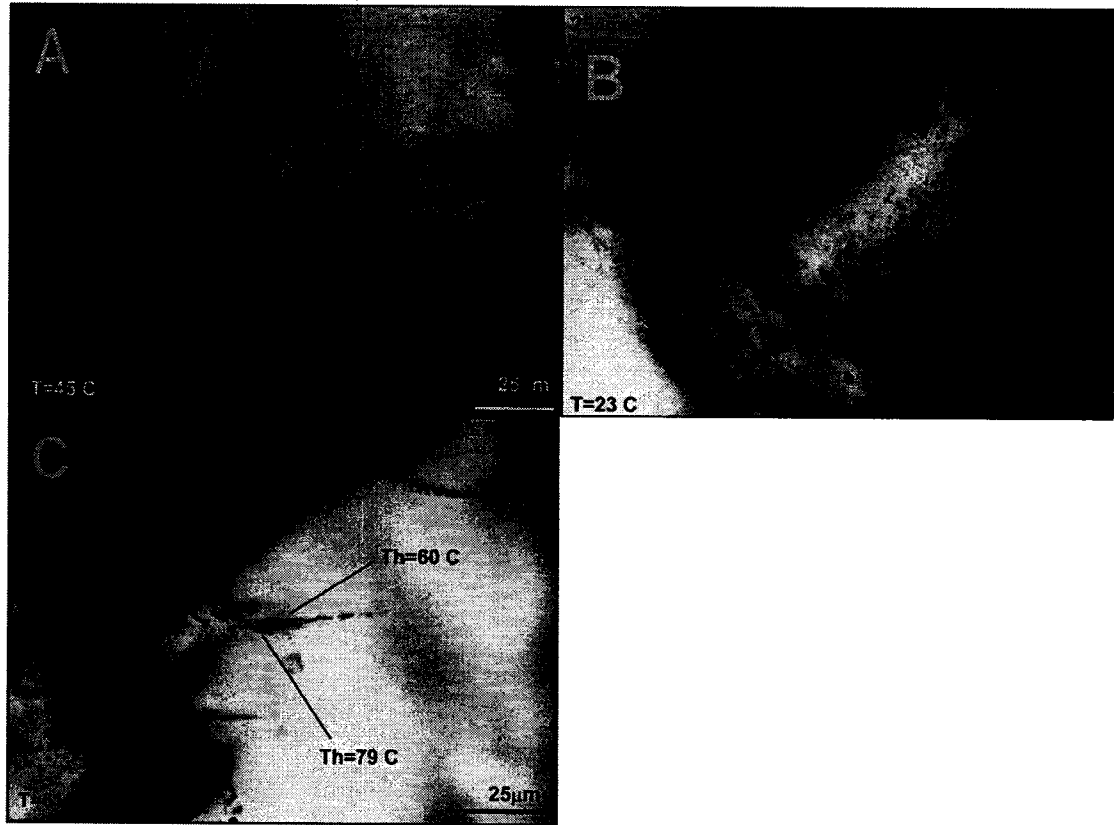


Plate 4.4

A. A calcite-hosted secondary inclusion trail photographed at 62°C in plane polarized light (from sample N81-68A 2969 375').

B. Photograph of a primary calcite-hosted fluid inclusion (L-V) at 70°C from sample N81-68A 2969 375' (viewed in plane polarized light).

C. Photograph of a primary calcite-hosted fluid inclusion (L-V) from sample N81-68A 2969 375'. Photographed at 40°C in plane polarized light.

D. A primary calcite-hosted fluid inclusion (L-V) from sample N81-68A 2969 375' photographed at 22°C in plane polarized light.

E. Photograph of a large primary calcite-hosted fluid inclusion from sample N81-98 3208 367' at -63°C in plane polarized light (note the secondary inclusion trail above and to the left of the specified inclusion).

F. Calcite-hosted primary fluid inclusion at -71°C from sample N81-98 3208 367' (photographed in plane polarized light).

G. A large primary fluid inclusion in calcite from sample N81-98 3181 287' photographed in plane polarized light at 23°C. Very small sphalerite-hosted inclusions are visible in the top portion of the photograph.

H. Photograph of the calcite-hosted inclusion from photograph (G) photographed under higher magnification and taken in plane polarized light at 25°C.

Plate 4.4

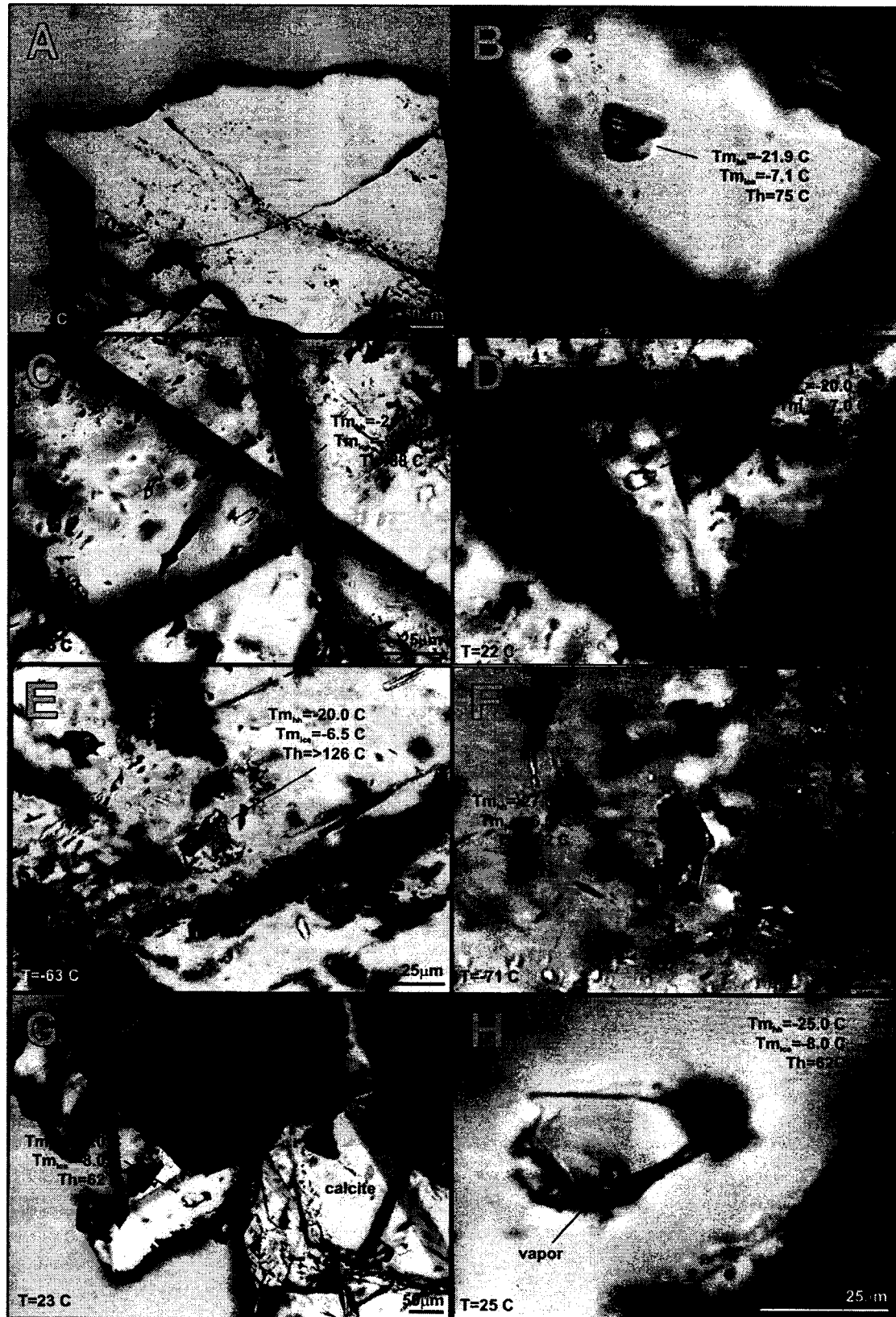


Plate 4.5

A. Photograph showing examples of necked secondary fluid inclusions in calcite from sample N81-98 3181 287'. Photographed in plane polarized light at 47°C.

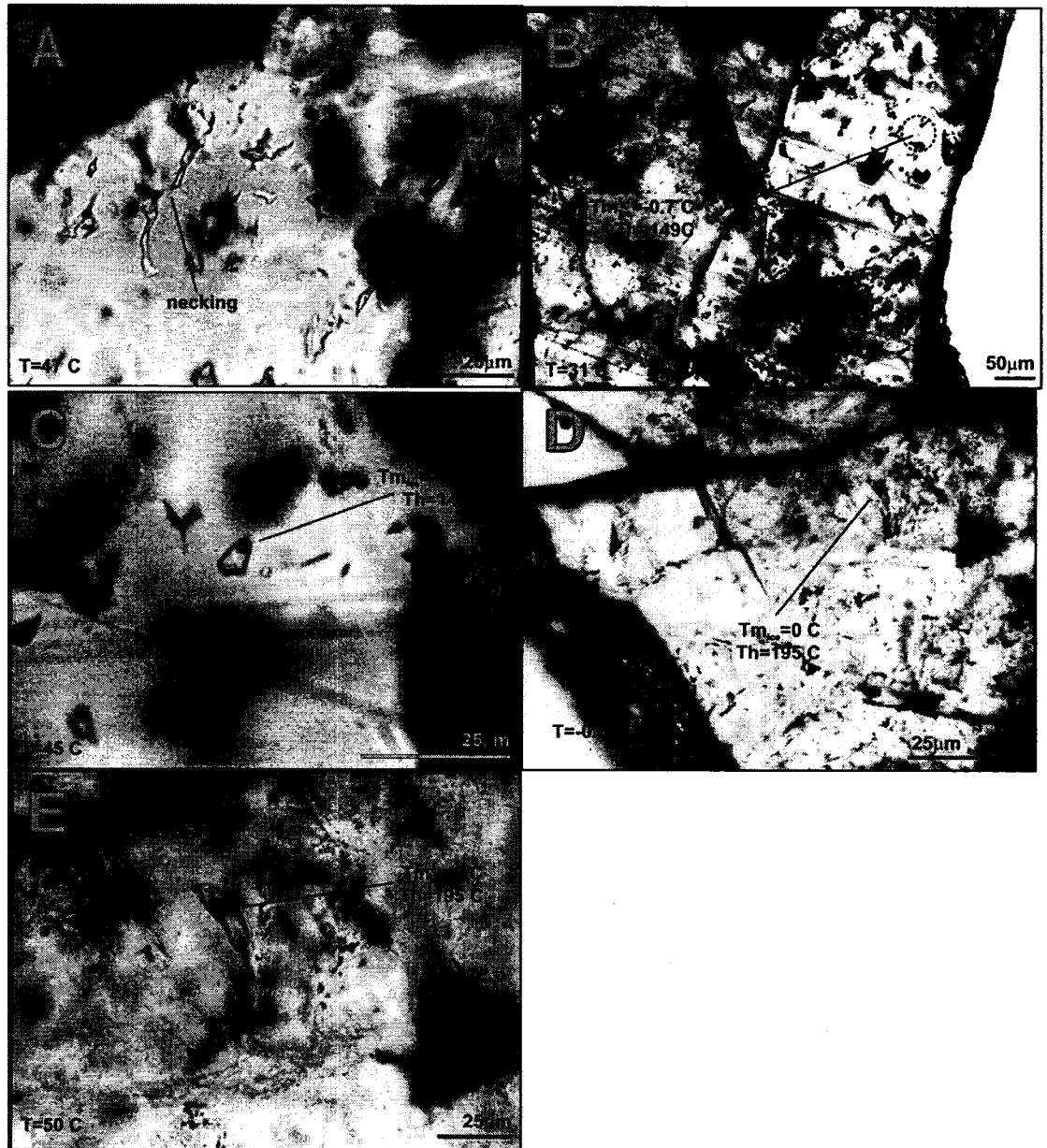
B. A calcite-hosted primary fluid inclusion (dashed circle) from sample N81-98 3214 photographed at 31°C in plane polarized light.

C. Photograph of the same fluid inclusion highlighted in photograph (B) except under a higher magnification. Photograph taken in plane polarized light at 45°C.

D. Calcite-hosted primary fluid inclusion with a  $T_{m_{ice}}$  value of 0°C from sample N81-98 3214. Photographed in plane polarized light at -0.6°C.

E. Photograph of the same inclusion highlighted in photograph (D) except under higher magnification and at 50°C (viewed in plane polarized light).

Plate 4.5



## CHAPTER 5

### BULK FLUID INCLUSION ANALYSIS

#### 5.1 Introduction

The objectives of the bulk fluid inclusion analyses were to: 1) ascertain the origin of mineralizing and non-mineralizing fluids in deposit N81; 2) provide insight into the fluid evolution (e.g. water-rock interaction) along the flow path to the site of mineralization; and 3) speculate whether mixing took place in the ore system. Bulk fluid inclusion studies allowed analysis of the cation and anion composition of fluid inclusions trapped in carbonates and sulphides in the N81 deposit. The objectives of this chapter were achieved by analyzing leachates produced by the crush-leach technique by ion chromatography, atomic absorption spectrometry (AAS) and inductively coupled plasma-mass spectrometry (ICP-MS). Data were acquired from host dolomite, coarse white dolomite, sulphide and calcite fluid inclusion leachate samples, which represented pre-, syn- and post-ore phases at the deposit. The results of this chapter were interpreted with the data from the petrographic and microthermometric analyses of Chapters 3 and 4. The analytical techniques of the three geochemical approaches used in this chapter are described in Section 2.3.2.

#### 5.2 Sample Selection

Carbonate and sulphide mineral phases were selected for bulk geochemical analysis based on the amount of material, purity and paragenetic relevance. Host dolomite, coarse white dolomite, sulphide and calcite samples were selected to represent the paragenetic sequence. In total, the crush-leach technique was carried out on 36 samples from 15 N81 deposit drill cores and one float sample from the P-41 pit. The leachate produced by the crush-leach technique was analyzed for major anions via ion chromatography and major and minor cations via AAS and ICP-MS analyses.

Thirty-six samples were analyzed for  $\text{Cl}^-$ ,  $\text{Br}^-$ ,  $\text{F}^-$ ,  $\text{SO}_4^{2-}$ ,  $\text{PO}_4^{3-}$  and  $\text{NO}_3^-$  by ion chromatography and routinely yielded data for  $\text{Cl}^-$ ,  $\text{Br}^-$ ,  $\text{F}^-$  and  $\text{SO}_4^{2-}$  (see Appendix IV). Host dolomite sample leachates from 5 drill cores were analyzed by ion chromatography and yielded 5  $\text{Cl}^-$ , 5  $\text{Br}^-$ , 5  $\text{F}^-$  and 5  $\text{SO}_4^{2-}$  concentrations. Coarse white dolomites from 5 drill cores were also analyzed and generated the following ion chromatographic data: 5  $\text{Cl}^-$ , 5  $\text{Br}^-$ , 5  $\text{F}^-$  and 5  $\text{SO}_4^{2-}$  values. Two samples of dolomite (unspecified variety) leachates were analyzed and yielded 2  $\text{Cl}^-$ , 1  $\text{Br}^-$ , 2  $\text{F}^-$  and 2  $\text{SO}_4^{2-}$  values. Sphalerite leachates from eight drill cores and one float sample were selected for ion chromatography and yielded 10  $\text{Cl}^-$  (including one duplicate),

9 Br<sup>-</sup> and 2 F<sup>-</sup> concentrations. Galena leachates from 4 drill cores yielded 4 Cl<sup>-</sup>, 4 Br<sup>-</sup> and one F<sup>-</sup> value. Sulphate concentrations for sphalerite and galena were not reported due to contamination issues (see Section 5.4.1). Calcite leachates from 9 drill cores and one float sample were analyzed and yielded 10 Cl<sup>-</sup>, 5 Br<sup>-</sup>, 9 F<sup>-</sup> and 10 SO<sub>4</sub><sup>2-</sup> values above the detection limits.

	HDOL	CWD	DOL	SPH	GN	CC
IC	5	5	3	9+1 DUP	4	10
AAS	5	5	2	8	2	10
ICP-MS	3	4	2	8	2	5

**Figure 5.1** Numeric summary of drill core and float samples analyzed by bulk geochemistry (IC = ion chromatography; AAS = atomic absorption spectroscopy; ICP-MS = inductively coupled plasma-mass spectrometry; HDOL = host dolomite; CWD = coarse white dolomite; DOL = dolomite (unspecified variety); SPH = sphalerite; GN = galena; CC = calcite; DUP = duplicate).

Thirty-two sample leachates were analyzed via AAS analysis and yielded data for Na, K and Li above the detection limits of the technique (Appendix V). Five drill core samples containing host dolomite were selected for AAS and yielded the following data: 5 Na, 3 K and one Li value. Five Na, 5 K and one Li value was attained from coarse white dolomite-hosted leachates from 5 drill cores. Two samples of dolomite (unspecified variety) leachates were analyzed and yielded 2 Na, and one K value. Sphalerite leachates from seven drill cores and one float sample were selected for AAS analysis and yielded 8 Na values. Two galena leachates were analyzed and data from them includes 2 Na levels. Nine drill core and one float sample calcite leachates yielded 10 Na, 5 K and one Li value.

Twenty-four separately picked La-doped leachates were analyzed by ICP-MS which routinely detected sixteen elements including Ca, Mg, Na, K, Fe, Mn, S, Ba, B, Cd, Co, Pb, Li, Ni, Sr and Zn (Appendix VI). Host dolomite from 3 drill core samples, coarse white dolomite from 4 drill samples and dolomite (unspecified variety) from 2 drills cores were selected for ICP-MS analysis. One float sample and 7 drill core samples containing sphalerite, 2 samples

containing galena and 4 drill core and one float sample containing calcite were also selected for ICP-MS analysis.

### 5.3 Suitability of Samples

Bulk fluid inclusion analyses can be carried out only if the samples are dominated by one fluid inclusion population. Inclusions in host and coarse white dolomite, and to a lesser extent sphalerite, were clearly primary and were abundant. Secondary inclusions were very rare in the coarse white dolomite and occurred occasionally in sphalerite phases and as such were thought to not have substantially affected the average salinity budget of the leachates. Therefore, these samples were very suitable for this kind of bulk study.

Calcite yielded similar microthermometric data (see Section 4.4.4) from primary and secondary inclusions. This similarity suggests that the secondary inclusions may have a composition similar to those of the primary inclusions and will not substantially affect the bulk geochemical analyses. Therefore, it is likely that in all the samples analysed the bulk geochemical data of this chapter should be representative of the fluids that precipitated the mineral phases.

## 5.4 Results

### 5.4.1 Contamination

Calcium concentrations for calcite leachates and calcium and magnesium concentrations for dolomite leachates were not reported as the leachates were dominated by the elements present in the host mineral. Similarly, sulphate concentrations for sphalerite and galena hosted leachates were not reported and lead and zinc concentration, respectively, were considered to have been contaminated by the host mineral for galena and sphalerite. Although mineral phases were carefully hand picked under a microscope it is evident from some of the geochemical data in some samples that tiny inclusions or intergrowths were present, which were not visible on the surface of the grains being picked. For example, the host dolomite phases often had growths of galena and sphalerite. Samples N81-69 2764 235' HDOL (177.01 ppm  $\text{SO}_4^{2-}$ ) and N81-69 2758 217' HDOL (364.07 ppm  $\text{SO}_4^{2-}$ ) had abnormally high  $\text{SO}_4^{2-}$  levels and both also had elevated Pb and/or Zn contents (see Table 5.7). Sample N81-69 2764 235' HDOL also may also have been contaminated by pyrite since it was the only sample where the Fe concentration was above the detection limit of the ICP-MS analysis. Host dolomite from sample N81-69 2766 240' had relatively elevated zinc and sulphur concentrations, which may

be due to some level of sphalerite contamination. Sample N81-98 3205 355' CC had an elevated  $\text{SO}_4^{2-}$  level (25.75 ppm) but contamination by celestite ( $\text{SrSO}_4$ ) could not be confirmed due to a lack of Sr data from the ICP-MS analysis. There is no indication that any of the phases of coarse white dolomite had been contaminated.

#### 5.4.2 Charge Balance

A major concern with crush-leach analysis is whether ionic concentrations in the leachates are purely fluid inclusion derived or whether there has been contamination by the host mineral. Charge balance calculations can be useful in assessing the quality of the data since the charge on most hydrothermal fluids is neutral (Shepherd et al., 1985). If cation and anion data are reported for the fluids, charge balances can be calculated using the equation from Shepherd et al. (1985) (see Figure 5.2). Charge balance calculations were carried out on samples analyzed by ion chromatography and AAS analyses. The charge balance calculation used anion data from ion chromatography ( $\text{Cl}^-$ ,  $\text{Br}^-$ ,  $\text{F}^-$  and  $\text{SO}_4^{2-}$ ) and major cation data from AAS analysis (Na, K and Li), both sets of data were acquired from the same leachate.

$$\text{CB} = \frac{\sum \text{charge} \times (\text{concentration/atomic weight})_{\text{cation}}}{\sum \text{charge} \times (\text{concentration/atomic weight})_{\text{anion}}}$$

**Figure 5.2** Charge balance (CB) equation based on Shepherd et al. (1985) (see Table 5.1 for concentration and charge balance data).

The charge balance values were generally consistent for all data. The charge balance from the host dolomite phases varied from 0.06 to 0.35, coarse white dolomite ranged from 0.13 to 0.25 and the unspecified dolomite phase had a charge balance of 0.13 (see Table 5.1). All of these values suggest an excess of anions in the fluids. Microthermometric data suggest the brines were Ca-rich so the cation deficiency was likely due to the lack of calcium and magnesium data.

Sample	Phase	Charge Balance	IC				AAS			
			ppm Cl	ppm Br	ppm F	ppm SO <sub>4</sub>	ppm Na	ppm K	ppm Li	
N81-65 0249	HDOL	0.29	76.98	0.530	0.177	10.17	21.50	7.00	-	
N81-69 2754 195'	HDOL	0.35	39.46	0.251	0.012	12.99	14.48	8.32	0.0024	
N81-69 2764 235'	HDOL	0.06	105.16	0.889	0.365	177.01	17.04	12.30	-	
N81-69 2766 240'	HDOL	0.06	46.39	0.298	0.254	54.66	9.00	-	-	
N81-65 0249	CWD	0.21	191.57	1.442	0.727	43.64	48.00	9.90	-	
N81-84 1078	CWD	0.25	183.06	1.289	0.483	5.04	41.70	7.80	-	
N81-98 3205 360'	CWD	0.22	201.62	1.463	0.542	13.87	42.75	8.40	-	
N81-98 3225 450'	CWD	0.13	472.76	4.065	0.534	93.50	72.40	17.20	0.0120	
N81-98 3205 355'	DOL	0.13	108.01	-	0.073	48.76	22.38	4.32	-	

**Table 5.1** Data used in the calculation of charge balance using ion chromatography (IC) and AAS data (HDOL=host dolomite, CWD=coarse white dolomite, DOL=dolomite (unspecified variety)).

#### 5.4.3 Ratios versus Absolute Data

Concentration data obtained from bulk geochemical analysis represent a specific volume of leachate analyzed. These values do not represent the concentration of the elements in a precipitating fluid; they represent the amount of ions/elements from an unknown number of fluid inclusions from a specific volume of leachate analyzed (e.g. fluid inclusion-rich coarse white dolomite will always have higher Cl<sup>-</sup> values than calcite which has much fewer less saline inclusions). In other words, higher salinity fluids would yield higher values of salt components such as Cl<sup>-</sup>. In order for comparisons to be carried out between samples, data is expressed in terms of molar element ratios (e.g. Cl/Br).

$$X \text{ (ppm)} = (\text{wt\% NaCl} \times 10000) \times \left[ \frac{\text{Cl}_{\text{a.w.}}}{\text{Cl}_{\text{a.w.}} + \text{Na}_{\text{a.w.}}} \right] \times \left[ \frac{X^*}{\text{Cl}_{\text{IC}}} \right]$$

**Figure 5.3** Formula used to calculate absolute concentrations using the salinity data acquired from microthermometry (Shepherd et al. (1985) (a.w. = atomic weight; IC = ion chromatography; X\* = raw data)

Absolute values were also presented in this chapter. These values were the calculated concentrations of elements within a precipitating fluid based on microthermometric analysis.

Ice melting temperatures yield data that can be calculated into a salinity wt% equivalent. Shepherd et al. (1985) developed a formula that incorporates salinity wt% equivalent, molecular weights and raw data from ion chromatography to give an absolute concentration of a specific element within a leachate (see Figure 5.3). This absolute value is a representation of the elemental concentration of a precipitating fluid in ppm. These values are presented in Tables 5.1, 5.3 and 5.4. Comparing data in terms of molar ratios and absolute concentrations, which incorporates molecular weights, provide insight into the origin of a fluid and its evolution along its flow path.

The AAS method had lower detection limits for Na, K and Li (0.0002, 0.003 and 0.002 ppm, respectively), in comparison to the ICP-MS analyses (2, 2 and 0.005 ppm, respectively). Na, K and Li values were also collected by ICP-MS analyses but AAS concentrations were used for all data plotting and conclusions. Salinities calculated from the ice melting temperatures along with the analyzed cation concentrations were used to determine absolute Na, K and Li values (Table 5.3). Concentrations from ICP-MS analyses and the AAS method were normalized to Na (Appendix VII).

#### 5.4.4 *Anion Data*

##### Host Dolomite

Chloride concentrations in host dolomite leachates ranged from 30.78 to 105.16 ppm and Br<sup>-</sup> concentrations varied from 0.2 to 0.89 ppm. Fluoride and SO<sub>4</sub><sup>2-</sup> concentrations ranged from 0.01 to 0.99 ppm and from 10.17 to 364.07 ppm, respectively. Molar ratios including Cl/Br, SO<sub>4</sub>/Br of host dolomite phases are reported in Appendix VIII. Cl/Br (molar) ratios ranged from 267 to 354 with an average ratio of 328. SO<sub>4</sub>/Br (molar) ratios ranged from 16 to 153 with an average molar ratio of 71. No absolute values were reported for Cl<sup>-</sup>, Br<sup>-</sup>, F<sup>-</sup> or SO<sub>4</sub><sup>2-</sup> due to an absence of microthermometric data for host dolomite.

##### Coarse white dolomite

Coarse white dolomites had numerous high salinity primary fluid inclusions and as such, their leachates had higher solute values when compared to other dolomite, sulphide or calcite leachates.

Leachates from coarse white dolomite separates produced Cl<sup>-</sup> values varying from 82.6 to 472.76 ppm, Br<sup>-</sup> values ranging from 0.46 to 4.07 ppm, F<sup>-</sup> concentrations ranging from 0.34 to 0.73 ppm and SO<sub>4</sub><sup>2-</sup> concentrations varying from 5.04 ppm to 43.64 ppm (Appendix IV).

Cl/Br (molar) ratios ranged from 262 to 405 with an average of 319 (n=5) and SO<sub>4</sub>/Br ratios gave an average value of 13 (n=5) and ranged from 3 to 25. Calculated absolute data for Cl<sup>-</sup>, Br<sup>-</sup>, F<sup>-</sup> and SO<sub>4</sub><sup>2-</sup> are reported in Table 5.2. Five absolute Cl<sup>-</sup> values ranged from 115300 to 165700 ppm (average = 144400 ppm). Molar Br<sup>-</sup> averaged 1050 ppm with minimum and maximum values of 640 and 1340 ppm. Fluoride values ranged from 180 to 500 ppm (average = 400 ppm; n = 5) and SO<sub>4</sub><sup>2-</sup> values ranged from 4600 to 30800 ppm (average = 16800 ppm; n = 5).

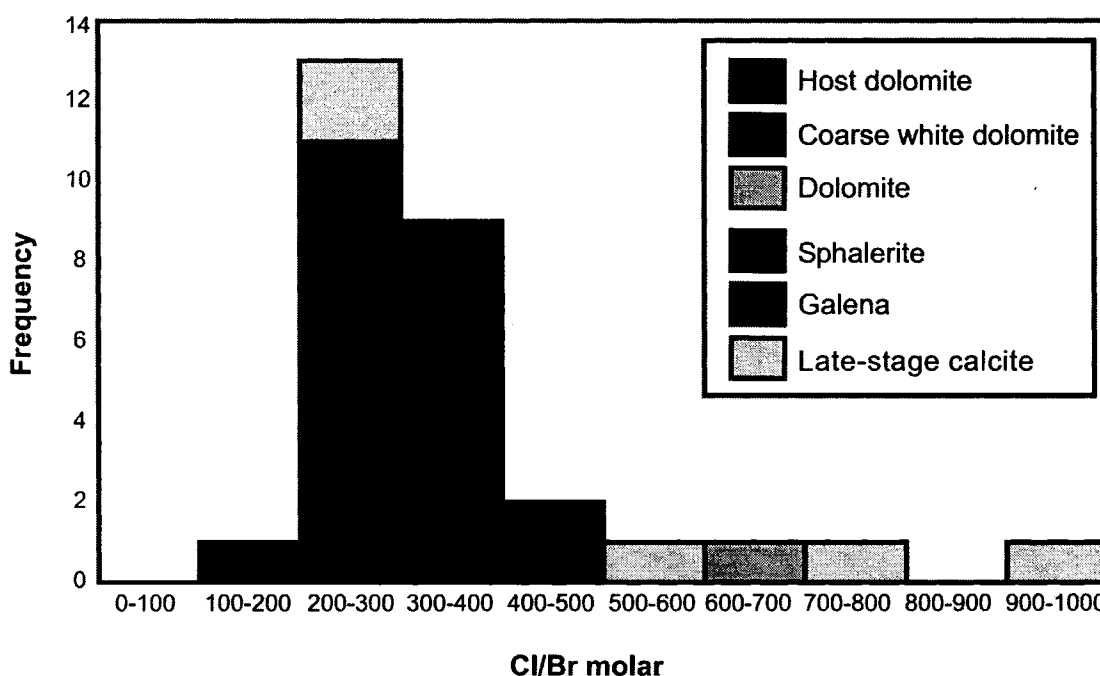


**Figure 5.4** Histogram of the molar Cl/Br ratio of fluid inclusions hosted by host dolomite, coarse white dolomite, dolomite, sphalerite, galena and calcite in the N81 deposit (present day seawater value is approximately 656 – from Fontes and Matray, 1993).

#### Dolomite (Unspecified Variety)

This category is a phase of dolomite that could not be confidently classified as either host or coarse white dolomite. The anion data for two unspecified dolomite phases (DOL) are reported in Appendix IV. The two samples had variable Cl<sup>-</sup> values of 13.73 (0.05 ppm Br<sup>-</sup>) and 108.01 ppm. Two F<sup>-</sup> and two SO<sub>4</sub><sup>2-</sup> components yielded data ranging from 0.07 to 0.18 ppm and 48.76 to 9.06 ppm, respectively. The two unspecified dolomite phases cannot be compared in

molar ratios of Cl/Br and SO<sub>4</sub>/Br because only one of the phases yielded a bromide value above the detection limit and no absolute values were reported due to a lack of salinity data.

### Sulphides

Sulphate concentrations for galena and sphalerite phases were not reported due an unknown degree of contamination by the host minerals and are shown as “HOST” in the tables of this text. Four galena leachate Cl<sup>-</sup> and Br<sup>-</sup> concentrations ranged from 3.01 to 8.02 ppm (average = 4.51 ppm) and 0.02 to 0.05 ppm (average = 0.04 ppm), respectively. Only one F<sup>-</sup> concentration is reported from galena derived leachates (0.05 ppm). Sphalerite leachate Cl<sup>-</sup> concentrations ranged from 2.54 ppm to 11.28 ppm (average = 7.49 ppm; n = 10). Nine Br<sup>-</sup> values ranged from 0.04 ppm to 0.09 ppm. Two F<sup>-</sup> values were reported, 0.03 and 0.08 ppm, most samples had F<sup>-</sup> values below the detection limits (Appendix IV). Nine sphalerite Cl/Br (molar) ratios ranged from 228 to 317 and had a similar average ratio of 271. Sphalerite leachates had one calculated absolute Cl<sup>-</sup> value of 126200 ppm and one molar bromide value of 1250 ppm (see Table 5.2). No microthermometry was performed on galena (see Section 4.1) and therefore it was not possible to calculate concentration data in the original fluid.

### Calcite

Calcite-hosted fluid inclusions had lower salinities than their coarse white dolomite and sphalerite phase counterparts and therefore, the leachates derived from calcites were less saline (smaller halogen concentrations) with bromine levels frequently below the detection limit. Chloride concentrations of leachates from calcite are reported in Appendix IV and ranged from 0.62 to 36 ppm. Bromide and F<sup>-</sup> concentrations had ranges of 0.03 to 0.3 ppm and 0.01 to 0.15 ppm, respectively. Sulphate concentrations from calcite phase leachates ranged from 0.31 to 40.93 ppm. Sample N81-68A 2969 375' had an elevated SO<sub>4</sub><sup>2-</sup> level (40.93 ppm) and also a high Sr value which may be indicative of celestite contamination. Leachates from calcite phases had Cl/Br (molar) ratios ranging from 271 to 975 (average = 561; n = 5) and SO<sub>4</sub>/Br (molar) ratios of 4 to 873 (average = 193; n = 5). Calculated chloride concentrations ranged from 30300 to 71000 ppm (average = 48100 ppm) and one bromide value of 220 ppm. Two fluoride values of 420 and 1030 ppm had an average value of 720 ppm. Absolute sulphate concentrations ranged from 21200 and 229200 ppm (Table 5.2).

Sample	Phase	ppm Cl <sup>-</sup>	ppm Br <sup>-</sup>	ppm F <sup>-</sup>	ppm SO <sub>4</sub> <sup>2-</sup>
N81-65 0249	CWD	131000	990	500	29800
N81-75 3386 322'	CWD	115300	640	480	8000
N81-84 1078	CWD	165700	1170	440	4600
N81-98 3205 360'	CWD	154000	1120	410	1100
N81-98 3225 450'	CWD	155900	1340	180	30800
N81-98 3205 360'	SPH	126200	1250	-	host
N81-68A 2969 375'	CC	71000	220	-	229200
N81-98 3208 367'	CC	43100	-	420	21200
N81-98 3214	CC	30300	-	1030	45400
<i>Seawater</i>	<i>SET</i>	<i>19780</i>	<i>68</i>	<i>-</i>	<i>2770</i>
<i>Gypsum ppt</i>	<i>SET</i>	<i>69000</i>	<i>234</i>	<i>-</i>	<i>10100</i>
<i>Halite ppt</i>	<i>SET</i>	<i>188200</i>	<i>950</i>	<i>-</i>	<i>28900</i>
<i>Epsomite ppt</i>	<i>SET</i>	<i>190500</i>	<i>2970</i>	<i>-</i>	<i>82200</i>
<i>Sylvite ppt</i>	<i>SET</i>	<i>223900</i>	<i>4770</i>	<i>-</i>	<i>56100</i>
<i>Carnallite ppt</i>	<i>SET</i>	<i>257600</i>	<i>5300</i>	<i>-</i>	<i>35400</i>
<i>Bischofite ppt</i>	<i>SET</i>	<i>337300</i>	<i>7530</i>	<i>-</i>	<i>34900</i>

**Table 5.2** Reported absolute anion values of this study (see Section 5.4.3) and seawater evaporation trajectory (SET) data from Fontes and Matray (1993) (CWD = coarse white dolomite; CC = calcite).

#### 5.4.5 Cation Data

##### Host Dolomite

AAS analyses produced Na concentrations ranging from 8.56 to 21.5 ppm, K concentrations with a range from 7 to 12.3 ppm and one Li concentration of 0.0024 ppm (see Appendix V). Most iron concentrations from leachates analyzed were below the detection limit (see Appendix VI), with the exception of one iron value (23.86 ppm) from sample N81-69 2764 235' (23.86 ppm). It is possible that the sample may be contaminated by pyrite (see Section 5.4.1). Manganese concentrations varied from 1.17 to 13.63 ppm (n=3), Ni from 0.060 to 0.342 ppm and Sr from 1.37 to 2.16 ppm. Sulphur varied from 30.00 to 239.68 ppm and the high value may be due to sulphide inclusions being present in the crushed phases. Lead and Zn concentrations ranged from 0.657 to 2.779 ppm and 3.81 to 13.44 ppm, respectively. Barium and B had ranges of 0.314 to 6.248 ppm and 0.06 to 0.40 ppm, respectively. Minor amounts of

Cd and Co were detected with maximum concentrations of 0.088 and 0.0514 ppm, respectively. Strontium concentrations were relatively consistent varying from 1.37 to 2.16 ppm.

Molar ratios were calculated for K/Na, Li/Na, Na/Br and K/Br and are reported in Appendix VIII. K/Na (molar) ratios ranged from 0.191 and 0.424 ppm (average = 0.318; n = 3) and one Li/Na value is reported (0.0005). Na/Br (molar) ratios varied from 67 to 201 (average = 132; n = 5). Three K/Br (molar) ratios had ranges of 27 to 68 (average = 41). Molecular weight ratios were calculated for the leachates analyzed by ICP-MS (Appendix IX). Two of the three Zn/Na ratios were considered to have been contaminated by trace sulphides. Pb/Na ratios had values of 0.0081 and 0.036 with one sample (N81-69 2764 235') considered to have been contaminated by galena yielding an elevated Pb/Na of 0.7545. Mn/Na values varied from 0.054 to 0.416 (average = 0.268; n = 3), Ba/Na varied from 0.0061 to 0.6140 (average = 0.0255; n = 3), B/Na range from 0.0142 to 0.0992 (average = 0.0449; n = 3) and Ni/Na from 0.0023 to 0.0157 (average = 0.0070; n = 3). Molecular weight ratios of Cd/Na and Co/Na varied from 0.0001 to 0.00106 (average = 0.00039; n = 3) and 0.00013 to 0.00234 (average = 0.00091; n = 3), respectively. Sr/Na ratios were relatively consistent varying slightly from 0.0332 to 0.0536 with an average of 0.0429 (n = 3).

#### Dolomite – Unspecified Variety

Two Na concentrations of 6.28 and 22.38 ppm and one K concentration of 4.32 ppm are reported in Appendix V. There is no Li data for unspecified dolomite phases. One phase of unspecified dolomite was normalized with Na data. The Fe concentration was below the detection limit. Manganese and Ni had values of 1.43 and 0.056 ppm, respectively. Barium was reported at 0.176 ppm, B at 0.11 ppm, Cd at 0.0008 and Co at 0.0014 ppm. Lead and Zn had concentrations of 0.233 and 5.37 ppm and S had a value of 67.14 ppm. Since S and Zn were both elevated in sample N81-98 3205 355' these values were likely to be the result of sphalerite in the sample. This phase has a strontium concentration of 1.29 ppm, which is similar to the strontium concentrations of the other dolomite phases analyzed.

Molar ratios for unspecified dolomite phases include one Na/Br (molar) ratio of 485 and one K/Na (molar) of 0.114 (Appendix VIII). This sample also had a Mn/Na (molar) ratio of 0.027 and a Ni/Na ratio of 0.001 (Appendix IX). The S/Na ratio (2.15) was similar to that of the host dolomite. Ba/Na and B/Na had values of 0.0013 and 0.0106, respectively. Cd/Na (molar) had a very small ratio of 0.000008 and Co/Na of 0.00002, which is similar to some of the host dolomite leachate data. Pb/Na (molar) and Zn/Na (molar) had ratios of 0.0012 and

0.084, respectively. The Sr/Na molar ratio is similar to those of coarse white dolomite leachates.

<b>Sample</b>	<b>Phase</b>	<b>ppm Na</b>	<b>ppm K</b>	<b>ppm Li</b>
N81-65 0249	CWD	32800	6770	-
N81-75 3386 322'	CWD	32800	3210	-
N81-84 1078	CWD	37700	7060	-
N81-98 3205 360'	CWD	32700	6420	-
N81-98 3225 450'	CWD	23900	5670	4
N81-98 3205 360'	SPH	47600	-	-
N81-68A 2969 375'	CC	35400	2910	-
N81-98 3208 367'	CC	1400	-	-
N81-98 3214	CC	17900	-	-
<i>Seawater</i>	<i>SET</i>	<i>11000</i>	<i>408</i>	<i>0.18</i>
<i>Gypsum ppt</i>	<i>SET</i>	<i>37800</i>	<i>1470</i>	<i>0.71</i>
<i>Halite ppt</i>	<i>SET</i>	<i>89000</i>	<i>5300</i>	<i>2.2</i>
<i>Epsomite ppt</i>	<i>SET</i>	<i>48200</i>	<i>17680</i>	<i>8.49</i>
<i>Sylvite ppt</i>	<i>SET</i>	<i>22100</i>	<i>25900</i>	<i>16.6</i>
<i>Carnallite ppt</i>	<i>SET</i>	<i>15000</i>	<i>17000</i>	<i>20.5</i>
<i>Bischofite ppt</i>	<i>SET</i>	<i>1680</i>	<i>860</i>	<i>20</i>

**Table 5.3** Reported absolute cation values of this study (based on AAS analyses and microthermometry) and seawater trajectory (SET) data in italics (from Fontes and Matray, 1993) (CWD=coarse white dolomite; SPH=sphalerite; CC=calcite).

#### Coarse White Dolomite

The leachates from five coarse white dolomite samples had Na concentrations ranging from 23.5 to 72.4 ppm, five K concentrations ranging from 2.3 to 17.2 ppm and one Li concentration of 0.012 ppm (Appendix V). The four coarse white dolomite leachate Mn concentrations ranged from 1.71 to 9.04 ppm and Ni varied from 0.046 to 0.139 ppm. All leachates had Fe concentrations below the detection limits of the ICP-MS analyses (0.05 ppm). Barium values ranged from 0.023 to 0.183 ppm and B varied more consistently between 0.11 and 0.18 ppm. Cadmium had minimum and maximum concentrations of 0.0002 and 0.0012 ppm and Co had one concentration value (0.0058 ppm) above the detection limit. Lead varied from 0.116 to 0.275 ppm and Zn from 0.14 to 4.28 ppm. Sulphur ranged from 12.21 to 23.17

ppm with one leachate having a concentration below the detection limit. Strontium varied from 1.46 to 6.42 ppm and is on average slightly higher in concentration than host dolomite leachates (Appendix VII).

Sample	Phase	ppm Ca	ppm Mg	ppm Na	ppm K	ppm Mn	ppm S	ppm Ba	ppm B	ppm Cd	ppm Co	ppm Pb	ppm Li	ppm Ni	ppm Sr	ppm Zn
N81-98 3225 450'	CWD	HOST	HOST	23875	4775	850	7640	57	57	0.09	2	4	10	19	1127	115
N81-75 3386 322'	CWD	n.a.	n.a.	n.a.	n.a.	n.a.	n.a.	n.a.	n.a.	n.a.	n.a.	n.a.	n.a.	n.a.	n.a.	n.a.
N81-65 0249	CWD	HOST	HOST	32832	3127	1173	10944	16	78	0.16	b.d.	79	13	31	996	422
N81-98 3205 360'	CWD	HOST	HOST	32671	b.d.	4434	9335	140	140	0.93	b.d.	210	b.d.	93	2007	3272
N81-84 1078	CWD	HOST	HOST	37725	b.d.	8174	b.d.	50	126	0.44	b.d.	138	b.d.	126	2704	126
<i>Seawater</i>	<i>SET</i>	<i>420</i>	<i>1320</i>	<i>n.a.</i>	<i>n.a.</i>	<i>n.a.</i>	<i>n.a.</i>	<i>n.a.</i>	<i>5</i>	<i>n.a.</i>	<i>n.a.</i>	<i>n.a.</i>	<i>n.a.</i>	<i>n.a.</i>	<i>8.18</i>	<i>n.a.</i>
<i>Gypsum ppt</i>	<i>SET</i>	<i>1540</i>	<i>4530</i>	<i>n.a.</i>	<i>n.a.</i>	<i>n.a.</i>	<i>n.a.</i>	<i>n.a.</i>	<i>15</i>	<i>n.a.</i>	<i>n.a.</i>	<i>n.a.</i>	<i>n.a.</i>	<i>n.a.</i>	<i>22.2</i>	<i>n.a.</i>
<i>Halite ppt</i>	<i>SET</i>	<i>237</i>	<i>20900</i>	<i>n.a.</i>	<i>n.a.</i>	<i>n.a.</i>	<i>n.a.</i>	<i>n.a.</i>	<i>59</i>	<i>n.a.</i>	<i>n.a.</i>	<i>n.a.</i>	<i>n.a.</i>	<i>n.a.</i>	<i>9.68</i>	<i>n.a.</i>
<i>Epsomite ppt</i>	<i>SET</i>	<i>0</i>	<i>56120</i>	<i>n.a.</i>	<i>n.a.</i>	<i>n.a.</i>	<i>n.a.</i>	<i>n.a.</i>	<i>216</i>	<i>n.a.</i>	<i>n.a.</i>	<i>n.a.</i>	<i>n.a.</i>	<i>n.a.</i>	<i>8.14</i>	<i>n.a.</i>
<i>Sylvite ppt</i>	<i>SET</i>	<i>0</i>	<i>72900</i>	<i>n.a.</i>	<i>n.a.</i>	<i>n.a.</i>	<i>n.a.</i>	<i>n.a.</i>	<i>343</i>	<i>n.a.</i>	<i>n.a.</i>	<i>n.a.</i>	<i>n.a.</i>	<i>n.a.</i>	<i>0</i>	<i>n.a.</i>
<i>Carnallite ppt</i>	<i>SET</i>	<i>0</i>	<i>85700</i>	<i>n.a.</i>	<i>n.a.</i>	<i>n.a.</i>	<i>n.a.</i>	<i>n.a.</i>	<i>370</i>	<i>n.a.</i>	<i>n.a.</i>	<i>n.a.</i>	<i>n.a.</i>	<i>n.a.</i>	<i>4.7</i>	<i>n.a.</i>
<i>Bischofite ppt</i>	<i>SET</i>	<i>60</i>	<i>122000</i>	<i>n.a.</i>	<i>n.a.</i>	<i>n.a.</i>	<i>n.a.</i>	<i>n.a.</i>	<i>450</i>	<i>n.a.</i>	<i>n.a.</i>	<i>n.a.</i>	<i>n.a.</i>	<i>n.a.</i>	<i>0.391</i>	<i>n.a.</i>

**Table 5.4** Cation concentrations (ppm) from ICP-MS analysis of this study and seawater trajectory (SET) data from Fontes and Matray (1993) (in italics) (all Fe values were below the detection limit and consequent absent from this table).

K/Na molar ratios of leachates from coarse white dolomite phases ranged from 0.058 to 0.14 (average = 0.109; n = 5). Although most of the leachate Li concentrations were below the detection limit, one Li/Na ratio was reported with a value of 0.0005. Five Na/Br (molar) values ranging from 62 to 178 (average = 114) and 5 K/Br (molar) ratios with ranges of 9 to 14 (average = 11) are shown in Appendix VIII. Mn/Na molar ratios varied from 0.015 to 0.091 with an average of 0.044. Ni/Na (molar) ratios had an average of 0.0008 and ranged from 0.0003 to 0.0013. Ba/Na (molar) and B/Na (molar) had average ratios of 0.0004 and 0.0066 and varied from 0.0001 to 0.0007 and 0.0051 to 0.0091, respectively. Four Cd/Na molecular weight ratios ranged from 0.000001 to 0.000006 (average = 0.000003). Only one Co/Na (molar) of 0.00003 was reported. Pb/Na (molar) and Zn/Na (molar) had averages of 0.0004 (0.0001 to 0.0007) and 0.0108 (0.001 to 0.035). Three S/Na (molar) ratios were quite

consistent and varied from 0.20 to 0.24 (average = 0.22). The Sr/Na (molar) ratios were also consistent ranging from 0.008 to 0.0188 (average = 0.0138; n = 4).

Microthermometric salinity data along with the analyzed cation concentrations were used to determine absolute values. Sodium, K and Li values for coarse white dolomites are reported in Table 5.3. Sodium values ranged from 23900 to 37700 ppm with an average molar value of 32000 ppm. Potassium values had an average of 5830 ppm and a ranged between 3210 and 7060 ppm. Only one lithium value of 4 ppm is reported. No molar data is reported for Fe (Table 5.4). Manganese and Ni both had four molar values ranging from 850 to 8174 ppm (average = 3658 ppm) and 19 to 126 ppm (average = 67 ppm). Barium varied from 16 to 140 ppm (average = 66 ppm; n = 4) and boron from 57 to 140 ppm (average = 100 ppm; n = 4). Four Cd values averaged 0.41 ppm and ranged from 0.09 to 0.93 ppm. Only one Co concentration was above the detection limit (2 ppm). Lead and Zn varied from 4 to 210 ppm (average = 108 ppm; n = 4) and 115 to 3272 ppm (average = 984 ppm; n = 4). Sulphur values from three coarse white dolomite phases varied from 7640 to 10944 ppm. Four Sr values averaged 1709 ppm and varied from 996 to 2704 ppm and are reported in Table 5.4.

Phase	molar Cl/Br	molar SO <sub>4</sub> /Br	molar K/Na	molar Li/Na	molar Na/Br	molar K/Br
Seawater	655.60	33.88	0.02181	0.00005	562.23	12.26
Gypsum ppt	664.59	35.90	0.02287	0.00006	561.45	12.84
Halite ppt	446.49	25.30	0.03502	0.00008	325.61	11.40
Epsomite ppt	144.56	23.02	0.21568	0.00058	56.41	12.17
Sylvite ppt	105.79	9.78	0.68910	0.00249	16.10	11.10
Carnallite ppt	109.54	5.56	0.66640	0.00453	9.84	6.56
Bischofite ppt	100.96	3.86	0.30100	0.03943	0.78	0.23

**Table 5.5** Seawater evaporation trajectory (SET) anion and cation molar ratio data from Fontes and Matray (1993).

### Sulphides

Sodium concentrations in galena and sphalerite leachates are reported in Appendix V. Potassium and Li concentrations were not analyzed. Galena leachates gave two Na values, 1.64 and 2.66 ppm. Eight sphalerite leachates were analyzed by AAS and produced Na

concentrations ranging between 1.94 and 3.87 ppm. No Na was detected in any sulphide phase with ICP-MS. High Pb levels in sphalerite suggest contamination by galena and conversely, high Zn levels in galena suggest contamination by sphalerite (see Section 5.4.1).

Due to a lack of K or Li concentration data only Na/Br is reported in Appendix VIII. Two Na/Br (molar) ratios in galena had values of 130 and 193 (average = 161). Sphalerite yielded 9 Na/Br (molar) ratios with an average of 146 and span between 111 and 184.

No absolute values were reported for galena since no microthermometry was performed on the sulphide. Only one value was reported for sphalerite in Table 5.3. An absolute Na value of 47600 ppm was reported for a single sphalerite phase.

### Calcite

Leachates from calcite phases had Na concentrations between 0.02 and 12.72 ppm (n = 10), K concentrations from 0.52 to 4.96 ppm (n = 5), and one Li concentration of 0.0018 ppm (see Appendix V).

Sodium levels were below the detection limit for ICP-MS analysis in all calcite phase samples. Therefore, using Na to normalize the ICP-MS La-doped leachate data to the AAS/IC leachate data was not possible and consequently no absolute ICP-MS cation concentrations are reported for calcite leachates. All phases were below the detection limit for iron. N81-68A 2969 375' had an abnormally high Sr value compared to the strontium data for the rest of the phases analyzed. The high strontium value is likely an indication of contamination by celestite.

Five K/Na molar ratios are reported in Appendix VIII ranging from 0.0488 and 0.367 (average = 0.205) and 1 Li/Na (molar) is reported at 0.0008. Na/Br (molar) ratios varied widely from 56 to 563 (average = 228; n = 5) and four K/Br (molar) ratios ranged from 27 to 66 with an average of 46.

Calcite leachates had a wide spread of absolute Na values ranging from 1400 to 35400 ppm (average = 18200; n = 3) and one absolute K value of 2910 ppm. The data set does not include any absolute Li values.

## **5.5 Discussion**

### *5.5.1 Na-Cl-Br Systematics*

In many geological systems halogens are considered to be conservative elements, and thus, they are useful in identifying the sources of fluids and processes acting upon the fluids during migration (Wilkinson, 2001). Bromine is an inert component of brines and does not

participate in diagenetic reactions (Carpenter, 1978) and as such is a useful tracer in brine origin and process studies. The most common salinity source of brines is evaporation of seawater and/or the dissolution of evaporites (Kesler et al., 1995). Halogen studies can discriminate between brines that originate as seawater, evaporated seawater before the precipitation of halite, evaporated seawater past the point of halite precipitation, salinity acquired from halite dissolution and mixing of any of these end-members (e.g. Carpenter, 1978; Hanor, 1994; Kesler et al., 1995).

The characterization of sedimentary basinal brines using Na-Cl-Br systematics was first proposed by Walter et al. (1990). The interpretation of data plotted on a Na/Br-Cl/Br diagram is based on three major points: 1) evaporating seawater (before the point of halite precipitation) retains a constant Cl/Br ratio (Carpenter, 1978); 2) Cl/Br ratios decrease when seawater is evaporated past the point of halite precipitation, as halite, when formed, effectively excludes Br from the mineral structure; and 3) Cl/Br and Na/Br ratios increase when brines are produced by the dissolution of halite, assuming no sinks for Na exist (Walter et al., 1990). Therefore, by plotting Cl/Br versus Na/Br it is possible to identify the origin of the chlorinity and the probable origin of a brine.

Reactions that occur along a fluid migration path, such as albitization, may affect the Na levels of a brine and can be discerned by comparison of the data to a line representing geochemical changes of seawater during evaporation, the seawater evaporation trajectory (SET). The SET, therefore, acts as a base-line which is used to indicate the possible origin of a fluid, the extent of evaporation or halite dissolution and other processes acting upon the fluid e.g. Na-Ca exchange reactions. The trajectory is used in Figures 5.5 to 5.13 and is derived from Fontes and Matray (1993) and reproduced in Tables 5.2 through 5.5.

#### 5.5.2 *Geochemical Implications for Fluid Sources*

The majority of the leachates analyzed had Cl/Br ratios that were lower than seawater (~656 from Fontes and Matray, 1993) (Figure 5.4) indicating that the fluids were relatively enriched in Br with respect to seawater. These values suggest that the fluids likely originated from evaporated seawater. Absolute Cl and Br levels were calculated from a small number of samples (coarse white dolomite, sphalerite and calcite) having salinity data obtained from microthermometry. The evaporative source of the fluids is confirmed by the absolute Cl and Br concentration data (Figure 5.5). Identification of potential end members (e.g. fluid mixing) can be made when the absolute data is plotted on a log-log plot. The coarse white dolomite and

sphalerite leachates plot near the SET and close to the point of halite precipitation, and thus can be interpreted as originating from evaporated seawater. The calcite leachate plots near the SET but has a larger Cl component, however, this is only one data point. Some of the calcite leachates had halogen ratios that were similar to those representing the ore fluid (see Figure 5.4), however, the average salinity of the calcite fluid is much less than that of the ore fluid. This indicates the calcite leachates may be representing a mixture of the ore fluid and a dilute end-member (e.g. meteoric water).

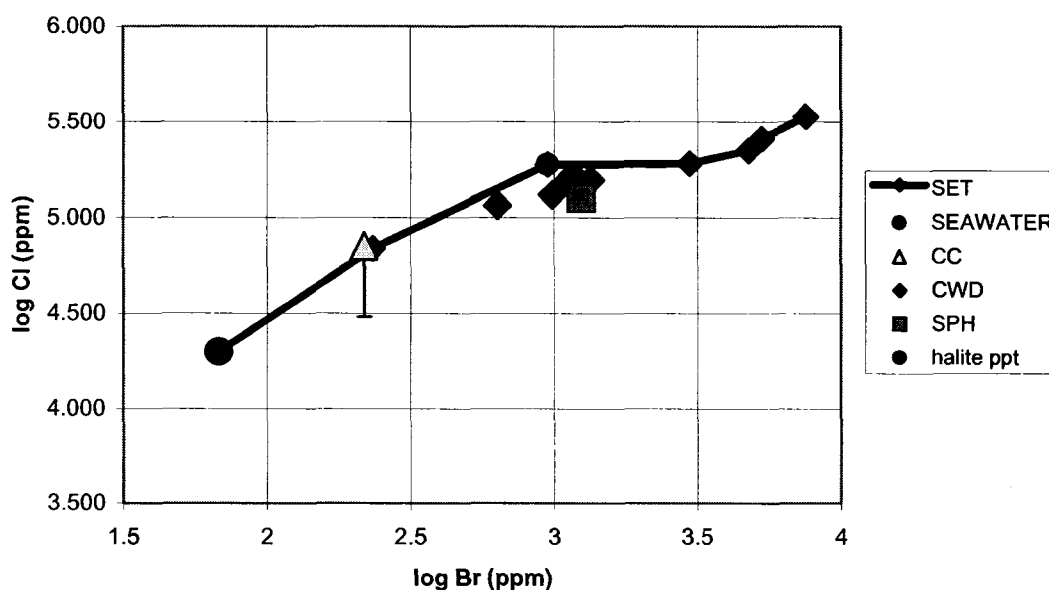


**Figure 5.5** Absolute Cl (ppm) and Br (ppm) concentrations including SET data from Fontes and Matray (1993) (CC=calcite; CWD=coarse white dolomite; SPH=sphalerite; ppt=precipitation). Calcite includes an error bar representing all log Cl (ppm) data.

The Na-Cl-Br systematics of host dolomite, coarse white dolomite and sulphide hosted leachates suggest that the fluids that formed all three mineral phases were derived from evaporated seawater (see Figure 5.6). The data suggest that the seawater was evaporated past the point of the precipitation of halite to form a Br-rich, bittern brine. Host dolomite leachates plot to the left of the SET, which indicate a loss of Na along the flow path. The same conclusion is made for the coarse white dolomite and sulphide leachates, which plot near or slightly to the left of the SET. Na-Cl-Br systematics confirm the textural relationship between coarse white dolomite and the sulphide mineralization (see Figure 5.6). Calcite-hosted leachate

Na-Cl-Br systematics vary considerably and suggest that the fluids that formed the mineral phases were derived from evaporated seawater and also a Cl-rich component. Some of the data plots near the SET in the same data cluster as the coarse white dolomite and sulphides but some of the data is very different. Two leachates had very large Cl/Br ratios and plot well above the SET with values between ~500 to 1000. These high Cl/Br ratios mean that the Cl has been added to the fluid (e.g. mixing) or the fluid is not from an evaporated seawater source.

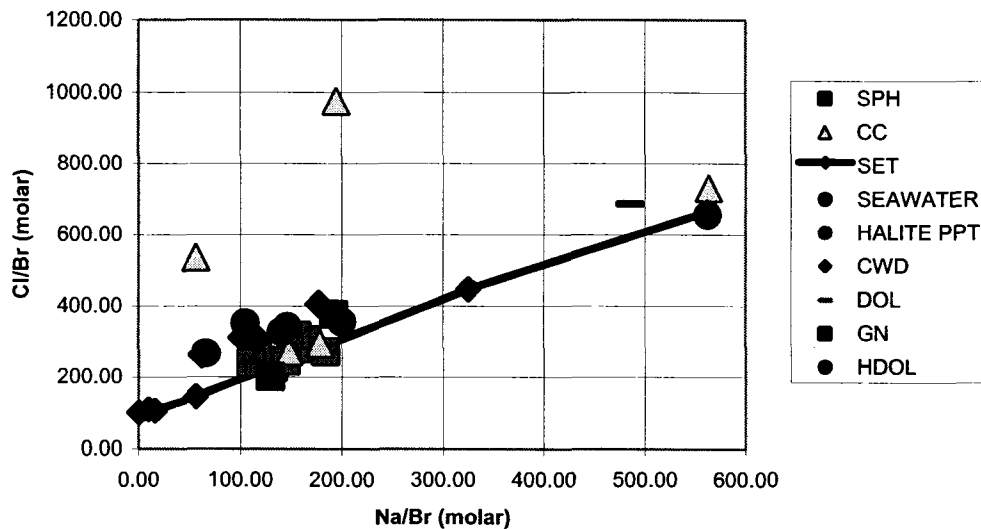


**Figure 5.6** Na-Cl-Br systematics including the SET data from Fontes and Matray (1993) (CC=calcite; CWD=coarse white dolomite; DOL=dolomite (unspecified variety); SPH=sphalerite; GN=galena; ppt=precipitation).

K-Cl-Br systematics show a large variation in potassium from evaporated seawater in the host dolomite and calcite leachates, which suggests that the element has been added to the fluid, likely along its flow path (see Figure 5.7). The K levels in the coarse white dolomite leachates plot on or near the SET, suggesting that the K levels of the ore fluid had not been significantly modified from those of evaporated seawater. Li-K-Na systematics show host dolomite and calcite leachates plotting to the right of the SET, which indicates a slight loss of Li along the flow path (see Figure 5.8). The ore fluid, represented by coarse white dolomite leachates, plots to the left of the SET and indicates a slight enrichment in Li. This data and its geochemical implications will be discussed more fully in Chapter 7.

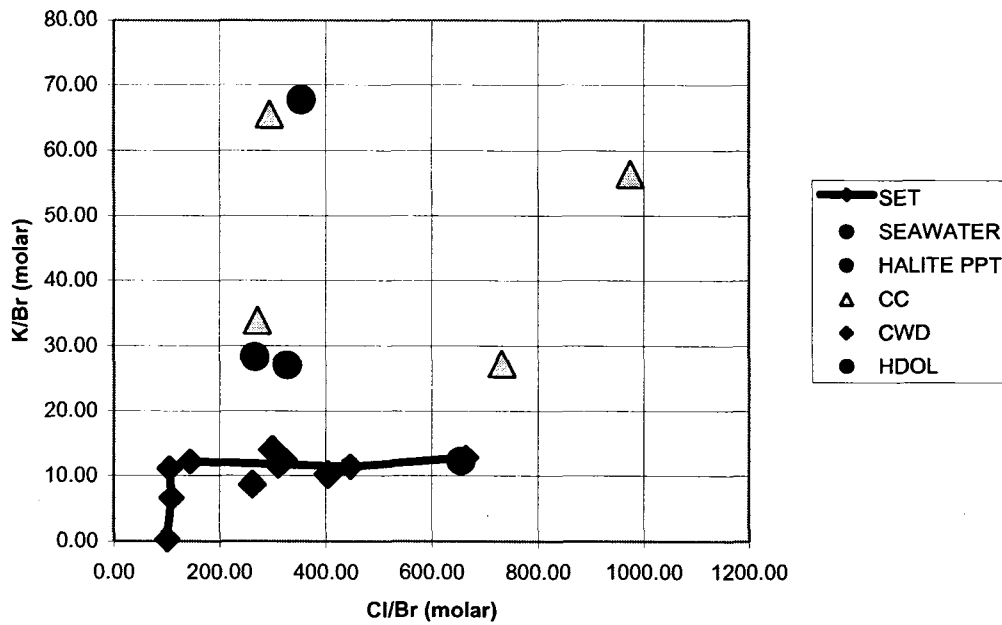


**Figure 5.7** K-Cl-Br systematics including the SET data from Fontes and Matray (1993) (CC=calcite; CWD=coarse white dolomite; HDOL=host dolomite; ppt=precipitation).

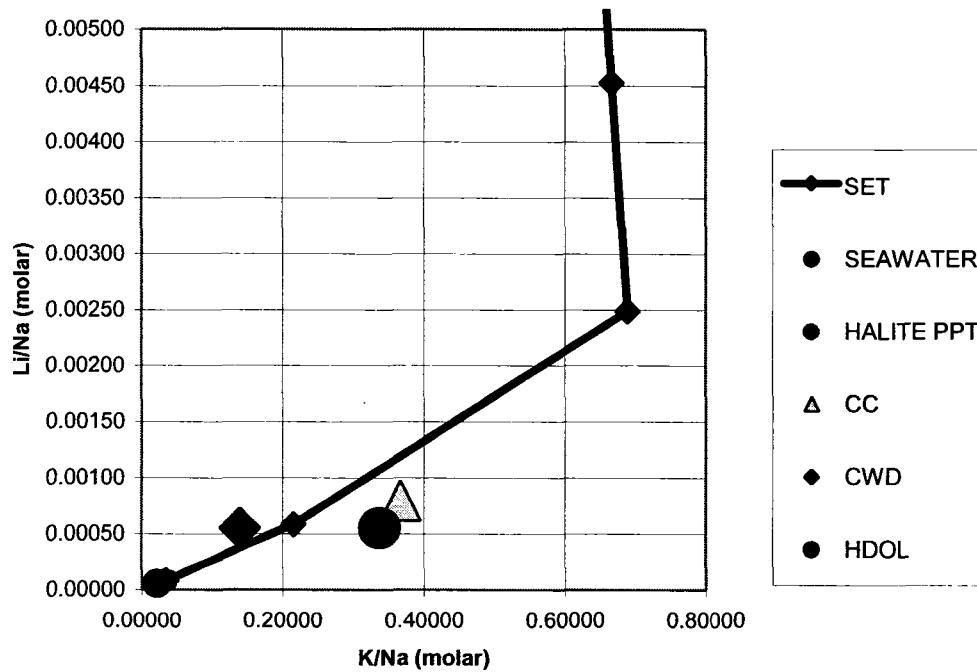


**Figure 5.8** Li-Na-K systematics including the SET data from Fontes and Matray (1993) (CC=calcite; CWD=coarse white dolomite; HDOL=host dolomite; ppt=precipitation).

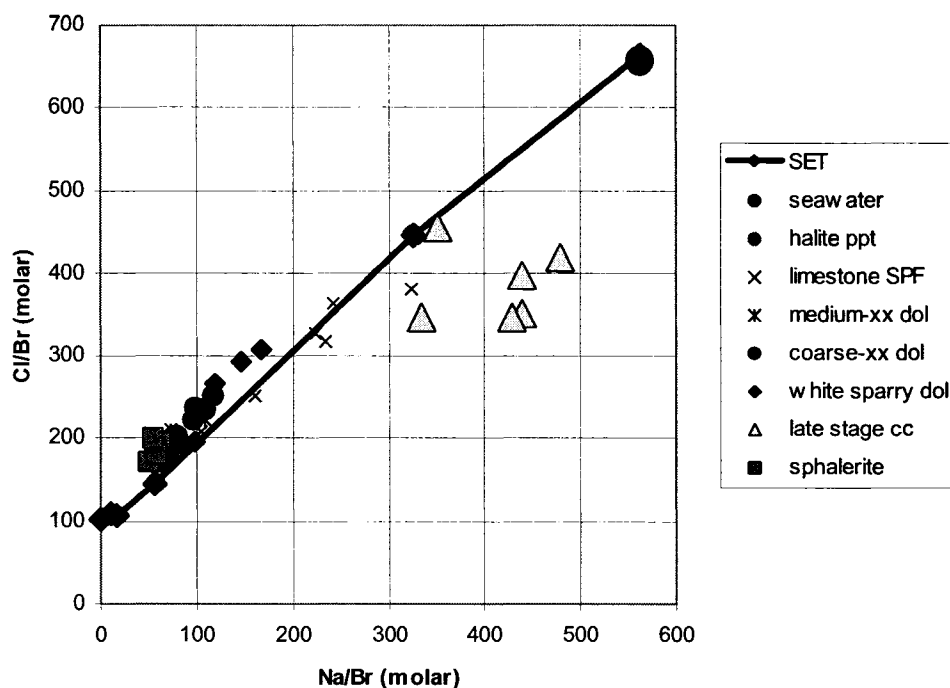


**Figure 5.9** Halogen and cation data from Telser (1999) and the SET data from Fontes and Matray (1993).

### 5.5.3 Comparison of Telser (1999) to this Study

A previous fluid inclusion crush leach study was carried out by Telser (1999) who studied Na-Cl-Br systematics and  $\delta D$ ,  $\delta^{13}C$ , and  $\delta^{18}O$  isotopic compositions at Pine Point. The study suggested that “coarse crystalline dolomite” (correlative to host dolomite of this study) and “white sparry dolomite” (coarse white dolomite in this thesis) were formed from the same fluid (Figure 5.9).

Telser (1999) found that the coarse crystalline dolomite had a Cl/Br range from 17 to 252 molar (average value of 77;  $n=20$ ) and Na/Br averaged 197 molar (ranging from 171 to 252;  $n=20$ ) (see Figure 5.10). Telser’s white sparry dolomite Cl/Br leachate data ranges from 188 to 307 (average = 250;  $n=5$ ) and Na/Br varies from 87 to 168 (average = 124;  $n=5$ ). These averages were roughly close to that of the averages of coarse white dolomite of this study (see Figure 5.11). Sphalerite Cl/Br ratios average 188 (171 to 200;  $n=6$ ) and Na/Br varies from 50 to 63 (average = 57;  $n=6$ ) (Figure 5.12). Both of these values were lower than those calculated from galena and sphalerite of this thesis. Late-stage calcite leachates from Telser (1999) yielded data for Cl/Br (average = 386;  $n=6$ ; 346 to 456) and Na/Br (average = 412;  $n=$

6; 334 to 478) (Figure 5.13). All Na-Cl-Br systematic data from this thesis and work by Telser (1999) are compared in Figures 5.10 to 5.13.

The bulk of Telser's data is similar to data of this study and has the same implications for fluid origins. However, a notable difference occurs in the calcite fluid inclusion chemistry. Data from Telser (1999) plot near or below the seawater evaporation trajectory and data from this study plot near or above the SET (see Figure 5.10). This discrepancy may be due to the analyses of different samples that had trapped fluids that were the result of mixing of various fluid end members.

#### *5.5.4 Comparison of Gleeson and Gromek (in press) to this Study*

Gleeson and Gromek (in press) include molar ratio data from matrix dolomite, coarse dolomite, sphalerite, galena and calcite from the southern Northwest Territories and Northern Alberta. The aim of this study was to see if a regional study of dolomites could be used as an exploration tool i.e. to ascertain if areas of mineralization could be identified from the fluid inclusion compositions. No samples from Pine Point were analysed in Gleeson and Gromek (in press). The regional data from the southern Northwest Territories are discussed in the following text. Matrix dolomite from the southern Territories is most closely correlative with host dolomite of this study and has a Cl/Br ratio range from 48 to 402 and a Na/Br range from 26 to 216 (see Figure 5.10). Coarse dolomite, correlative to coarse white dolomite of this thesis, has a large Cl/Br ratio variation from 171 to 1015 and a Na/Br ratio range from 7 to 336 (see Figure 5.11). Sphalerite and galena molar ratio data from the Westmin area, a prospect next to Pine Point, ranges in Cl/Br from 176 to 358 and 259 to 280, respectively. Na/Br ratios vary in sphalerite from 112 to 316 and in galena from 72 to 156 (see Figure 5.12). Calcite leachates from Gleeson and Gromek (in press) had Cl/Br ratios ranging from 14 to 611 and Na/Br ratios from 9 to 465 (see Figure 5.13). Gleeson and Gromek (in press) include leachates analyzed from a large area surrounding the Pine Point deposit and consequently differences in geochemical data were expected upon comparison to the N81 deposit. Much of the molar ratio data of this thesis appears to fall within or plots near the data found in the more regional southern Northwest Territories leachate study. Calcite leachate Cl/Br and Na/Br values are highly variable in both Gleeson and Gromek (in press) and this thesis indicating a complexity in the fluid (e.g. potential mixing).

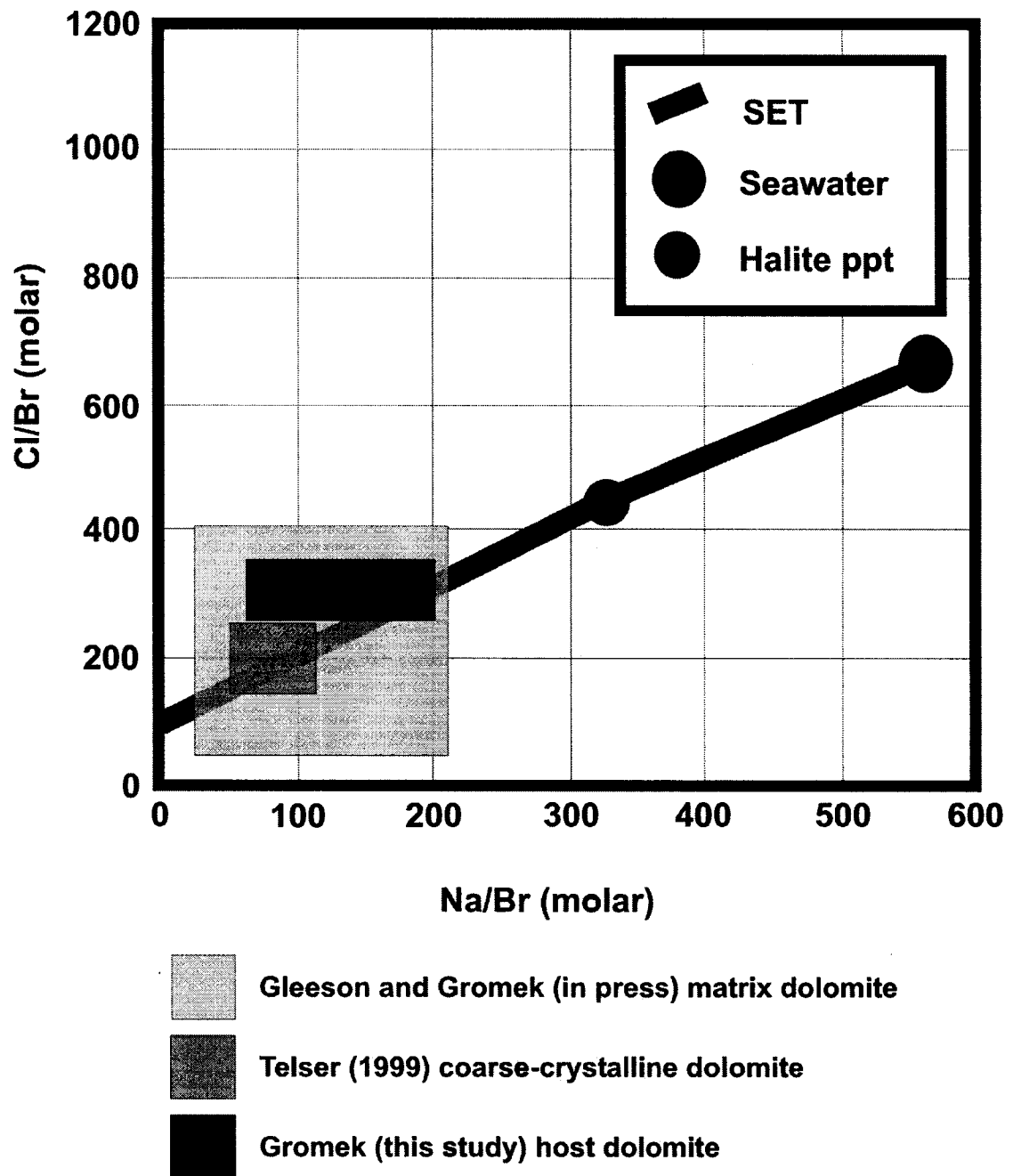


**Figure 5.10** Range data for host dolomite and correlative units from Gleeson and Gromek (in press) and Telser (1999) plotted on a Na-Cl-Br diagram (after Kelser et al., 1995).

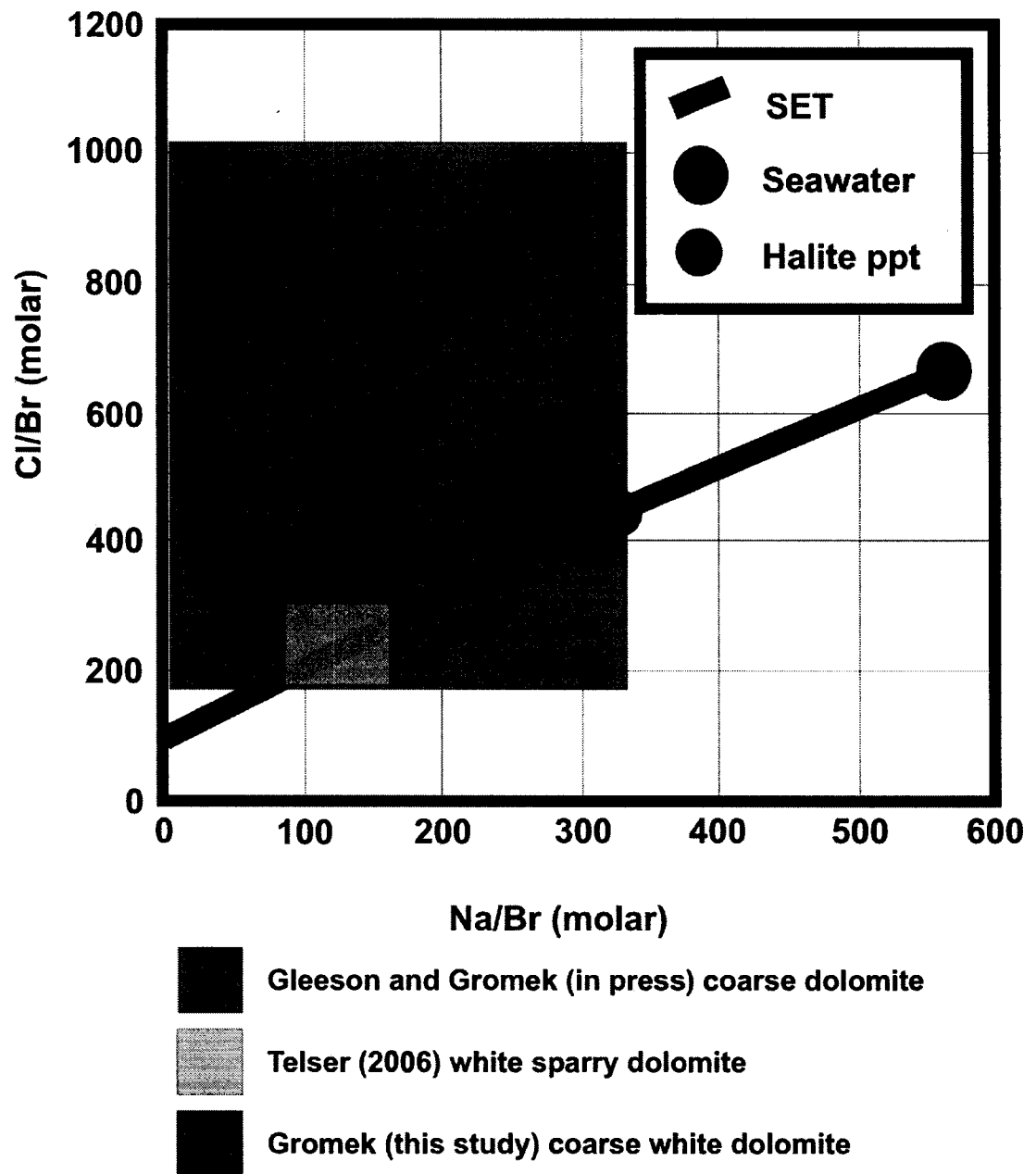


**Figure 5.11** Range data for coarse white dolomite and correlative units from Gleeson and Gromek (in press) and Telser (1999) plotted on a Na-Cl-Br diagram (after Kelser et al., 1995).

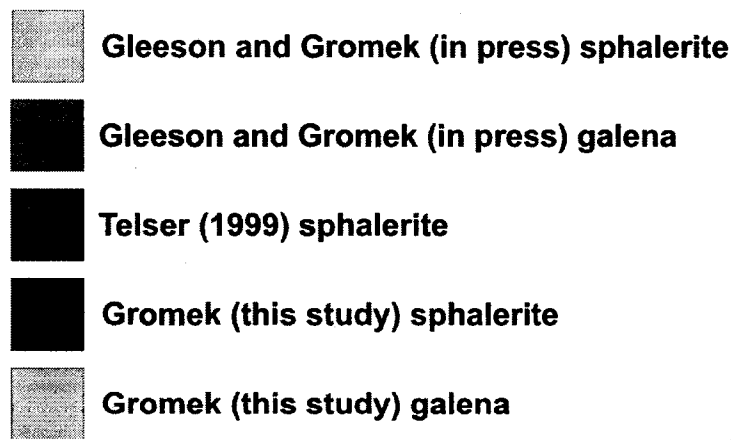
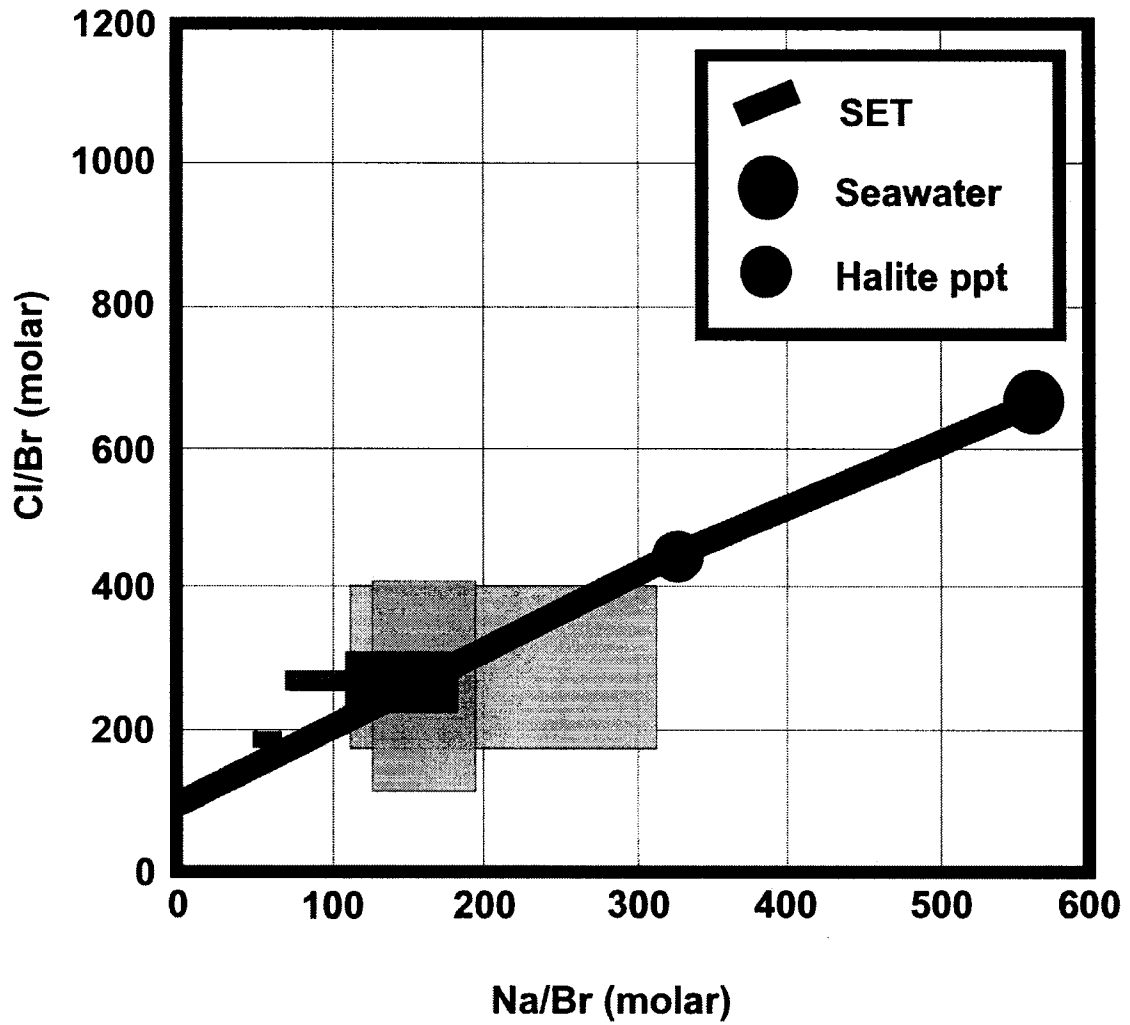


**Figure 5.12** Range data for sulphides from this study, Gleeson and Gromek (in press) and Telser (1999) plotted on a Na-Cl-Br diagram (after Kelser et al., 1995).

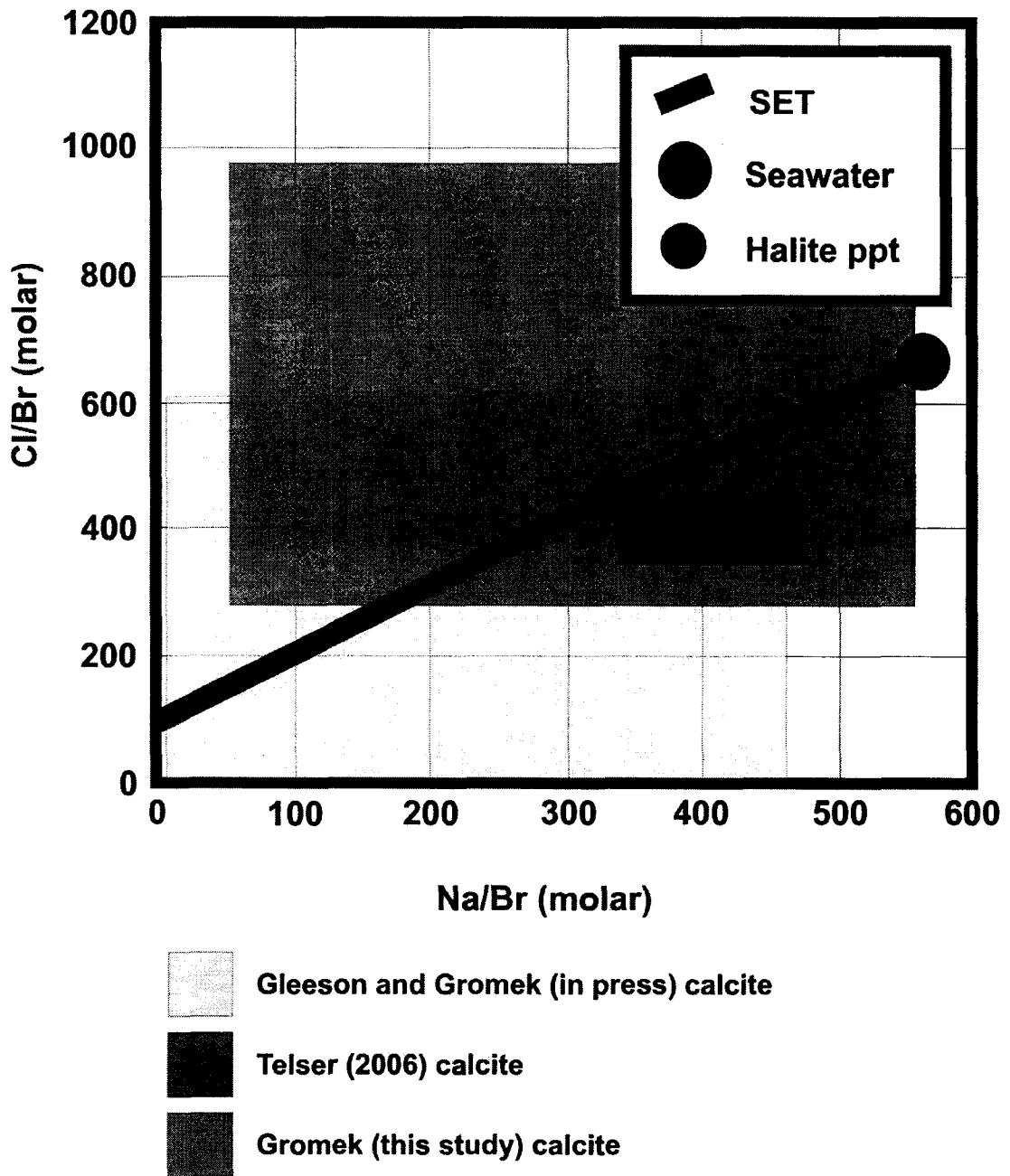


**Figure 5.13** Range data for calcites from this study, Gleeson and Gromek (2006) and Telser (1999) plotted on a Na-Cl-Br diagram (after Kelser et al., 1995).

## **5.6 Remarks**

This chapter characterizes the elemental geochemistry of the fluids involved in the N81 deposit. Halogen and cation ratios of fluid inclusion leachates help to decipher the origin of the salt content of the fluids and processes acting upon them. The data suggest that at least two fluids were present. The bulk of the leachates analysed had Cl/Br ratios that indicate the pre-ore and ore fluids were relatively enriched in Br and likely originated from evaporated seawater. Data from leachates representing the post-ore fluid indicate that a more dilute Cl-rich fluid is present and may be mixing with the ore. Cation data suggests that a variable amount of water-rock interaction has occurred and consequently modified the K and Na levels of the fluids. Chapter 6 will present Sr isotopic data to further constrain the origins and water-rock interactions that may have changed the composition of the fluids.

## CHAPTER 6

### STRONTIUM ISOTOPE GEOCHEMISTRY

#### 6.1 Introduction

Strontium isotope  $^{87}\text{Sr}/^{86}\text{Sr}$  studies provide insight on the origin of Sr in a fluid and can constrain if the fluid originated as seawater and/or if there have been interactions with other fluids or rock units. Strontium isotopic compositions in minerals formed from seawater are assumed to be equal to their seawater source since minimal isotopic fractionation occurs during precipitation (Veizer and Compston, 1974 and Burke et al., 1982). In fluids derived from seawater, variance from the original  $^{87}\text{Sr}/^{86}\text{Sr}$  seawater composition occurs during diagenetic modification by or mixing with other fluids from different sources (Veizer and Compston, 1974; Burke et al., 1982). For example, these fluids can be enriched in radiogenic  $^{87}\text{Sr}$  by interaction with feldspars and clays in basement rocks or clastic sediments (Mountjoy et al., 1992). Basinal fluids in the Western Canadian Sedimentary basin can be compared to the MASIRBAS (Maximum Sr Isotope Ratio of Basinal Shale) (Machel and Cavell, 1999) to indicate if they have acquired  $^{87}\text{Sr}$  from a metamorphic component derived from Precambrian rocks. Thus, strontium isotopes can provide information on the origin, evolution and migration pathways of fluids.

The objectives of this strontium isotopic study were to: 1) define the strontium isotopic composition of pre-, syn- and post-ore carbonate phases in the ore deposit; 2) gain insight into the origin and evolution of the precipitating fluids and, 3) indicate whether mixing is taking place within the deposit. These objectives were achieved by in-situ strontium isotope geochemical analyses (see Section 2.3.3) carried out on carbonate mineral phases including host, coarse white dolomite and calcite. These phases represent the pre-, main stage and post-ore stages of the main paragenetic sequence. In-situ strontium isotope analysis, via MC-ICP-MS, was carried out on fourteen samples from nine drill holes. The in-situ nature of the analysis allows for a quantity of specific mineral crystals and/or individual growth zones (e.g. saddle-shaped rims) to be analyzed. A total of 112  $^{87}\text{Sr}/^{86}\text{Sr}$  values were obtained from three host dolomite, four coarse white dolomite and/or saddle dolomite and seven calcite samples.

#### 6.2 Strontium Isotopic Results

##### 6.2.1 Host Dolomite

Phases from three drill core samples were analyzed yielding seven strontium isotopic ratios and total Sr ion signals (volts) (Appendix X). Four host dolomite samples had an average

Sr ratio 0.7082. This value is comparable to the Middle Devonian  $^{87}\text{Sr}/^{86}\text{Sr}$  seawater signature of 0.7080 (average between 0.7078 and 0.7082) estimated from the  $^{87}\text{Sr}/^{86}\text{Sr}$  seawater variation curve of Burke et al., 1982. All host dolomite phases (including 3 samples partially replaced by coarse white dolomite - HDOL(R)) had Sr isotope values varying from 0.7058 to 0.7097 and have an average  $^{87}\text{Sr}/^{86}\text{Sr}$  value of 0.7085 (see Figure 6.1).

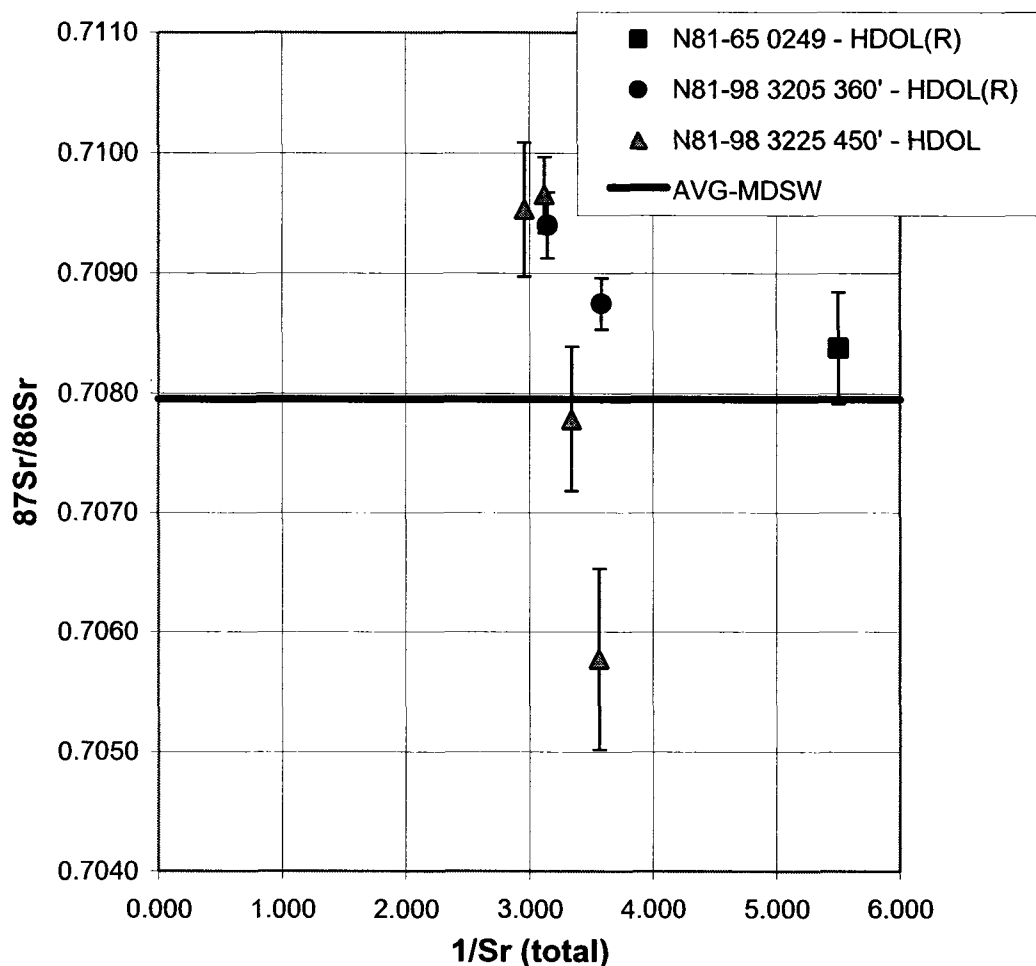


**Figure 6.1** Strontium isotopic composition of host dolomite (AVG-MDSW = average Middle Devonian seawater from Burke et al., 1982 (0.7080); HDOL=host dolomite; HDOL(R)=host dolomite partially replaced by coarse white dolomite).

Sample N81-65 0249 appeared to have some coarse white dolomite replacement (HDOL(R)) and gave one  $^{87}\text{Sr}/^{86}\text{Sr}$  measurement of 0.7084 and a total Sr ion signal of 0.1818 volts. N81-98 3205 360' also appeared to be partially replaced by dolomite and had an average  $^{87}\text{Sr}/^{86}\text{Sr}$  ratio of 0.7091 (average total Sr ion signal = 0.2985 volts). Four  $^{87}\text{Sr}/^{86}\text{Sr}$  values from

N81-98 3225 450' varied from 0.7058 and 0.7097 (average = 0.7082) and had total Sr ion signals ranging from 0.2807 to 0.3378 volts (average = 0.3095 volts) (see Appendix X and Appendix XI).

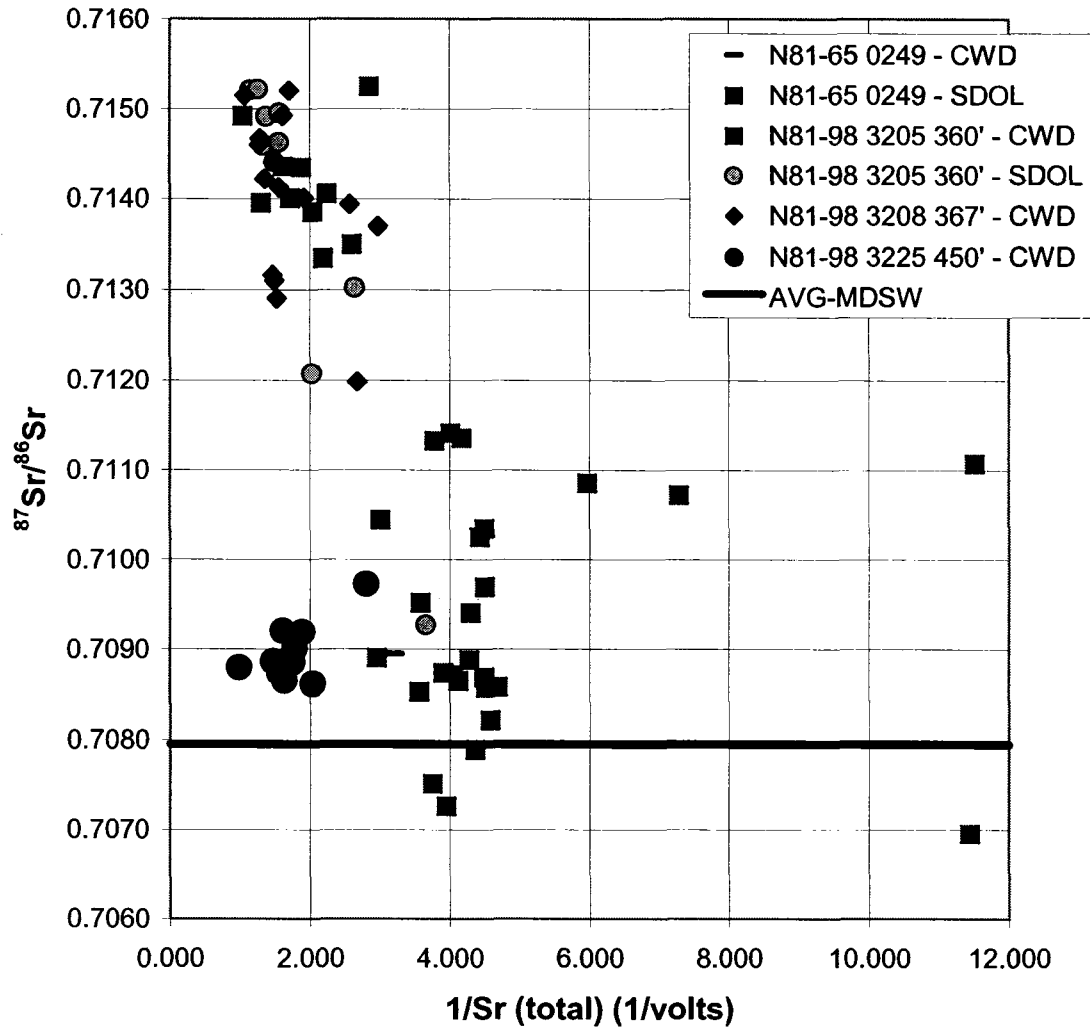


**Figure 6.2** Strontium isotopic compositions of coarse white and saddle dolomite (AVG-MDSW = average Middle Devonian seawater from Burke et al., 1982 (0.7080); CWD=coarse white dolomite; SDOL=saddle dolomite).

### 6.2.2 Coarse White Dolomite

Coarse white dolomite frequently displayed saddle textures in the samples analyzed. An attempt to determine if the saddle-textured type differed isotopically from the non-saddle

textured type of coarse white dolomite was made and as such saddle dolomite (SDOL) is discussed separately in Section 6.2.3.

Fifty-two coarse white dolomite  $^{87}\text{Sr}/^{86}\text{Sr}$  ratios and total Sr ion signals were acquired from four drill core samples in Appendix X. Coarse white dolomite ranged from 0.7073 to 0.7152 with an average  $^{87}\text{Sr}/^{86}\text{Sr}$  of 0.7116 (Figure 6.2). This average  $^{87}\text{Sr}/^{86}\text{Sr}$  ratio was more radiogenic than both the host dolomite analyzed in this study and the  $^{87}\text{Sr}/^{86}\text{Sr}$  value for Middle Devonian seawater.

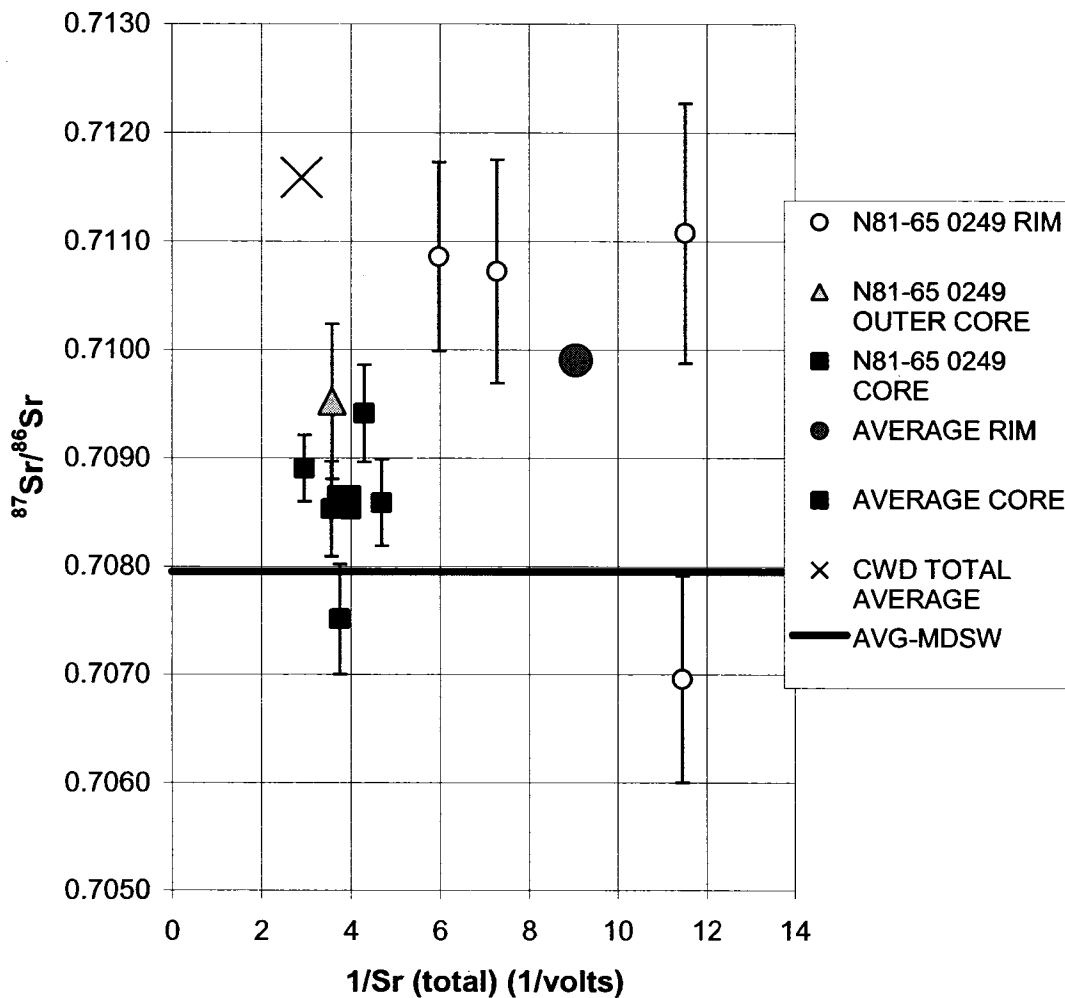


**Figure 6.3** Strontium isotopic compositions of saddle dolomite growth zones for sample N81-65 0249 (AVG-MDSW = average Middle Devonian seawater from Burke et al., 1982 (0.7080); CWD=coarse white dolomite).

Two N81-65 0249 samples of coarse white dolomite yielded  $^{87}\text{Sr}/^{86}\text{Sr}$  ratios of 0.7088 and 0.7090 (average = 0.7089) and total Sr ion signals of 0.2476 and 0.3122 volts (average = 0.2799 volts). N81-98 3205 360' coarse white dolomites had an average  $^{87}\text{Sr}/^{86}\text{Sr}$  value of 0.7113 with a minimum of 0.7073 and a maximum of 0.7152 ( $n = 25$ ) and total Sr ion signals ranged from 0.2185 to 0.9563 volts. Coarse white dolomite from sample N81-98 3225 450' has an average  $^{87}\text{Sr}/^{86}\text{Sr}$  value of 0.7090 and minimum and maximum Sr isotope values of 0.7086 and 0.7097, respectively. Sr ion signals ranged from 0.3568 to 1.0103 volts (average = 0.6067;  $n = 10$ ). Sample N81-98 3208 367' had a similar average total Sr ion signal (0.6243 volts;  $n = 15$ ) with a range of 0.3364 to 0.9334 volts. Sr isotope ratios varied from 0.7120 to 0.7152 with the most radiogenic average Sr isotope value of all the coarse white dolomite ratios (0.7140).

### 6.2.3 Saddle Dolomite

This study views saddle dolomite (SDOL) as a textural variety of coarse white dolomite (CWD). The nature of the in-situ isotopic analyses allowed specific areas, such as rims and cores, of coarse white dolomite that had saddle-texture development to be analyzed.

Saddle dolomite from two drill cores (N81-65 0249 and N81-98 3205 360') had an average value of 0.7117 ( $n = 21$ ) and varied from 0.7070 to 0.7152. Sample N81-65 0249 saddle dolomites yielded an average  $^{87}\text{Sr}/^{86}\text{Sr}$  value of 0.7092 ( $n = 10$ ) with a minimum of 0.7070 and maximum of 0.7111 (Figure 6.3). Total Sr ion signals ranged from 0.0868 to 0.3383 volts (average = 0.2090;  $n = 10$ ). Saddle dolomite analyses from sample N81-98 3205 360' had  $^{87}\text{Sr}/^{86}\text{Sr}$  values ranging from 0.7093 to 0.7152 (average = 0.7140;  $n = 11$ ) and total Sr ion signals ranging from 0.2736 to 0.8684 volts (average = 0.2090) (Figure 6.4).

Laser in-situ analysis allowed for the analysis of growth zones in single crystals. Multiple saddle dolomite rims, boundaries and cores were analyzed and are compared in Figures 6.3 and 6.4. The two samples analyzed have discrete isotopic characteristics and plot in two clusters except for two data points with low total Sr levels (both from sample N81-65 0249—see above).

Sample N81-98 3205 360' was more radiogenic and had higher total Sr ion signals (lower  $1/\text{Sr}_{\text{total}}$ ) than N81-65 0249 (Figure 6.2). The strontium isotope ratios showed a general trend of a more radiogenic composition at the rims (Figures 6.3 and 6.4). One "boundary" value plotted at an intermediate level in between the average rim and core values. Sample N81-65 0249 had core strontium values that plot in a cluster with relatively consistent Sr isotope and  $1/\text{Sr}_{\text{total}}$  values.

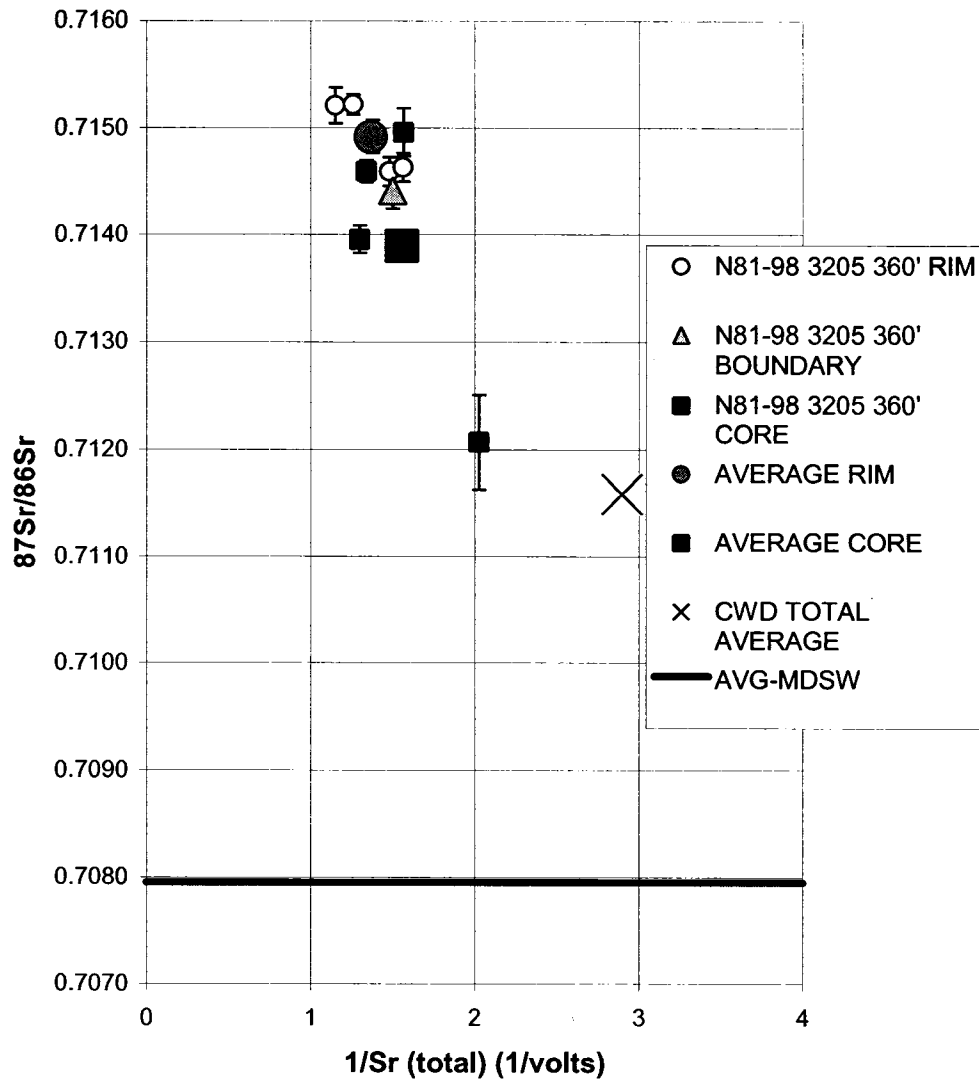


**Figure 6.4** Strontium isotopic compositions of saddle dolomite growth zones for sample N81-98 3205 360' (AVG-MDSW = average Middle Devonian seawater from Burke et al., 1982 (0.7080); CWD=coarse white dolomite).

Rim  $1/\text{Sr}_{\text{total}}$  values were more varied and plotted between 6.0 and 11.5  $\text{volts}^{-1}$ . All but one of the rim values was more radiogenic than core strontium isotopes. One value from an “outer core” zone was more radiogenic than all core values and less radiogenic than rim values. This appeared to be an intermediate isotopic composition and fell in between the average rim and core values. A general trend appeared in the previous plots from the two samples with rims yielding more radiogenic compositions than their cores.

The inverse of the total Sr ion signal in saddle dolomite versus the coarse white dolomite is compared in Figure 6.2. Other than two coarse white dolomites (both from N81-65 0249) having exceptionally high  $1/Sr_{total}$  values (low total Sr values), the plot shows two defined clusters of data, with both the coarse white and saddle dolomite spanning both of these groups. The average Sr isotopic and ion signal values for all of the coarse white dolomites (including saddle dolomite) plotted in between these two clusters.

#### 6.2.4 Calcite

Thirty-two calcite Sr isotope values were generally more radiogenic (average ratio of 0.7149) than both their dolomite counterparts and had a range of 0.7107 to 0.7186 (see Appendix X). N81-65 0249 had the most radiogenic average  $^{87}Sr/^{86}Sr$  ratio (0.7161) with maximum and minimum values of 0.7174 and 0.7153, respectively. Total Sr ions signals varied from 0.41 to 0.4928 volts (average = 0.4469 volts;  $n = 5$ ). Seven total Sr ions signals from sample N81-68A 2969 375' varied more considerably from 0.3065 to 2.8146 volts (average = 0.8542 volts) and had an average  $^{87}Sr/^{86}Sr$  ratio of 0.7149 (0.7140 to 0.7155). Sample N81-84 1078 had an average Sr isotope value of 0.7160 (0.7159 to 0.7161;  $n = 3$ ) and total strontium ion signals ranging from 0.8737 to 1.0301 volts (average = 0.9372 volts). Two N81-98 3181 287' calcite phases yielded an average Sr isotopic ratio of 0.7155 and a 0.2400 volt average total Sr ion signal (see Appendix X). Sample N81-98 3205 355' had an average  $^{87}Sr/^{86}Sr$  ratio of 0.7145 (0.7107 to 0.7154;  $n = 6$ ) and an average total Sr ion signal of 0.4034 volts (0.3305 to 0.5257 volts). N81-98 3214 had the lowest  $^{87}Sr/^{86}Sr$  ratio of all the average values (0.7130) and the six samples analyzed ranged from 0.7117 to 0.7139 and had average total Sr ion signal of 1.0433 volts. Three  $^{87}Sr/^{86}Sr$  values from calcite of N81-98 3225 450' varied from 0.7157 to 0.7160 (average = 0.7158) and had total Sr ion signals spanning from 0.5347 to 0.7489 volts (average = 0.6516 volts) (see Figure 6.5).

### 6.3 Comparison to Previous Work

#### 6.3.1 Host dolomite

Host dolomite, coarse white dolomite and calcite  $^{87}Sr/^{86}Sr$  ratios are compared to previous Pine Point Sr isotopic studies (see Appendix XII and Figure 6.7). The total strontium isotopic data presented here substantially increases the amount of Sr data collected from Pine Point and introduces new results. The Pine Point host dolomite of this study is equivalent to “fine crystalline dolomite” of Mountjoy et al. (1992) and Qing (1998) and to “Presqu'île

dolomite” of Medford et al. (1983) (see also Figure 6.7). Host dolomite is generally comparable in Sr isotopic composition to “fine crystalline dolomite” and “Presqu’ile dolomite” although three points from this study are considerably more radiogenic.

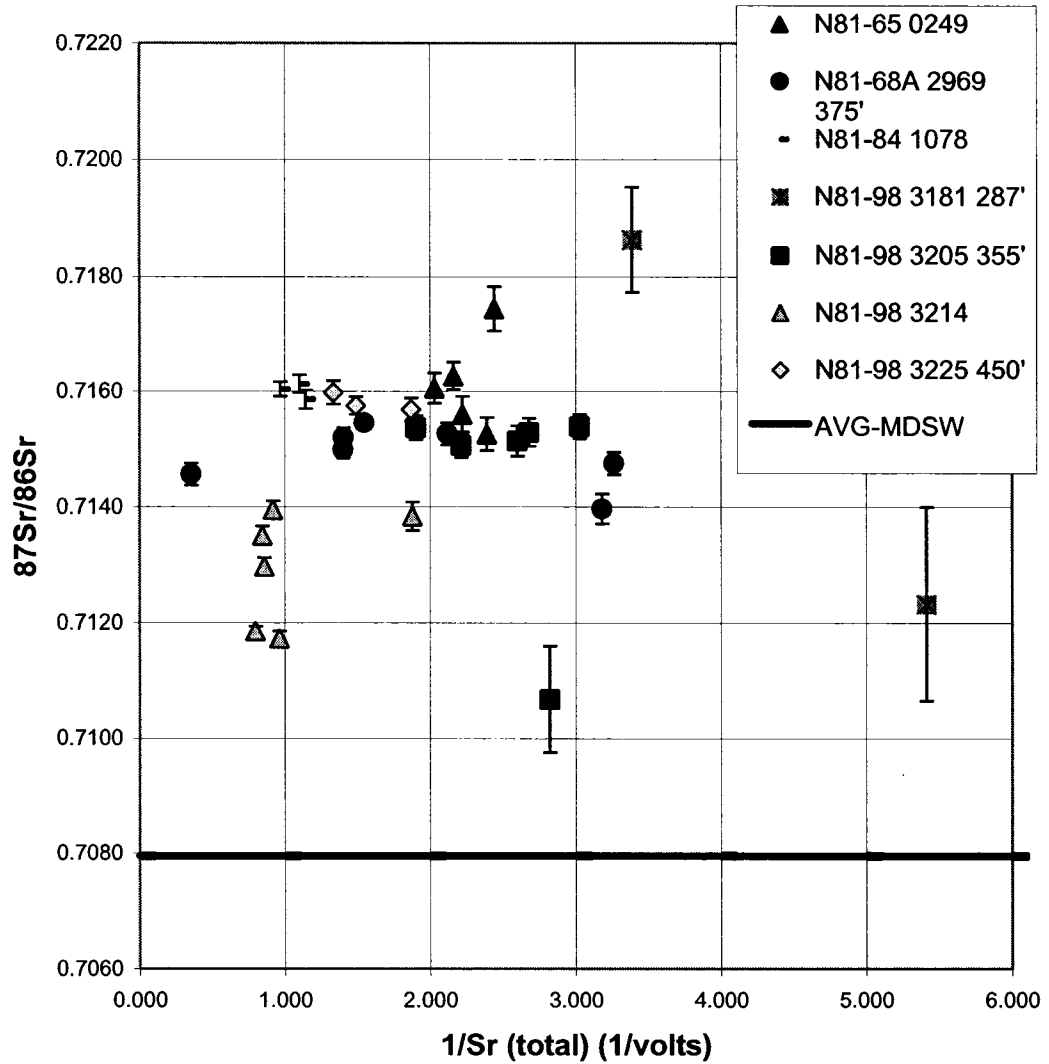


**Figure 6.5** Strontium isotopic compositions of calcite (AVG-MDSW = average Middle Devonian seawater from Burke et al., 1982 (0.7080)).

### 6.3.2 Coarse White Dolomite and Saddle Dolomite

The maximum value of  $^{87}\text{Sr}/^{86}\text{Sr}$  in coarse white dolomite equivalent phases has been reported by most previous workers to be 0.7085 (e.g. Mountjoy et al., 1992 and Qing, 1998). This study reports many coarse white dolomite phases with much more radiogenic strontium isotope values (up to 0.7152) (see Appendix X). The radiogenic nature of the coarse white dolomites suggests a source of radiogenic strontium is needed in the system. The average  $^{87}\text{Sr}/^{86}\text{Sr}$  composition for the seventy-three coarse white dolomites of this study is much more radiogenic than all previous data compared to it (Figure 6.7). All the Qing and/or Mountjoy data for saddle dolomite range from 0.70807 to 0.70850. Maxwell (1976) reports one “sparry dolomite” phase strontium composition of 0.7096. Al-Aasm et al. (2000) analyzed saddle dolomites of the Sulphur Point and Slave Point formations in northern Alberta and, these dolomites range from 0.70810 to 0.71024 and 0.70860 to 0.71035, respectively.

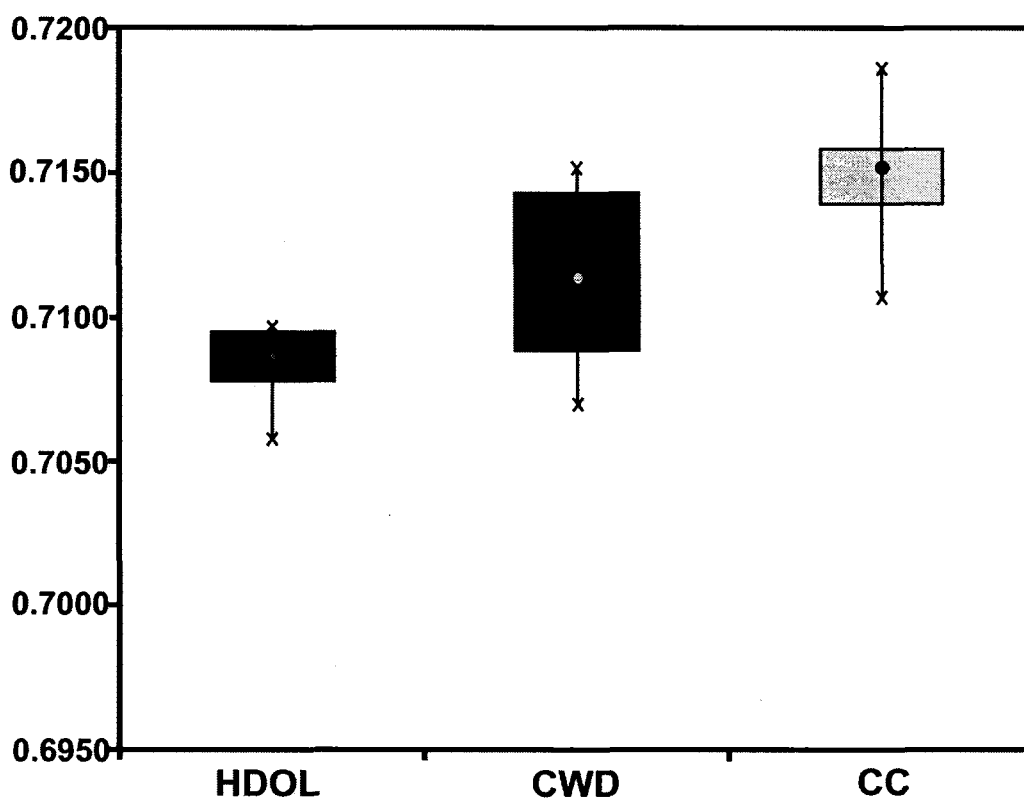


**Figure 6.6** Box and whisker plot of host dolomite (HDOL), coarse white dolomite (CWD) and calcite (CC) phases. The circles mark the median value of the three individual data sets.

### 6.3.3 Calcite

Previous studies have recognized variable strontium isotopic compositions in calcites. Our data concur with the general variability of calcite compositions although these new data do extend the compositions toward a more radiogenic end member (Figure 6.7). The late-stage calcite compositions are most radiogenic all of three phases analyzed in this study and agree with previous calcite strontium isotope work at Pine Point (Maxwell, 1976; Medford et al., 1983; Mountjoy et al., 1992; among others). The radiogenic nature of the calcites implies an interaction with an external  $^{87}\text{Sr}$ -enriched fluid or rock unit.

### 6.4 Geochemical Implications for Fluid Sources

The strontium isotopic compositions of the host dolomite suggest this phase formed from Middle Devonian seawater, since, the average host dolomite  $^{87}\text{Sr}/^{86}\text{Sr}$  composition (0.7078 to 0.7082) is statistically indistinguishable from Middle Devonian seawater (0.7080) (Burke et al., 1982). This concurs with the views of Medford et al. (1983), Mountjoy et al. (1992) and Qing (1998). However, the isotopic values range from an anomalously low value of 0.7058 to a slightly more radiogenic value of 0.7097, suggesting the conditions producing the host dolomite are more complex than simply Middle Devonian seawater. The fluids were likely somewhat influenced by a radiogenic strontium component. The “Medium crystalline dolomite” strontium isotopic compositions of Mountjoy et al. (1992) and Qing (1998) range from 0.70812 to 0.70871 (average = 0.7084) and 0.7081 to 0.7087, respectively. Mountjoy et al. (1992) notes the slightly radiogenic nature of these dolomites and suggests that an introduction of  $^{87}\text{Sr}$  from formation waters different than those of Middle Devonian seawater likely caused the increase in radiogenic strontium values. Qing (1998) suggests “burial dolomitizing fluids” which are slightly radiogenic, “neomorphic alteration during later burial diagenesis” and/or that the dolomites could have been neomorphosed by hydrothermal fluids in the subsurface to explain the elevated strontium ratios.

Coarse white dolomite strontium ratios are more radiogenic than Middle Devonian seawater and must have been enriched by  $^{87}\text{Sr}$  from another source. Medford et al. (1983) state that ore-associated dolomite veins likely reflect an “imprint” of a solution enriched in  $^{87}\text{Sr}$ . Their study’s findings of the radiogenic nature of the dolomites (mean  $^{87}\text{Sr}/^{86}\text{Sr}$  ratio of 0.7110) are remarkably similar to the values reported here from coarse white dolomites and saddle dolomites (average 0.7116). Mountjoy et al. (1992) re-evaluated samples from Medford et al.

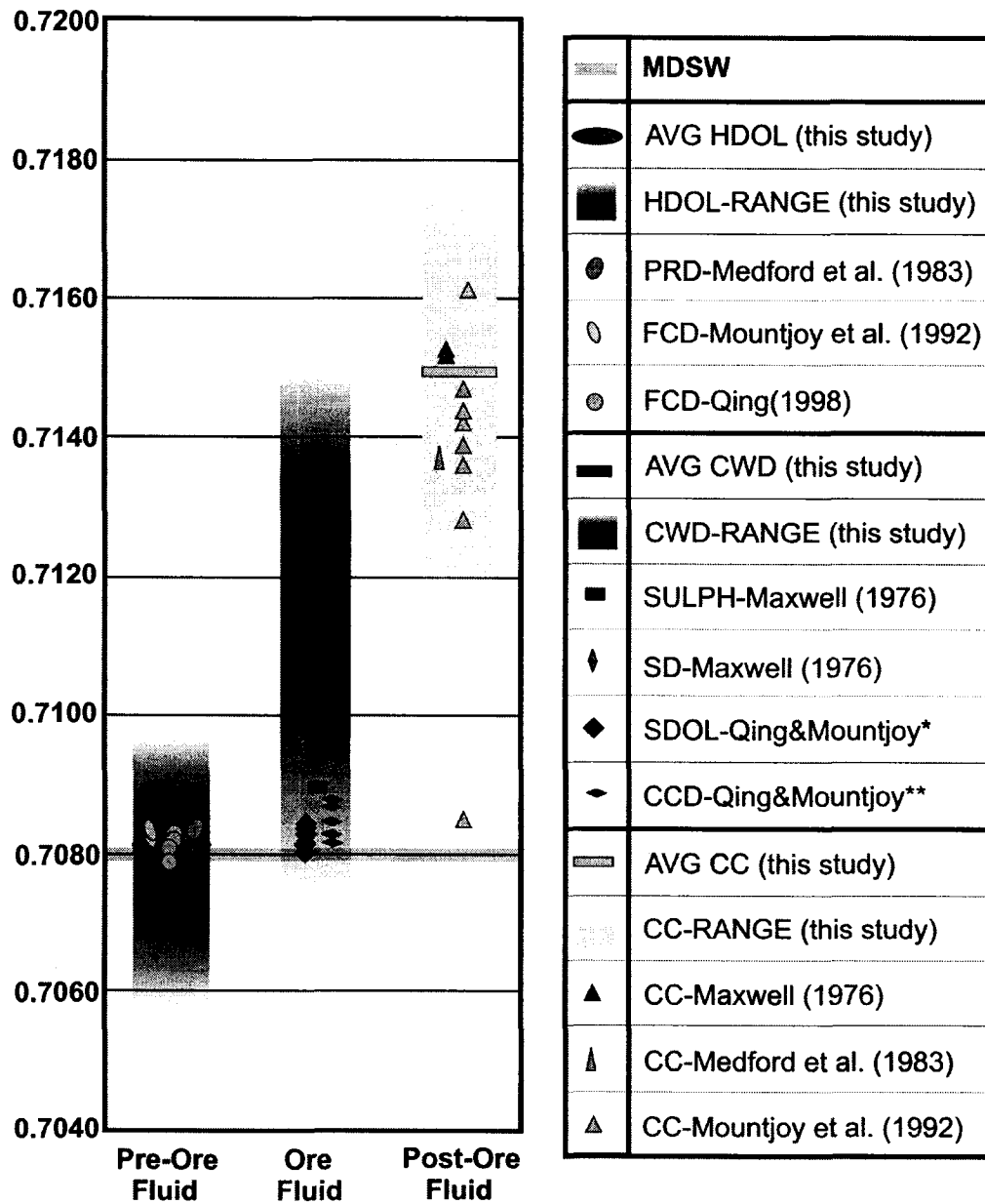


**Figure 6.7** Comparison plot of strontium various isotopic studies at Pine Point. Shaded areas are the range of strontium isotope data from this study. (HDOL=host dolomite; CWD=coarse white dolomite; CC=calcite; PRD=Presqu'île dolomite; FCD=Fine-grained crystalline dolomite; SULPH=sulphides; SD=sparry dolomite; SDOL=saddle dolomite; CCD=coarse crystalline dolomite; AVG=average; MDSW = Middle Devonian seawater range from Burke et al., 1982 (0.7078-0.7082; \*=data from Mountjoy et al. (1992), Qing (1998), Qing and Mountjoy (1994), Qing and Mountjoy (1992); \*\*=data from Mountjoy et al. (1992) and Qing and Mountjoy (1994)).

(1983) and suggested the radiogenic values of some samples were in fact due to a mixture of saddle dolomite and white calcite. The in-situ nature of the strontium isotopic analysis of this study validates the study of Medford et al., (1983) and clearly shows that saddle dolomite  $^{87}\text{Sr}/^{86}\text{Sr}$  ratios have radiogenic values that can exceed those found in their study (average = 0.7117). The data presented here also show that the isotopic composition of the coarse white dolomites is often above the MASIRBAS value of 0.7120 (Machel and Cavell, 1999). Deeper subsurface saddle dolomites with radiogenic strontium isotopic compositions and Pine Point saddle dolomites (0.70807-0.70847; average = 0.7083) were reported by Mountjoy et al. (1992) and were suggested to be formed from the mixing of a  $^{87}\text{Sr}$ -enriched fluid and a “less enriched one”. Qing and Mountjoy (1992 and 1994) report Pine Point saddle dolomite strontium composition ranges identical to those of Mountjoy et al. (1992). The authors suggest that saddle dolomite and their “coarse crystalline dolomite” formed from a “diagenetic fluid with similar chemical compositions” and the less radiogenic nature of their saddle dolomites could be due to the dissolution of Middle Devonian limestones.

Calcite  $^{87}\text{Sr}/^{86}\text{Sr}$  values are the most radiogenic of all phases analyzed (average = 0.7149). Maxwell (1976) and Medford et al. (1983) report calcite at radiogenic values of 0.7152 to 0.7153 and 0.7137, respectively. Mountjoy et al. (1992) suggest that radiogenic calcite may be caused by a mixture of Shield-derived waters and basin brines.

Plate 6.0

A. Photograph of a Sr-isotope laser track in host dolomite from sample N81-65 0249 that has been partially replaced by coarse white dolomite ( $^{87}\text{Sr}/^{86}\text{Sr} = 0.7084$ ). The sample was photographed in plane polarized light.

B. Photograph of sphalerite (bottom left) and a Sr-isotope laser track in host dolomite which has been partially replaced by coarse white dolomite ( $^{87}\text{Sr}/^{86}\text{Sr} = 0.7087$ ) (viewed in plane polarized light).

C. Same field of view as previous photograph (B) except viewed in crossed polarized light.

D. Photograph of a Sr-isotope laser track in host dolomite from sample N81-98 3225 450' (viewed in plane polarized light). This sample yielded the lowest  $^{87}\text{Sr}/^{86}\text{Sr}$  ratio of this study (0.7058). The blue markings are a pen outline.

E. Sr-isotope laser track in host dolomite from sample N81-98 3225 450' photographed in plane polarized light ( $^{87}\text{Sr}/^{86}\text{Sr} = 0.7078$ ). The blue markings are a pen outline.

F. Photograph of a Sr-isotope laser track in host dolomite from sample N81-98 3225 450' viewed in plane polarized light ( $^{87}\text{Sr}/^{86}\text{Sr} = 0.7097$ ). The red markings are a pen outline.

G. Same field of view as previous photograph (G) except viewed in crossed polarized light.

Plate 6.0

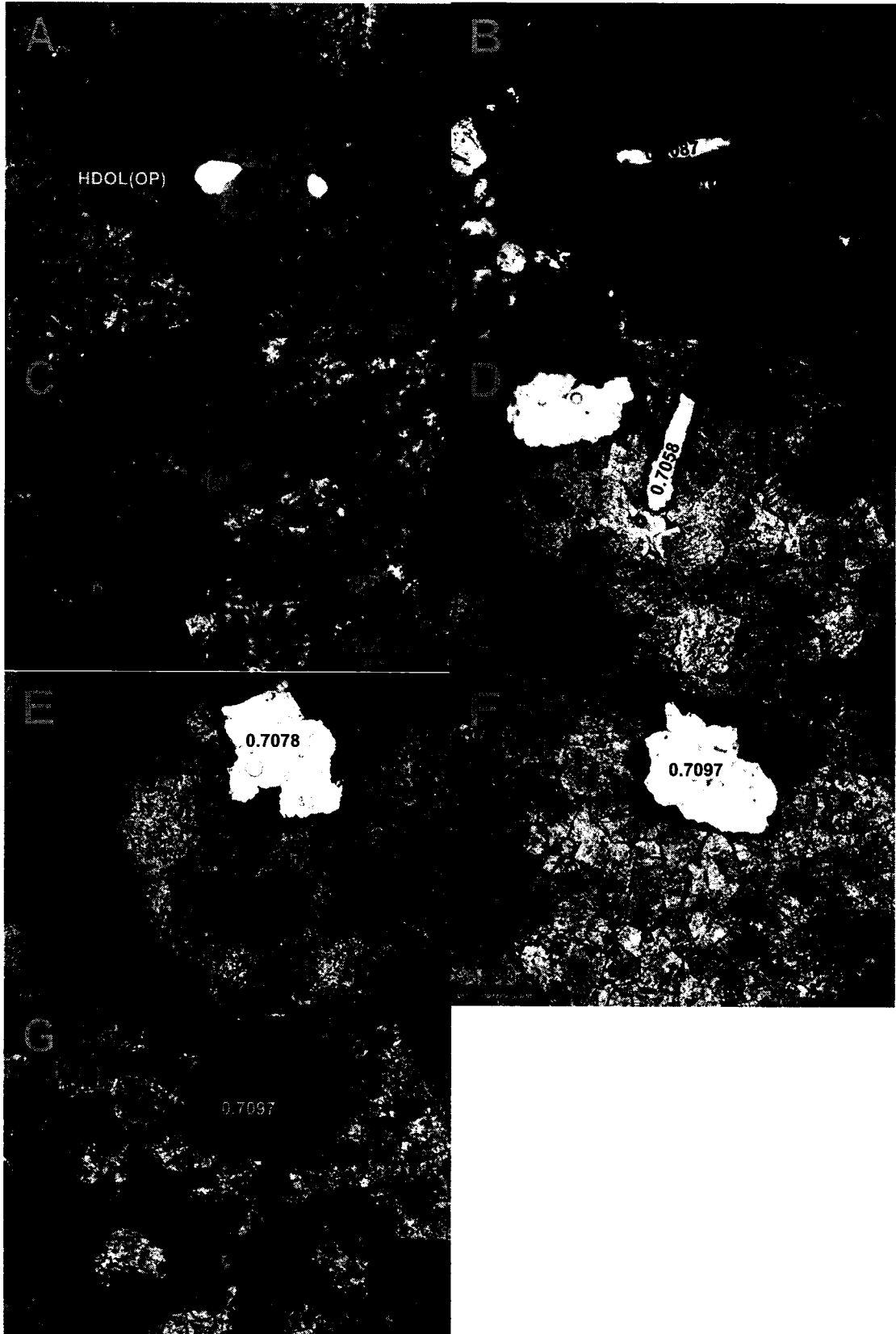


Plate 6.1

A. Photograph of coarse white dolomite with an  $^{87}\text{Sr}/^{86}\text{Sr}$  value of 0.7090 from sample N81-65 0249. The photograph was taken in plane polarized light.

B. Photograph of a coarse white dolomite-hosted Sr-isotope track from sample N81-65 2049 with an  $^{87}\text{Sr}/^{86}\text{Sr}$  value of 0.7088 and viewed in plane polarized light.

C. Photograph of three strontium isotope laser tracks along the rim, boundary and core zones of a saddle form of coarse white dolomite from sample N81-65 0249. The strontium isotope ratios become more radiogenic from core, boundary to rim with values of 0.7089, 0.7095 and 0.7109, respectively. Calcite is visible in the top portion of the photograph with a slight red staining.

D. Photograph showing saddle textured coarse white dolomite (SDOL) rim and core from sample N81-65 0249. The  $^{87}\text{Sr}/^{86}\text{Sr}$  value for the rim is more radiogenic at 0.7111 whereas the core has a value of 0.7075 (CC=calcite).

E. Photograph of a rim and core zone in saddle dolomite from sample N81-65 0249 with  $^{87}\text{Sr}/^{86}\text{Sr}$  values of 0.7104 and 0.7086, respectively (SDOL=saddle dolomite; CC=calcite).

F. Same Sr isotopic tracks as in photograph (E) except under higher magnification (SDOL=saddle dolomite; CC=calcite).

G. Photograph of a boundary between the rim and core of a saddle dolomite crystal from sample N81-65 0249 ( $^{87}\text{Sr}/^{86}\text{Sr} = 0.7094$ ) (SDOL=saddle dolomite; CC=calcite).

H. Photograph of a rim and core from a saddle dolomite crystal from sample N81-65 0249 (SDOL=saddle dolomite).

Plate 6.1

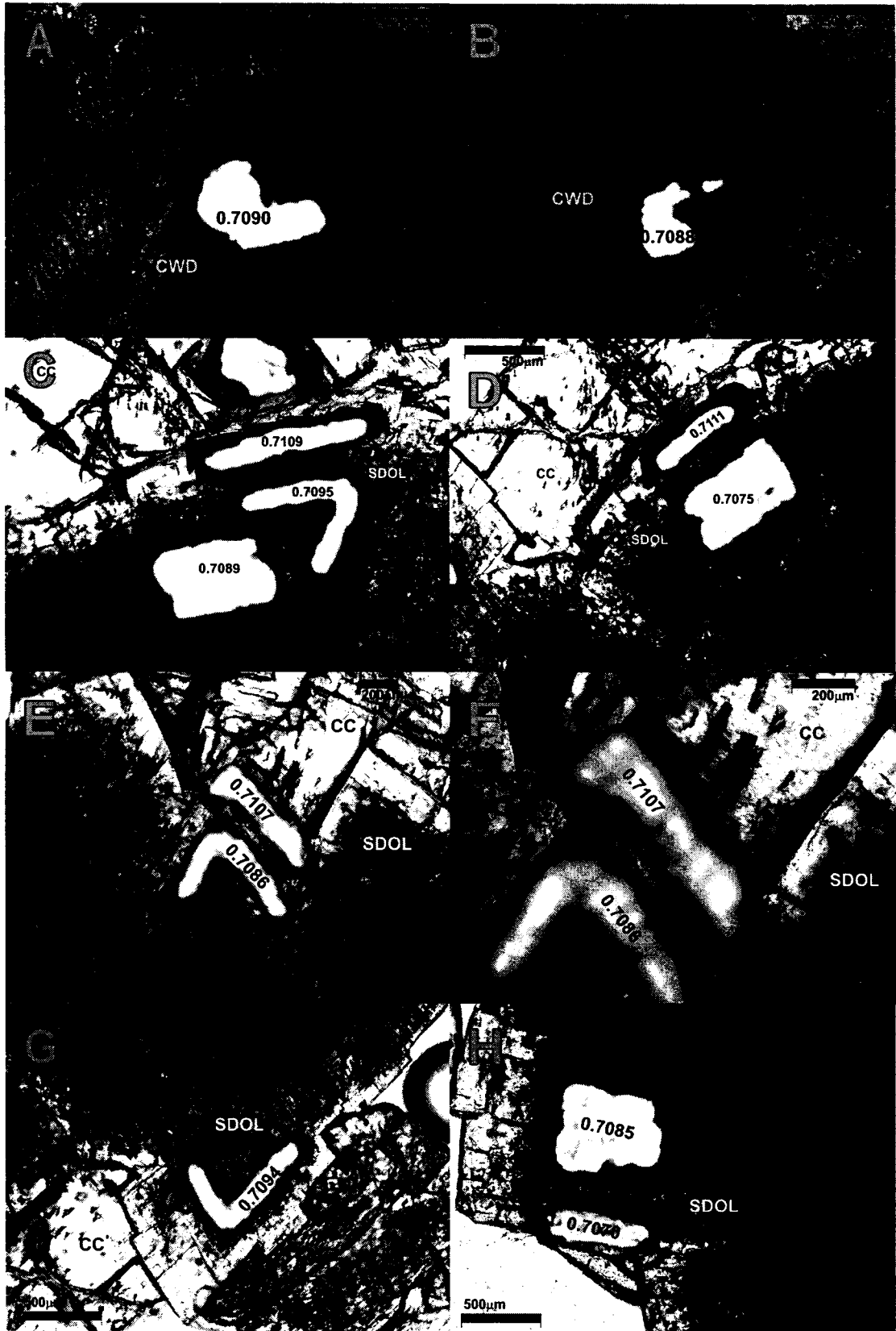


Plate 6.2

- A. Photograph of two Sr-isotope laser tracks in coarse white dolomite from sample N81-98 3205 360' viewed in plane polarized light ( $^{87}\text{Sr}/^{86}\text{Sr} = 0.7114$  and  $0.7130$ ).
- B. Same field of view as photograph (A) except viewed under crossed polarized light.
- C. Photograph of a strontium isotope laser track in coarse white dolomite, surrounded by colloform sphalerite, from sample N81-98 3205 360' viewed in plane polarized light ( $^{87}\text{Sr}/^{86}\text{Sr} = 0.7139$ ).
- D. Same field of view as photograph (C) except viewed under crossed polarized light.
- E. Photograph of a Sr-isotope laser track in coarse white dolomite from sample N81-98 3205 360' viewed in plane polarized light ( $^{87}\text{Sr}/^{86}\text{Sr} = 0.7114$ ).
- F. Same field of view as photograph (E) except viewed under crossed polarized light.
- G. Photograph of a Sr-isotope track in coarse white dolomite from sample N81-98 3205 360' viewed in plane polarized light ( $^{87}\text{Sr}/^{86}\text{Sr} = 0.7144$ ).
- H. Same field of view as photograph (G) except viewed under crossed polarized light.

Plate 6.2



Plate 6.3

- A. Photograph of a Sr-isotope laser track in coarse white dolomite surrounded by sphalerite from sample N81-98 3205 360' and viewed in plane polarized light ( $^{87}\text{Sr}/^{86}\text{Sr} = 0.7086$ ).
- B Same field of view as photograph (A) except viewed under crossed polarized light.
- C. This image was photographed in plane polarized light and contains two Sr-isotopic tracks in coarse white dolomite from sample N81-98 3205 360' ( $^{87}\text{Sr}/^{86}\text{Sr} = 0.7149$  and  $0.7153$ ) (SPH=sphalerite).
- D. Same field of view as photograph (C) except viewed under crossed polarized light.
- E. Photograph of strontium isotopic tracks in coarse white dolomite ranging in  $^{87}\text{Sr}/^{86}\text{Sr}$  from 0.7140 to 0.7146 from sample N81-98 3205 360' (photographed in plane polarized light).
- F. Photograph of coarse white dolomite from sample N81-98 3205 360' showing 5 laser tracks and 2 laser spot Sr-isotopic analyses ranging in  $^{87}\text{Sr}/^{86}\text{Sr}$  values from 0.7121 to 0.7152 from (viewed in plane polarized light).
- G. Photograph of two coarse white dolomite-hosted Sr-isotopic laser tracks from sample N81-98 3205 360' viewed in plane polarized light ( $^{87}\text{Sr}/^{86}\text{Sr} = 0.7140$  and  $0.7141$ ).
- H. Photograph of 3 strontium isotopic laser tracks in coarse white dolomite from sample N81-98 3205 360' ( $^{87}\text{Sr}/^{86}\text{Sr} = 0.7073, 0.70870$  and  $0.7113$ ). The photograph was taken in plane polarized light.

Plate 6.3

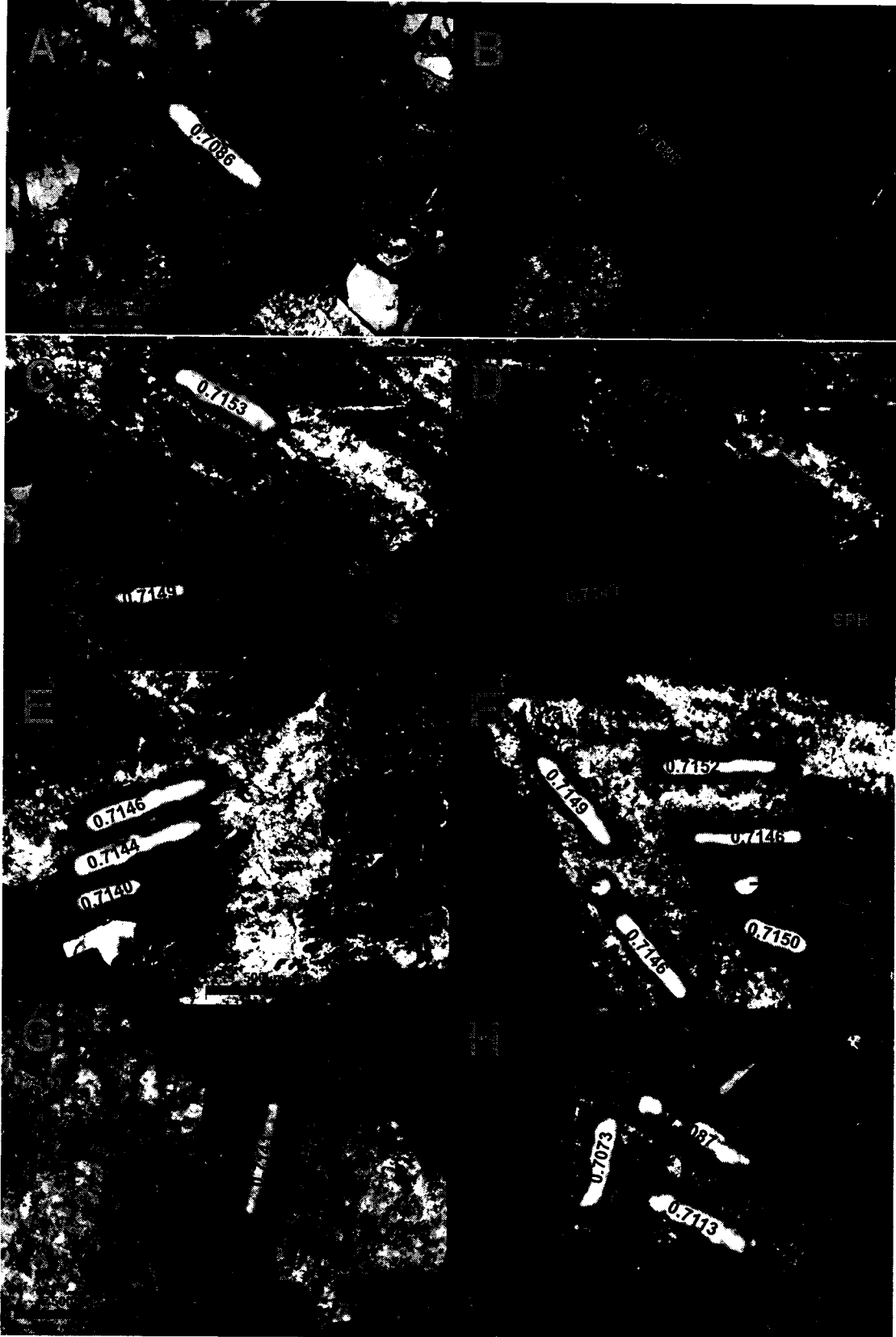


Plate 6.4

A. Photograph of a Sr-isotope laser track in coarse white dolomite from sample N81-98 3225 450' viewed in plane polarized light ( $^{87}\text{Sr}/^{86}\text{Sr} = 0.7089$ ).

B. A Sr-isotope laser track in coarse white dolomite from sample N81-98 3225 450' photographed in plane polarized light ( $^{87}\text{Sr}/^{86}\text{Sr} = 0.7092$ ).

C. Photograph of a strontium isotope track ( $^{87}\text{Sr}/^{86}\text{Sr}$  value of 0.7137) in coarse white dolomite from sample N81-98 3208 367' (viewed in plane polarized light).

D. Photograph of two strontium isotope laser tracks with  $^{87}\text{Sr}/^{86}\text{Sr}$  values of 0.7146 and 0.7152 from sample N81-98 3208 367' viewed in plane polarized light.

Plate 6.4

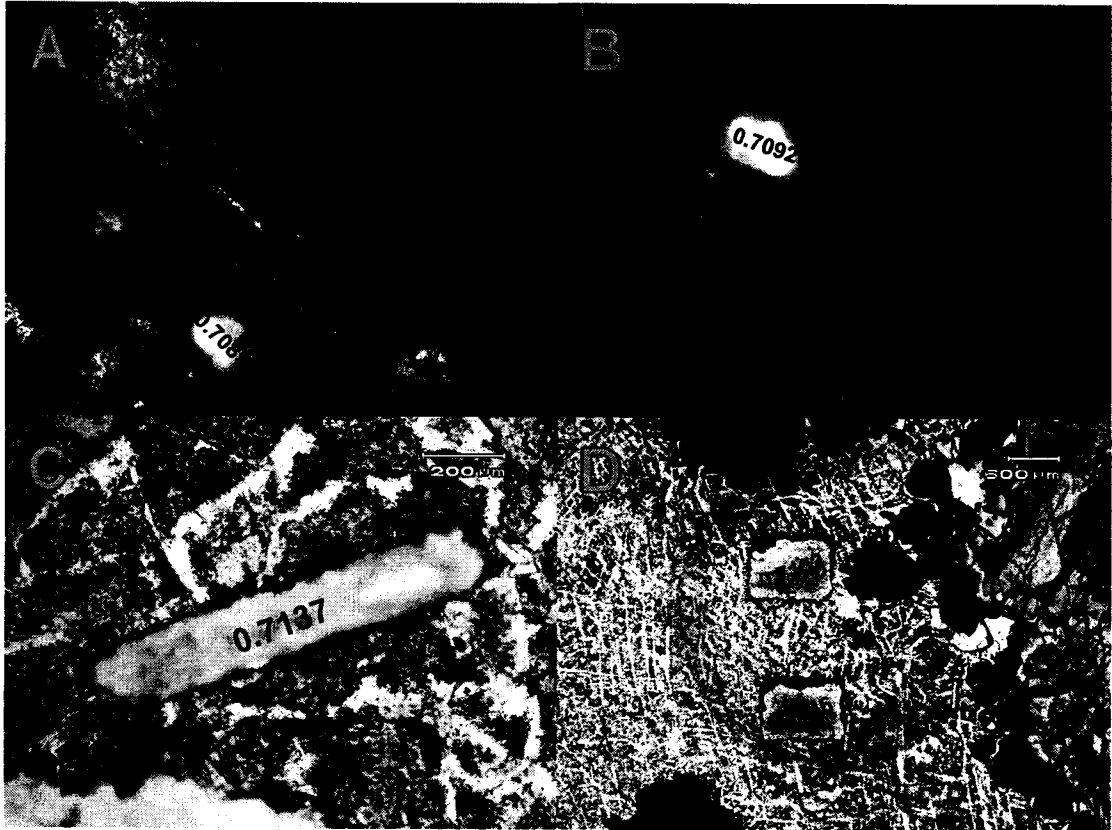


Plate 6.5

- A. Photograph of strontium isotope tracks in calcite from sample N81-65 0249 viewed in plane polarized light ( $^{87}\text{Sr}/^{86}\text{Sr}$  values of 0.7152 and 0.7163).
- B. Photograph of a calcite-hosted strontium laser track ( $^{87}\text{Sr}/^{86}\text{Sr}$  value of 0.7186), sphalerite and galena from sample N81-98 3181 287' (viewed in plane polarized light).
- C. A strontium isotopic laser track in calcite from sample N81-98 3181 287' photographed in plane polarized light ( $^{87}\text{Sr}/^{86}\text{Sr} = 0.7123$ ).
- D. Same view as above photograph (C) except viewed in crossed polarized light.
- E. Photograph of three strontium isotope tracks in calcite from sample N81-98 3205 355' viewed in plane polarized light ( $^{87}\text{Sr}/^{86}\text{Sr} = 0.7153, 0.7154$  and  $0.7154$ ).
- F. Strontium isotope tracks in calcite from sample N81-98 3205 355' viewed in plane polarized light. Both of the laser tracks have identical  $^{87}\text{Sr}/^{86}\text{Sr}$  values of 0.7151.
- G. Photograph of a Sr-isotope laser track in calcite from sample N81-98 3214 (viewed in plane polarized light) ( $^{87}\text{Sr}/^{86}\text{Sr} = 0.7117$ ).
- H. Same view as above photograph (G) except viewed in crossed polarized light.

Plate 6.5



Plate 6.6

- A. Photograph of a Sr-isotope laser track in calcite from sample N81-98 3214 taken in plane polarized light ( $^{87}\text{Sr}/^{86}\text{Sr} = 0.7138$ ).
- B. Same view as above photograph (A) except viewed in crossed polarized light.
- C. A Sr-isotope laser track in calcite from sample N81-98 3214 viewed in plane polarized light ( $^{87}\text{Sr}/^{86}\text{Sr} = 0.7118$ ). Dark reddish-brown sphalerite is present in the right portion of the photograph.
- D. Photograph of a Sr-isotope laser track in calcite from sample N81-98 3214 (viewed in plane polarized light) ( $^{87}\text{Sr}/^{86}\text{Sr} = 0.7135$ ).
- E. Photograph of a Sr-isotope laser track in calcite from sample N81-98 3225 450' viewed in plane polarized light ( $^{87}\text{Sr}/^{86}\text{Sr} = 0.7157$ ).
- F. Same view as above photograph (E) except viewed in crossed polarized light.
- G. Photograph of a calcite-hosted Sr-isotope laser track from sample N81-98 3225 450' viewed in plane polarized light ( $^{87}\text{Sr}/^{86}\text{Sr} = 0.7160$ ).
- H. Same view as above photograph (G) except viewed in crossed polarized light.

Plate 6.6



Plate 6.7

A. Photograph showing calcite with a Sr-isotope laser track and saddle textured coarse white dolomite (left dark portion of the field of view) from sample N81-98 3225 450' (viewed in plane polarized light). This calcite has an  $^{87}\text{Sr}/^{86}\text{Sr}$  ratio of 0.7158.

B. Same view as above photograph (A) except viewed in crossed polarized light.

C. Calcite-hosted strontium isotope track with an  $^{87}\text{Sr}/^{86}\text{Sr}$  value of 0.7152 from sample N81-98 2696 375' (viewed in plane polarized light).

D. Same view as above photograph (C) except viewed in crossed polarized light.

E. Photograph of a strontium isotope track in calcite with an  $^{87}\text{Sr}/^{86}\text{Sr}$  value of 0.7146 from sample N81-98 2696 375' (photographed in plane polarized light).

F. Same view as above photograph (E) except viewed in crossed polarized light.

Plate 6.7



## CHAPTER 7

### DISCUSSION

#### 7.1 Introduction

The overall objective of this thesis is to characterize the mineralizing and non-mineralizing fluids involved at Pine Point with particular focus on the N81 deposit. Individually, Chapters 4 through 6 focussed on specific geochemical objectives, which were based on the petrographic analysis of Chapter 3. The objective of this final chapter is to integrate the findings of all the previous chapters into a synopsis of the origin and evolution of the fluids involved in the deposit.

#### 7.2 Summary of Fluids Involved in the N81 Deposit

##### 7.2.1 *Pre-Ore Fluid*

Data obtained from the analysis of host dolomite and its fluid inclusion leachates represents the pre-ore fluid in the N81 deposit. No microthermometric analysis was possible on host dolomite and therefore, there is no data to constrain the total salinity and/or temperatures of this phase. The pre-ore fluid at the N81 deposit is characterized by an average  $^{87}\text{Sr}/^{86}\text{Sr}$  ratio of 0.7082. Halogen and cation bulk geochemical studies gave an average Cl/Br of 328 and Na/Br of 132, which are comparable to the ratios of the fluid responsible for the sulphide mineralization but much lower than those of the post-ore fluid (see Table 7.1). Host dolomite leachates have a large variation in K from evaporated seawater (see Figure 5.7). The variable increase in K suggests that the element has been added to the fluid along the flow path. Lithium values are below those of evaporated seawater and indicate a slight loss of Li along the flow path (see Figure 5.8).

##### 7.2.2 *Ore-Stage Fluid*

Petrographic, microthermometric and bulk geochemical analysis from Chapters 3 through 5 demonstrate that the fluids that formed coarse white dolomite are associated with sphalerite and galena mineralization. The ore-stage fluid of the N81 deposit is consequently represented by data obtained from coarse white dolomite and the sulphides. Ore-associated coarse white dolomite has an average  $^{87}\text{Sr}/^{86}\text{Sr}$  ratio of 0.7116, which is more radiogenic than that of the pre-ore fluid and less radiogenic than that of the post-ore fluid. Molar Cl/Br ratios from phases representing the ore fluid ranged from 271 to 319 which are slightly less than those of the pre-ore fluid and much less than those of the post-ore fluid (e.g. average Cl/Br = 561).

Molar Na/Br averages in the ore fluid ranged from 114 to 161, which are comparable to those of the pre-ore fluid but less than those of the post-ore fluid (see Table 7.1). The fluid responsible for the sphalerite mineralization is a warm saline brine with an average homogenization temperature of 74°C and a salinity of 21 wt% equivalent CaCl<sub>2</sub>+NaCl. Coarse dolomite-hosted fluid inclusions, which represent a fluid intimately related to the mineralization, yielded a comparable minimum trapping temperature of 82°C and a similar average salinity (23 wt% CaCl<sub>2</sub>+NaCl). Hydrohalite melting temperatures from primary fluid inclusions in coarse white dolomite indicate the ore-fluid is a highly calcic brine. Potassium levels indicate that the K content of the ore fluid has not been significantly modified from evaporated seawater. The ore fluid is slightly enriched in Li compared to evaporated seawater.

	<i>Pre-Ore Fluid</i>	<i>Ore Fluid</i>			<i>Post-Ore Fluid</i>
	HDOL	CWD	SPH	GN	CC
Cl/Br (molar)	328	319	271	287	561
Na/Br (molar)	132	114	146	161	228
SO <sub>4</sub> /Br (molar)	71	13	-	-	193
K/Na (molar)	0.318	0.109	-	-	0.205
Li/Na (molar)	0.0005	0.0005	-	-	0.0008
K/Br (molar)	41	11	-	-	46
Cl (ppm)	-	14400	126200	-	48100
Br (ppm)	-	1050	1250	-	220
SO <sub>4</sub> (ppm)	-	16800		-	33300
Na (ppm)	-	32000	47600	-	18200
K (ppm)	-	5830	-	-	2910
Li (ppm)	-	4	-	-	-

**Table 7.1** Average halogen and cation molar ratios and absolute values for pre-ore, ore and post-ore fluids in the N81 deposit.

### 7.2.3 *Post-Ore Fluid*

Data from late-stage calcite typifies the post-ore fluid in the N81 deposit. The post-ore fluid is the most radiogenic (average <sup>87</sup>Sr/<sup>86</sup>Sr = 0.7149) of the three main fluids (pre-ore, ore-stage and post-ore) involved in the N81 deposit. The average Cl/Br and Na/Br ratios are the

highest of all the fluids. The ore-stage fluid average absolute Cl, Br and Na values differed drastically from those of the post-ore fluid. Absolute concentrations of Cl, Br and Na are considerably lower than those of the ore fluid (see Table 7.1) as a result of the lower fluid salinity. Homogenization and ice melting temperatures from primary calcite-hosted inclusions indicate that the post-ore fluid is warmer (92°C) and much less saline (9 wt% NaCl-CaCl<sub>2</sub> equivalent) than the ore-forming fluid. Additionally, the post-ore fluid has a remarkably different salt component indicating a NaCl-rich brine with a minimal CaCl<sub>2</sub> component. K-Cl-Br systematics show a large variation in potassium from evaporated seawater in calcite leachates representing the post-ore fluid suggesting that the element has been added to the fluid, likely along its flow path (see Figure 5.7). Li-K-Na systematics indicate that the calcite leachates have a slight loss of Li along the flow path (see Figure 5.8).

### 7.3 Fluid Origins and Water-Rock Interactions

Strontium isotopic and bulk fluid inclusion data constrain the origin and water-rock interactions that alter the composition of a fluid. The following sections include discussions on data obtained from Sr and bulk fluid inclusion analyses of phases representing pre-ore, ore-stage and post-ore fluids.

#### 7.3.1 *Nature of Clastics and Basement Rocks*

A common observation in the pre-ore, ore-stage and post-ore fluids of this study is the presence of radiogenic Sr. Bulk geochemical data suggest that most of the phases analysed were formed from evaporated seawater yet many of the phases have elevated <sup>87</sup>Sr levels. As such, this section outlines radiogenic Sr levels in rocks that may be acting as sources for the elevated <sup>87</sup>Sr.

Lonnee (2005) analyzed potential Sr source rocks in northeastern British Columbia to suggest possible sources of radiogenic Sr present in some carbonates of the Slave Point formation (e.g. saddle dolomites). Crystalline basement rocks (e.g. blastomylonite, gneiss, diabase, meta-argillite, diorite, quartzite and granodiorite) were analyzed and had <sup>87</sup>Sr/<sup>86</sup>Sr ratios ranging from 0.7219 to 0.8234. A single Cambrian sandstone sample (underlying the Devonian strata) was analyzed and had an <sup>87</sup>Sr/<sup>86</sup>Sr ratio of 0.7198. The study also analyzed Phanerozoic basinal shales that ranged in <sup>87</sup>Sr/<sup>86</sup>Sr ratios from 0.7088 to 0.7123. Connolly et al. (1990) analyzed 3 Cambrian shales in the Alberta basin (<sup>87</sup>Sr/<sup>86</sup>Sr ratios ranging from 0.7431 to 0.7757) and two Precambrian greenstones (<sup>87</sup>Sr/<sup>86</sup>Sr ratios of 1.0932 and 1.3097). Machel and

Cavell (1999) suggested that any carbonate phase that has an  $^{87}\text{Sr}/^{86}\text{Sr}$  ratio higher than 0.7120 (MASIRBAS) would have been formed from a fluid that has a “basin-external” Sr component derived from Precambrian rocks. Additionally, they also suggested that the shales that underlie much of the Devonian strata would not be able to liberate  $^{87}\text{Sr}/^{86}\text{Sr}$  ratios higher than 0.7120. The above mentioned data suggests that  $^{87}\text{Sr}$  is potentially being introduced into some carbonates of the Pine Point region by fluids from or interaction with clastics or basement rocks.

### 7.3.2 *Pre-Ore Fluid*

Host dolomite of this thesis is comprised of multiple phases of finer-grained dolomite and recrystallization evidence is present in some of the host dolomite phases. This phase was not the focus of this study, with the exception of the Sr study, and therefore, multiple generations of cements are likely to have been analysed. However, the new data presented here show that the host dolomites are geochemically very complex and further work should be carried out to characterize the fluids responsible for the precipitation of this phase.

The average  $^{87}\text{Sr}/^{86}\text{Sr}$  ratio of host dolomites indicates that the pre-ore fluid in the N81 deposit was derived from Middle Devonian seawater (see section 6.2.1), which is in agreement with the findings of Medford et al. (1983), Mountjoy et al. (1992) and Qing (1998). This is consistent with the Na-Cl-Br systematics of host dolomite leachates, which suggest that the fluid responsible for the precipitation of host dolomite was derived from seawater evaporated past the point of precipitation of halite (see section 5.5.2 and Figure 5.6).

Although the average  $^{87}\text{Sr}/^{86}\text{Sr}$  ratio of the host dolomite analyzed (0.7082) is very similar to that of Middle Devonian seawater as given in Burke et al. (1982) (average of 0.7080), the large variation between the minimum and maximum strontium ratios (0.7058 to 0.7097) indicates that the fluid origin is more complex than simply Middle Devonian seawater. This variation may be masked if conventional bulk isotopic studies are used. Sample N81-98 3225 450' has in fact a radiogenic Sr component, a depleted  $^{87}\text{Sr}$  component and an  $^{87}\text{Sr}/^{86}\text{Sr}$  ratio that is comparable to Middle Devonian seawater.

The highest  $^{87}\text{Sr}/^{86}\text{Sr}$  ratio of 0.7097 is more radiogenic than the strontium data from previous workers (see Figure 6.7). The high  $^{87}\text{Sr}/^{86}\text{Sr}$  ratios in the host dolomite could be caused by interaction with rocks or fluids derived from the underlying shales since the ratios are less than 0.7120 (MASIRBAS) or a slight component of basement sourced highly radiogenic fluid. The anomalously low value of 0.7058 is very different from all work done by previous

authors and is difficult to interpret. The low  $^{87}\text{Sr}/^{86}\text{Sr}$  value is lower than Middle Devonian or any seawater compositions through Phanerozoic time (Burke et al., 1982). Interestingly, low  $^{87}\text{Sr}/^{86}\text{Sr}$  ratios (as low as 0.7058) from Upper Cretaceous waters were measured from reservoirs in the Alberta Basin (Connelly et al., 1990). The low values were suggested to be derived from water-rock interaction. The single anomalously low value from this study indicates that the fluid responsible for precipitating the host dolomite interacted with a rock or a fluid that encountered a rock that is depleted in  $^{87}\text{Sr}$  (e.g. ocean basalts). It is highly unlikely the fluids will have encountered such a unit in the sedimentary sequences. At this time, and without further study, it is not possible to identify the source of this low  $^{87}\text{Sr}/^{86}\text{Sr}$  ratio, although it may be derived from interaction with mafic rocks, presumably in the basement.

Mixing between these different end-members could cause an increase in the amount of  $^{87}\text{Sr}$  in the precipitating host dolomite cements. It is possible that the radiogenic and depleted Sr signatures are the result of the introduction of Sr from extraneous fluids and/or are acquired during the migration and interaction of the fluids with rocks on the flow paths. Regardless, the precipitating dolomite cements clearly contain the variable Sr signatures of the fluids that they were precipitating from. This study uses in-situ Sr analyses in the N81 deposit which can delineate the Sr isotope ratios of specific cements and perhaps the bulk crush Sr analysis of previous studies is representing a mixture of all these cements (e.g. seawater-derived, depleted  $^{87}\text{Sr}$  and radiogenic Sr fluids). A mixture of an  $^{87}\text{Sr}$ -depleted fluid and a radiogenic Sr-rich fluid could produce a fluid with an  $^{87}\text{Sr}/^{86}\text{Sr}$  ratio near that of Middle Devonian seawater (e.g. the average  $^{87}\text{Sr}/^{86}\text{Sr}$  ratio of host dolomite from this thesis). However, this idea is based on only two data points from a small host dolomite data set and, thus, is merely speculative and further work is needed to test this hypothesis.

Cation data from bulk fluid inclusion analysis provide further insight into the interactions of these fluids. Although the halogen data clearly show that the fluids that formed the host dolomite originated as evaporated seawater, the data plot (on a Na-Cl-Br plot) just to the left of the seawater evaporation trajectory suggesting that there has been a change in the Na content of the fluids along the flow path to the site of precipitation (see Figure 5.6). In other words, compared to the SET, there has been a loss of Na likely from water-rock interaction. This trend was also observed by Telser (1999) and Gleeson and Gromek (in press) (see Figures 5.10 and 5.11). Depletion in Na can be caused by albitization in which Na is exchanged for Ca in plagioclase (Banks et al., 2002) and the Br concentration remains constant (Viets et al., 1996). This reaction has been used in the past to explain high Ca contents in basinal brines.

For example, Spencer (1987) states that the most important reaction between subsurface brines in the Western Canada Sedimentary Basin and the Precambrian basement is albitization of feldspars. An interaction with clastics containing feldspars that are being albitized could also produce the depletion in Na.

The K-Cl-Br systematics show variability in K concentration of the pre-ore fluid. Elevated K levels can also be caused by albitization of feldspars (Banks et al., 2002), the dissolution of K-bearing minerals (Viets et al., 1996; Cai et al., 2001) and/or illitization of feldspars (Gleeson et al., 2001; Cai et al., 2001). The decrease in Na and increase in K related to albitization of K-feldspars combined with the radiogenic signature of some of the host dolomite samples suggest that the fluid responsible had interaction with underlying clastics or the basement rocks.

### 7.3.3 *Ore Fluid*

Microthermometry of fluid inclusions from sphalerite and coarse white dolomite indicates the mineralizing fluid is a 23wt% CaCl<sub>2</sub>-NaCl calcic-brine with a minimum trapping temperature of 82°C. Figures 4.7 and 4.8 show the wide range in ore fluid salinity and salt composition and the fairly consistent homogenization temperatures, which suggest that mixing may be occurring and be responsible for the precipitation of the ore minerals.

The strontium isotope ratios from coarse white dolomites, representing the ore fluid, have an average <sup>87</sup>Sr/<sup>86</sup>Sr of 0.7116. This value is considerably more radiogenic than the average for the host dolomites (0.7082). As discussed above, however, the range in the Sr isotope values and therefore, the complexity in the fluid system, is masked by the average value. The minimum value (0.7073) is similar to, but slightly below, the <sup>87</sup>Sr/<sup>86</sup>Sr value for Middle Devonian seawater. This slightly depleted <sup>87</sup>Sr/<sup>86</sup>Sr ratio indicates that the ore-fluid may have encountered <sup>87</sup>Sr-depleted rocks or fluid (see above). The highest (radiogenic) <sup>87</sup>Sr/<sup>86</sup>Sr ratio in this phase (0.7152) indicates that the fluids have either interacted with radiogenic rocks (e.g. the basement or clastics) or with radiogenic fluids that have come up from the basement or underlying clastics (e.g. along structures). Figure 6.2 shows that two isotopically discrete fluids may be responsible for the precipitation of the coarse white dolomite (and therefore the mineralization). One group of data plots well above the MASIRBAS (0.7120) line and one plots in between the <sup>87</sup>Sr/<sup>86</sup>Sr ratio for Devonian seawater (0.7080) and the MASIRBAS line. The wide range of ratios suggests a mixture of Middle Devonian seawater and a radiogenic fluid (e.g. pulses). Connolly et al. (1990), Mountjoy et al. (1992) and

Machel et al. (1996) suggest that  $^{87}\text{Sr}$  enriched fluids were tectonically expelled along faults in Cambrian shales and the Precambrian basement and therefore, may represent the highly radiogenic end-member visible in Figure 6.2. A general trend appears in saddle dolomite rims and cores, with rims yielding more radiogenic compositions than their cores (see Section 6.2.3). This suggests that the cores and rims may be representing different fluids or fluids from different sources.

The similarity between coarse white dolomite, sphalerite and galena leachates using Na-Cl-Br systematics confirms that the three phases are related (see Figure 5.5). The bulk of the data plot close to the SET near the point of halite precipitation and are interpreted to be formed from seawater evaporated past the point of halite precipitation. Spencer (1987) suggests that the source of the  $\text{CaCl}_2$ -rich brines in the Western Canada Sedimentary Basin is a mixture of residual evaporite brines and seawater or meteoric water. Our data, on the whole, do not support this since the absolute Cl and Br data plotted on a log-log plot (Figure 5.8) show a slight variability in the ore fluid. The bulk of the data plot close to the SET near the point of halite precipitation and are interpreted to be formed from seawater evaporated past the point of halite precipitation. One sample lies near the SET but before the precipitation of halite, which indicates a more dilute end member is present and potential evidence for mixing. Data from both the strontium and bulk geochemistry analyses suggests that the ore-fluid is derived from Middle Devonian seawater beyond the point of halite precipitation that has acquired radiogenic Sr by water-rock interaction or by mixing with a fluid that has an  $^{87}\text{Sr}$  radiogenic signature.

The fluid inclusion leachates from the coarse white dolomites and sulphides plot slightly to the left of the SET indicating a loss of Na. Depletion in Na can be caused by albitization of Ca or K feldspars (Banks et al., 2002) (see above). The ore fluid is enriched in Ca with some coarse white dolomite-hosted fluid inclusions having salts composed of nearly pure  $\text{CaCl}_2$  (see section 4.4.2). The high Ca content of the ore-depositing brines can be caused by dolomitization, albitization and/or the dissolution of gypsum (Carpenter, 1978; Land and Prezbindowski, 1981; Viets et al., 1996; Gleeson and Gromek, in press; among others). In combination with the Na depletion it is possible that albitization of Ca-feldspar is important.

The K level of the ore fluid has not been enriched like the pre-ore fluid has been (see Figure 5.6). K-Cl-Br systematics show the ore-fluid leachate data plotting on or near the SET (both below and above). Causes for K enrichment are outlined in the previous section and a possible cause for the depletion of K is the precipitation of K-bearing minerals (Viets et al., 1996) or the albitization of K-feldspars (Banks et al., 2002). If the ore fluid has derived its  $^{87}\text{Sr}$

from basement rocks then it must be doing so without significant addition of K or some precipitation of K-bearing mineral phases has occurred along the flow path to the site of mineralization.

The lithium content of the ore fluid plots near and slightly to the left of the SET in Figure 5.7, suggesting that the fluids are enriched in Li relative to seawater. Lithium is common in micas and therefore, the increase in the ore fluid may be due to an interaction with mica-bearing rocks from the basement (Banks et al., 2002). Shield brines from Yellowknife gold mines have Li values that are relatively similar or unchanged from seawater suggesting that Li is conservative at lower temperatures when fluids are interacting with basement rocks (Bottomley et al., 1999).

#### 7.3.4 *Post-Ore Fluid*

The post-ore fluid in the N81 deposit is represented by microthermometric, isotopic and geochemical data from late-stage calcite and petrographically associated with sulphur and bitumen. The late-stage fluid that precipitated calcite has a salinity of 9wt% NaCl + CaCl<sub>2</sub> and was formed at a minimum average temperature of 92°C. The post-ore fluid is on average warmer than the ore-fluid (92°C versus ~78°C) and ranges up to approximately 200°C. The fluid is also less saline and is dominated by NaCl instead of CaCl<sub>2</sub> and is very different from the fluid responsible for the ore mineralization.

The average <sup>87</sup>Sr/<sup>86</sup>Sr ratio of the post-ore fluid is the highest of all three fluids and does not fall within the Middle Devonian seawater range (all ratios fall in between 0.7107 and 0.7186). This suggests that the post-ore fluid had a significant interaction with clastics and/or basement rocks or the fluid is sourced in the clastics or basement rocks and is coming up along structures into the deposit. The majority of the data lie above the MASIRBAS (0.7120) (Machel and Cavell, 1999) and as such the source for the radiogenic Sr is likely derived from basement rocks.

Halogen and cation ratios provide more information on a potential source for this type of fluid. The Cl/Br and Na/Br ratios are considerably higher than the pre-ore and ore fluid although the absolute Cl and Na (ppm) values for the post-ore fluid are the lowest (due to the lower salinity of the fluid). Na-Cl-Br systematics (see Figure 5.5) show that the post-ore fluid has highly variable levels of Cl, Br and Na. Data from two of the five calcite-derived leachates plot on the seawater evaporation trajectory past the point of halite precipitation (close to those of the ore fluid), two plot far above the SET with elevated Cl levels (Cl/Br ratios up to 975) and

one value plots slightly to the right of seawater (see Figure 5.5) indicating a minor level of halite dissolution or mixing (see below). The elevated Cl/Br levels indicate that the fluids have acquired Cl relative to Br, which differs from the pre-ore and ore-fluid. Although two calcite samples have Cl/Br and Na/Br ratios that are very similar to the ore fluid, the salinity is less than half the salinity of the ore fluid. This suggests that the post-ore fluid may represent a mixture of the ore fluid and meteoric water. Microthermometric data also suggests that a low salinity fluid (e.g. meteoric fluid) plays a role in the precipitation of calcite. Chloride and Br concentrations of a calcite leachate from sample N81-68A 2969 375' are shown in Figure 5.5 and this leachate is the same as the data point that plots very close to seawater in the Cl/Br-Na/Br plot (Figure 5.6). Although only one data point is present, the data show that the post-ore fluid is distinct from the ore fluid. The leachate plots on the seawater evaporation trajectory half way in between the ore fluid and seawater, which suggests dilution by another fluid. The K values differ considerably from the ore fluid but some are comparable to those of the host dolomite (Figure 5.6). The K is enriched in all the samples, which indicates albitization of feldspars as before, dissolution of K-bearing minerals and/or illitization of feldspars (Viets et al., 1996; Gleeson et al., 2001; Cai et al., 2001; Banks et al., 2002). The high Cl/Br ratio further distinguishes the post-ore fluid data from the data of the other fluids. The log Cl-log Br plot shows how the ore and post-ore fluid are very different in Cl/Br ratios (see Figure 5.5). The post-ore fluid plots near the SET but slightly to the right indicating some halite dissolution may have occurred. The spread of data reiterates the possibility of at least two fluids being responsible for the precipitation of late-stage calcite, one being sourced from Middle Devonian seawater and a more dilute and/or radiogenic fluids.

#### **7.4 The Role of Fluid Mixing in Mineralization of the N81 Deposit**

One of the objectives of this thesis was to constrain whether mixing took place in the deposit and whether it played a role in the ore mineralization. The role of fluid mixing at Pine Point has been proposed by many authors (Kyle, 1977; Haynes and Kesler, 1987; Viets et al., 1996; Adams et al., 2000; Gleeson and Turner, in press; among others) and geochemical data from this study confirms the importance of fluid mixing in the N81 deposit.

Microthermometric data from coarse white dolomites indicate that at least two fluids are responsible for the ore mineralization, a saline ~25wt% equiv., CaCl<sub>2</sub>-NaCl brine and less saline, ~20wt% CaCl<sub>2</sub>-NaCl and less calcic brine (see Figures 4.7 and 4.8). The wide range of Sr isotope ratios from coarse white dolomite suggest the ore fluid is derived from a mixture of

Middle Devonian seawater and a fluid with a radiogenic Sr signature. Figure 6.2 clearly shows coarse white dolomite has two discrete Sr isotope compositions and therefore suggests mixing of at least two fluid members. Sr isotopic analyses of rims and cores of saddle dolomite further confirm the presence of at least two fluids. The rims are on average more radiogenic than the cores and the boundaries between the two have intermediate  $^{87}\text{Sr}/^{86}\text{Sr}$  ratios (see Figure 6.3 and 6.4). This indicates a potential evolution of the ore fluid towards a more radiogenic signature with continued development of the saddle shaped coarse white dolomite (e.g. via pulses of radiogenic fluid). If a metalliferous radiogenic fluid was periodically coming up from the basement along faults and encountering an ambient brine in the barrier (e.g. evaporated Devonian seawater), the mixture could create a fluid with a varied Sr and evaporated seawater signature. Interestingly, the late-stage calcite is most radiogenic and may represent the radiogenic fluid coming up from the basement but running out of ambient fluid that would dilute it, therefore, retaining the highest  $^{87}\text{Sr}$  values. However, the late-stage fluid also seems to have a component of a warmer dilute fluid (e.g. meteoric water). This fluid may have circulated and interacted with the basement picking up a radiogenic Sr signature and heat.

In terms of halogens and cations, the ore fluid data is generally consistent in reference to the SET (see Figure 5.5) but a small trend paralleling the trajectory is visible. A disparity is visible in the log Cl-log Br plot where most of the data plot close to the SET near the point of halite precipitation but one sample plots before the point of halite precipitation. This may also indicate a mixture of fluids being responsible for the ore mineralization.

### **7.5 Source of the Metals**

The source of the metals at Pine Point is unknown though many authors have hypothesized their origins (Roedder (1968); Campbell (1966); Skall (1975); Krebs and MacQueen (1984); among others). In general, five possible metal sources exist: 1) shales from the surrounding Mackenzie basin; 2) clastics underlying the carbonate sequences; 3) the carbonate host; 4) evaporites (e.g. Elk Point Basin), and, 5) basement rocks. Roedder (1968) suggests that base metals in the Pine Point area may have been leached from crystalline basement and/or sedimentary rocks by hot upward flowing brines that later mixed with fresh and cold surface waters. Similarly, Krebs and MacQueen (1984), Campbell (1966), Skall (1975) and Hitchon (1993) suggest that ore mineralization, and related saddle dolomite formation, may have been caused by hydrothermal solutions ascending through pathways in hinge zones of the McDonald Fault. Although Rhodes et al. (1984) contested this fluid system

(due to no signs of vertical displacement), Skall (1975) suggested small-scale movements may have occurred and increased the capacity of the conduit system. Beales and Jackson (1966) and Jackson and Beales (1967) suggest that compacting shales from the Mackenzie Basin supplied the metals. They argue that the compacted shales could release water that could carry the high amounts of Pb and Zn. Kyle (1981) suggests that the host carbonate strata, associated evaporites and the clastic aquifers that the brines passed through may be a source for the metals. Sasaki and Krouse (1969) discuss S isotopes and their signatures ( $\sim +20.1\%$ ) and indicate that the sulphide S is derived from Middle Devonian seawater sulphate (e.g. evaporites of the Elk Point Basin). Data from this study suggests that the fluid responsible for the ore mineralization is a calcic, evaporated Middle Devonian seawater-sourced brine with some level of radiogenic Sr input, likely from interaction with crystalline basement rocks or basement associated fluids and/or clastics.

Coarse white dolomite Zn/Pb molar ratio data from this study ranges from 2.9 to 95.0 (Table 7.1) and suggest that the brines responsible for the mineralization are higher in Zn than Pb. Hitchon (2006) states that most of the formation waters in the Alberta basin have Pb>Zn and that these types of fluids would not be able to produce the Zn>Pb mineralization at Pine Point. Consequently, the study suggests geothermal fluids ascending along the Great Slave Lake Shear Zone (e.g. McDonald Fault) as a source for the metals at Pine Point.

Sample	Zn/Pb
N81-65 0249	16.8
N81-84 1078	2.9
N81-98 3205 360'	49.3
N81-98 3225 450'	95.0

**Table 7.2** Cation molar ratio data (Zn/Pb) from ICP-MS analysis of 4 coarse white dolomite samples.

### 7.6 Timing of Mineralization and formation of the deposits

The Pine Point deposits are epigenetic, however, the timing of the mineralization is contentious. Proposed times include, but are not limited to Late Devonian (Nakai et al., 1993-Rb-Sr dating), Pennsylvanian (Kyle, 1981-Pb isotopes), Pennsylvanian to Early Tertiary (Cumming et al., 1990-Pb isotopes), Cretaceous (Arne, 1991-apatite fission track) and Late

Cretaceous to Early Tertiary (Garven, 1985-computer modelling). Halogen data suggests that the ore fluid originated as evaporated seawater (see Figures 5.5 and 5.6) and Sr isotopes indicate that some of the fluid has a Middle Devonian seawater signature.

There are two major fluid flow models attributed to the Mississippi Valley-type mineralization at Pine Point. The first model suggests that fluid circulation is related to the Cretaceous-Tertiary Laramide orogeny (Garven, 1985; Qing and Mountjoy, 1992; among others) and the second relates fluid movement to Antler orogenic processes during Late Devonian to Early Mississippian time (e.g. Nesbitt and Muehlenbachs, 1994; Nelson et al., 2002; among others).

Garven (1985) suggested that ore mineralization and dolomitization in the Pine Point region occurred during post-Cretaceous time and is related to the emergence of Rocky Mountains, which induced gravity-driven fluid flow. The flow system was suggested to be able to have flow rates, temperatures and metal contents that could produce the Zn-Pb mineralization at Pine Point. Garven (1985) negated the role of heat sources from the basement and possible hot brine pulses being involved in the mineralization. Data from this thesis indicates that the ore fluid has a radiogenic component that originated from the underlying clastics and/or basement rocks and therefore, does not agree with the statement. Post-ore fluids analyzed in this thesis suggest that meteoric fluids are likely mixing with other fluids to precipitate the calcite and this meteoric fluid may be related to the topographic recharge that Garven (1985) suggests is present in the barrier. The gravity-driven Laramide orogeny-associated model of Garven (1995) was elaborated on by Qing and Mountjoy (1992). The authors suggest that dolomitization and mineralization were related to warm radiogenic basinal fluids that migrated updip along the Presqu'ile Barrier and mixed with cooler and less radiogenic ambient formation waters. This movement and interaction was also suggested to be responsible for the progressive decline in  $^{87}\text{Sr}/^{86}\text{Sr}$  towards the east end of the barrier (e.g. Pine Point ore region). Strontium data from this thesis indicates that the deposit fluid history is more complex e.g. depleted Sr, radiogenic Sr and Middle Devonian seawater-derived fluids are involved in the ore mineralization. There does not appear to be a gradual evolution but more likely pulses of radiogenic fluid coming into the system.

Nesbitt and Muehlenbachs (1994) suggested that the ore mineralization at Pine Point was formed during the Late Devonian to Early Mississippian and discount the involvement of a Tertiary fluid (using  $\delta\text{D}$  data). They suggest that the warm brines originated in shales (to the west of the deposit) and migrated through the Presqu'ile Barrier until they cooled and

precipitated the base metals. If the metals were sourced from shales, the Sr isotopic composition of the ore fluid should reflect this. Basinal shales analyzed by Lonnee (2005) range from 0.7088 to 0.7123 and the ore fluid from this study ranges up to 0.7152, therefore, there must be a more radiogenic component than shales (e.g. basement) or multiple fluids (e.g. shale and basement derived fluids). Nelson et al. (2002) also suggest that the mineralization at Pine Point is related to Middle Paleozoic tectonics rather than those of the Cretaceous-Tertiary. Ore mineralization and hydrothermal dolomite in the Pine Point region (and also in other deposits of the Western Canada Sedimentary Basin and the Canadian Cordillera) are suggested to have been produced by fluids migrating along “reactivated back-arc structures and permeable stratified units” (Nelson et al., 2002). This rifted back-arc tectonic setting suggests that thermal convection could be driving the fluids that produce the mineralization and hydrothermal dolomite. The elevated temperatures and enriched  $^{87}\text{Sr}$  levels could have originated as hydrothermal solutions migrating through intrabasinal faults. Radiogenic strontium isotopic data from this thesis agrees with the theory that hydrothermal brines flowing upward from the basement and/or clastics are carrying the radiogenic strontium signature (and likely the metals) to the site of ore deposition.

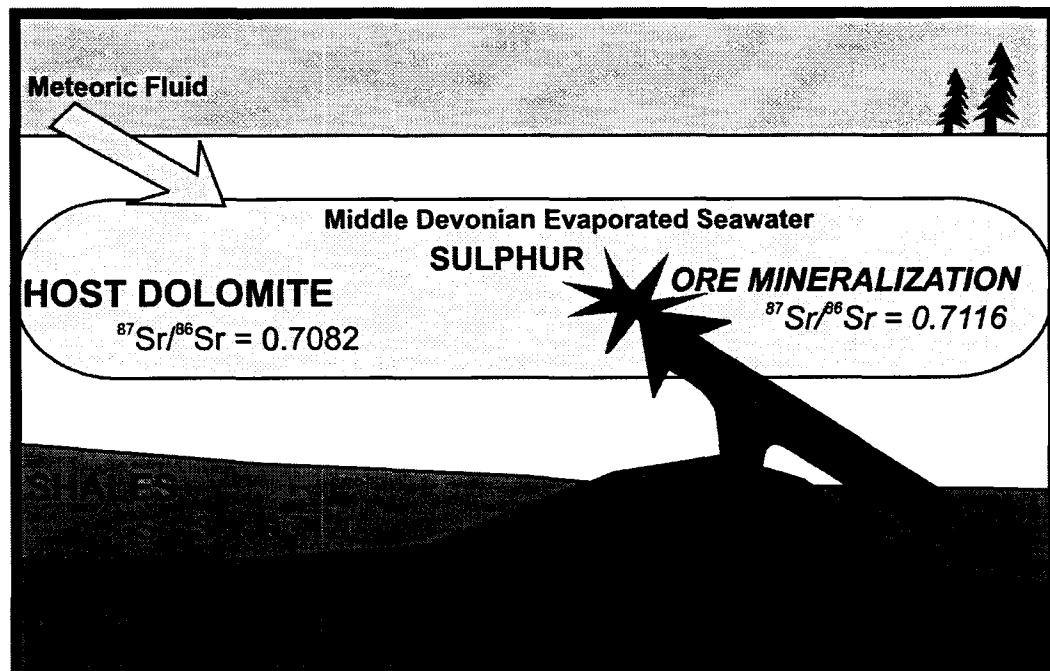


**Figure 7.1** Simplified diagram of  $^{87}\text{Sr}$  and metal sources in the N81 deposit.

Data from this thesis does not categorically fit into one of the previously mentioned models. Although some ideas from certain models agree with some of the data from this thesis, some also negate certain aspects of the models. The complexity of the system has been confirmed along with the likelihood of fluid mixing playing a role in the deposit. For example, Sr data provides evidence that radiogenic (warmer) fluids are mixing with ambient (cooler) formation waters yet microthermometric data suggest that the ore fluid is relatively isothermal with only salinity and salt composition varying considerably. A possible explanation for this could be that the cooler ambient fluid was much more abundant and the radiogenic warmer fluid was being introduced in pulses (e.g. along faults from the underlying clastics and/or basement). The ambient fluid would therefore, retain an evaporated signature and relatively consistent overall temperature while the Sr ratios would be generally increasing with time. The metals would be precipitating during this mixture until all the ambient fluid available for reaction with the radiogenic fluid was exhausted. This steady increase in Sr with time is seen in the rims of saddle dolomite being more radiogenic than cores. The late-stage highly radiogenic fluid that is precipitating the calcite could be a mixture of radiogenic basement fluids and exhausted ambient formation waters and a later meteoric water influx.

## CHAPTER 8

### CONCLUSIONS

1. The pre-ore fluid in the N81 deposit has a complex strontium isotopic composition containing depleted Sr, seawater-derived and radiogenic Sr signatures (average  $^{87}\text{Sr}/^{86}\text{Sr}$  ratio of 0.7082; range of 0.7058 to 0.7097). The pre-ore fluid has halogen and cation ratios that indicate an evaporated seawater origin and a loss of Na and Li along the flow path.
2. The fluid responsible for base metal mineralization in the N81 deposit was a high salinity (23 wt% equivalent  $\text{CaCl}_2\text{-NaCl}$ ), calcic, warm brine (82°C). The ore-stage fluid has a complex strontium isotopic composition with an average  $^{87}\text{Sr}/^{86}\text{Sr}$  ratio of 0.7116 with minimum and maximum values of 0.7073 and 0.7152 (spanning depleted Sr, seawater-derived and radiogenic Sr compositions). Halogen and cation data from mineral leachates representing the ore fluid suggest that the fluid likely originated from evaporated seawater. The fluid appears to have been slightly depleted in Na and enriched in Li along the flow path to the site of mineralization.
3. Geochemical studies of late-stage calcite suggest the post-ore fluids were  $\text{NaCl-CaCl}_2$  brines with a salinity of 0 to 15wt%  $\text{NaCl-CaCl}_2$  (average of 9 wt%  $\text{NaCl-CaCl}_2$ ) and contained a strongly radiogenic  $^{87}\text{Sr}/^{86}\text{Sr}$  signature (0.7149). The fluids have halogen compositions comparable to a mixture of a more saline brine with meteoric water, which may have occurred during meteoric recharge of the aquifer.
4. The bulk of the fluids involved in the N81 deposit have halogen contents that suggest that the ore minerals were formed from fluids that originated as surficially evaporated seawater. Relative to a modern evaporated seawater composition, most of the fluids have lost some Na along the fluid migration path, possibly due to the albitization of feldspars. The elevated level of Ca in the mineralizing fluids has likely been caused by dolomitization, albitization and/or the dissolution of gypsum.
5. The wide range of strontium isotopic ratios found in single ore-related dolomite crystals suggest that the fluids that formed the N81 deposit had variable origins or water-rock interaction histories. There is a general trend of the fluids becoming more radiogenic with the progression of the paragenetic sequence (e.g. host dolomite → coarse white dolomite → calcite)

which is corroborated, on a smaller scale, by the rims of saddle dolomite being more radiogenic than the cores. The ore fluid appears to have three strontium isotopic components with Middle Devonian evaporated seawater, radiogenic and depleted Sr signatures. The radiogenic Sr is likely derived from fluids ascending via faults from the underlying clastics and/or basement rocks. The depleted Sr signature indicates that an interaction with an  $^{87}\text{Sr}$  depleted rock or fluid that encountered such a rock type has occurred (e.g. mafic rocks in the basement).

6. Sr isotope data suggests that the pre-ore and ore-fluids have interacted with fluids from or rocks of the underlying clastics. The Sr data also suggests that the ore-fluids and post-ore fluids have likely had interaction with the basement and/or fluids from the basement.

7. The importance of mixing in the N81 deposit is supported by the geochemical data. A minimum of two fluids are responsible for the mineralization, a saline ~25wt% equivalent  $\text{CaCl}_2\text{-NaCl}$ , highly calcic brine and less saline ~20wt%  $\text{CaCl}_2\text{-NaCl}$ , moderately calcic brine. Strontium isotope data suggests the ore fluid is a mixture of evaporated Middle Devonian seawater and fluid with a radiogenic Sr component. The wide range of halogen compositions and microthermometric data of the post-ore fluid suggests that more than one fluid was responsible for it. The post-ore fluid has likely been mixed with a more dilute, potentially meteoric fluid.

## CHAPTER 9

### REFERENCES

Adams, J.J., Rostron, B.J. and Mendoza, C.A., Evidence for two-fluid mixing at Pine Point, NWT: *Journal of Geochemical Exploration*, v. 69-70, p. 103-108.

Al-Aasm, I., Lonnee, J. and Clarke, J., 2000, Multiple fluid flow events and the formation of saddle dolomite: examples from Middle Devonian carbonates of the Western Canada Sedimentary Basin: *Journal of Geochemical Exploration*, v. 69-70, p. 11-15.

Arne, D.C., 1991, Regional thermal history of the Pine Point area, Northwest Territories, Canada, from apatite fission-track analysis: *Economic Geology*, vol.86, p.428-435.

Banks, D.A., Boyce, A.J. and Samson, I.M., 2002, Constraints on the origins of fluid forming Irish Zn-Pb-Ba deposits: Evidence from the composition of fluid inclusions: *Economic Geology*, v. 97, p. 471-480.

Beales, F.W. and Jackson, S.A., 1966, Precipitation of lead-zinc ores in carbonate reservoirs as illustrated by Pine Point ore field, Canada: *Transactions of the Institute of Mining and Metallurgy*, v. 75, p. B278-B285

Bodnar, R.J., 2003, Introduction to aqueous-electrolyte fluid inclusions, in I. Samson, A. Anderson and D. Marshall, eds., *Fluid Inclusions: Analysis and Interpretation: Mineralogical Association of Canada, Short Course Series*, v. 32, p. 81-100.

Bottomley, D.J., Katz, A., Chan, L.H., Starinsky, A., Douglas, M., Clark, I.D. and Roven, J.G., 1999, The origin and evolution of Canadian Shield brines: evaporation or freezing of seawater? New lithium isotope and geochemical evidence from the Slave craton: *Chemical Geology*, v. 155, p. 295-320.

Burke, W.H., Denison, R.E., Hetherington, E.A., Koepnick, R.B., Nelson, H.F. and Otto, J.B., 1982, Variation of seawater  $^{87}\text{Sr}/^{86}\text{Sr}$  throughout Phanerozoic time: *Geology*, v. 10, p. 516-519.

Cai, C., Franks, S.G. and Aagaard, Per, 2001, Origin and migration of brines from Paleozoic strata in Central Tarim, China: constraints from  $^{87}\text{Sr}/^{86}\text{Sr}$ ,  $\delta\text{D}$ ,  $\delta^{18}\text{O}$  and water chemistry: *Applied Geochemistry*, v.16, p. 1269-1284.

Campbell, N., 1996, The lead-zinc deposits of Pine Point: *Canadian Institution of Mining and Metallurgy Bulletin*, v. 59, p. 953-960.

Carpenter, A.B., 1978, Origin and chemical evolution of brines in sedimentary basins: Oklahoma Geological Survey Circular, v. 79, p. 50-88.

Connolly, C.A., Walter, L.M., Baadsgaard, H. and Longstaffe, F.J., 1990, Origin and evolution of formation waters, Alberta Basin, Western Canada Sedimentary Basin. II. Isotope systematics and water mixing: Applied Geochemistry, v. 5, p. 397-413.

Cumming, G.L., Kyle, J.R. and Sangster, D.F., 1990, Pine Point: A case history of lead isotope homogeneity in a Mississippi Valley-type district: Economic Geology, v. 85, p. 133-144.

Fontes, J.C. and Matray, J.M., 1993, Geochemistry and origin of formation brines from the Paris Basin, France 1. Brines associated with Triassic salts: Chemical Geology, v. 109, p. 149-175.

Garven, G., 1985, The role of regional fluid flow in the genesis of the Pine Point Deposit, Western Canada Sedimentary Basin: Economic Geology, v. 80, p. 307-324.

Gleeson, S.A., Wilkinson, J.J., Stuart, F.M. and Banks, D.A., 2001, The origin and evolution of base metal mineralizing brines and hydrothermal fluids, South Cornwall, UK: Geochimica et Cosmochimica Acta, v. 65, p. 2067-2079.

Gleeson, S.A. and Gromek, P., in press, The origin of hydrothermal sulphide and dolomite mineralising fluids in southern Northwest Territories and northern Alberta, in P.K. Hannigan, ed., Potential for carbonate-hosted lead-zinc Mississippi Valley-type mineralization in northern Alberta and southern Northwest Territories Geoscience Contributions, Targeted Geoscience Initiative: Geological Survey of Canada, Bulletin.

Gleeson, S.A. and Turner, W.A., in press, The origin of the Pine Point Pb-Zn mineralizing fluids and coarse and saddle dolomite formation in southern Northwest Territories: Geofluids.

Goldstein, R.H., 2003, Petrographic analysis of fluid inclusions, in I. Samson, A. Anderson and D. Marshall, eds., Fluid Inclusions: Analysis and Interpretation: Mineralogical Association of Canada, Short Course Series, v. 32, p. 9-53.

Goldstein, R.H. and Reynolds, T.J., 1994, Systematics of fluid inclusions in diagenetic minerals: SEPM Short Course, vol. 31, 199 p.

Hanor, J.S., 1994, Origin of saline fluids in sedimentary basins, in J. Parnell, ed., Special Publication of the Geological Society of London, v. 78, p. 151-174.

- Haynes, F.M., and Kesler, S.E., 1987, Chemical evolution of brines during Mississippi Valley-type mineralization: Evidence from East Tennessee and Pine Point: *Economic Geology*, v. 82, p. 53-71.
- Hitchon, B., 1993, Geochemistry of formation water, northern Alberta, Canada: their relation to the Pine Point ore deposit: Alberta Geological Survey, Open File Report, 1993-14.
- Hitchon, B., 2006, Lead and zinc in formation waters, Alberta Basin, Canada: Their relation to the Pine Point ore fluid: *Applied Geochemistry*, v. 21, p. 109-133.
- Jackson, S.A. and Beales, F.W., 1967, An aspect of sedimentary basin evolution: the concentration of Mississippi Valley-type ores during late stages of diagenesis: *Bulletin of Canadian Petroleum Geology*, v. 15, p. 383-433.
- Kesler, S.E., Appold, M.S., Martini, A.N., Walter, L.M., Huston, T.J. and Kyle, J.R., 1995, Na-Cl-Br systematics of mineralizing brines in Mississippi Valley-type deposits: *Geology*, v. 23, p. 641-644.
- Krebs, W. and Macqueen, R., 1984, Sequence of diagenetic and mineralization events, Pine Point lead-zinc property, NWT: *Bulletin of Canadian Petroleum Geology*, v. 32, p. 434-464.
- Kyle, J.R., 1977, Development of sulfide-hosted structures and Mineralization, Pine Point, Northwest Territories: unpublished Ph.D. thesis, University of Western Ontario, p.226.
- Kyle, J.R., 1981, Geology of the Pine Point lead-zinc district, in K.H.Wolf, ed., *Handbook of strata-bound and stratiform ore deposits*: Elsevier Publishing Co., Amsterdam, v.9, p. 643-741.
- Land, L.S. and Prezbindowski, D.R., 1981, The origin and evolution of saline formation water, Lower Cretaceous carbonates, south-central Texas, U.S.A.: *Journal of Hydrology*, v.54, p. 51-74.
- Lonnee, J.S., 2005, Diagenetic evolution of the Slave Point Formation, Clarke Lake, British Columbia, Canada: unpublished Ph.D. thesis, University of Alberta, p.434.
- Machel, H.G., Cavell, P.A. and Patey, K.S., Isotopic evidence for carbonate cementation and recrystallization, and for tectonic expulsion of fluids into the Western Canada Sedimentary Basin: *Geological Society of America Bulletin*, v. 108, p. 1108-1119.

Machel, H.G. and Cavell, P.A., 1999, Low-flux, tectonically-induced squeegee fluid flow ("hot flash") into the Rocky Mountain Foreland Basin: *Bulletin of Canadian Petroleum Geology*, V. 47, p. 510-533.

Maxwell, R.J., 1976, A study of rubidium, strontium, and strontium isotopes in some mafic and sulphide minerals: unpublished M.Sc. thesis, University of British Columbia.

Medford, G.A., Maxwell, R.J. and Armstrong, R.L., 1983,  $^{87}\text{Sr}/^{86}\text{Sr}$  ratio measurements on sulfides, carbonates, and fluid inclusions from Pine Point, Northwest Territories, Canada: An  $^{87}\text{Sr}/^{86}\text{Sr}$  ratio increase accompanying the Mineralizing Process: *Economic Geology*, v. 78, p. 1375-1378.

Mountjoy, E.W., Qing, H. and McNutt, R., 1992, Sr isotopic composition of Devonian dolomites, western Canada: significance regarding sources of dolomitizing fluids: *Applied Geochemistry*, v.7, p. 59-75.

Nakai, S., Halliday, A.N., Kesler, S.E., Jones, H.D., Kyle, J.R. and Lane, T.E., 1993, Rb-Sr dating of sphalerites from Mississippi Valley-type (MVT) ore deposits: *Geochimica et Cosmochimica Acta*, v. 57, p. 417-427.

Nelson, J., Paradis, S., Christensen, J. and Gabites, J., 2002, Canadian Cordilleran Mississippi Valley-type deposits: A case for Devonian-Mississippian back-arc hydrothermal origin: *Economic Geology*, v. 97, p. 1013-1036.

Nesbitt, B.E. and Muehlenbachs, K., 1994, Paleohydrogeology of the Canadian Rockies and origins of brines, Pb-Zn deposits and dolomitization in the Western Canada Sedimentary Basin: *Geology*, v. 22, p. 243-246.

Norris, A.W., 1965, Stratigraphy of Middle Devonian and older Paleozoic rocks of the Great Slave Lake region, Northwest Territories: *Geological Survey Canada, Memoir 322*.

Oakes, C.S., Bodnar, R.J. and Simonson, J.M., 1990, The system  $\text{NaCl-CaCl}_2\text{-H}_2\text{O}$ : I. The ice liquidus at 1 atm total pressure: *Geochimica et Cosmochimica Acta*, v. 54, p. 603-610.

Qing, H., 1991, Diagenesis of Middle Devonian Presqu'ile dolomite Pine Point NWT and adjacent subsurface: unpublished Ph.D. thesis, McGill University.

Qing, H., 1998, Geochemical constraints on the origin and timing of palaeofluid flow in the Presqu'ile barrier reef, Western Canada Sedimentary Basin, in J.Parnell, ed., *Dating of Fluid Flow and Fluid-Rock Interaction: Geological Society, London, Special Publications*, 144, p. 173-187.

Qing, H., 1998, Petrography and geochemistry of early-stage, fine- and medium-crystalline dolomites in the Middle Devonian Presqu'ile Barrier at Pine Point, Canada: *Sedimentology*, v. 45, p. 433-446.

Qing, H. and Mountjoy, E., 1990, Petrography and diagenesis of the Middle Devonian Presqu'ile barrier: implications on formation of dissolution vugs and breccias at Pine Point and adjacent subsurface, District of Mackenzie: Geological Survey of Canada, Paper 901-D, p. 37-45.

Qing, H. and Mountjoy, E., 1992, Large-scale fluid flow in the Middle Devonian Presqu'ile barrier, Western Canada Sedimentary Basin: *Geology*, v. 20, p. 903-906.

Qing, H. and Mountjoy, E., 1994, Formation of coarsely crystalline, hydrothermal dolomite reservoirs in the Presqu'ile Barrier, Western Canada Sedimentary Basin: *AAPG Bulletin*, v. 78, p. 55-77.

Rhodes, D., Lantos, E.A., Lantos, J.A., Webb, R.J. and Owens, D.C., 1984, Pine Point ore bodies and their relationship to the stratigraphy, structure, dolomitization and karstification on the Middle Devonian Barrier Complex: *Economic Geology*, v. 79, p. 991-1055.

Roedder, E., 1968, Temperature, salinity, and origin of the ore-forming fluids at Pine Point, Northwest Territories, Canada, from fluid inclusion studies: *Economic Geology*, v. 63, p. 439-450.

Roedder, E., 1984, Fluid Inclusions: Mineralogical Society of America, *Reviews in Mineralogy*, v. 12, 646 p.

Sasaki, A. and Krouse, H.R., 1969, Sulfur isotopes and the Pine Point lead-zinc mineralization: *Economic Geology*, v. 64, p. 718-730.

Schmidberger S.S., Simonetti A., Francis D., 2003, Small-scale Sr isotope investigation of clinopyroxenes from peridotite xenoliths by laser ablation MC-ICP-MS – implications for mantle metasomatism: *Chemical Geology*, v. 199, p.317-329.

Shepherd, T.J., Rankin, A.H. and Alderton, D.H.M., 1985, A practical guide to fluid inclusion studies: Blackie & Son Ltd., Glasgow, 239 p.

Skall, H., 1975, The paleoenvironment of the Pine Point lead-zinc district: *Economic Geology*, v. 70, p. 22-47.

Spencer, R.J., 1987, Origin of Ca-Cl brines in Devonian formations, Western Canada Sedimentary Basin: Applied Geochemistry, v. 2, p. 373-384.

Telser, H., 1999, Significance of inclusion fluid chemistry for the origin of the Pine Point mineralization, NWT: unpublished M.Sc. thesis, University of Leoben.

Turner, W.A., 2003, Microthermometric study of fluids associated with Pb-Zn mineralization in the vicinity of the Pine Point mining camp: C.S. Lord Northern Geoscience Centre, Yellowknife. NWT Open File Report 2006-06, 30 p.

Viets, J.G., Hofstra, A.H. and Emsbo, P., 1996, Solute compositions of fluid inclusions in sphalerite from North American and European Mississippi-Valley type ore deposits: Ore fluids derived from evaporated seawater: Society of Economic Geologists Special Publication No.4, p. 465-482..

Viezer, J. and Compston, W., 1974,  $^{87}\text{Sr}/^{86}\text{Sr}$  composition of seawater during the Phanerozoic: *Geochemica et Cosmochemica Acta*, v. 38, p. 1461-1484.

Walter, L.M., Stueber, A.M. and Huston, T.J., 1990, Br-Cl-Na systematics in Illinois basin fluids: Constraints on fluid origin and evolution: *Geology*, v. 18, p. 315-318.

Wilkinson, J.J., 2001, Fluid inclusions in hydrothermal ore deposits: *Lithos*, v. 55, p. 229-272.

**APPENDIX I**  
**FLUID INCLUSION MICROTHERMOMETRIC RESULTS**

List of fluid inclusion microthermometric results.

List of abbreviations:

CWD = coarse white dolomite  
SPH = sphalerite  
CC = calcite  
P = primary  
S = secondary  
PS = psuedosecondary  
ID = indeterminable  
L-V = liquid-vapour  
L-HC = liquid-hydrocarbon  
DOF = degree of fill  
Tf = first melting temperature  
T<sub>m<sub>HH</sub></sub> = hydrohalite melting temperature  
T<sub>m<sub>ice</sub></sub> = ice melting temperature  
Th = homogenization temperature

Sample	Host	Type	Phase Type	DOF	Length (μm)	Tf (°C)	T <sub>mHH</sub> (°C)	T <sub>mIce</sub> (°C)	Th (°C)
N81-65 0249	CWD	P	L-V	0.95	4				82
N81-65 0249	CWD	P	L-V	0.95	3				73
N81-65 0249	CWD	P	L-V	0.9	4				74
N81-65 0249	CWD	P	L-V	0.95	4				91
N81-65 0249	CWD	P	L-V	0.95	4				82
N81-65 0249	CWD	P	L-V	0.95	5			-15.5	87
N81-65 0249	CWD	P	L-V	0.95	9		-33.5	-21.2	72
N81-65 0249	CWD	P	L-V	0.95	9		-37.7	-20.7	88
N81-65 0249	CWD	P	L-V	0.95	7		-31.0	-19.9	88
N81-65 0249	CWD	P	L-V	0.95	4			-18.1	85
N81-65 0249	CWD	P	L-V	0.95	5				81
N81-65 0249	CWD	P	L-V	0.95	6		-35.3		74
N81-65 0249	CWD	P	L-V	0.95	8				70
N81-65 0249	CWD	P	L-V	0.95	4				87
N81-65 0249	CWD	P	L-V	0.9	28		-36.0	<-16.1	85
N81-65 0249	CWD	P	L-V	0.9	4				79
N81-68A 2969 375'	CC	P	L-V	0.95	4				65
N81-68A 2969 375'	CC	P	L-V	0.95	3			-8.8	67
N81-68A 2969 375'	CC	P	L-V	0.95	16				66
N81-68A 2969 375'	CC	P	L-V	0.95	4				66
N81-68A 2969 375'	CC	P	L-V	0.95	11				68
N81-68A 2969 375'	CC	P	L-V	0.95	12				92
N81-68A 2969 375'	CC	P	L-V	0.95	22	<-46	-21.9	-7.1	75
N81-68A 2969 375'	CC	P	L-V	0.95	12				71
N81-68A 2969 375'	CC	P	L-V	0.95	10		-21	-9.0	66
N81-68A 2969 375'	CC	P	L-V	0.95	8				66
N81-68A 2969 375'	CC	P	L-V	0.95	10		-20	-7.0	59
N81-68A 2969 375'	CC	S	L-V	0.95	12			-7.5	67
N81-68A 2969 375'	CC	S	L-V	0.95	6				64
N81-68A 2969 375'	CC	S	L-V	0.95	4				58
N81-68A 2969 375'	CC	S	L-V	0.95	8		-20	-8.0	>37.1
N81-68A 2969 375'	CC	ID	L-V	0.95	16			-10.9	53
N81-68A 2969 375'	CC	ID	L-V	0.95	6			-7.7	62
N81-68A 2969 375'	CC	ID	L-V	0.95	5		-25	-5.1	68
N81-75 3386 322'	CWD	P	L-V	0.95	5	<-60			86
N81-75 3386 322'	CWD	P	L-V	0.95	16				82
N81-75 3386 322'	CWD	P	L-V	0.95	10	~-75			75
N81-75 3386 322'	CWD	P	L-V	0.95	5				89
N81-75 3386 322'	CWD	P	L-V	0.95	7		<-57.0	-14.8	88
N81-75 3386 322'	CWD	P	L-V	0.95	9	<-70		-15.3	88
N81-75 3386 322'	CWD	P	L-V	0.95	6				86
N81-75 3386 322'	CWD	P	L-V	0.95	8				85
N81-75 3386 322'	CWD	P	L-V	0.95	7		<-35.0	-16.5	86
N81-75 3386 322'	CWD	P	L-V	0.95	10			-17.0	85

N81-75 3386 322'	CWD	P	L-V	0.95	5				80
N81-75 3386 322'	CWD	P	L-V	0.95	4				86
N81-75 3386 322'	CWD	P	L-V	0.95	7				86
N81-75 3386 322'	CWD	P	L-V	0.95	6				85
N81-75 3386 322'	CWD	P	L-V	0.95	5			-14.3	84
N81-75 3386 322'	CWD	P	L-V	0.95	5			-13.7	83
N81-75 3386 322'	CWD	P	L-V	0.95	6				80
N81-75 3386 322'	CWD	P	L-V	0.95	10				90
N81-75 3386 322'	CWD	P	L-V	0.95	17	<-65	-49.0	-16.5	88
N81-75 3386 322'	CWD	P	L-V	0.95	8				88
N81-75 3386 322'	CWD	P	L-V	0.95	17	<-60	-41.8	-15.5	87
N81-75 3386 322'	CWD	P	L-V	0.95	6				87
N81-75 3386 322'	CWD	P	L-V	0.95	8				87
N81-75 3386 322'	CWD	P	L-V	0.95	14	<-65	-49.0		87
N81-75 3386 322'	CWD	P	L-V	0.95	11			-15.6	86
N81-75 3386 322'	CWD	P	L-V	0.95	4				86
N81-75 3386 322'	CWD	P	L-V	0.95	9				86
N81-75 3386 322'	CWD	P	L-V	0.95	10				86
N81-75 3386 322'	CWD	P	L-V	0.9	17		>-55 & <-35	-13.7	85
N81-75 3386 322'	CWD	P	L-V	0.95	9	<-65	-49.5	-16.0	84
N81-75 3386 322'	CWD	P	L-V	0.95	10				84
N81-75 3386 322'	CWD	P	L-V	0.95	4				83
N81-75 3386 322'	CWD	P	L-V	0.95	17				83
N81-75 3386 322'	CWD	P	L-V	0.95	10	<-70	-35.8	-15.6	81
N81-75 3386 322'	CWD	P	L-V	0.95	4			<-9.9	80
N81-75 3386 322'	CWD	P	L-V	0.95	11	<-65	-50.3	-16.2	80
N81-75 3386 322'	CWD	P	L-V	0.95	4				79
N81-75 3386 322'	CWD	P	L-V	0.95	5			-12.6	77
N81-75 3386 322'	CWD	P	L-V	0.95	7				64
N81-84 1078	CWD	P	L-V	0.95	16.8	<-60	-32	-27.0	117
N81-84 1078	CWD	P	L-V	0.95	8	<-60	-38	-25.3	91
N81-84 1078	CWD	P	L-V	0.95	9.6	<-72	-50.4	-28.1	84
N81-84 1078	CWD	P	L-V	0.9	3.6				127
N81-84 1078	CWD	P	L-V	0.95	2			<-11.0	128
N81-84 1078	CWD	P	L-V	0.95	2.4			-28.0	122
N81-84 1078	CWD	P	L-V	0.95	7.2	<-60		-27.0	77
N81-84 1078	CWD	P	L-V	0.95	5.6	<-60			81
N81-84 1078	CWD	P	L-V	0.95	3.2		-49.3		84
N81-84 1078	CWD	P	L-V	0.95	4.8	<-68	-45	-24.0	
N81-84 1078	CWD	P	L-V	0.95	5.2	<-63		-28.0	78
N81-84 1078	CWD	P	L-V	0.95	6.4	<-72	-41	-28.0	83
N81-84 1078	CWD	P	L-V	0.95	3.6				72
N81-84 1078	CC	P	L-V	0.95	5.6				62
N81-84 1078	CC	S	L-V	0.95	9.2			>-8.8	68
N81-84 1078	CC	S	L-V	0.95	12	<-64		-8.8	71
N81-98 3181 287'	CC	P	L-V	0.95	11.2				61
N81-98 3181 287'	CC	P	L-V	0.95	6.4		<-24	-6.5	66

N81-98 3181 287'	CC	P	L-V	0.95	10.8				67
N81-98 3181 287'	CC	P	L-V	0.95	5.6				72
N81-98 3181 287'	CC	P	L-V	0.95	12				65
N81-98 3181 287'	CC	P	L-V	0.95	12.8				70
N81-98 3181 287'	CC	P	L-V	0.95	13.6				68
N81-98 3181 287'	CC	P	L-V	0.95	45.2	<-60	-25.0	-8.0	62
N81-98 3181 287'	CC	P	L-V	0.9	16				57
N81-98 3181 287'	CC	P	L-V	0.95	24			-11.3	62
N81-98 3181 287'	CC	P	L-V	0.95	6.4	<-52	<-21	-5.9	60
N81-98 3181 287'	CC	S	L-V	0.95	16.8	<-50	-30	-6.9	73
N81-98 3181 287'	CC	ID	L-V	0.9	12.4				83
N81-98 3205 360'	CWD	P	L-V	0.95	10		-56.5		57
N81-98 3205 360'	CWD	P	L-V	0.95	8	<-65		-22.0	79
N81-98 3205 360'	CWD	P	L-V	0.95	8	<-65		-22.0	79
N81-98 3205 360'	CWD	P	L-V	0.95	7	<-65	-45.0	-22.5	89
N81-98 3205 360'	CWD	P	L-V	0.95	10	<-65		-23.0	89
N81-98 3205 360'	CWD	P	L-V	0.95	10	<-65	-45.0	-26.0	84
N81-98 3205 360'	CWD	P	L-V	0.9	7		-54.0	-27.9	86
N81-98 3205 360'	CWD	P	L-V	0.95	5			-28.3	63
N81-98 3205 360'	CWD	P	L-V	0.95	4			-28.8	76
N81-98 3205 360'	CWD	P	L-V	0.9	6				96
N81-98 3205 360'	CWD	P	L-V	0.9	5				82
N81-98 3205 360'	CWD	P	L-V	0.95	6				74
N81-98 3205 360'	CWD	P	L-V	0.95	6				71
N81-98 3205 360'	CWD	P	L-V	0.95	5				68
N81-98 3205 360'	CWD	P	L-V	0.9	3				66
N81-98 3205 360'	CWD	P	L-V	0.9	4				66
N81-98 3205 360'	CWD	P	L-V	0.95	3				65
N81-98 3205 360'	CWD	P	L-V	0.95	5				65
N81-98 3205 360'	CWD	P	L-V	0.9	3				62
N81-98 3205 360'	CWD	P	L-V	0.9	3				60
N81-98 3205 360'	CWD	P	L-V	0.95	7				59
N81-98 3205 360'	CWD	P	L-V	0.95	6				56
N81-98 3205 360'	CWD	P	L-V	0.95	6			<-27.4	76
N81-98 3205 360'	CWD	P	L-V	0.95	5			<-20.0	75
N81-98 3205 360'	CWD	P	L-V	0.95	10			<-20.0	65
N81-98 3205 360'	CWD	P	L-V	0.95	18	<-63	-32.0	-16.5	78
N81-98 3205 360'	CWD	ID	L-V	0.75	14	<-57	>-36	-9.0	124
N81-98 3205 360'	CWD	ID	L-V	0.9	10	<-57			81
N81-98 3205 360'	CWD	ID	L-V	0.95	5				85
N81-98 3205 360'	CWD	ID	L-V	0.95	4			-22.0	85
N81-98 3205 360'	SPH	P	L-V	0.95	15			-17.7	80
N81-98 3205 360'	SPH	P	L-V	0.9	4			-17.7	71
N81-98 3205 360'	SPH	P	L-V	0.9	3				67
N81-98 3205 360'	SPH	P	L-V	0.95	7			-16.9	76
N81-98 3205 360'	SPH	S	L-V	0.9	7				79
N81-98 3205 360'	SPH	S	L-V	0.9	6				60

N81-98 3205 360'	SPH	ID	L-V	0.95	7			-15.7	71
N81-98 3205 360'	SPH	ID	L-V	0.95	5			-16.3	70
N81-98 3205 360'	SPH	ID	L-V	0.95	10			-11.3	58
N81-98 3208 367'	CC	P	L-V	0.9	13.6		<-16.6	-0.1	138
N81-98 3208 367'	CC	P	L-V	0.9	7.2				104
N81-98 3208 367'	CC	P	L-V	0.9	9.6				144
N81-98 3208 367'	CC	P	L-V	0.9	10				113
N81-98 3208 367'	CC	P	L-V	0.95	26	<-50	-20.0	-6.5	>126
N81-98 3208 367'	CC	P	L-V	0.95	19.2				147
N81-98 3208 367'	CC	P	L-V	0.9	18.8				156
N81-98 3208 367'	CC	P	L-V	0.9	72				154
N81-98 3208 367'	CC	P	L-V	0.9	33.2	<-72	-27.5	-6.5	152
N81-98 3208 367'	CC	P	L-V	0.9	23.6				142
N81-98 3208 367'	CC	P	L-V	0.9	19.2	<-60	-20.6	-4.6	128
N81-98 3208 367'	CC	P	L-V	0.95	32		-23.0	-6.3	71
N81-98 3208 367'	CC	P	L-V	0.95	8.8				70
N81-98 3208 367'	CC	P	L-V	0.95	24.8		-20.0	-6.4	67
N81-98 3208 367'	CC	P	L-V	0.95	9.6				60
N81-98 3208 367'	CC	P	L-V	0.95	12				60
N81-98 3208 367'	CC	P	L-V	0.95	11.6			-5.1	56
N81-98 3208 367'	CC	P	L-V	0.95	8.8				151
N81-98 3208 367'	CC	P	L-V	0.95	13.6			-0.1	95
N81-98 3208 367'	CC	P	L-V	0.95	10	<-76		-6.3	63
N81-98 3208 367'	CC	S	L-V	0.95	<4				100
N81-98 3208 367'	CC	S	L-V	0.95	<4				74
N81-98 3208 367'	CC	S	L-V	0.95	6.4				109
N81-98 3208 367'	CC	S	L-V	0.95	3.6				103
N81-98 3208 367'	CC	S	L-V	0.95	10				62
N81-98 3208 367'	CC	PS	L-V	0.95	5.6				64
N81-98 3208 367'	CC	PS	L-V	0.95	3.6				63
N81-98 3208 367'	CC	PS	L-V	0.95	7.2				66
N81-98 3208 367'	CC	ID	L-V	0.95	6			< -3.0	56
N81-98 3208 367'	CC	ID	L-V	0.95	5.2				55
N81-98 3208 367'	CC	ID	L-V	0.95	10				114
N81-98 3208 367'	CC	ID	L-V	0.95	3.6			-9.0	112
N81-98 3208 367'	CC	ID	L-V	0.95	6				64
N81-98 3208 367'	CC	ID	L-V	0.95	7.6				64
N81-98 3208 367'	CC	ID	L-V	0.95	7.2			-4.9	69
N81-98 3208 367'	CC	ID	L-V	0.95	16.8	<-76	-25.5	-6.0	66
N81-98 3208 367'	CC	HC	L-HC		13.6				-
N81-98 3214	CC	P	L-V	0.95	8	<-46			91
N81-98 3214	CC	P	L-V	0.95	24	<-37			126
N81-98 3214	CC	P	L-V	0.95	8			-0.1	149
N81-98 3214	CC	P	L-V	0.95	6			-9.9	162
N81-98 3214	CC	P	L-V	0.85	24			0.0	195
N81-98 3225 450'	CWD	P	L-V	0.95	4	<-65	-45	-28.0	103
N81-98 3225 450'	CWD	P	L-V	0.95	4.4	<-60		-23.0	88

N81-98 3225 450'	CWD	P	L-V	0.95	4	<-60		-21.0	85
N81-98 3225 450'	CWD	P	L-V	0.95	6.8	<-60	-51.5	-26.0	80
N81-98 3225 450'	CWD	P	L-V	0.95	6	<-65	-52		70

**APPENDIX II**  
**FLUID INCLUSION CALCULATED SALINITIES**

Calculated salinities based on Bodnar, 1993.

List of abbreviations:

CWD = coarse white dolomite  
SPH = sphalerite  
CC = calcite  
P = primary  
S = secondary  
ID = indeterminable  
L-V = liquid-vapour  
DOF = degree of fill  
 $T_{m_{ice}}$  = ice melting temperature  
Th = homogenization temperature

Sample	Host	FI Phase		DOF	Length( $\mu\text{m}$ )	$T_{m_{ice}}$ ( $^{\circ}\text{C}$ )	abs $T_{m_{ice}}$	Salinity
		Type	Type					wt% NaCl (equivalent)
N81-65 0249	CWD	P	L-V	0.95	5	-15.5	15.5	19.0
N81-65 0249	CWD	P	L-V	0.95	9	-21.2	21.2	23.2
N81-65 0249	CWD	P	L-V	0.95	9	-20.7	20.7	22.8
N81-65 0249	CWD	P	L-V	0.95	7	-19.9	19.9	22.3
N81-65 0249	CWD	P	L-V	0.95	4	-18.1	18.1	21.0
N81-65 0249	CWD	P	L-V	0.9	28	<-16.1	16.1	19.5
N81-75 3386 322'	CWD	P	L-V	0.95	7	-14.8	14.8	18.5
N81-75 3386 322'	CWD	P	L-V	0.95	9	-15.3	15.3	18.9
N81-75 3386 322'	CWD	P	L-V	0.95	7	-16.5	16.5	19.8
N81-75 3386 322'	CWD	P	L-V	0.95	10	-17.0	17.0	20.2
N81-75 3386 322'	CWD	P	L-V	0.95	5	-14.3	14.3	18.0
N81-75 3386 322'	CWD	P	L-V	0.95	5	-13.7	13.7	17.5
N81-75 3386 322'	CWD	P	L-V	0.95	17	-16.5	16.5	19.8
N81-75 3386 322'	CWD	P	L-V	0.95	17	-15.5	15.5	19.0
N81-75 3386 322'	CWD	P	L-V	0.95	11	-15.6	15.6	19.1
N81-75 3386 322'	CWD	P	L-V	0.9	17	-13.7	13.7	17.5
N81-75 3386 322'	CWD	P	L-V	0.95	9	-16.0	16.0	19.4
N81-75 3386 322'	CWD	P	L-V	0.95	10	-15.6	15.6	19.1
N81-75 3386 322'	CWD	P	L-V	0.95	11	-16.2	16.2	19.6
N81-75 3386 322'	CWD	P	L-V	0.95	5	-12.6	12.6	16.5
N81-84 1078	CWD	P	L-V	0.95	16.8	-27.0	27	26.8
N81-84 1078	CWD	P	L-V	0.95	8	-25.3	25.3	25.8
N81-84 1078	CWD	P	L-V	0.95	9.6	-28.1	28.1	27.5
N81-84 1078	CWD	P	L-V	0.95	2.4	-28.0	28	27.4
N81-84 1078	CWD	P	L-V	0.95	7.2	-27.0	27	26.8
N81-84 1078	CWD	P	L-V	0.95	4.8	-24.0	24	25.0
N81-84 1078	CWD	P	L-V	0.95	5.2	-28.0	28	27.4
N81-84 1078	CWD	P	L-V	0.95	6.4	-28.0	28	27.4
N81-98 3205 360'	CWD	P	L-V	0.95	8	-22.0	22.0	23.7
N81-98 3205 360'	CWD	P	L-V	0.95	8	-22.0	22.0	23.7
N81-98 3205 360'	CWD	P	L-V	0.95	7	-22.5	22.5	24.0
N81-98 3205 360'	CWD	P	L-V	0.95	10	-23.0	23.0	24.3
N81-98 3205 360'	CWD	P	L-V	0.95	10	-26.0	26.0	26.2
N81-98 3205 360'	CWD	P	L-V	0.9	7	-27.9	27.9	27.4
N81-98 3205 360'	CWD	P	L-V	0.95	5	-28.3	28.3	27.6
N81-98 3205 360'	CWD	P	L-V	0.95	4	-28.8	28.8	27.9
N81-98 3225 450'	CWD	P	L-V	0.95	4	-28.0	28	27.4
N81-98 3225 450'	CWD	P	L-V	0.95	4.4	-23.0	23	24.3
N81-98 3225 450'	CWD	P	L-V	0.95	4	-21.0	21	23.0
N81-98 3225 450'	CWD	P	L-V	0.95	6.8	-26.0	26	26.2

N81-98 3205 360'	CWD	P	L-V	0.95	18	-16.5	16.5	19.8
N81-98 3205 360'	CWD	ID	L-V	0.75	14	-9.0	9.0	12.8
N81-98 3205 360'	CWD	ID	L-V	0.95	4	-22.0	22.0	23.7
N81-98 3205 360'	SPH	P	L-V	0.95	15	-17.7	17.7	20.7
N81-98 3205 360'	SPH	P	L-V	0.9	4	-17.7	17.7	20.7
N81-98 3205 360'	SPH	P	L-V	0.95	7	-16.9	16.9	20.1
N81-98 3205 360'	SPH	ID	L-V	0.95	7	-15.7	15.7	19.2
N81-98 3205 360'	SPH	ID	L-V	0.95	5	-16.3	16.3	19.7
N81-98 3205 360'	SPH	ID	L-V	0.95	10	-11.3	11.3	15.3
N81-68A 2969 375'	CC	P	L-V	0.95	3	-8.8	8.8	12.6
N81-68A 2969 375'	CC	P	L-V	0.95	22	-7.1	7.1	10.6
N81-68A 2969 375'	CC	P	L-V	0.95	10	-9.0	9	12.8
N81-68A 2969 375'	CC	P	L-V	0.95	10	-7.0	7	10.5
N81-98 3181 287'	CC	P	L-V	0.95	6.4	-6.5	6.5	9.9
N81-98 3181 287'	CC	P	L-V	0.95	45.2	-8.0	8.0	11.7
N81-98 3181 287'	CC	P	L-V	0.95	24	-11.3	11.3	15.3
N81-98 3181 287'	CC	P	L-V	0.95	6.4	-5.9	5.9	9.1
N81-98 3208 367'	CC	P	L-V	0.9	13.6	-0.1	0.1	0.2
N81-98 3208 367'	CC	P	L-V	0.95	26	-6.5	6.5	9.9
N81-98 3208 367'	CC	P	L-V	0.9	33.2	-6.5	6.5	9.9
N81-98 3208 367'	CC	P	L-V	0.9	19.2	-4.6	4.6	7.3
N81-98 3208 367'	CC	P	L-V	0.95	32	-6.3	6.3	9.6
N81-98 3208 367'	CC	P	L-V	0.95	24.8	-6.4	6.4	9.7
N81-98 3208 367'	CC	P	L-V	0.95	11.6	-5.1	5.1	8.0
N81-98 3208 367'	CC	P	L-V	0.95	13.6	-0.1	0.1	0.2
N81-98 3208 367'	CC	P	L-V	0.95	10	-6.3	6.3	9.6
N81-98 3214	CC	P	L-V	0.95	8	-1.0	1.0	1.7
N81-98 3214	CC	P	L-V	0.95	8	-0.1	0.7	1.2
N81-98 3214	CC	P	L-V	0.95	6	-9.9	9.9	13.8
N81-98 3214	CC	P	L-V	0.85	24	0.0	0	0.0
N81-68A 2969 375'	CC	S	L-V	0.95	12	-7.5	7.5	11.1
N81-68A 2969 375'	CC	S	L-V	0.95	8	-8.0	8	11.7
N81-84 1078	CC	S	L-V	0.95	12	-8.8	8.8	12.6
N81-98 3181 287'	CC	S	L-V	0.95	16.8	-6.9	6.9	10.4
N81-68A 2969 375'	CC	ID	L-V	0.95	16	-10.9	10.9	14.9
N81-68A 2969 375'	CC	ID	L-V	0.95	6	-7.7	7.7	11.3
N81-68A 2969 375'	CC	ID	L-V	0.95	5	-5.1	5.1	8.0
N81-98 3208 367'	CC	ID	L-V	0.95	3.6	-9.0	9.0	12.8
N81-98 3208 367'	CC	ID	L-V	0.95	7.2	-4.9	4.9	7.7
N81-98 3208 367'	CC	ID	L-V	0.95	16.8	-6.0	6.0	9.2

**APPENDIX III**  
**PINE POINT MICROTHERMOMETRIC DATA FROM PREVIOUS AUTHORS**

List of microthermometric results from the Pine Point mine site and the surrounding ore-related regions.

CWD = coarse white dolomite  
SPH = sphalerite  
CC = calcite  
CEL = celestite  
P = primary fluid inclusions  
PP = Pine Point  
PQB = Presqu'ile Barrier  
NW AB= northwestern Alberta  
 $T_{m_{HH}}$  = hydrohalite melting temperature  
 $T_{m_{ice}}$  = ice melting temperature  
 $T_h$  = homogenization temperature

Author	Type	T <sub>mHH</sub>		Na:Ca	T <sub>mice</sub>		Salinity (wt% NaCl equiv.)	Th	
		(°C)	n <sub>TmHH</sub>		(°C)	n <sub>Tmice</sub>		(°C)	n <sub>Th</sub>
<i>This study (2006)</i>	PP CWD P	-43.4	25	0.05	-21.0	40	23.4	82	98
<i>This study (2006)</i>	PP SPH P	-	-	-	-17.4	3	20.7	74	4
<i>This study (2006)</i>	PP CC P	-22.1	9	0.88	-5.8	20	8.9	92	47
<i>This study (2006)</i>	PP ORE FLUID	-43.4	25	0.05	-20.7	43	23.2	82	102
Roedder (1968)	PP SPH	-	-	-	-	133	25	51 to 97	112
Roedder (1968)	PP DOL	-	-	-	-	4	~21	90 to 100	23
Roedder (1968)	PP CC	-	-	-	-	14	~5	-	-
Kyle (1981)	PP SPH	-	-	-	-	31	20	51 to 99	56
Kyle (1981)	PP CEL	-	-	-	-	4	10 to 15	86 to 98	4
Qing (1991)	PP N81 PIT SDOL	-	-	-	-22.8	2	24.5	106	13
Qing (1991)	PP N81 PIT CC	-	-	-	-4.5	8	7.1	95	8
Qing (1991)	PP AREA SDOL	-	-	-	-20.3	71	10 to 31	133	144
Qing (1991)	PP AREA CC	-	-	-	-10.3	36	6 to 19	142	49
Qing & Mountjoy (1992)	PQB SDOL	-	-	-	-	-	-	92 to 178	-
Qing & Mountjoy (1992)	PP SDOL	-	-	-	-	-	-	92 to 106	-
Al-Aasm et al. (2000)	NW AB SDOL	-	-	-	-7 to - 9.5	-	10.9 to 13.6	170 to 230	-
Turner (2003)	PP AREA ORE FLUID	-	-	<0.1	-	-	25 to 27	96	-
Turner (2003)	PP AREA CC	-	-	0.4 to 1	-	-	9	85	-
Turner (2003)	PP N81-65 0249 (DOL)	-38.4	5	0.12	18.8	5	21.7	87	4
Turner (2003)	PP N81-98 3208 (SPH)	>-52	3	>0.05	-31.6	3	30	60	2
Turner (2003)	PP N81-98 3208 (CC)	-	-	-	-0.7	2	1.2	105	1

**APPENDIX IV  
GEOCHEMICAL DATA FROM ION CHROMATOGRAPHY**

Anion data from ion chromatography (HDOL=host dolomite; DOL=dolomite (unspecified variety); CWD=coarse white dolomite; SPH=sphalerite; GN=galena; CC=calcite; b.d.=below detection limit; n.d.=not determined; DUP=duplicate (see Section 5.2); host= $\text{SO}_4^{2-}$  data is not reported for sulphide hosted fluid inclusions (see Section 5.4.1). The detection limits are 0.02 for  $\text{Cl}^-$ ,  $\text{Br}^-$  and  $\text{F}^-$  and 0.05 for  $\text{SO}_4^{2-}$  (ppm).

Sample	Phase	ppm Cl <sup>-</sup>	ppm Br <sup>-</sup>	ppm F <sup>-</sup>	ppm SO <sub>4</sub> <sup>2-</sup>
N81-65 0249	HDOL	76.98	0.53	0.18	10.17
N81-69 2754 195'	HDOL	39.46	0.25	0.01	12.99
N81-69 2758 217'	HDOL	30.78	0.2	0.99	364.07
N81-69 2764 235'	HDOL	105.16	0.89	0.37	177.01
N81-69 2766 240'	HDOL	46.39	0.3	0.25	54.66
N81-65 0249	CWD	191.57	1.44	0.73	43.64
N81-75 3386 322'	CWD	82.6	0.46	0.34	5.73
N81-84 1078	CWD	183.06	1.29	0.48	5.04
N81-98 3205 360'	CWD	201.62	1.46	0.54	13.87
N81-98 3225 450'	CWD	472.76	4.07	0.53	93.5
N81-98 3205 355'	DOL	108.01	n.d.	0.07	48.76
N81-98 3208 367'	DOL	13.73	0.05	0.18	9.06
N81-68A 2969 375'	SPH	5.29	0.04	b.d.	HOST
N81-69 2754 195'	SPH	10.28	0.07	0.08	HOST
N81-69 2764 235'	SPH	6.19	0.05	b.d.	HOST
N81-98 3181 287'	SPH	2.54	b.d.	b.d.	HOST
N81-98 3205 355'	SPH(DUP)	6.27	0.05	b.d.	HOST
N81-98 3205 355'	SPH(DUP)	6.49	0.06	b.d.	HOST
N81-98 3205 360'	SPH	7.88	0.08	b.d.	HOST
N81-98 3208 367'	SPH	7.61	0.07	b.d.	HOST
N81-98 3214	SPH	11.28	0.09	b.d.	HOST
Pit P-41(float)	SPH	11.08	0.08	0.03	HOST
N81-69 2758 217'	GN	3.01	0.04	0.05	HOST
N81-69 2764 235'	GN	8.02	0.05	b.d.	HOST
N81-98 3181 287'	GN	3.93	0.04	b.d.	HOST
N81-98 3205 355'	GN	3.09	0.02	b.d.	HOST
N81-65 0249	CC	8.08	0.03	0.05	0.58
N81-68A 2969 375'	CC	12.67	0.04	b.d.	40.93
N81-75 3358 260'	CC	13.03	b.d.	0.12	2.04
N81-75 3386 322'	CC	14.28	0.03	0.08	2.45
N81-84 1078	CC	36	0.3	0.02	1.61
N81-98 3205 355'	CC	2.85	b.d.	0.05	25.75
N81-98 3208 367'	CC	0.62	b.d.	0.01	0.31

N81-98 3214	CC	4.31	b.d.	0.15	6.46
N81-98 3225 450'	CC	19.06	0.15	0.07	2
Pit P-41(float)	CC	3.61	b.d.	0.01	0.53

**APPENDIX V**  
**GEOCHEMICAL DATA FROM AAS ANALYSIS**

Cation data from AAS analysis (HDOL=host dolomite; CWD =coarse white dolomite; DOL=dolomite (unspecified variety); SPH=sphalerite; GN=galena; CC=calcite; b.d.=below detection limit; n.a.=not analyzed). The detection limits for Na, K and Li are 0.0002, 0.003 and 0.002 ppm, respectively.

Sample	Phase	ppm Na	ppm K	ppm Li
N81-65 0249	HDOL	21.5	7	b.d.
N81-69 2754 195'	HDOL	14.48	8.32	0.0024
N81-69 2758 217'	HDOL	8.56	n.a	n.a
N81-69 2764 235'	HDOL	17.04	12.3	n.a
N81-69 2766 240'	HDOL	9	n.a	n.a
N81-65 0249	CWD	48	9.9	b.d.
N81-75 3386 322'	CWD	23.5	2.3	n.a
N81-84 1078	CWD	41.7	7.8	b.d.
N81-98 3205 360'	CWD	42.75	8.4	b.d.
N81-98 3225 450'	CWD	72.4	17.2	0.012
N81-98 3205 355'	DOL	22.38	4.32	n.a
N81-98 3208 367'	DOL	6.28	n.a	n.a
N81-68A 2969 375'	SPH	2.33	n.a	n.a
N81-69 2754 195'	SPH	3.28	n.a	n.a
N81-69 2764 235'	SPH	2.24	n.a	n.a
N81-98 3181 287'	SPH	n.a	n.a	n.a
N81-98 3205 355'	SPH	1.94	n.a	n.a
N81-98 3205 360'	SPH	2.97	n.a	n.a
N81-98 3208 367'	SPH	2.92	n.a	n.a
N81-98 3214	SPH	3.1	n.a	n.a
Pit P-41(float)	SPH	3.87	n.a	n.a
N81-69 2764 235'	GN	2.66	n.a	n.a
N81-98 3181 287'	GN	1.64	n.a	n.a
N81-65 0249	CC	0.55	n.a	n.a
N81-68A 2969 375'	CC	6.32	0.52	n.a
N81-75 3358 260'	CC	4.72	0.72	n.a
N81-75 3386 322'	CC	1.85	0.91	n.a
N81-84 1078	CC	12.72	4.96	b.d.
N81-98 3205 355'	CC	0.9	n.a	n.a
N81-98 3208 367'	CC	0.02	n.a	n.a
N81-98 3214	CC	2.55	n.a	n.a
N81-98 3225 450'	CC	7.5	4.68	0.0018
Pit P-41(float)	CC	0.33	n.a	n.a

**APPENDIX VI**  
**GEOCHEMICAL DATA FROM ICP-MS ANALYSIS**

Cation data from ICP-MS analysis (HDOL=host dolomite; CWD=coarse white dolomite; DOL=dolomite (unspecified variety); SPH=sphalerite; GN=galena; CC=calcite; host=Ca, Mg, S, Pb, Zn data that is not reported for certain leachates (see Section 5.4.1); data below the detection limits of the technique are indicated as <detection limit (see Section 2.3.2)).

Sample	Phase	Ca	Mg	Na	K	Fe	Mn	S	Ba	B
N81-69 2758 217'	HDOL	HOST	HOST	3	21	<0.05	2.98	84	0.11	0.14
N81-69 2764 235'	HDOL	HOST	HOST	3	4	4.2	2.4	10	1.1	0.03
N81-69 2766 240'	HDOL	HOST	HOST	3	<2	<0.05	0.39	10	0.16	0.02
N81-65 0249	CWD	HOST	HOST	21	2	<0.05	0.75	7	0.01	0.05
N81-84 1078	CWD	HOST	HOST	6	<2	<0.05	1.3	<2	0.008	0.02
N81-98 3205 360'	CWD	HOST	HOST	7	<2	<0.05	0.95	2	0.03	0.03
N81-98 3225 450'	CWD	HOST	HOST	25	5	<0.05	0.89	8	0.06	0.06
N81-98 3205 355'	DOL	HOST	HOST	8	<2	<0.05	0.51	24	0.063	0.04
N81-98 3208 367'	DOL	HOST	HOST	<2	<2	<0.05	0.63	2	0.008	0.02
N81-68A 2969 375'	SPH	1400	4	<2	<2	0.53	0.47	HOST	0.01	<0.01
N81-69 2754 195'	SPH	668	375	<2	<2	18.6	2.56	HOST	0.522	<0.01
N81-69 2764 235'	SPH	587	194	<2	<2	18.3	2.5	HOST	0.48	<0.01
N81-98 3205 355'	SPH	943	24	<2	<2	4	0.51	HOST	0.04	<0.01
N81-98 3205 360'	SPH	408	91.4	<2	<2	14.8	0.65	HOST	0.077	0.02
N81-98 3208 367'	SPH	1310	44	<2	<2	4.9	1.2	HOST	0.28	<0.01
N81-98 3214	SPH	1070	29	<2	<2	9.14	0.67	HOST	0.02	<0.01
Pit P-41(float)	SPH	992	195	<2	<2	0.75	1	HOST	0.03	<0.01
N81-69 2764 235'	GN	110	36	<2	<2	3.4	0.32	HOST	0.2	<0.01
N81-98 3181 287'	GN	119	14	<2	<2	1.6	0.3	HOST	0.02	<0.01
N81-65 0249	CC	HOST	11	<2	<2	<0.05	0.69	<2	<0.005	0.02
N81-68A 2969 375'	CC	HOST	6.1	<2	<2	<0.05	0.43	4	0.008	0.08
N81-84 1078	CC	HOST	13	<2	<2	<0.05	0.76	<2	0.007	0.04
N81-98 3214	CC	HOST	8.4	<2	<2	<0.05	<0.2	3	0.02	0.02
Pit P-41(float)	CC	HOST	3	<2	<2	<0.05	0.2	<2	0.005	0.02

CONTINUED...

Sample	Phase	ppm Cd	ppm Co	ppm Pb	ppm Li	ppm Ni	ppm Sr	ppm Zn
N81-69 2758 217'	HDOL	0.00140	0.018	0.974	0.01	0.12	0.48	4.71
N81-69 2764 235'	HDOL	0.01550	0.002	20.4	<0.005	0.02	0.38	20
N81-69 2766 240'	HDOL	0.00010	0.001	0.219	<0.005	0.02	0.613	1.27
N81-65 0249	CWD	0.00010	<0.0005	0.0508	0.008	0.02	0.637	0.27
N81-84 1078	CWD	0.00007	<0.0005	0.022	<0.005	0.02	0.43	0.02
N81-98 3205 360'	CWD	0.00020	<0.0005	0.045	<0.005	0.02	0.43	0.701
N81-98 3225 450'	CWD	0.00009	0.002	0.004	0.01	0.02	1.18	0.12
N81-98 3205 355'	DOL	0.00030	0.0005	0.0833	<0.005	0.02	0.46	1.92
N81-98 3208 367'	DOL	0.00009	<0.0005	0.0756	<0.005	<0.005	0.33	0.38
N81-68A 2969 375'	SPH	0.00060	<0.0005	3.06	<0.005	<0.01	0.523	HOST
N81-69 2754 195'	SPH	0.00170	0.0008	5.81	<0.005	0.02	0.26	HOST
N81-69 2764 235'	SPH	0.00270	<0.0005	4.6	<0.005	0.01	1.33	HOST
N81-98 3205 355'	SPH	0.00030	<0.0005	1.4	<0.005	0.009	0.31	HOST
N81-98 3205 360'	SPH	0.00020	<0.0005	0.86	<0.005	0.01	0.14	HOST
N81-98 3208 367'	SPH	0.00020	0.0005	0.1	<0.005	0.02	0.33	HOST
N81-98 3214	SPH	0.00040	<0.0005	0.52	<0.005	0.01	0.24	HOST
Pit P-41(float)	SPH	0.00220	<0.0005	1.2	<0.005	0.02	0.076	HOST
N81-69 2764 235'	GN	0.26500	0.0005	HOST	<0.005	0.02	0.2	15
N81-98 3181 287'	GN	0.08210	<0.0005	HOST	<0.005	0.02	0.099	22
N81-65 0249	CC	0.00010	<0.0005	0.01	<0.005	0.02	0.18	0.45
N81-68A 2969 375'	CC	0.00010	<0.0005	0.14	<0.005	0.02	1.82	0.253
N81-84 1078	CC	<0.00005	<0.0005	0.0773	<0.005	0.02	0.29	0.01
N81-98 3214	CC	0.00008	<0.0005	<0.0005	<0.005	0.01	0.511	0.26
Pit P-41(float)	CC	0.00005	<0.0005	0.1	<0.005	0.002	0.051	0.17

**APPENDIX VII**  
**NORMALIZED CATION CONCENTRATIONS (ICP-MS)**

Cation values from ICP-MS analysis normalized to Na concentrations of AAS analysis (HDOL=host dolomite; CWD=coarse white dolomite; DOL=dolomite (unspecified variety); b.d.=below detection limit).

Sample	Phase	ppm Ca	ppm Mg	ppm Na	ppm K	ppm Fe	ppm Mn	ppm S	ppm Ba
N81-69 2758 217'	HDOL	HOST	HOST	8.56	59.92	b.d.	8.5	239.68	0.314
N81-69 2764 235'	HDOL	HOST	HOST	17.04	22.72	23.86	13.63	56.8	6.248
N81-69 2766 240'	HDOL	HOST	HOST	9	b.d.	b.d.	1.17	30	0.48
N81-65 0249	CWD	HOST	HOST	48	4.57	b.d.	1.71	16	0.023
N81-84 1078	CWD	HOST	HOST	41.7	b.d.	b.d.	9.04	b.d.	0.056
N81-98 3205 360'	CWD	HOST	HOST	42.75	b.d.	b.d.	5.8	12.21	0.183
N81-98 3225 450'	CWD	HOST	HOST	72.4	14.48	b.d.	2.58	23.17	0.174
N81-98 3205 355'	DOL	HOST	HOST	22.38	b.d.	b.d.	1.43	67.14	0.176

CONTINUED...

Sample	Phase	B ppm	Cd ppm	Co ppm	Pb ppm	Li ppm	Ni ppm	Sr ppm	Zn ppm
N81-69 2758 217'	HDOL	0.4	0.004	0.0514	2.779	0.029	0.342	1.37	13.44
N81-69 2764 235'	HDOL	0.17	0.088	0.0114	115.872	b.d.	0.114	2.16	113.6
N81-69 2766 240'	HDOL	0.06	0.0003	0.003	0.657	b.d.	0.06	1.84	3.81
N81-65 0249	CWD	0.11	0.0002	b.d.	0.116	0.018	0.046	1.46	0.62
N81-84 1078	CWD	0.14	0.0005	b.d.	0.153	b.d.	0.139	2.99	0.14
N81-98 3205 360'	CWD	0.18	0.0012	b.d.	0.275	b.d.	0.122	2.63	4.28
N81-98 3225 450'	CWD	0.17	0.0003	0.0058	0.012	0.029	0.058	3.42	0.35
N81-98 3205 355'	DOL	0.11	0.0008	0.0014	0.233	b.d.	0.056	1.29	5.37

**APPENDIX VIII**  
**ANION AND CATION MOLAR RATIO RESULTS (IC AND AAS)**

Anion and cation molar ratio data (HDOL=host dolomite; DOL=dolomite (unspecified variety); CWD=coarse white dolomite; SPH=sphalerite; GN=galena; CC=calcite; b.d=below detection limit; n.d=not determined; DUP=duplicate (see Section 5.2); host= $\text{SO}_4^{2-}$  data is not reported for sulphide hosted fluid inclusions (see Section 5.4.1)).

Sample	Phase	Cl/Br	SO <sub>4</sub> /Br	K/Na	Li/Na	Na/Br	K/Br
N81-65 0249	HDOL	327	16	0.191	b.d.	141	27
N81-69 2754 195'	HDOL	354	43	0.338	0.0005	201	68
N81-69 2758 217'	HDOL	342	1492	n.a.	n.a.	147	n.a.
N81-69 2764 235'	HDOL	267	166	0.424	n.a.	67	28
N81-69 2766 240'	HDOL	351	153	n.a.	n.a.	105	n.a.
N81-65 0249	CWD	299	25	0.121	b.d.	116	14
N81-75 3386 322'	CWD	405	10	0.058	n.a.	178	10
N81-84 1078	CWD	320	3	0.11	b.d.	112	12
N81-98 3205 360'	CWD	311	8	0.116	b.d.	102	12
N81-98 3225 450'	CWD	262	19	0.14	0.0005	62	9
N81-98 3205 355'	DOL	n.d.	n.d.	0.114	n.a.	n.a.	n.d.
N81-98 3208 367'	DOL	688	167	n.a.	n.a.	485	n.a.
N81-68A 2969 375'	SPH	271	HOST	n.a.	n.a.	184	n.a.
N81-69 2754 195'	SPH	317	HOST	n.a.	n.a.	156	n.a.
N81-69 2764 235'	SPH	279	HOST	n.a.	n.a.	156	n.a.
N81-98 3181 287'	SPH	b.d.	HOST	n.a.	n.a.	b.d.	n.a.
N81-98 3205 355'	SPH(DUP)	283	HOST	n.a.	n.a.	b.d.	n.a.
N81-98 3205 355'	SPH(DUP)	240	HOST	n.a.	n.a.	111	n.a.
N81-98 3205 360'	SPH	228	HOST	n.a.	n.a.	132	n.a.
N81-98 3208 367'	SPH	245	HOST	n.a.	n.a.	145	n.a.
N81-98 3214	SPH	276	HOST	n.a.	n.a.	117	n.a.
Pit P-41(float)	SPH	305	HOST	n.a.	n.a.	164	n.a.
N81-69 2758 217'	GN	161	HOST	n.a.	n.a.	n.a.	n.a.
N81-69 2764 235'	GN	377	HOST	n.a.	n.a.	193	n.a.
N81-98 3181 287'	GN	201	HOST	n.a.	n.a.	130	n.a.
N81-98 3205 355'	GN	410	HOST	n.a.	n.a.	b.d.	n.a.
N81-65 0249	CC	536	14	n.a.	n.a.	56	n.a.
N81-68A 2969 375'	CC	732	873	0.048	n.a.	563	27
N81-75 3358 260'	CC	b.d.	b.d.	0.090	n.a.	b.d.	b.d.
N81-75 3386 322'	CC	975	62	0.289	n.a.	195	56
N81-84 1078	CC	271	4	0.229	b.d.	148	34
N81-98 3205 355'	CC	b.d.	b.d.	n.a.	n.a.	b.d.	n.a.
N81-98 3208 367'	CC	b.d.	b.d.	n.a.	n.a.	b.d.	b.d.
N81-98 3214	CC	b.d.	b.d.	n.a.	n.a.	b.d.	b.d.
N81-98 3225 450'	CC	294	11	0.367	0.0008	179	66
Pit P-41(float)	CC	b.d.	b.d.	n.a.	n.a.	b.d.	b.d.

**APPENDIX IX**  
**CATION MOLAR RATIO RESULTS (ICP-MS)**

Cation molar ratio data from ICP-MS analysis (HDOL=host dolomite; DOL=dolomite (unspecified variety); CWD=coarse white dolomite; b.d.=below detection limit).

	N81-69		N81-69		N81-65	N81-98		N81-84	N81-98		N81-98			
Sample	2758	217'	2764	235'	2766	240'	0249	3205	360'	1078	3225	450'	3205	355'
Phase	HDOL	HDOL	HDOL	HDOL	CWD	CWD	CWD	CWD	CWD	CWD	CWD	CWD	DOL	DOL
Fe/Na	b.d.	0.576	b.d.	b.d.	b.d.	b.d.	b.d.	b.d.	b.d.	b.d.	b.d.	b.d.	b.d.	b.d.
Zn/Na	0.552	2.343	0.149	0.005	0.035	0.001	0.002	0.084						
Mn/Na	0.416	0.335	0.054	0.015	0.057	0.091	0.015	0.027						
S/Na	20.08	2.39	2.39	0.24	0.20	b.d.	0.23	2.15						
Ba/Na	0.0061	0.0614	0.0089	0.0001	0.0007	0.0002	0.0004	0.0013						
B/Na	0.0992	0.0213	0.0142	0.0051	0.0091	0.0071	0.0051	0.0106						
Cd/Na	0.0001	0.00106	0.00001	0.000001	0.000006	0.000002	0.000001	0.000008						
Co/Na	0.00234	0.00026	0.00013	b.d.	b.d.	b.d.	0.00003	0.00002						
Pb/Na	0.036	0.7545	0.0081	0.0003	0.0007	0.0004	0.0001	0.0012						
Ni/Na	0.0157	0.0026	0.0026	0.0004	0.0011	0.0013	0.0003	0.001						
Sr/Na	0.0420	0.0332	0.0536	0.008	0.0161	0.0188	0.0124	0.0151						

**APPENDIX X**  
**IN-SITU Sr ISOTOPE RESULTS (MC-ICP-MS)**

List of strontium isotope results and total strontium ion signals from N81 deposit drill cores (HDOL=host dolomite; HDOL(R)=host dolomite partially replaced by coarse white dolomite; CWD=coarse white dolomite; SDOL=saddle dolomite (see Section 6.2.3); CC=calcite).

Sample	Phase	$^{87}\text{Sr}/^{86}\text{Sr}$	$^{87}\text{Sr}/^{86}\text{Sr}$ Error	(volts) $\text{Sr}_{\text{total}}$	$\text{Sr}_{\text{total}}$ Error	(1/Volts <sup>-1</sup> ) 1/ $\text{Sr}_{\text{total}}$
N81-65 0249	CC	0.7153	0.0003	0.42	0.03	2.39
N81-65 0249	CC	0.7163	0.0002	0.46	0.02	2.16
N81-65 0249	CC	0.7161	0.0003	0.49	0.03	2.03
N81-65 0249	CC	0.7174	0.0004	0.41	0.02	2.44
N81-65 0249	CC	0.7156	0.0003	0.45	0.03	2.22
N81-68A 2969 375'	CC	0.7152	0.0002	0.71	0.02	1.41
N81-68A 2969 375'	CC	0.7153	0.0002	0.47	0.01	2.12
N81-68A 2969 375'	CC	0.7155	0.0001	0.65	0.01	1.55
N81-68A 2969 375'	CC	0.7147	0.0002	0.31	0.01	3.26
N81-68A 2969 375'	CC	0.7150	0.0002	0.71	0.01	1.4
N81-68A 2969 375'	CC	0.7140	0.0003	0.32	0.01	3.18
N81-68A 2969 375'	CC	0.7146	0.0002	2.82	0.21	0.36
N81-84 1078	CC	0.7159	0.0002	0.87	0.03	1.15
N81-84 1078	CC	0.7161	0.0002	0.91	0.04	1.1
N81-84 1078	CC	0.7160	0.0001	1.03	0.04	0.97
N81-98 3181 287'	CC	0.7123	0.0016	0.19	0.04	5.41
N81-98 3181 287'	CC	0.7186	0.0009	0.29	0.07	3.39
N81-98 3205 355'	CC	0.7153	0.0002	0.37	0.01	2.68
N81-98 3205 355'	CC	0.7154	0.0002	0.53	0.01	1.9
N81-98 3205 355'	CC	0.7107	0.0009	0.35	0.06	2.82
N81-98 3205 355'	CC	0.7154	0.0002	0.33	0.01	3.03
N81-98 3205 355'	CC	0.7151	0.0003	0.39	0.01	2.6
N81-98 3205 355'	CC	0.7151	0.0002	0.45	0.01	2.21
N81-98 3214	CC	0.7139	0.0002	1.09	0.07	0.92
N81-98 3214	CC	0.7130	0.0002	1.16	0.04	0.86
N81-98 3214	CC	0.7118	0.0001	1.25	0.02	0.8
N81-98 3214	CC	0.7138	0.0002	0.53	0.01	1.88
N81-98 3214	CC	0.7135	0.0002	1.18	0.07	0.85
N81-98 3214	CC	0.7117	0.0001	1.04	0.03	0.96
N81-98 3225 450'	CC	0.7157	0.0002	0.54	0.01	1.87
N81-98 3225 450'	CC	0.7160	0.0002	0.75	0.01	1.34
N81-98 3225 450'	CC	0.7158	0.0002	0.67	0.02	1.49
N81-65 0249	CWD	0.7090	0.0002	0.31	0.01	3.2
N81-65 0249	CWD	0.7088	0.0003	0.25	0.01	4.04
N81-65 0249	SDOL	0.7109	0.0009	0.17	0.01	5.97
N81-65 0249	SDOL	0.7070	0.001	0.09	0.01	11.45
N81-65 0249	SDOL	0.7107	0.0010	0.14	0.01	7.28
N81-65 0249	SDOL	0.7111	0.0012	0.09	0.01	11.52
N81-65 0249	SDOL	0.7095	0.0007	0.28	0.02	3.58

N81-65 0249	SDOL	0.7075	0.0005	0.27	0.02	3.75
N81-65 0249	SDOL	0.7094	0.0004	0.23	0.01	4.3
N81-65 0249	SDOL	0.7089	0.0003	0.34	0.01	2.96
N81-65 0249	SDOL	0.7085	0.0004	0.28	0.01	3.57
N81-65 0249	SDOL	0.7086	0.0004	0.21	0.01	4.69
N81-98 3205 360'	CWD	0.7086	0.0005	0.22	0.01	4.52
N81-98 3205 360'	CWD	0.7114	0.0004	0.25	0.01	4.01
N81-98 3205 360'	CWD	0.7103	0.0004	0.22	0.01	4.50
N81-98 3205 360'	CWD	0.7139	0.0003	0.49	0.03	2.04
N81-98 3205 360'	CWD	0.7089	0.0004	0.23	0.01	4.28
N81-98 3205 360'	CWD	0.7087	0.0003	0.22	0.01	4.49
N81-98 3205 360'	CWD	0.7079	0.0005	0.23	0.01	4.36
N81-98 3205 360'	CWD	0.7133	0.0002	0.46	0.02	2.19
N81-98 3205 360'	CWD	0.7104	0.0003	0.33	0.01	3.01
N81-98 3205 360'	CWD	0.7135	0.0003	0.38	0.01	2.6
N81-98 3205 360'	CWD	0.7152	0.0004	0.35	0.02	2.85
N81-98 3205 360'	CWD	0.7149	0.0002	0.96	0.08	1.05
N81-98 3205 360'	CWD	0.7086	0.0005	0.24	0.01	4.12
N81-98 3205 360'	CWD	0.7143	0.0003	0.53	0.01	1.88
N81-98 3205 360'	CWD	0.7103	0.0006	0.23	0.01	4.43
N81-98 3205 360'	CWD	0.7082	0.0003	0.22	0.01	4.58
N81-98 3205 360'	CWD	0.7073	0.0004	0.25	0.01	3.95
N81-98 3205 360'	CWD	0.7087	0.0003	0.26	0.01	3.91
N81-98 3205 360'	CWD	0.7113	0.0003	0.26	0.01	3.78
N81-98 3205 360'	CWD	0.7097	0.0004	0.22	0.01	4.5
N81-98 3205 360'	CWD	0.7141	0.0002	0.45	0.02	2.24
N81-98 3205 360'	CWD	0.7140	0.0002	0.58	0.02	1.72
N81-98 3205 360'	SDOL	0.7093	0.0004	0.27	0.01	3.66
N81-98 3205 360'	CWD	0.7130	0.0002	0.38	0.01	2.64
N81-98 3205 360'	CWD	0.7114	0.0003	0.24	0.01	4.17
N81-98 3205 360'	SDOL	0.7152	0.0002	0.87	0.06	1.15
N81-98 3205 360'	SDOL	0.7146	0.0001	0.68	0.01	1.48
N81-98 3205 360'	SDOL	0.7152	0.0001	0.79	0.01	1.26
N81-98 3205 360'	SDOL	0.7146	0.0001	0.75	0.02	1.34
N81-98 3205 360'	SDOL	0.7149	0.0002	0.73	0.02	1.38
N81-98 3205 360'	SDOL	0.7121	0.0004	0.49	0.03	2.03
N81-98 3205 360'	SDOL	0.7150	0.0002	0.64	0.02	1.57
N81-98 3205 360'	SDOL	0.7146	0.0001	0.64	0.01	1.56
N81-98 3205 360'	SDOL	0.7144	0.0002	0.67	0.01	1.5
N81-98 3205 360'	SDOL	0.7140	0.0001	0.77	0.01	1.3
N81-98 3205 360'	CWD	0.7144	0.0001	0.62	0.02	1.62
N81-98 3208 367'	CWD	0.7137	0.0007	0.34	0.04	2.97

N81-98 3208 367'	CWD	0.7129	0.0002	0.65	0.03	1.53
N81-98 3208 367'	CWD	0.7139	0.0006	0.39	0.06	2.57
N81-98 3208 367'	CWD	0.7120	0.0005	0.37	0.03	2.67
N81-98 3208 367'	CWD	0.7132	0.0004	0.68	0.07	1.47
N81-98 3208 367'	CWD	0.7144	0.0003	0.67	0.04	1.49
N81-98 3208 367'	CWD	0.7140	0.0007	0.52	0.04	1.92
N81-98 3208 367'	CWD	0.7142	0.0003	0.74	0.02	1.36
N81-98 3208 367'	CWD	0.7149	0.0003	0.62	0.03	1.62
N81-98 3208 367'	CWD	0.7131	0.0002	0.67	0.04	1.49
N81-98 3208 367'	CWD	0.7141	0.0002	0.64	0.04	1.56
N81-98 3208 367'	CWD	0.7147	0.0002	0.77	0.04	1.29
N81-98 3208 367'	CWD	0.7152	0.0002	0.93	0.03	1.07
N81-98 3208 367'	CWD	0.7152	0.0002	0.58	0.04	1.71
N81-98 3208 367'	CWD	0.7146	0.0002	0.78	0.03	1.28
N81-98 3225 450'	CWD	0.7090	0.0004	0.56	0.06	1.78
N81-98 3225 450'	CWD	0.7092	0.0003	0.53	0.03	1.89
N81-98 3225 450'	CWD	0.7088	0.0001	1.01	0.02	0.99
N81-98 3225 450'	CWD	0.7089	0.0002	0.68	0.01	1.48
N81-98 3225 450'	CWD	0.7087	0.0002	0.61	0.01	1.64
N81-98 3225 450'	CWD	0.7087	0.0002	0.64	0.01	1.56
N81-98 3225 450'	CWD	0.7092	0.0001	0.62	0.01	1.61
N81-98 3225 450'	CWD	0.7089	0.0002	0.57	0.01	1.75
N81-98 3225 450'	CWD	0.7086	0.0002	0.49	0.01	2.04
N81-98 3225 450'	CWD	0.7097	0.0003	0.36	0.02	2.8
N81-65 0249	HDOL(R)	0.7084	0.0005	0.18	0.01	5.5
N81-98 3205 360'	HDOL(R)	0.7087	0.0002	0.28	0.01	3.59
N81-98 3205 360'	HDOL(R)	0.7094	0.0003	0.32	0.01	3.15
N81-98 3225 450'	HDOL	0.7097	0.0003	0.32	0.01	3.12
N81-98 3225 450'	HDOL	0.7095	0.0006	0.34	0.02	2.96
N81-98 3225 450'	HDOL	0.7058	0.0008	0.28	0.01	3.56
N81-98 3225 450'	HDOL	0.7078	0.0006	0.30	0.01	3.34

**APPENDIX XI**  
**AVERAGE Sr ISOTOPE RESULTS**

List of average strontium isotope results and total strontium ion signals (volts) from N81 deposit drill cores (HDOL=host dolomite; HDOL(R)=host dolomite partially replaced by coarse white dolomite; CWD=coarse white dolomite; SDOL=saddle dolomite (see Section 6.2.3); CC=calcite).

Sample	Phase	n	$^{87}\text{Sr}/^{86}\text{Sr}$	$^{87}\text{Sr}/^{86}\text{Sr}$	Average $^{87}\text{Sr}/^{86}\text{Sr}$	$^{87}\text{Sr}/^{86}\text{Sr}$
			Minimum	Maximum		Error
AVERAGE N81-65 0249	CC	5	0.7153	0.7174	0.7161	0.0003
AVERAGE N81-68A 2969 375'	CC	7	0.7140	0.7155	0.7149	0.0002
AVERAGE N81-84 1078	CC	3	0.7159	0.7161	0.7160	0.0001
AVERAGE N81-98 3181 287'	CC	2	0.7123	0.7186	0.7155	0.0012
AVERAGE N81-98 3205 355'	CC	6	0.7107	0.7154	0.7145	0.0003
AVERAGE N81-98 3214	CC	6	0.7117	0.7139	0.7130	0.0002
AVERAGE N81-98 3225 450'	CC	3	0.7157	0.7160	0.7158	0.0002
AVERAGE N81-65 0249	CWD&SDOL	12	0.7070	0.7111	0.7092	0.0006
AVERAGE N81-98 3205 360'	CWD&SDOL	36	0.7073	0.7152	0.7121	0.0003
AVERAGE N81-98 3208 367'	CWD	15	0.7120	0.7152	0.7140	0.0003
AVERAGE N81-98 3225 450'	CWD	10	0.7086	0.7097	0.7090	0.0002
AVERAGE N81-65 0249	HDOL(R)	1	0.7084	0.7084	0.7084	0.0005
AVERAGE N81-98 3205 360'	HDOL(R)	2	0.7087	0.7094	0.7091	0.0002
AVERAGE N81-98 3225 450'	HDOL	4	0.7058	0.7097	0.7082	0.0006

CONTINUED...

Sample	Phase	$Sr_{total}$		$1/Sr_{total}$		Average
		Minimum	Maximum	Minimum	Maximum	$1/Sr_{total}$
AVERAGE N81-65 0249	CC	0.41	0.49	2.03	2.44	2.25
AVERAGE N81-68A 2969 375'	CC	0.31	2.81	0.36	3.26	1.9
AVERAGE N81-84 1078	CC	0.87	1.03	0.97	1.15	1.07
AVERAGE N81-98 3181 287'	CC	0.18	0.3	3.39	5.41	4.4
AVERAGE N81-98 3205 355'	CC	0.33	0.53	1.9	3.03	2.54
AVERAGE N81-98 3214	CC	0.53	1.25	0.8	1.88	1.04
AVERAGE N81-98 3225 450'	CC	0.53	0.75	1.34	1.87	1.57
AVERAGE N81-65 0249	CWD&SDOL	0.09	0.34	2.96	11.52	5.52
AVERAGE N81-98 3205 360'	CWD&SDOL	0.22	0.96	1.05	4.58	2.82
AVERAGE N81-98 3208 367'	CWD	0.34	0.93	1.07	2.97	1.73
AVERAGE N81-98 3225 450'	CWD	0.36	1.01	0.99	2.8	1.76
AVERAGE N81-65 0249	HDOL(R)	0.18	0.18	5.5	5.5	5.5
AVERAGE N81-98 3205 360'	HDOL(R)	0.28	0.32	3.15	3.59	3.37
AVERAGE N81-98 3225 450'	HDOL	0.28	0.34	2.96	3.56	3.25

**APPENDIX XII**  
**Sr ISOTOPIC DATA FROM PREVIOUS AUTHORS**  
**(PINE POINT AND RELATED AREAS)**

List of strontium isotope results from the Pine Point ore district and related areas (PP=Pine Point; PreC=Precambrian; Mid Devo=Middle Devonian; AB=Alberta).

Sample	Phase	$^{87}\text{Sr}/^{86}\text{Sr}$
Burke et al. (1982)	Middle Devonian seawater	0.7080
Mountjoy et al. (1992)	Fine-crystalline dolomite (PP 2822)	0.70822
Mountjoy et al. (1992)	Fine-crystalline dolomite (PP W17)	0.70833
Mountjoy et al. (1992)	Medium-crystalline dolomite (PP 2822)	0.70871
Mountjoy et al. (1992)	Medium-crystalline dolomite (PP 2822)	0.70812
Mountjoy et al. (1992)	Medium-crystalline dolomite (PP 3305)	0.70846
Mountjoy et al. (1992)	Coarse-crystalline dolomite (PP 2822)	0.70829
Mountjoy et al. (1992)	Coarse-crystalline dolomite (PP 2822)	0.70880
Mountjoy et al. (1992)	Coarse-crystalline dolomite (PP Y53)	0.70816
Mountjoy et al. (1992)	Coarse-crystalline dolomite (PP N81)	0.70850
Mountjoy et al. (1992)	Coarse-crystalline dolomite (PP N81)	0.70866
Mountjoy et al. (1992)	Saddle Dolomite (PP 2822)	0.70847
Mountjoy et al. (1992)	Saddle Dolomite (PP Y53)	0.70816
Mountjoy et al. (1992)	Saddle Dolomite (PP N81)	0.70807
Mountjoy et al. (1992)	Saddle Dolomite (PP N81)	0.70821
Mountjoy et al. (1992)	Saddle Dolomite (PP M64)	0.70831
Mountjoy et al. (1992)	Saddle Dolomite (PP M64)	0.70840
Mountjoy et al. (1992)	Saddle Dolomite (PP P77)	0.70818
Mountjoy et al. (1992)	Saddle Dolomite (PP P77)	0.70821
Mountjoy et al. (1992)	white anhedral calcite (201 PP 2870)	0.71420
Mountjoy et al. (1992)	white anhedral calcite (201 PP 2870)	0.71438
Mountjoy et al. (1992)	white anhedral calcite (203 PP N81)	0.71360
Mountjoy et al. (1992)	white anhedral calcite (204 PP M64)	0.71468
Mountjoy et al. (1992)	white anhedral calcite (206 PP I65)	0.71282
Mountjoy et al. (1992)	white anhedral calcite (206 PP I65)	0.71388
Mountjoy et al. (1992)	white anhedral calcite (209 PP M64)	0.70849
Mountjoy et al. (1992)	semi-translucent calcite (PP 2822)	0.71612
Maxwell (1976)	PP1 sparry dolomite	0.7096
Maxwell (1976)	PP1 late calcite	0.7153
Maxwell (1976)	PP2 calcite	0.7152
Maxwell (1976)	PP1 euhedral sphalerite	0.7120
Maxwell (1976)	PP1 crystalline galena	0.7090
Maxwell (1976)	PP4 galena	0.7121
Medford et al. (1983)	Presqu'île facies dolomite (avg)	0.7084
Medford et al. (1983)	calcite (avg)	0.7137
Qing (1998)	fine crystalline dolomite	0.7079
Qing (1998)	fine crystalline dolomite	0.7081
Qing (1998)	fine crystalline dolomite	0.7079
Qing (1998)	altered fine crystalline dolomite	0.7082
Qing (1998)	altered fine crystalline dolomite	0.7083
Qing (1998)	medium crystalline dolomite	0.7081
Qing (1998)	medium crystalline dolomite	0.7085
Qing (1998)	medium crystalline dolomite	0.7087
Qing (1998)other	Pit M-64 saddle dolomite	0.70831
Qing (1998)other	Pit M-64 saddle dolomite	0.70840
Qing (1998)other	Pit P77 saddle dolomite	0.70818
Qing (1998)other	Pit P77 saddle dolomite	0.70818

Qing (1998)other	Pit Y53 saddle dolomite	0.70816
Qing (1998)other	Pit N81 saddle dolomite	0.70821
Qing (1998)other	Pit N81 saddle dolomite	0.70807
Qing (1998)other	Pit N81 saddle dolomite	0.70847
Qing and Mountjoy (1994)	saddle dolomite	0.70810
Qing and Mountjoy (1994)	saddle dolomite	0.70820
Qing and Mountjoy (1994)	saddle dolomite	0.70820
Qing and Mountjoy (1994)	saddle dolomite	0.70820
Qing and Mountjoy (1994)	saddle dolomite	0.70820
Qing and Mountjoy (1994)	saddle dolomite	0.70830
Qing and Mountjoy (1994)	saddle dolomite	0.70840
Qing and Mountjoy (1994)	saddle dolomite	0.70850
Qing and Mountjoy (1994)	coarse crystalline dolomite	0.70820
Qing and Mountjoy (1994)	coarse crystalline dolomite	0.70830
Qing and Mountjoy (1994)	coarse crystalline dolomite	0.70850
Qing and Mountjoy (1994)	coarse crystalline dolomite	0.70870
Qing and Mountjoy (1994)	coarse crystalline dolomite	0.70880
Qing and Mountjoy (1992)	saddle dolomite (avg)	0.70830
Connolly et al (1990)	Mid Devo Elk Point dolomite (AB basin)	0.70922
Al-Aasm et al. (2000)	Sulphur Point saddle dolomite(low)	0.70810
Al-Aasm et al. (2000)	Sulphur Point saddle dolomite(high)	0.71024
Al-Aasm et al. (2000)	Slave Point saddle dolomite(low)	0.70860
Al-Aasm et al. (2000)	Slave Point saddle dolomite(high)	0.71035